

A GROUND BASED INVESTIGATION OF HIGH
LATITUDE ELF RADIO SIGNALS

by

P.S. CANNON B.Sc., MSc.

A thesis submitted for the degree
of Doctor of Philosophy

Department of Physics
University of Southampton

January 1981.

UNIVERSITY OF SOUTHAMPTON

ABSTRACT

FACULTY OF SCIENCE

PHYSICS

Doctor of Philosophy

A GROUND BASED INVESTIGATION OF HIGH LATITUDE ELF RADIO SIGNALS

by Paul Stephen Cannon

The operation and calibration of a network of ELF/VLF radio goniometer receivers is outlined. The design of a frequency shift key encoded, digital clock, to provide time encoding and decoding of data tapes, is presented. Long term stability is provided by synchronisation to the VLF Omega navigation network. Goniometer experiments conducted between 1976 and 1979 and analyses of data from two experiments are presented.

The first are analyses of goniometer data recorded during the flight of Skylark rocket SL1424; launched from the Andøya range, Norway. At this time an ELF chorus event was observed by the Geos-2 satellite, the rocket and by the network of goniometer receivers. The times of risers received during and directly after the flight, and the bearing of certain of these risers from Tromsø are given.

The second, involves a new non-linear ionospheric effect, discovered from the analyses of data obtained in Scandinavia during 1979. Apart from signals of natural origin timing signals, six pips which occurred on the hour, were received. The pips, of frequency $1\text{kHz} \pm 0.5\text{Hz}$, duration $105 \pm 8\text{ms}$, and field strength $\sim 0.1\text{pT}$ at Sodankyla, Finland, exhibit a favoured source location $\sim 150\text{km}$ south-south-east of Sodankyla. A close association between the reception of these ELF pips and the auroral electrojet is demonstrated by the positive temporal correlation between ELF pip generation and periods of enhanced local magnetic activity and, also by the spatial correlation between source location and the latitude over Finland at which riometer absorption is a maximum. The latter is interpreted as indicating the electrojet position. The originating signals are shown to emanate from one or more Soviet LF/MF broadcast transmitters, all several hundred km or more from the favoured generation region. It is proposed that the 1kHz amplitude modulated waves heat the auroral D region, modulating the large electrojet current which radiates at 1kHz . Various mechanisms which can account for such a localised generation region far from the transmitters are discussed. The data argue strongly in favour of a mechanism involving periodic in-phase heating of the ionosphere by two or more synchronised transmitters. The most likely solutions involve transmissions on 173kHz , 263kHz , 281kHz and 549kHz . A 0.5K peak to peak sinusoidal electron temperature variation superimposed upon a 2K temperature rise is predicted for the combined effect of these transmitters. An estimate of the corresponding 1kHz magnetic field variations, is in good agreement with the experimental fields.

The design of a low noise ELF radio receiver with optional passbands, 0.3Hz to 700Hz , 0.3Hz to 40Hz , and 200Hz to 700Hz and, noise thresholds of $4.5 \times 10^{-7} \text{V Hz}^{-\frac{1}{2}}$ at 10Hz and $1.9 \times 10^{-7} \text{V Hz}^{-\frac{1}{2}}$ for frequencies $>200\text{Hz}$, is presented. An integral comb filter provides attenuation (48dB) of mains fundamental interference and its harmonics up to 1600Hz . A mu-metal core, multi-turn antenna, and matching preamplifier, are described; the predicted sensitivity is $1.4\text{pT Hz}^{-\frac{1}{2}}$ at 10Hz and $0.35\text{pT Hz}^{-\frac{1}{2}}$ at 200Hz . The antenna is characterised in terms of equivalent lumped circuit elements, the values of which are experimentally determined. A method of field amplitude calibration is compared with the Helmholtz coil technique. Agreement is to within 5% . Fluctuations of the Schumann resonance fundamental and harmonic frequencies at Lavangsdalen on 28 March 1979 are examined with a 15 minute resolution. Their correlation with sudden ionospheric disturbances and with other geophysical events is investigated. The experimental frequency variations are, in some cases, at variance with the theoretical predictions of Madden and Thompson (1965).

To Viv

ACKNOWLEDGMENTS

To conduct an experimental programme abroad, often in conjunction with other universities and/or institutions, requires the help and co-operation of many people. To subsequently perform the data reduction and interpretation requires yet more assistance, in terms of supplementary data and advice. To those omitted below I extend my sincerest apologies but also thanks for their help.

I wish to thank my supervisor Dr. Michael J. Rycroft for giving me the opportunity to work in this fascinating field of research and for his guidance and encouragement, over the last few years. My thanks also go to Mrs. Mary Rycroft for her hospitality during my various visits to Cambridge. I would also like to thank the Professors of Physics and in particular Professor G.W. Hutchinson for use of the departmental facilities. My thanks go to Miss P. Rothwell for help and encouragement over the past year. Additionally, thanks go to the other members of the Space Radio Physics Group, all of whom managed a goniometer receiving station on one or more occasions; namely Messrs. R. Brittain, P. Kiernan, and M. Saunders, Miss M. Madden and; Drs. G. Williams and H. Strangeways. Without their help these experiments could never have taken place. Much of the equipment described in this thesis was constructed and maintained by the Physics departmental electronics workshop; my thanks go to Messrs. Garment, Bopola, Danaford and Friis for their expertise and help.

At Sheffield University I would like to thank Professor T. Kaiser and Dr. K. Bullough for permission to use various of their facilities. In addition discussions and help given by Drs L.J.C. Woolliscroft, A.J. Smith and Messrs. I.D. Smith and B. Madahar have been of immense value.

Abroad I would especially like to thank Dr. T. Turunen at the Sodankyla Geophysical Observatory, Finland, for many interesting and helpful discussions. Thanks also go to Dr. Turunen for arranging the Finnish magnetometer and riometer data and for help during our experiments in Scandinavia. Also in Finland I would like to thank Mr. J. Sivussami of the Finnish Monitoring Service for conducting some subsidiary investigations on my behalf. In Norway thanks go to Dr. Brekke and Mr. T. Negård at the Nordlys Observatoriet, Tromsø for help with

the Lavangsdalen monitoring hut.

I would like to thank Dr. T. Jones at Leicester University for obtaining the STARE data on my behalf and the Max Planck Institute, W. Germany for providing it. Mr. R. Meacham at the B.B.C. Monitoring Service and Mr. R. Gressmann at the European Broadcasting Union are due thanks for providing data which helped identify the causative transmitters.

I would also thank Anne Le Brun for her speedy and accurate typing of this thesis.

I would like to take this opportunity to thank my parents for everything they have done for me and the support that they have given me over the past years.

Lastly, but not least, I wish to mention my wife Viv, whose help and encouragement has been of inestimable value during both the research and the writing of this thesis. To her go my sincerest thanks.

'Some say that the Northern Lights
are the glare of the Arctic ice and snow;
And some that it's electricity
and nobody seems to know.'

- From the "Ballad of the Northern Lights"
by R.W. Service

CONTENTS

	<u>Page no.</u>
<u>Chapter 1</u> THE NEAR EARTH SPACE PLASMA ENVIROMENT: A REVIEW	
1.1 Introduction	1
1.2 The Ionosphere	1
1.3 The Morphology Of The Magnetosphere	5
1.4 Magnetospheric And Auroral Ionsopheric Current Systems	12
 <u>Chapter 2</u> SOME ELF/VLF RADIO SIGNALS: THEIR GENERATION AND PROPAGATION	
2.1 Introduction	14
2.2 History	15
2.3 Characteristics Of Natural ELF/VLF Signals Propagating Only Between The Earth And The Ionosphere	17
2.4 Characteristics Of ELF/VLF Signals Propagating Through The Magnetosphere	19
2.5 Active ELF/VLF Stimulation Experiments In The Ionosphere And Magnetosphere	26
 <u>Chapter 3</u> THE VLF GONIOMETER SYSTEM - THEORY AND PRACTICE	
3.1 Introduction	32
3.2 The Theory Of Goniometers	32
3.3 A Practical Goniometer System	34
3.4 Azimuthal Calibration	44
3.5 Data Recording	45
3.6 Analysis Equipment	46
 <u>Chapter 4</u> A BATTERY POWERED TIME ENCODED CLOCK FOR USE IN A GONIOMETER ELF/VLF RECORDING SYSTEM	
4.1 Introduction	48
4.2 Design Requirements	48
4.3 Considered Solutions	48
4.4 Introduction To The Time Encoded Clock	50
4.5 Clock Description and Operation	51
4.6 Goniometer Interfacing: Time Encode/ Decode Module	54
4.7 Whistler Analyser Interface	55

	<u>Page no.</u>
4.8 Performance	57
<u>Chapter 5</u> GONIOMETER EXPERIMENTS DURING THE PERIOD 1977 to 1979	
5.1 Introduction	59
5.2 Project Trigger	62
5.3 Project Porcupine	62
5.4 Iceland Campaign	63
5.5 Second British High Latitude Campaign (H.L.C.)	63
5.6 Second British H.L.C. (Repeat)	64
5.7 Second British H.L.C. (Repeat)	64
5.8 1979 Spring Campaign	71
<u>Chapter 6</u> RADIATION OF 1kHz TIMING SIGNALS VIA THE NIGHT-TIME AURORAL IONOSPHERE - DATA ANALYSES AND INTERPRETATION	
6.1 Introduction	73
6.2 The Experiment	73
6.3 Identification Of Transmitter(s) Responsible	74
6.4 VLF Goniometer System Tests	79
6.5 Analysis Equipment	88
6.6 Investigation of the Pips	89
6.7 Summary Of Major Results And Initial Conclusions	110
<u>Chapter 7</u> ELF PIP GENERATION MECHANISMS	
7.1 Introduction	114
7.2 The Location Of The Generation Region	114
7.3 Heating Effects From Each Transmitter	123
7.4 Conclusions - The Generation Mechanism	126
7.5 Physical Plausibility Of ELF Pip Generation By LF/MF Modulation Of The Electrojet	129
7.6 Final Summary And Conclusions	136
<u>Chapter 8</u> AN ELF RECEIVER FOR THE FREQUENCY RANGE 0.3 Hz to 700 Hz	
8.1 Introduction	139
8.2 Design Constraints	139

	<u>Page no.</u>
8.3 System Overview	140
8.4 Amplifiers: Offsets, Noise and Device Selection	143
8.5 Receiver Circuitry	149
8.6 A Comb Bandstop Filter For Use In An ELF Receiver	157
8.7 Performance	166
8.8 Future Work	171
8.9 Assessment	171
 <u>Chapter 9</u> A MU-METAL CORED ANTENNA AND ITS ASSOCIATED PREAMPLIFIER	
9.1 Introduction	173
9.2 The Use Of A High Magnetic Permeability Core	173
9.3 The Antenna Gain Factor	174
9.4 Physical Description And Construction Of The Mu-Metal Cored Antenna	176
9.5 The Electrical Characteristics Of The Antenna	176
9.6 Field Calibration	183
9.7 The Preamplifier	186
9.8 Noise Performance Of The Mu-Metal Antenna And Preamplifier	187
9.9 System Sensitivity	196
9.10 Conclusions And Further Work	196
 <u>Chapter 10</u> SOME RESULTS FROM THE ELF RECEIVER	
10.1 Introduction	200
10.2 Power Spectra Reduction Of ELF Data	200
10.3 Equipment Performance	201
10.4 An Investigation Of High Latitude Schumman Resonance Frequency Variations On 28 March 1979	204
 <u>Chapter 11</u> SOME FURTHER SUGGESTIONS FOR ELF RESEARCH	214
11.1 The Future For Broad Band Goniometer Experiments In The Scandinavian Auroral Zone	214
11.2 Some Further 'Pip' Experiments	216
 REFERENCES	218

		<u>Page no.</u>
APPENDIX 1	GONIOMETER SYSTEM PREAMPLIFIER	229
APPENDIX 2	CIRCUIT DESCRIPTION OF THE DIGITAL TIME ENCODED CLOCK	231
APPENDIX 3	FIELD SITE OPERATION OF THE ELF RECEIVER SYSTEM	249
APPENDIX 4	A HELMHOLTZ COIL CALIBRATION SYSTEM	251

CHAPTER ONE

The Near Earth Space Plasma Environment: A Review

1.1 Introduction

This thesis is concerned with the study of various naturally occurring and artificially stimulated radio signals in the extremely low frequency (ELF) band (3 Hz to 3kHz). Some such signals provide a remote diagnostic tool for the investigation of the space plasma (ionized gas) environment, out to several earth radii. Others are studied in order to obtain a better understanding of their generation mechanisms in, and their propagation characteristics through, the various media in this region.

This environment may be subdivided into three regions which are, in increasing distance from the earth; the earth-ionosphere cavity or waveguide, the ionosphere, and the magnetosphere. The first is simply the non-ionized region between the earth and the bottom side ionosphere. It is the latter two regions that form the basis of the discussion in this chapter. The propagation of certain ELF and very low frequency (VLF) (3kHz to 30kHz) radio waves through these regions is reviewed in Chapter 2.

1.2 The Ionosphere

1.2.1 Introduction

The ionization of the earth's atmosphere which produces the ionosphere is caused by several mechanisms. The most important of these, at non auroral latitudes, are the sun's X-ray, ultra-violet, and Lyman α radiations together with cosmic rays. At high latitudes, particularly during magnetically active periods, the effects of energetic charged particles are important.

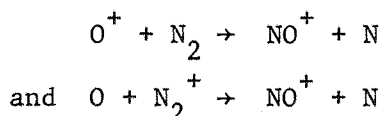
The rate of ionization at any altitude depends upon the atmospheric composition as well as the characteristics of the incident radiation at that height. As the solar radiation propagates down through the neutral atmosphere the various frequency (energy) bands of this radiation are attenuated by different amounts. At the same time the composition of the atmosphere alters with altitude. Consequently, different ionization processes become predominant at different heights resulting in a layered structure. The principal layers are designated

D,E,F1 and F2, each being characterised by a different set of ionization processes. Figure 1.1 shows an electron density profile through a 'typical' midlatitude ionosphere for daytime and nighttime conditions. These differ because of the lack of ionizing solar radiation during the nighttime.

This thesis is concerned primarily with the D and E regions of the ionosphere and this review will restrict itself to these regions. A review of the D region is presented in Thomas (1971) and also in texts such as Rishbeth and Garriott (1969), Ratcliffe (1972) and Hargreaves (1979) which treat all these regions in some detail.

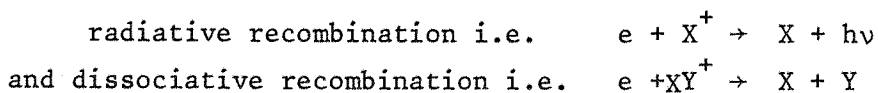
1.2.2 The Non-Auroral Quiet Time E Region

The E region peaks near 105 km altitude, see figure 1.1, and results from extreme ultra-violet radiation (E.U.V.) between 800 Å and 1026 Å producing O_2^+ , and X-rays from 10 to 100 Å. The X-rays can ionize all constituents, particularly forming N_2^+ , O_2^+ and O^+ , although the degree of ionization from this source is highly dependent upon the solar activity. Experimentally NO^+ and O_2^+ are found to be the most copious ions in this region. NO^+ can be formed by the charge exchange reaction:



Similar reactions convert other atomic ions into molecular ions.

Recombination is primarily by:



where X and Y represent different atomic species, h is Planck's constant and ν the frequency of the emitted photon. Of the above recombination processes the second dominates because conservation of energy and momentum can be most easily satisfied when two bodies are produced.

1.2.3 The Non-Auroral Quiet Time D Region

The D region is the lowest layer of the ionosphere extending from ~ 50 km to ~ 90 km. Being the lowest lying region it is produced by

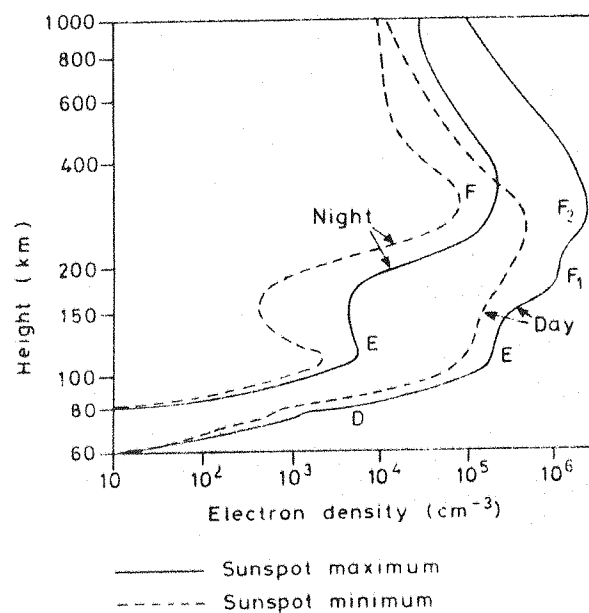
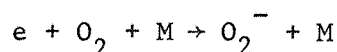


Figure 14 Typical vertical profiles of the mid-latitude ionosphere. (From wallchart *Aerospace Environment*, W. Swider, Air Force Geophysics Laboratory, Hanscom Air Force Base, Massachusetts.)

the most penetrating of the ionizing radiations. It is characteristically a region of very weakly ionized plasma, the neutral density exceeding the electron/ion densities by several orders of magnitude. The electron density exhibits a strong diurnal variation being some two orders of magnitude higher during the day.

The three main production sources are: X-rays (wavelengths 1 to 10 Å) between 85km and 95km, Lyman α between 75km and 85km and cosmic rays below 75km. The importance of Lyman α (1216 Å) as an ionizing agent in the D-region is due to an atmospheric window near 1216 Å which allows radiation to penetrate deeply into the atmosphere. The energy of the Lyman α photon is, however, only 10.14 eV which is insufficient to ionize the major gases. It is, however, sufficient to ionize the minor gases such as nitric oxide (NO), methyl radicals (CH₃) and trace gases from meteors. Thus these minor gases play an important role in the maintenance and chemistry of the D-region.

The recombination processes in this region are complex due to the production of negative ions by three body attachment processes such as:



Here M represents any molecule.

The ozone layer at ~ 50km plays a significant role in the reduction of these negative ions (Turco and Sechrist, 1972).

1.2.4 The Polar And Auroral E and D Regions During Disturbed Periods

While most of the ionospheric phenomena observed at low and middle latitude can be properly explained in terms of ionization by electromagnetic radiation, this is not so in the auroral and polar ionosphere. In these regions the ionization produced by the energetic particles can be at least as important as the electromagnetic radiation. Three types of high latitude ionospheric modification due to charged particles are distinguished (Landmark, 1968). Firstly, Polar Cap Absorption (P.C.A.) Events which are caused by the so called solar cosmic rays consisting of high energy (1 to 100 MeV) protons and alpha particles. These arrive about fifteen minutes after a solar flare causing high D region ionization over the whole polar cap region. Strong riometer (Relative Ionospheric Opacity Meter) (Little and

Leinbach, 1958) absorption is measured at these times. Secondly, Auroral Absorption Events, which can also be identified using riometer. These are mainly caused by electrons of energy 50 to 500 keV, associated with geomagnetic substorms. High D region ionization over only the auroral region, results. Thirdly, Sporadic E ionization which is associated with the visual aurora (Wagner et al., 1973) at about 110km. This is caused by protons of energy 50 to 200 keV and electrons of energy 5 to 30 keV.

Figure 1.2 shows several D region auroral electron density profiles derived from rocket flights during auroral absorption events, after Jespersen et al. (1966). These flights were made from the Andøya rocket range in Norway. Figure 1.2 should be compared with figure 1.3 which shows nighttime midlatitude D/E region profiles determined from Wallops Island, U.S.A., (Belrose, 1966). We note that even at times of zero riometer absorption the auroral electron densities are higher than the mid latitude densities at the same height. Belrose et al. (1966) suggest that weak electron fluxes probably result in enhancement of the nighttime auroral electron densities, even during so called quiet times.

1.3 The Morphology Of The Magnetosphere

1.3.1 Introduction

This region has been discussed many times typically by Axford (1969), Ratcliffe (1972) and Dungey (1976).

The magnetosphere is strictly defined as that region of plasma, above the ionosphere, where the geomagnetic field dominates over other factors controlling the motion of the charged particles. The principal constituents of the region are protons, electrons and alpha particles; unlike the ionosphere which also contains a high percentage of heavier molecular and atomic ions.

The structure of the accepted open field magnetospheric model is shown in figure 1.4 and is described below. (The formation of the magnetospheric cavity is addressed in section 1.3.9).

1.3.2 The Magnetospheric Boundary Or Magnetopause

Physically the magnetopause defines a surface such that at every

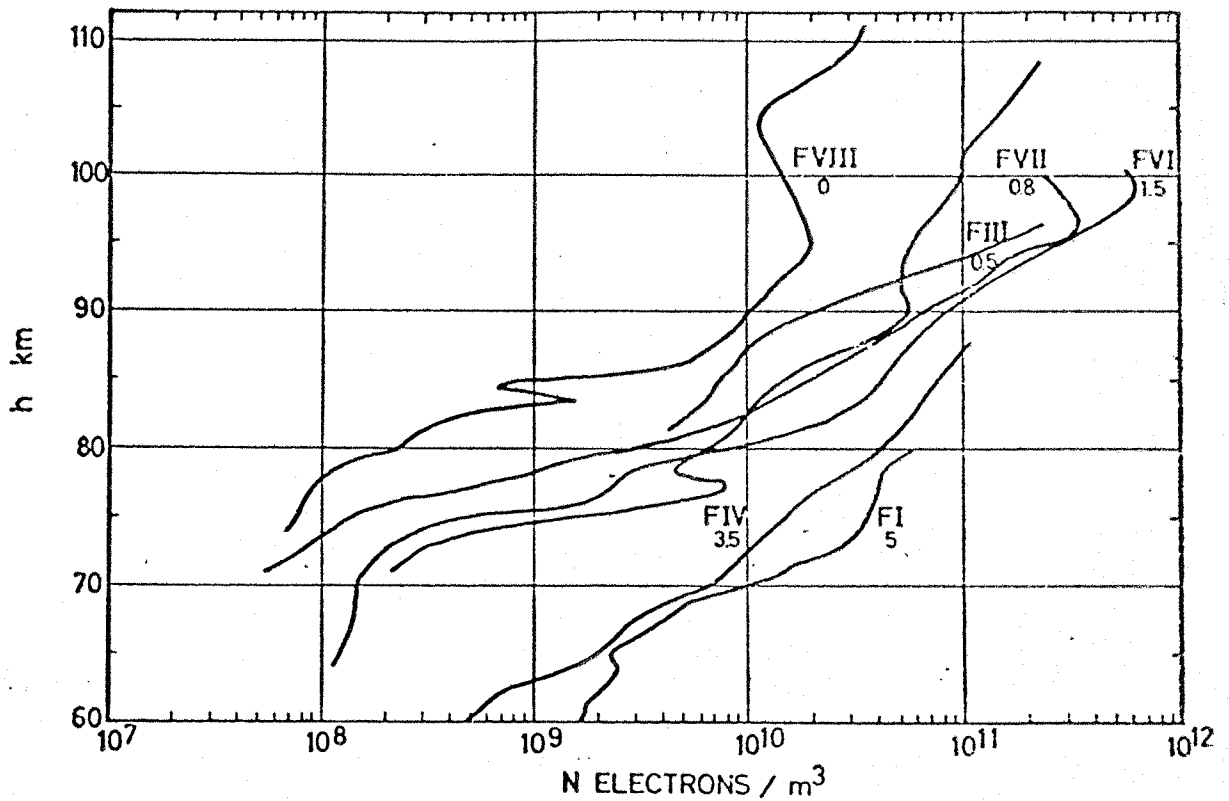


Fig. 1:2 Electron density profiles during Auroral absorption events showing riometer absorption in dB (after Jespersen et al, 1966)

Daytime Flights : FI, FIV.

Nighttime Flights : FII, FV, FVI, FVII, FVIII.

Flight FII occurred 14 Dec, 1962.

Flights FVI and FVII occurred 22 March, 1964.

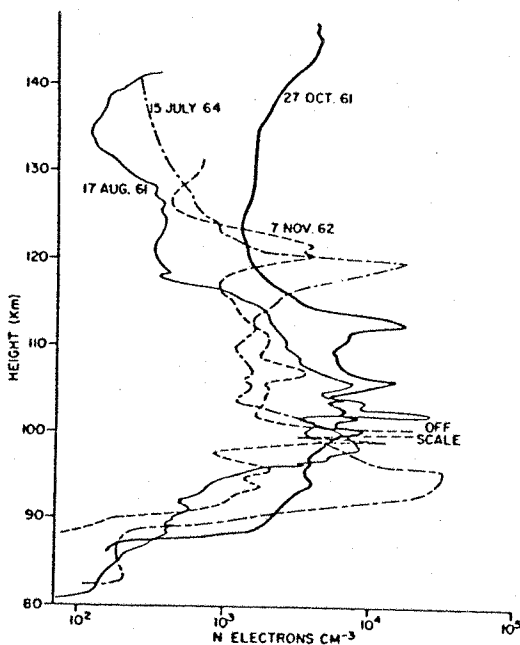


Fig. 1:3 Electron density-height profiles for the E region at night over Wallops Island measured by rocket-borne Langmuir probes (after Smith, 1965).

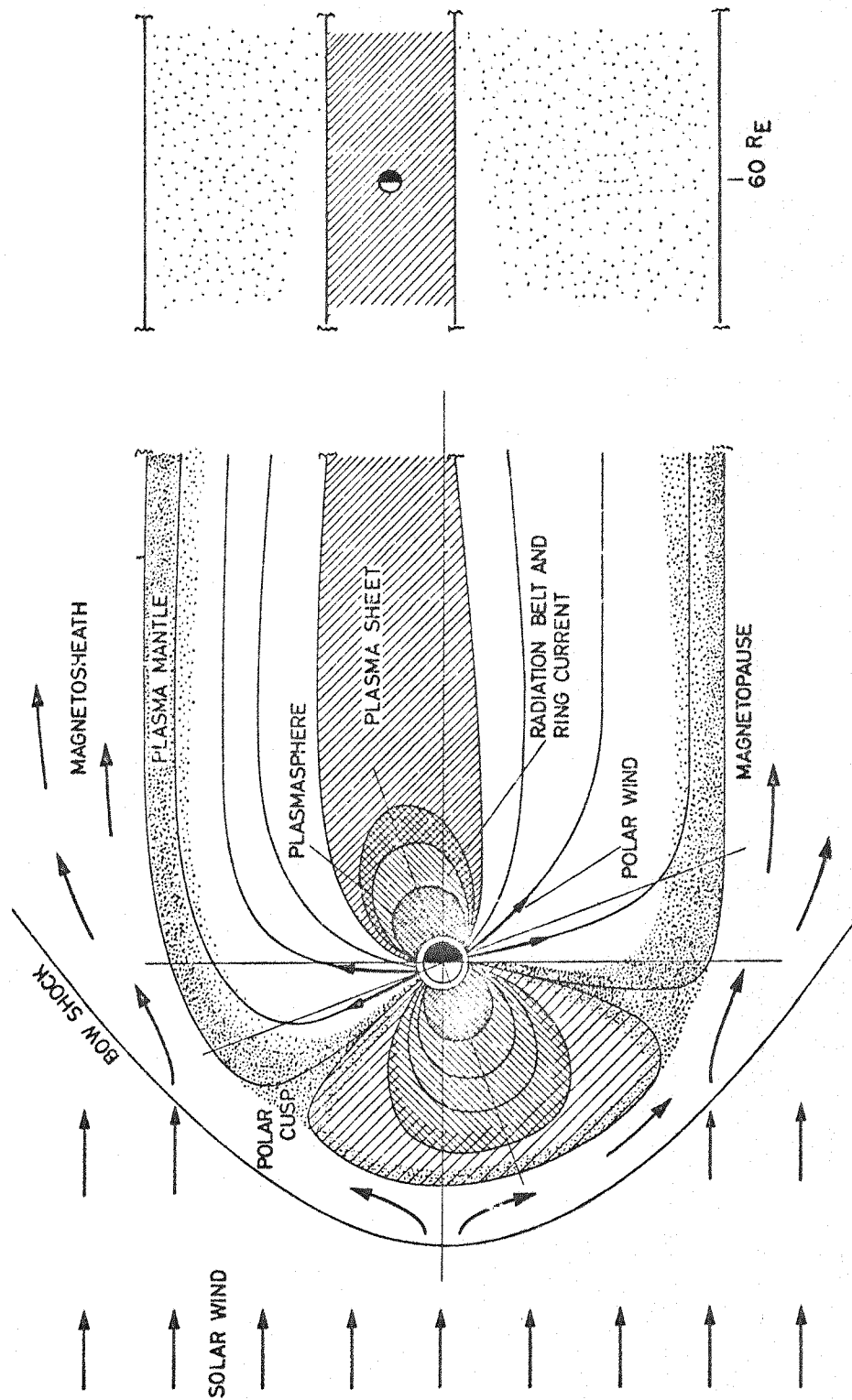


Fig. 1:4 The Magnetosphere (from Akasofu , 1977 after Rosenbauer, H. et al, 1975)

point the pressure of the solar wind (section 1.3.9) is balanced by the pressure of the geomagnetic field. The dayside magnetopause occurs at about $10 R_E$ ($1 R_E$ = one earth radius from the centre of the earth) during periods of low solar activity.

1.3.3 Shock

The bow shock, formed upstream of the magnetopause, is the result of the 300 to 500 km s^{-1} solar wind velocity exceeding the local Alfvén velocity of $\sim 50 \text{ km s}^{-1}$. The latter is the magnetohydrodynamic (M.H.D.) equivalent of the speed of sound.

1.3.4 Sheath

The magnetosheath is a region of turbulent plasma which has been thermalised by passage through the shock wave in the solar wind.

1.3.5 The Polar Cusps

Geomagnetic field lines in the cusp (magnetic field) regions are connected to the magnetopause or magnetosheath. Dayside field lines at lower latitudes are closed, and those connected to higher latitudes are open. The projection of the polar cusp onto the dayside ionosphere defines the dayside auroral oval, the region of maximum auroral activity.

1.3.6 The Tail

The tail results from the distortion of the approximately dipolar geomagnetic field by the solar wind. It extends out to at least $10^3 R_E$ on the night side (Ness et al., 1967) and forms, in three dimensions, a cylinder parallel to the wind direction. As a result of the magnetosheath plasma flowing past the geomagnetic field a large scale electric field exists in the tail, directed in the dawn to dusk direction. Field strengths of 0.3 mV m^{-1} , resulting in a potential difference across the tail of $> 40 \text{ kV}$, are typical.

The tail itself can be subdivided into two regions. Firstly, the outer lobes which are regions of relatively high magnetic field strength ($10 - 30 \text{ nT}$) and few particles (typically 10^4 m^{-3}). (The magnetic field is directed earthwards in the northern hemisphere and in the opposite direction in the southern). Secondly, the plasma sheet which bisects

the tail in the equatorial plane. It is a region of relatively low field strength, (typically 2 to 5 nT) but high charged particle density, (typically 10^5 m^{-3}) (Akasofu, 1977). The sheet, detectable from about $7 R_E$ outwards and several earth radii thick connects to the night-side auroral oval.

1.3.7 The Plasmasphere

The plasmasphere is an inner region of closed magnetic field lines extending out to about $4 R_E$ during average solar and geomagnetic activity. It is populated by low energy thermal electrons, typically 0.1 eV, with a density of 10^9 m^{-3} and corotates with the earth. The region attempts to be in diffusive equilibrium with the ionosphere below.

1.3.8 The Van Allen Radiation Belts

There are two radiation belts that is regions containing very high energy ($>40 \text{ keV}$) charged particles. The inner belt, centred on $\sim 1.5 R_E$ is populated by protons with energies between 100 keV and 100 MeV, indirectly produced by cosmic ray interaction with the neutral atmosphere. The outer belt, centred on $\sim 3.5 R_E$, is populated by electrons with energies generally exceeding 1.6 MeV. These are considered to be injected by a mechanism associated with geomagnetic storms. The belts, particularly the outer belt, contribute to the ring currents, see section 1.4.

1.3.9 The Solar Wind And Formation Of The Magnetospheric Cavity

Figure 1.3 shows the magnetosphere to be highly asymmetric. This is the result of the solar wind plasma which flows continuously from the sun at speeds generally between 200 and 700 kms^{-1} and with a particle density of about $5 \times 10^6 \text{ m}^{-3}$. (When a solar flare occurs it may, however, gust to 1000 kms^{-1} with a density of 10^7 m^{-3}). Due to the high electrical conductivity of the wind, the interplanetary magnetic field (I.M.F.) may be thought of as being frozen into, and carried along by it.

Experimental satellite studies have shown that the magnetic field has a small component directed either northward or southward, usually maintaining one configuration for several days on end. Current theories which predict an open magnetosphere are generally based on

Dungey (1961) and require a southward component in the I.M.F. At these times a neutral point can be formed on the dayside, resulting in field line connection between the terrestrial field and the I.M.F. (Russell and Elphic, 1978). These merged field lines, themselves frozen into the wind, are then swept around to the nightside to form the tail. Field line reconnection subsequently takes place in the equatorial plane plasma sheet with the resulting field lines and plasma moving eastward and sunward. This circulation of plasma is known as convection and is illustrated in figure 1.5. During geomagnetically quiet periods the overall rate of field line reconnection in the tail of the magnetosphere is equal to the rate at which interplanetary magnetic field lines connect with geomagnetic field lines on the upstream side.

Mechanisms which can maintain this general magnetospheric shape during periods of prolonged northward I.M.F. are ill defined. Some level of convection is required to explain the polar quiet time currents (c.f. Ratcliffe, 1972) and this could be satisfied by a model proposed by Axford and Hines (1961). This relies upon an undefined frictional coupling between the solar wind and the magnetosphere. In this view closed field lines from the dayside are pulled around the flanks of the magnetosphere and then released to return along the noon-midnight meridian in the tail. This results in a closed magnetosphere. Recently, Maezawa (1976) has proposed an open field model which combines frictional coupling and a neutral point on the dawn dusk meridian.

1.3.10 The Magnetospheric Substorm Akasofu (1968, 1977), McPherron (1979)

The substorm, a concept propounded by S.I. Akasofu, is (McPherron, 1979) "a transient process initiated on the nightside of the earth in which a significant amount of energy derived from the solar wind - magnetospheric interaction is deposited in the auroral ionosphere and magnetosphere". Originally most observations of high latitude disturbances were presented in terms of average behaviour and it seemed to be sufficient to think in terms of quasi-steady convection where the convection driven by the wind reacted almost immediately to variations of the latter. It was, however, demonstrated by Axford (1969) that polar magnetic disturbances had only a statistical relationship to variations in the solar wind. The substorm concept proposes that convection is not necessarily steady state and that field line

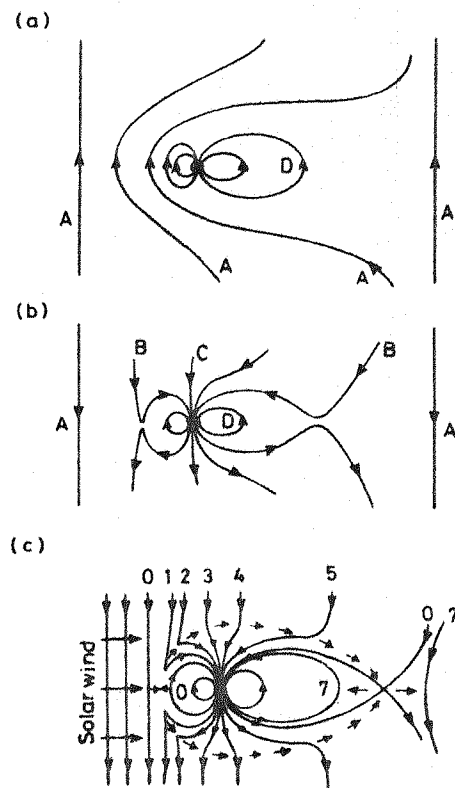


Figure 1-5 Terrestrial and solar-wind fields in polar section: (a) with northward IMF, giving a closed magnetosphere; (b) with southward IMF, giving an open magnetosphere; (c) showing the circulation due to the flow of the solar wind. ((a) and (b) after C.T. Russell, *Critical Problems of Magnetospheric Physics*, 1972, with permission of the National Academy of Sciences, Washington, DC, after J.W. Dungey; (c) after R.H. Levy *et al.*, *Am. Inst. Aeronaut. Astronaut. J.* 2, 2065, 1964.)

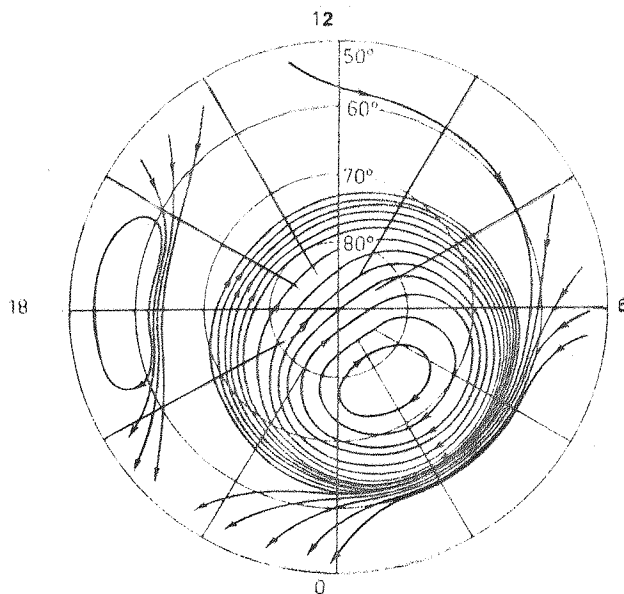


Fig. 1-6 Equivalent current system for the daily magnetic variation (Feldstein, Y. I.: *Planetary Space Sci.* 14, 121, 1966).

reconnection in the tail can be inhibited. The result is a growth phase where magnetic energy is extracted from the solar wind and stored in the tail. In the simplest models, neutral sheet field line connection subsequently takes place, suddenly and explosively, releasing this stored energy into the ionosphere. The processes responsible for the onset of this expansion phase are unknown (McPherron, 1979). Finally the magnetosphere enters a recovery phase when it relaxes to its quiet state. The substorm phenomenon, is highly correlated with the direction of the I.M.F., ceasing when it points northward for a long period and reappearing when it turns southward (McPherron, 1979). Frequently during a southward period more than one substorm expansion phase occurs, these often being so temporally close that they are virtually indistinguishable (Wiens and Rostoker, 1975).

The substorm manifests itself in many ways but most dramatically by increases in the intensity, and changes in position and form, of the Aurora Borealis. Other less dramatic results include modifications to the ring currents (section 1.4), modifications to the ionospheric current system (section 1.4) and modifications to the ionospheric electron density profile due to associated charged particle precipitation (section 1.2.4).

1.4 Magnetospheric And Auroral Ionospheric Current Systems

Various current systems flow in the magnetosphere and these are often resolved into the following groups (Potemra, 1979):

- (1) Auroral ionospheric currents, see below.
 - (2) Field aligned or Birkeland currents, first proposed by Birkeland in 1908 but only recently confirmed by rocket and satellite measurements, flowing between the magnetosphere and ionosphere and vice versa.
 - (3) Magnetospheric ring currents due to geomagnetic B field gradient and curvature drift of electrons and protons injected into the closed magnetic field line region (figure 1.4) during the substorm growth phase (Huage and Soraas, 1975). These are generally studied using ground based magnetometers.
 - (4) Magnetospheric boundary and tail currents deduced from large scale observations of magnetic fields in space.
- In most magnetospheric models these systems are linked by closed, three dimensional, electric currents (Sugiura, 1975; Heikkila, 1978).

In this thesis primary interest lies in (1) above. These currents were the first system to be studied continuously, this by surface magnetometers from which equivalent horizontally flowing auroral electrojet current systems have been deduced. Figure 1.6 shows a system after Feldstein (1966) which shows the stronger westward electrojet in the morning sector and the weaker, and slightly lower latitude eastward electrojet in the evening sector. More recently these currents have been studied using Incoherent Scatter Radar techniques (Kamide and Brekke, 1975, 1977; Banks and Doupnik, 1975) and also using the Scandinavian Twin Auroral Radar Experiment (STARE) (Greenwald et al., 1978). Brekke and Rino (1978) have successfully determined the current density of the electrojet, with a height resolution of 10 km, using incoherent scatter techniques. During a geomagnetically disturbed period the maximum westward electrojet current density was $40 \mu\text{A}/\text{m}^2$ occurring at heights below 120 km. The maximum eastward electrojet current density was $15 \mu\text{A}/\text{m}^2$ at ~ 130 km altitude.

(Defence Meteorological Satellite Photograph)

Kamide and Akasofu (1975) have shown, using D.M.S.P. satellite photographs, that the westward electrojet flows along the region of diffuse aurora (Akasofu, 1974) in the midnight sector as well as in the vicinity of the westward travelling surge in the evening sector, see below (Rostoker, 1975). The eastward electrojet is found to flow mainly equatorward of the discrete aurora (auroral arcs) in the evening sector and there is some indication that it flows in the ionosphere along the diffuse aurora.

During the substorm growth phase equatorward motion of the nighttime electrojet occurs. The expansion phase is associated with the westward travelling surge (auroral spiral) which flows along a preexisting arc. The surge carries the leading edge of the westward electrojet (Rostoker et al., 1975). Behind the surge a poleward expansion of the westward electrojet occurs (Nielsen and Greenwald, 1978). During the recovery stage a poleward leap of the westward electrojet takes place with an associated reduction in intensity (McPherron, 1979).

CHAPTER TWO

Some ELF/VLF Radio Signals: Their Generation And Propagation

2.1 Introduction

All the radio signals reviewed in this chapter and investigated in this thesis require some type of interaction, within the magnetospheric or ionospheric plasma, for either their generation or their characteristic frequency time variations. Thus the propagation characteristics of signals from ELF/VLF transmitters, such as the Omega navigation system (Burgess and Jones, 1975), are not studied.

This thesis is concerned with the generation, propagation and reception of several different types of ELF radio signals. The bulk of the analysis reports an investigation of what is believed to be demodulation of an ELF modulated broadcast service, LF/MF signal by a non-linear process in the auroral ionosphere (see Chapters 6 and 7). Various other analyses are, however, reported, including a study of an ELF chorus event (see Chapter 5). Additionally a short examination of Schumann Resonances of the earth-ionosphere spherical shell cavity has been undertaken (Chapter 10) obtained using the equipment described in Chapters 8 and 9.

The purpose of this chapter is to provide some insight into the physical mechanisms which generate these signals and, their mode of propagation through the ionosphere and magnetosphere, and to report on previous work in these fields. Apart from considering the generation mechanism of Schumann Resonances, propagation within the earth-ionosphere waveguide is not addressed. Galejs (1972) treats this subject in some detail.

All signals described in this chapter may be detected by what is essentially a highly sensitive, wide band, audio amplifier fed by a long wire or loop antenna. Such receivers are described in Chapters 3, 8 and 9.

Unless otherwise stated ground based reception is assumed.

2.2 History

The first report of naturally occurring ELF/VLF signals was made in Austria in the year 1886 when falling frequency signals, (whistlers), were heard on a 22 km telephone line (Fuchs, 1938). Subsequently, various other emissions were reported which we now recognise as tweeks, risers, fallers and chorus (Helliwell, 1965).

Some research was conducted during the 1920's and 30's on whistlers (Eckersley, 1935) but due to the lack of suitable analysis equipment little progress was made. After a lapse of 20 years, however, interest in ELF/VLF research, particularly whistlers and chorus revived; this resulting from the development of the sound spectrograph which displayed frequency time information.

It was principally Storey (e.g. 1953) who put the subject of magnetospheric ELF/VLF propagation on a firm physical footing. In particular he proposed that whistlers were produced by energy, from lightning discharges, echoing back and forth along the geomagnetic field lines. To account for the degree of dispersion his theory required an unexpectedly high electron density in the outer ionosphere, thus providing the first evidence for the magnetospheric plasma.

At approximately the same time Schumann (1952) suggested that lightning flashes might also excite the so called earth-ionosphere cavity, setting up a system of standing waves around the earth. Resonant frequencies of ~ 8 Hz, 14 Hz, 20 Hz, 26 Hz etc. were predicted; representing the fundamental and harmonics of the cavity. These were subsequently detected (Balser and Wagner, 1962; Rycroft, 1965).

From the mid 1950's to date there has been considerable interest in ELF/VLF radio signal generation and propagation within the ionosphere, magnetosphere and earth-ionosphere waveguide cavity. Initially experimenters used ground based instruments, however, since the mid 1960's considerable use has been made of rocket and satellite instrumentation. Figure 2.1 shows the great variety of magnetospherically propagating signals (ELF/VLF) which have been detected and investigated, over the last 30 years (Shawhan, 1979). In particular, recent years have brought the advent of combined charged particle and wave experiments on board rockets and satellites. This has given a more integrated view of the magnetospheric and ionospheric processes. Rycroft (1972) reviews progress made in ELF/VLF research to that date.

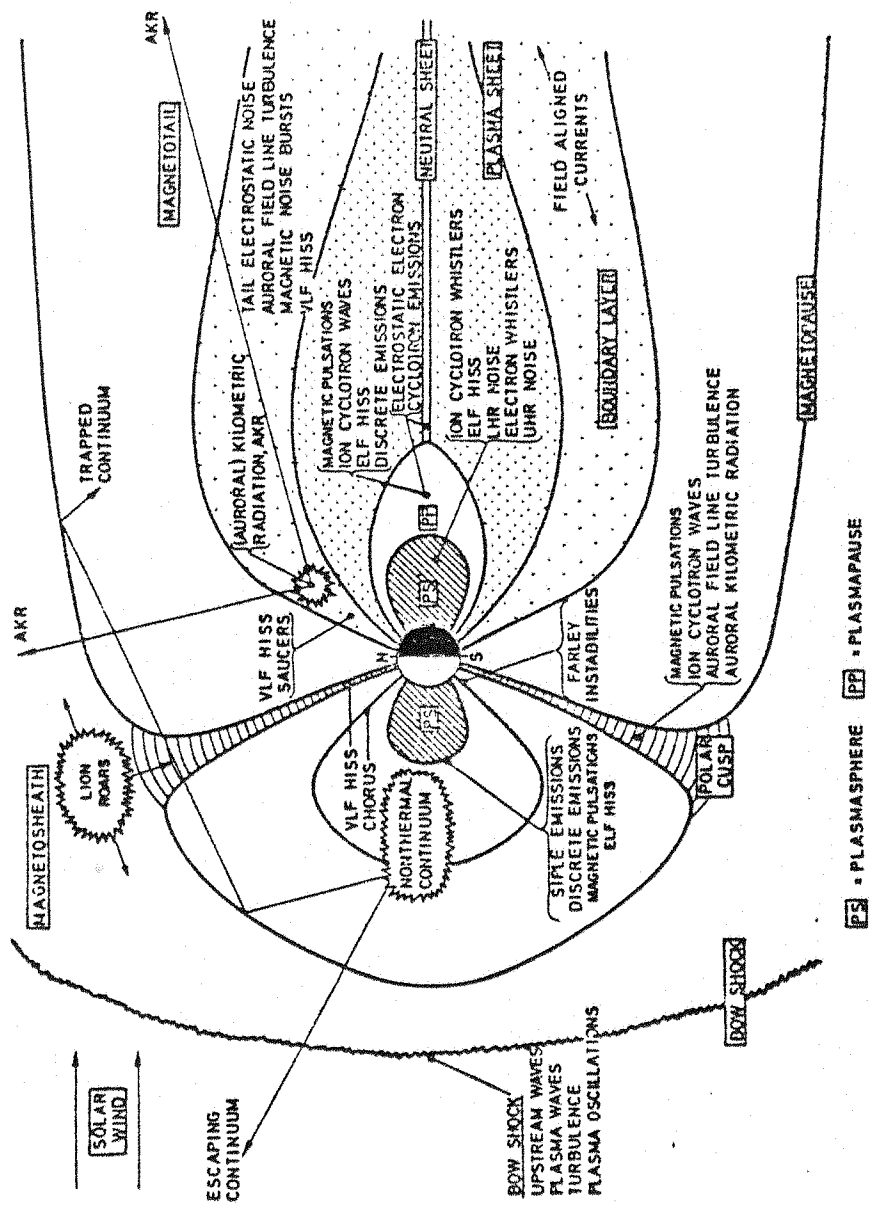


Figure 2.1 Types of magnetospheric plasma waves and regions of occurrence in a noon-midnight meridian cross-section of the Earth's magnetosphere [from Shawhan, 1978].

The above experiments may all be described as passive; the experimenter waits for Nature to create the radio signals. Many attempts have, however, been made to stimulate such emissions artificially in what are known as active experiments (Rycroft, 1980). In these experiments the ionosphere and/or magnetosphere is modified in a controlled manner and the stimulated signals interpreted in terms of the modification.

The earliest indication that man could change the ionosphere/magnetosphere occurred in 1933 when Tellegen (1933) reported that signals received in Holland from the Swiss radio station at Beromunster (650kHz) appeared to be modulated with signals from the powerful station at Luxembourg (252kHz, 200 kW). It was subsequently discovered that this phenomenon, called cross modulation, was quite common when the unwanted, or disturbing, station was located near the transmission path of the wanted station to the receiver. Bailey and Martyn (1934) explained the effect by the following argument. The electric field of the disturbing wave imparts energy to the D region electrons. This energy is converted into heat by electron-neutral collisions thus raising the electron temperature and, hence, the electron collision frequency. When the angular frequency of the wanted wave is much greater than the collision frequency, the absorption of the wanted wave is proportional to the collision frequency and, thus, it varies with the electron temperature which, in turn, varies with the modulation of the disturbing signal.

Since this discovery, several specially designed experiments have been carried out to investigate this effect and others. Some of these experiments, resulting in the generation of ELF signals, are reviewed in section 2.5.

2.3 Characteristics Of Natural ELF/VLF Signals Propagating Only Between The Earth And The Ionosphere.

2.3.1 Spherics

Spherics (atmospherics) are wide band impulsive signals produced by lightning flashes. Propagation takes place in the earth-ionosphere waveguide; the signals are heard as sharp clicks or crackles.

2.3.2 Tweeks

Tweeks are the result of spherics which have propagated a substantial distance (> 1000 km) in the waveguide. They are characterised by the prolonged travel time experienced by frequencies close to the waveguide cut-off frequency; typically 1.8kHz.

2.3.3 Schumann Resonances

Schumann (1952) addressed the problem of estimating the resonant frequency and harmonics of the entire waveguide system; these being excited by lightning discharges. The energy in these resonant modes propagates as a zeroth-order T.M. mode; the electric field of the mode being vertical and constant throughout the height of the guide. Since, in general, the number of lightning strokes is high at any one time and, because the attenuation of signals is low at these frequencies, it is impossible to distinguish the waveforms of individual flashes. It is consequently necessary to investigate these signals via an examination of the background noise power density spectrum.

Schumann showed (e.g. Chapman and Llanwyn-Jones, 1964; Rycroft, 1964) that the vertical component of the electric field is represented by an expression of the form:

$$E(f) = A(f) \sum_n \frac{f S_o^2}{f_n^2 - f^2 S_o^2} \Phi(n) C_n(\theta)$$

where n represents the order of the cavity resonator modes ($n = 0, 1, 2, 3$ etc.), and $A(f)$ is a term, related to the energy spectrum of the exciting discharge, which varies slowly with frequency compared with the terms inside the summation. θ , is the polar angle relative to the source and the point of observation. $\Phi(n)$ and $C_n(\theta)$ are functions of n and θ only. S_o is related to the propagation constant, P such that $P = i 2\pi f S_o / c$, where c is the velocity of light. f_n is the resonance of the n^{th} order mode for a perfectly conducting ground and ionosphere and is defined by $f_n = c\sqrt{n(n+1)} / 2\pi R$, R being the radius of the earth. For a perfectly conducting ionosphere $S_o = 1$.

In reality, however, the ionosphere has finite conductivity and S_o is complex. As a consequence the resonant frequencies and Q values are lower than those predicted for a perfectly conducting ionosphere

(e.g. Rycroft, 1965; Galejs, 1972). For a sharply bounded, homogeneous, isotropic ionosphere:

$$S_o = 1 - \frac{1}{h} \left(\frac{i^3}{\mu_o \sigma_I 2\pi f} \right)^{\frac{1}{2}}$$

where h is the height of the ionosphere, μ_o the permeability of free space and σ_I the ionospheric conductivity, (Chapman and Llanwyn-Jones, 1964).

Most theoretical efforts have been directed towards improving the ionospheric models on which the resonant frequency estimates are based. Chapman and Llanwyn-Jones (1964) have used a two-layer model ionosphere, Galejs (1972) describes an exponential conductivity versus height profile. Both models give good agreement with experimentally determined resonant frequencies. Madden and Thompson (1965) have estimated the effects of additional ionization, due to high altitude nuclear detonations and sudden ionospheric disturbances, on the mode resonant frequencies.

2.4 Characteristics Of ELF/VLF Signals Propagating Through The Magnetosphere

2.4.1 Introduction

Before reviewing such ELF/VLF signals it is first necessary to address the method of propagation.

2.4.2 The Magneto-Ionic Theory And Whistler Mode Propagation

The whistler mode describes the means by which ELF/VLF radiation propagates through the magnetosphere. It is one solution of the Appleton-Hartree equation which characterises the refractive index of a homogeneous ionized medium permeated by a static magnetic field. In this theory the medium is assumed to consist of neutral particles and equal numbers of positive and negative charges. At whistler frequencies the motion of the ion is considered negligible due to its large mass relative to that of the electron. With these approximations the Appleton-Hartree equation is written as: (Ratcliffe, 1959; Helliwell, 1965).

$$n^2 = 1 - \frac{X}{\frac{1-jZ - \frac{1}{2}Y_T^2}{1-X-jZ} \pm \frac{1}{1-X-jZ} \left[\frac{1}{4} Y_T^4 + Y_L^2 (1-X-jZ)^2 \right]^{\frac{1}{2}}} \quad \text{equation 2.1}$$

where X, Y and Z are dimensionless quantities.

$$Z = \frac{v_e}{\omega}, \quad X = \frac{\omega_N^2}{\omega^2}, \quad Y = \frac{\omega_{Be}}{\omega}, \quad Y_L = \frac{\omega_L}{\omega}, \quad Y_T = \frac{\omega_T}{\omega}$$

where ω_N is the angular plasma frequency; ω_{Be} is the electron gyrofrequency; $\omega_L = \omega_{Be} \cos \theta$ and $\omega_T = \omega_{Be} \sin \theta$ are respectively the longitudinal and transverse components of ω_{Be} , with θ the angle between the wave normal and the imposed magnetic field; and v_e the collision frequency of the electrons with an average heavy neutral particle.

Great simplifications can be made to equation 2.1 when θ is sufficiently small; that is $Y_T = 0$ is a good approximation. This is the quasi-longitudinal (Q.L.) approximation. Helliwell (1965) has shown that in the magnetosphere this approximation holds for θ up to $\sim 45^\circ$. It is demonstrated below that generally θ is substantially less than this value. With the further simplification that $Z = 0$ in the magnetosphere equation 2.1 reduces to:

$$n^2 = 1 - \frac{X}{1 \pm |Y_L|} \quad \text{equation 2.2}$$

In the magnetosphere $\frac{X}{1 \pm |Y_L|} \gg 1$ and hence this in turn reduces to:

$$n^2 = \frac{X}{Y_L - 1} = \frac{\omega_N^2}{\omega(\omega_{Be} \cos \theta - \omega)} \quad \text{equation 2.3}$$

where the positive sign has been neglected since it represents a non propagating wave (imaginary refractive index) through the magnetosphere.

This expression shows that whistler mode propagation is restricted to frequencies below the local electron gyro frequency.

The validity of this approximation, that θ is small, is now considered. Two different mechanisms exist to guide the wave along the magnetic field direction.

The first is due to the anisotropy of the magnetospheric plasma, due to the geomagnetic field, which results in a refractive index dependent upon direction. Storey (1953) showed that providing $\omega \leq \omega_{Be}$ the wave direction is limited to a cone of half angle $19^{\circ}29'$ either side of the magnetic field. That is ELF/VLF waves, which are less than ω_{Be} , will be guided by the magnetic field from one hemisphere to another, thus satisfying the Q.L. approximation.

This was originally thought to be a sufficient condition for whistler mode propagation; however, Yarbrough (1961) showed that a small critical angle existed between the high refractive index ionosphere and the atmosphere. The consequence of this was that it was extremely likely that whistler mode signals would become totally internally reflected and never be received on the ground. This was contrary to experimental knowledge. The idea of the magnetospheric duct was consequently introduced (Smith et al., 1960; Smith, 1961). These are field aligned regions of enhanced or depleted electron density and serve to guide the wave along the field when the signal frequencies are $0 < \omega/\omega_{Be} \leq 0.5$ and $0 < \omega/\omega_{Be} \leq 1$ respectively (Jarvis, 1976). Helliwell (1965) shows that trapping is most likely in an enhancement. This forms the second guiding mechanism.

2.4.3 Whistlers

Whistlers are dispersed forms of atmospherics. Some of the electromagnetic energy from a lightning flash can couple into the ionosphere and magnetosphere where it propagates from one hemisphere to the other, sometimes being received on the ground after one or more such hops, see figure 2.2 (Helliwell, 1965).

Of particular interest are nose whistlers (so called because of the shape of their frequency time profiles, see figure 2.2). The nose marks the frequency with minimum propagation time measured relative to the causative spheric (Helliwell, 1965). The nose frequency and corresponding time delay have been interpreted in terms of the minimum electron gyrofrequency over the path (Angerami, 1966) and the total electron density along the propagation duct. Rycroft (1974) reviews such theories. When the whistler has no nose frequency and/or when the causative spheric is not received, methods have been developed to determine these parameters, typically Rycroft and Mathur (1973), Ho and Bernard (1973) and Tarcsai (1975).

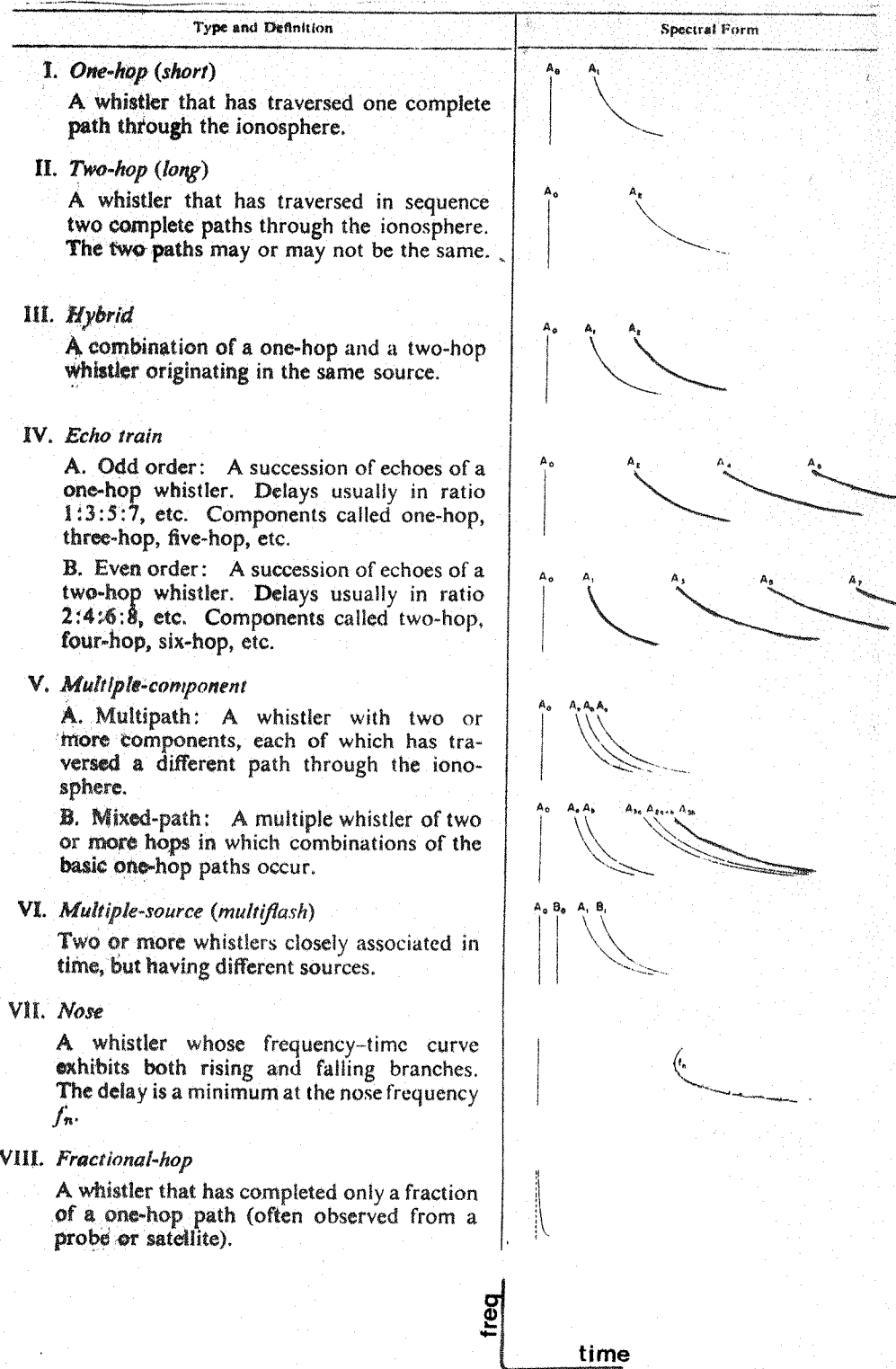


Fig. 2:2 Illustrating the many types of whistler and combinations of whistlers which have been investigated by various research workers (after Hellwell, 1965).

2.4.4 Natural ELF/VLF Magnetospheric Emissions

2.4.4.1 Introduction

The remaining natural ELF/VLF, magnetospherically propagating radio signals are thought to find their birth place in the magnetosphere. In the following a short description is given of the more common signals and this will be followed by a brief discussion of some proposed discrete emission and chorus generation mechanisms.

2.4.4.2 Hiss Or Continuous Emissions

Hiss is a broad band emission whose spectrum resembles band limited noise. Various magnetospheric sources have been proposed, see figure 2.1. Two principal varieties are defined, plasmaspheric hiss and auroral hiss. Hiss has been detected over a wide frequency range, from 0.7kHz to $> 100\text{kHz}$, with bandwidths of typically a few kilohertz or more.

2.4.4.3 Discrete Emissions

Natural discrete emissions are spontaneous, magnetospherically generated signals of a few seconds duration at the most. They can be rising tones, falling tones, or any combination of the two. A rising tone followed by a falling tone is known as a hook. Helliwell (1965) presents an extremely comprehensive review of the dynamic spectra of these various signals. The generation of all these emissions is thought to involve a transverse electron cyclotron resonance interaction between the whistler mode waves and the high energy Van Allen belt or ring current electrons (Brice, 1964) described in Chapter 1.

Occasionally the discrete emissions are triggered by whistlers and appear to occur near both the lower frequency and higher whistler cut off frequencies (Matsumoto and Kimura, 1971).

2.4.4.4 Chorus

The reception of the aforementioned discrete emissions is rare compared to the reception of many overlapping rising frequency elements, or chorus. Each such element is typically one second in duration.

Chorus was first reported by Burton (1930) but gained its name from the work of Storey (1953) who reported that early morning chorus sounded like birds singing, viz dawn chorus. The principal generation region for these signals is believed to be in the equatorial plane near the plasmopause in the region occupied by the outer Van Allen Belt and ring currents.

Ground based work has included that of Pope (1963), Ungstrup and Juckerott (1963) and Adjepong (1972). Ionospheric and low altitude satellite measurements have been reported by Taylor and Gurnett (1968), Barrington et al. (1971) and Thorne et al. (1977). High altitude satellite measurements include those of Tsurutani and Smith (1974) and Burton and Holzer (1974).

Cannon et al. (1980) report simultaneous, and conjugate, ground based, ionospheric, and satellite measurements of a chorus event, some results of which are reported in Chapter 5.

2.4.4.5 Generation of Discrete ELF/VLF Emissions And Chorus

Various emission generation mechanisms have been postulated, however, all theories are based upon a resonant interaction between a wave, with electric field \underline{E} , and a flux of energetic electrons in which energy is transferred from the electrons to the wave. Rycroft (1972) reviews these various mechanisms. In the following the basic concepts are considered.

Following Brice (1964) the change in energy Δw of a charged particle of charge e , moving a distance Δs at velocity \underline{V} in time Δt , in a wave electric field \underline{E} and geomagnetic field \underline{B} is given by:-

$$\Delta w = e (\underline{E} + \underline{V} \times \underline{B}) \cdot \Delta s$$

$$\Delta w = e (\underline{E} + \underline{V} \times \underline{B}) \cdot \underline{V} \Delta t$$

$$\Delta w = e \underline{E} \cdot \underline{V} \Delta t \quad \text{equation 2.4}$$

Thus, providing that \underline{E} and \underline{V} are in phase, there will be a net energy exchange between electrons and wave.

The helical motion of a charged particle in a magnetic field may be described by two velocities, one parallel and one perpendicular to the magnetic field. If α is the pitch angle of the helix then $V_{\perp} = V \cos \alpha$ and $V_{\parallel} = V \sin \alpha$ and two possible resonant conditions

result:

$$E_{\parallel} \cdot V_{\parallel} = \text{constant} \quad \text{equation 2.5a}$$

$$E_{\perp} \cdot V_{\perp} = \text{constant} \quad \text{equation 2.5b}$$

Equation 2.5a is the condition for longitudinal resonance, equation 2.5b that for transverse resonance.

The transverse resonance condition is satisfied where the Doppler shifted wave frequency, seen by the electrons, equals the electron gyro-frequency, and where both rotate about the geomagnetic field in the same sense. Since equation 2.3 showed that waves may only propagate in the whistler mode at frequencies less than the electron gyrofrequency (f_{Be}) the waves and electrons must be travelling in opposite directions. Equation 2.5b thus requires that:

$$V_p \frac{(f_{Be} - f)}{f} = -\gamma V_{\parallel} \cos \theta \quad \text{equation 2.6}$$

where the negative sign indicates waves and particles travelling in opposite directions, V_p is the wave phase velocity, $\gamma = (1 - V_{\parallel}^2/c^2)^{-1/2}$, and θ is the angle between the wave normal and the geomagnetic field.

When $\gamma = 1$, the non relativistic approximation, the condition for resonance thus becomes:

$$\frac{\omega_{Be} - \omega}{k} = -V_{\parallel} \cos \theta \quad \text{equation 2.7a}$$

$$\text{or } f = f_{Be} / (1 - n(f, \theta) V_{\parallel} / c) \quad \text{equation 2.7b}$$

where $V_p = \omega/k = c/n$

c being the velocity of light, n the refractive index of the medium, and k the wave vector.

Brice (1963) postulated that the Doppler shifted cyclotron radiation, travelling back along the incoming electron stream, phase bunched the incoming electrons so that they radiated coherently. In this way a sustained oscillation could be set up. Brice (1964), by squaring equation 2.7a and multiplying by $m/2$ (where m is the electron mass), showed that the electron energies required for resonance in the equatorial plane were less than those required at other locations.

Since magnetospheric energetic electrons are more plentiful at lower energies Helliwell (1963) considered that the resonant interaction was most likely to occur in the equatorial plane.

Although Brice (1964) explained the presence of an emission his theory did not predict the spectral forms of the signals. This was resolved by Helliwell (1967) in his consistent wave or phenomenological theory. This theory requires that the spatial variations of the electron gyrofrequency and the Doppler shifted wave frequency be matched, thus enabling the wave to remain in resonance with the electron for a longer time. Unlike Brice (1964) who considered a fixed interaction region, Helliwell (1967) considered the movement of the interaction region. The geomagnetic field gradient, and the feedback delay due to the finite wave and electron velocities cause a characteristic rate of change of frequency, which depends on the initial frequency of the instability and the position of the interaction region. Hence the spectral shapes of the emissions can be explained in terms of movement of the interaction region, as shown in figure 2.3. It is clear from equation 2.7b that, as the interaction region moves from the equator along a field line, to where f_{Be} is larger, a rising frequency emission will be generated. Other emissions can be explained by different movements of the interaction region.

2.5 Active ELF/VLF Stimulation Experiments In The Ionosphere And Magnetosphere

2.5.1 Introduction

Active experiments are designed to modify the ionosphere and magnetosphere in a controlled manner in order to study the plasma processes which result. Amongst other effects a variety of waves may be excited, some of these falling in the ELF band.

One of four stimulation techniques are generally employed. The first is the modification of the ionosphere and magnetosphere by the release of chemically active gases. Everhard-Bakker et al. (1976) report short ELF risers and fallers subsequent to such a release of barium. A second technique uses charged particle accelerators onboard rockets and satellites to inject a beam of electrons or ions into the plasma. A third technique uses VLF radiation, propagating in the whistler mode, from ground based transmitters to stimulate plasma instabilities in the magnetosphere (e.g. Stiles et al., 1975). The

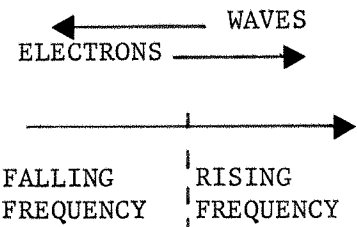
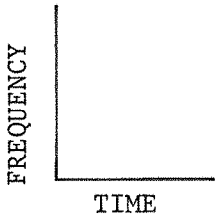


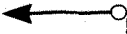







LOCUS OF INTERACTION REGION	SPECTRAL FORM	NAME
 <p>Diagram showing wave and electron directions and frequency regions. A horizontal line has a left-pointing arrow labeled 'WAVES' and a right-pointing arrow labeled 'ELECTRONS'. Below the line, a vertical dashed line separates the 'FALLING FREQUENCY' region on the left from the 'RISING FREQUENCY' region on the right.</p>	 <p>Diagram showing the axes for the spectral form: a vertical axis labeled 'FREQUENCY' and a horizontal axis labeled 'TIME'.</p>	
 <p>Diagram showing the interaction region (represented by a circle) moving to the right, indicated by a right-pointing arrow.</p>		RISING TONE (riser)
 <p>Diagram showing the interaction region (represented by a circle) moving to the left, indicated by a left-pointing arrow.</p>		FALLING TONE
 <p>Diagram showing the interaction region (represented by a circle) moving to the right, indicated by a right-pointing arrow.</p>		HOOK
 <p>Diagram showing the interaction region (represented by a circle) moving to the left, indicated by a left-pointing arrow.</p>		INVERTED HOOK
 <p>Diagram showing the interaction region (represented by a circle) oscillating, indicated by a vertical wavy arrow.</p>		OSCILLATING TONE

Fig. 2.3 Diagram showing how different movements of the interaction region (○→) produce different VLF spectral shapes, for waves moving ← and electrons moving → (Helliwell, 1967).

fourth technique uses ground based transmitters to modify the ionosphere. (Such a modification is described in Chapters 6 and 7). This technique is usually concerned with producing changes in the upper ionosphere (150 - 400km) using powerful HF transmitters operating at frequencies close to the F-region critical frequencies (3 to 10MHz). Many experiments have been conducted at middle latitudes using the Plattville heating facility in Colorado, U.S.A. and the facility at Arecibo, Puerto Rico. Utlaut (1975) reviews the copious ionospheric effects resulting from these experiments. There are, however, few reports of ELF/VLF signals being generated using this technique.

Showen (1972) obtained significant heating of the D/E region by illuminating the ionosphere at 40MHz and, stimulated by these results, Willis and Davis (1973) theoretically addressed the possibility of heating the lower E region using long pulse length HF transmissions. They suggested that such pulsed heating could perturb the low latitude ionospheric dynamo current, thereby leading to a perceptable variation (at ~ 1 Hz) in the magnetic field strength measured on the ground. Getmensev et al. (1974) and Kapustin et al. (1977) also report some applicable results. The former report non-linear detection of 6MHz signals modulated at frequencies between 1.3kHz and 7.3kHz and broadcast from a low latitude purpose built transmitter. The latter report a similar but accentuated effect from a like experiment conducted in auroral regions. Kapustin et al. (1977) found that the intensity of the radiation at the modulation frequency depended on the distance between the auroral electrojet and the heated ionospheric region, and also on the strength of the jet. Stubbe and Kopka (1979) describe the design of an HF ionospheric modification experimental facility to be built near Tromsø, Norway in order to investigate similar auroral region effects. The theoretical aspects of this experiment are discussed in Stubbe and Kopka (1977).

2.5.2 A Simplified Theory Of D and Lower E Region Ionospheric Heating

The wealth of observable, non-linear ionospheric phenomena arises from the dependence of electron collision frequency on the electron temperature (Walker, 1979).

In the collision dominated D and lower E regions (in which this thesis is most interested), the principal modification, due to the

incident radio wave, will be one of electron heating (Gurevich, 1978; Walker, 1979). The heating results from electrons acquiring considerable energy from the incident field between collisions, and because the electron-neutral and electron-ion heat losses, on collision, are relatively small. These are hindered by the very low electron to neutral/ion mass ratio. As a result, the ionospheric electrons may be heated even in a comparatively weak field.

The following simplified theory, adapted from Hibberd (1955) and Gurevich (1978) illustrates how D-region ionospheric heating occurs. Following Gurevich (1978) a wave with electric field \underline{E} and angular frequency ω is considered to pass through a slab of ionospheric plasma with an average electron to neutral collision frequency ν_e . This field will act upon the electrons and accelerate them. Collisions will, however, retard them and, given time, a stationary state will be set up. If the ion motions are neglected (since $\omega \gg \omega_{Bi}$, where ω_{Bi} is the ion gyrofrequency), application of Newton's second law of motion gives the directional velocity, V_e , of the average electron:

$$m \frac{dV_e}{dt} = -e\underline{E} - e(\underline{V}_e \times \underline{B}) - m \nu_e \underline{V}_e \quad \text{equation 2.8}$$

where \underline{B} is the imposed geomagnetic field and m is the electron mass.

The change in electron temperature due to this incident wave is found by considering the conservation of energy. In unit time the wave electric field performs work equal to $\underline{J} \cdot \underline{E} = -Ne \underline{V}_e \cdot \underline{E}$ on the plasma, where N is the electron number density and \underline{J} is the current density. Conversely, during this time electrons lose energy via collisions and thus:

$$\frac{d}{dt} \left[\frac{3}{2} N \kappa T_e \right] = Ne \underline{V}_e \cdot \underline{E} - \frac{3}{2} \delta \nu_e N \kappa (T_e - T) \quad \text{equation 2.9}$$

where δ is the average fraction of energy transferred to a neutral in one collision with an electron, T_e is the modified electron temperature due to the wave, and T is the unmodified neutral/electron temperature. A Maxwellian particle energy distribution is assumed.

If $B = 0$ and $\underline{E} = E_0 \cos \omega t$, V_e can be conveniently obtained from equation 2.8 by using the identity:

$$\int e^{at} \cos bt = \frac{1}{a^2 + b^2} (ae^{at} \cos bt + be^{at} \sin bt)$$

$$\text{i.e. } V = \frac{E_o e}{m(v_e^2 + \omega^2)} (v_e \cos \omega t + \omega \sin \omega t) \quad \text{equation 2.10}$$

On substitution into equation 2.9 this gives:

$$\frac{dT_e}{dt} = \frac{e^2 E_o^2}{3\kappa m(\omega^2 + v_e^2)} (v_e + v_e \cos 2\omega t + \omega \sin 2\omega t) - \delta v_e (T_e - T) \quad \text{equation 2.11}$$

The steady state solution of equation 2.11 is:-

$$T_e = T + \frac{e^2 E_o^2}{3\kappa m \delta(\omega^2 + v_e^2)} + \frac{e^2 E_o^2}{3\kappa m(\omega^2 + v_e^2)} \left[\frac{(\delta v_e^2 - 2\omega^2) \cos 2\omega t}{4\omega^2 + \delta^2 v_e^2} \right] + \frac{2\omega v_e \sin \omega t}{4\omega^2 + \delta^2 v_e^2} \quad \text{equation 2.12}$$

which providing $\omega \gg \delta v_e$, a condition readily met in the D region, reduces to:

$$\Delta T = (T_e - T) = \frac{e^2 E_o^2}{3\kappa m \delta(\omega^2 + v_e^2)} \quad \text{equation 2.13}$$

It is convenient to define a quantity E_p the plasma field:-

$$E_p = \left[\frac{3\kappa T m}{e^2} \delta(\omega^2 + v_e^2) \right]^{\frac{1}{2}} \quad \text{equation 2.14}$$

Consequently equation 2.13 can be rewritten as:

$$\frac{\Delta T}{T} = \left[\frac{E_o}{E_p} \right]^2 \quad \text{equation 2.15}$$

Hence, to first order, the fractional electron temperature enhancement settles on a certain average value dependent upon the square of the peak incident field strength.

Note that in this derivation it has been tacitly assumed that neither δ nor v_e are functions of T_e . Although this is not true, inclusion of this dependency does not invalidate equation 2.15 to first order (Gurevich, 1978).

Now consider an amplitude modulated (A.M.) wave, incident upon the ionosphere, described by:

$$E = E_o \left[1 + M \cos \Omega t \right] \cos \omega t \quad \text{equation 2.16}$$

where M is the modulation index, and Ω is the modulation frequency.

An identical analysis to that described above gives the temperature perturbation due to this A.M. signal. Substitution of equation 2.16 in 2.8 gives:

$$V = \frac{eE_o}{m} \left[\frac{v_e \cos \omega t + \omega \sin \omega t}{v_e^2 + \omega^2} + \frac{M}{2} \left(\frac{v_e \cos(\omega-\Omega)t + (\omega-\Omega) \sin(\omega-\Omega)t}{v_e^2 + (\omega-\Omega)^2} \right) \right. \\ \left. + \frac{M}{2} \left(\frac{v_e \cos(\omega+\Omega)t + (\omega+\Omega) \sin(\omega+\Omega)t}{v_e^2 + (\omega+\Omega)^2} \right) \right] \quad \text{equation 2.17}$$

which on substitution in equation 2.9 gives:

$$\frac{1}{\delta v_e} \frac{dT_e}{dt} = \frac{E_o^2}{E_p^2} T \left[1 + \frac{M^2}{2} + 2M \cos \Omega t + \frac{M^2}{2} \cos 2\Omega t + \text{terms in } \omega \text{ and } 2\omega \right. \\ \left. - (T_e - T) \right] \quad \text{equation 2.18}$$

providing $\omega \approx \omega + \Omega \approx \omega - \Omega$ i.e. $\omega \gg \Omega$

Once again if $\omega \gg \delta v_e$ the expression for the resulting temperature change can be considerably simplified:

$$\text{Defining: } \Delta T_e = \Delta_o T_e + \Delta_\Omega T_e,$$

where $\Delta_o T_e$ is the time independent perturbation

and $\Delta_\Omega T_e$ is the time dependent perturbation,
integration of equation 2.18 gives:

$$\frac{\Delta_o T_e}{T} = \left[\frac{E_o}{E_p} \right]^2 \left[1 + \frac{M^2}{2} \right] \quad \text{equation 2.19}$$

$$\text{and } \frac{\Delta_\Omega T_e}{T} = \left[\frac{E_o}{E_p} \right]^2 2M \left\{ \frac{1}{\Omega^2 + \delta^2 v_e^2} \left[\delta^2 v_e^2 \cos \Omega t + \Omega \delta v_e \sin \Omega t \right] \right. \\ \left. + \frac{M}{4(\Omega^2 + \delta^2 v_e^2)} \left[\delta^2 v_e^2 \cos 2\Omega t + 2\Omega \delta v_e \sin 2\Omega t \right] \right\} \quad \text{equation 2.20}$$

Hence, an incident modulated wave can cause both constant and periodically varying, at the modulation frequency Ω (and 2Ω), variations in the electron temperature. The impact of such variations in auroral latitudes is discussed in Chapter 7.

CHAPTER THREE

The VLF Goniometer System - Theory and Practice

3.1 Introduction

Several ELF/VLF goniometer experiments have been conducted by the Space Radio Physics Group, Southampton, England, during the period January 1977 to December 1979, and are discussed in Chapter 5.

These generally involved setting up multiple goniometer ground stations in Scandinavia. Each goniometer receiver gives, subject to certain assumptions (see section 3.2), the azimuthal bearing of an ELF/VLF signal source in the ionosphere. Hence, in addition to the spectral and amplitude information normally associated with wide band ELF/VLF measurements, the use of two or more such receivers enables the source location to be found by triangulation.

In this chapter the theory of the goniometer is reviewed, together with a description of the experimental system at March, 1979. Furthermore the experimental procedures will be described.

The primary results of this thesis, see Chapter 6, refer to the system in operation during March/April, 1979.

3.2 The Theory Of Goniometers

The theory of the goniometer, as applied to ELF/VLF direction finding studies, has been discussed by Bullough and Sagredo (1973).

Consider one horizontally propagating plane wave, of angular frequency ω , with its wavefront in a vertical plane, incident upon two vertically mounted orthogonal antenna loops A and B, at an angle θ to the plane of A. After some amplification the output from each channel may be expressed as:

$$V_A = K_1(\omega) \sin(\omega t + \beta(\omega)) \cos \theta$$

$$V_B = K_2(\omega) \sin \omega t \sin \theta$$

where $K_1(\omega)$ and $K_2(\omega)$ give a measure of the gain of each channel and where $\beta(\omega)$ is a measure of the differential phase response. Consider $K_1 = K_2 = K$ and $\beta(\omega) = 0$, then, multiplying V_A by $V_m \sin \omega_m t$ and V_B by

$V_m \cos \omega_m t$ and adding gives:

$$\text{equation 3.1} \quad V = V_A + V_B = V_m K \sin \omega t \sin (\theta + \omega_m t)$$

Here $\omega_m t$ is a goniometer generated modulation signal. The modulated output voltage, V , is directly proportional to that which would be obtained by a single loop mechanically rotated about a vertical axis at a frequency $\omega_m/2\pi$ Hz. The goniometer output is thus an electrical and, consequently more rugged, simulation of a mechanical system. Note that minima in the resultant output voltage occur when $\theta + \omega_m t = 0, \pi$ etc. and maxima occur when $\theta + \omega_m t = \pi/2, 3\pi/2$ etc. It is evident that, if a reference pulse is generated once every revolution, i.e. at north, the phase difference between the reference and a modulation envelope minimum gives a measure of the bearing angle, θ . It can also be seen, however, that a 180° ambiguity exists in bearings obtained using this technique.

In the development of the theory it has been assumed that $K_1(\omega) = K_2(\omega)$ and $\beta(\omega) = 0$, that is the goniometer channels A and B are amplitude and phase matched. It has also been tacitly assumed that the modulation signals are in quadrature and of the same amplitude. These various conditions cannot be met in practise and frequency dependent and frequency independent deviations from equation 3.1 can be expected (Jarvis, 1976). This results in an apparent bearing which is not equal to the real bearing, (see section 3.4).

Additionally various assumptions (underlined) have been made in the theory concerning the incoming wave. A general ELF/VLF radio wave with its source in the ionosphere could be the sum of many multipath waves, inclined to the horizontal, which are elliptically polarised, with the major axis of the polarisation ellipse inclined to the horizontal. Bullough and Sagredo (1973) examined the problem of ellipticity and inclination showing that the bearing errors were small providing that the signal had propagated some distance from the ionospheric exit point. As such the wave is inclined at some small angle to the horizontal and also becomes nearly vertically plane polarized due to the high ground conductivity (Nambra, 1931).

More recently, however, Strangeways (1977) has conducted a sophisticated computer analysis accounting for all the factors above. He demonstrated that the bearing errors due to wave polarisation and

multipath propagation are of opposite sign providing some reduction in the errors. He found, however, that multipath errors increase as the source to receiver distance increases, this being due to the relatively larger amplitudes of the multi-hop signals. The overall result is an increase in bearing errors as the source to receiver distance increases. Strangeways (1977) reports that for a constant frequency emission the bearing angle error, on a signal source over 200 km distant, is generally less than 20° , although for a limited frequency range it may be higher.

When the bearing can be averaged over 2kHz, i.e. with whistlers, a reduction in these errors to 10° or less can be obtained.

3.3 A Practical Goniometer System

3.3.1 Introduction

The equipment used in this study is based upon the goniometer system designed by Bullough et al. (1973). Jarvis (1976) has described the use of a goniometer system by Southampton University, and this section describes modifications and additions made since that time. Only the antennae and the goniometer receiver remain essentially unchanged.

Some of the following is a précis of the Southampton University ELF/VLF Goniometer Manual, 1979 (Cannon et al., 1979).

3.3.2 System Overview

The ELF/VLF goniometer system used in this work is shown in figure 3.1. Two crossed loop antennae feed two identical channels comprising a low noise preamplifier, attenuator, and goniometer receiver, the output of which feeds a stereo direct record magnetic tape recorder. The antenna - preamplifier sensitivity is $\sim 4 \times 10^{-16} \text{ V}^2/\text{Hz}$ at 1kHz (Bullough, 1976). Due to mains harmonic interference adequate sensitivity can only be obtained $> 5\text{km}$ from a mains supply and consequently all equipment is battery operated. Both amplitude and azimuthal bearing calibrations are carried out using a small coil, fed from a signal generator, mounted at the centre of the loops.

Battery operated test and calibration equipment, including an oscilloscope, was available. In addition communications between goniometer recording stations, and where applicable between these

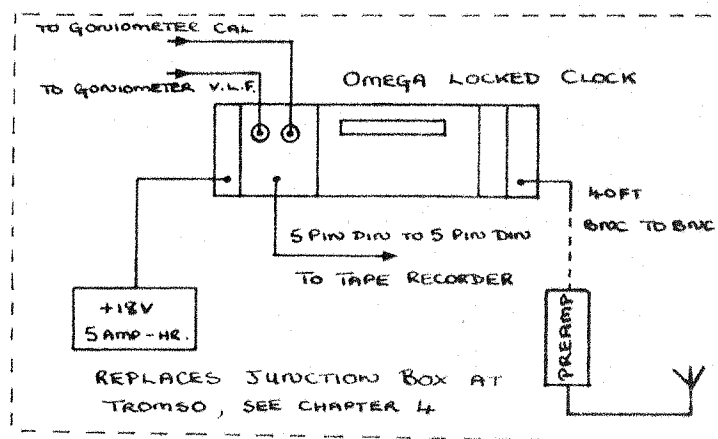
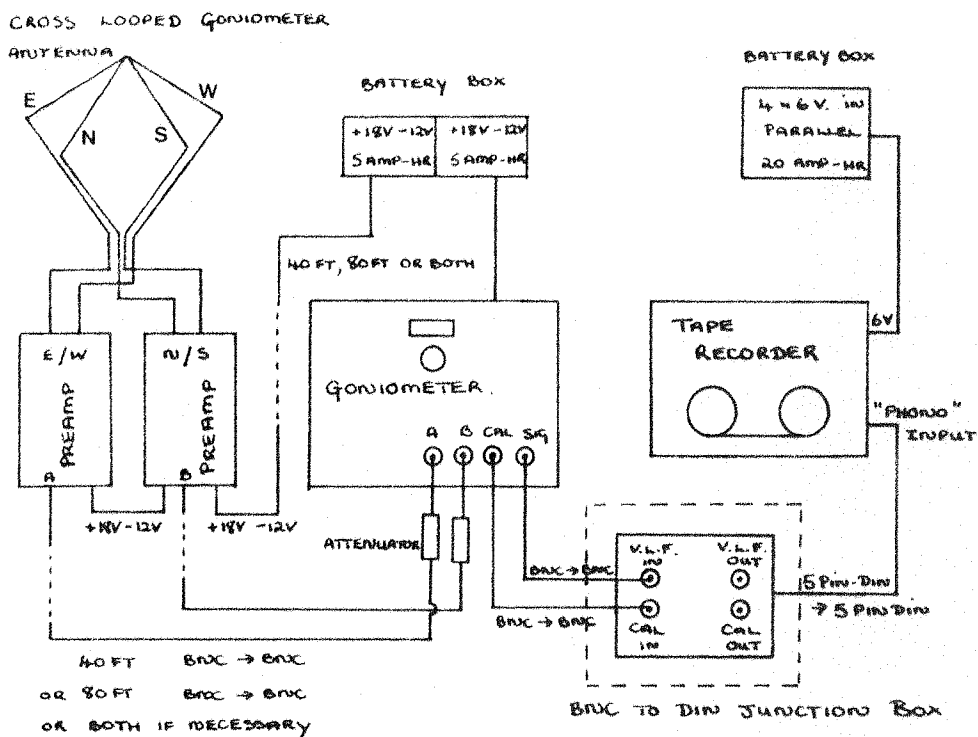


Fig. 3:1 Goniometer System In Use March 1979

stations and the Andøya Rocket Range, Norway, was provided by battery operated HF (150 watt peak envelope power) single side band transceivers. Cannon et al.(1979) discuss the use of the transceiver in this context. Site timing was provided by digital watches, updated daily from commercial timing information (W.W.V., B.B.C. etc.) received on battery operated communication receivers.

3.3.3 The Antenna

3.3.3.1 Description

The antennae used consisted of two diamond shaped, orthogonal, magnetic field sensing, loops each 58m^2 in area. These were mounted in a vertical plane using a 42 ft (12.8 metres) aluminium mast and suitable guying, (Cannon et al.,1979) see figure 3.2. The single turn antenna was constructed from heavy duty RG 213/U coaxial cable, where the inner core formed the antenna and the outersheath (braid) an electrostatic screen and shorted turn at high ($> 70\text{kHz}$) frequencies. The effect of the screening is addressed in some detail in Chapter 6.

Table 6.2 gives typical antenna characteristics.

3.3.3.2 Practical Details

The antennae were mounted in geographic north-south, east-west planes by sighting along the antennae loops and guy ropes using a prismatic compass. An accuracy of better than $\pm 1^\circ$ could be obtained. Each recording station utilised a geographic frame of reference in order to make later data analysis easier.

3.3.4 The Preamplifier

3.3.4.1 Description

The differential input preamplifiers, one for each channel (i.e. antenna) are based upon the design of Cantarano and Pallotino (1970) who give an excellent description of the design philosophy. The design was adapted for ELF/VLF work by Morgan (1976). These preamplifiers replaced the preamplifiers used by Jarvis (1976), which were mounted within the goniometer, and which had a reduced sensitivity. A circuit diagram is shown in figure A1.1, Appendix 1.

The design utilizes two field effect transistor (F.E.T.) devices in cascode as a front end. These transistors have an input referred

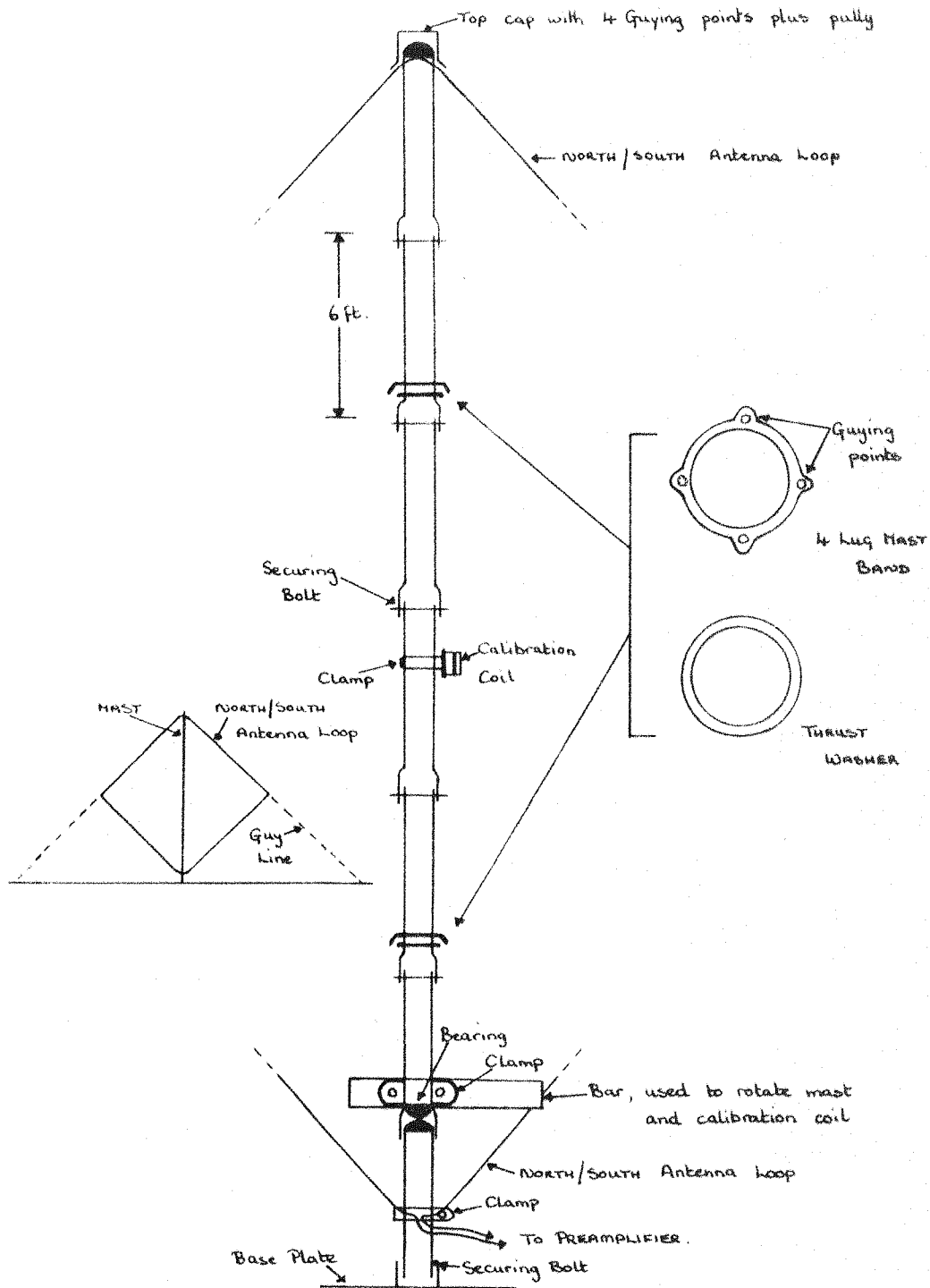


Fig. 3:2 Southampton University Goniometer Antennae
(one only shown) and Supporting Mast.
- antennae loops are hoisted using a halyard

voltage noise of only $3\text{nV}/(\text{Hz})^{\frac{1}{2}}$ for frequencies over 100Hz giving good sensitivity. In addition, in order to maximise the signal to noise ratio, an input transformer has been utilised to match the low impedance antenna to the high input impedance (low input referred current noise) of the F.E.T. (Motchbacher and Fitchen, 1973). Smith and Bullough (1976) have experimentally demonstrated that for an almost identical preamplifier, the preamplifier plus antenna noise is comparable to the thermal noise contributed by the antenna only. They concluded that the system is antenna noise limited (thermal noise limited), rather than preamplifier noise limited.

The input transformer has the additional effect of introducing a resonance which, due to the high impedance F.E.T. loading, has a fairly high Q (~ 10). With the addition of some tens of picofarads the resonant frequency has been adjusted by the author to approximately the earth-ionosphere waveguide cut-off frequency, giving additional sensitivity at these frequencies.

The preamplifier gain is determined, excluding the effect of the input transformer, by the 91K and 91Ω feedback resistors, the quotient of these defining the gain, 60 dB (figure A1.1). At three variable frequencies, however, the gain can be reduced by about 18 dB. A high Q, LC filter circuit (figure A1.1) placed in parallel with the 91K resistor reduces the gain near the tuned circuit resonance but has little effect away from resonance. These filters were used to attenuate (notch) unwanted high field strength VLF transmitters between $\sim 12\text{kHz}$ and $\sim 20\text{kHz}$ which would otherwise reduce the system dynamic range in Scandinavia.

Figure 3.3 depicts the response of the two matched preamplifiers used at Sodankyla, March 1979. The input transformer resonating at 1.025kHz clearly defines the response of the preamplifier up to the notch frequencies and also provides some low frequency (mains harmonic) cut off.

3.3.4.2 Preamplifier Calibration and Crosstalk

Absolute phase and amplitude matching of the two preamplifiers is not a problem, providing the difference remains approximately constant as the frequency is varied, since system calibration can account for this (section 3.4). Large variations in the differential amplitude and phase, as a function of frequency are, however, a problem, since interpolation

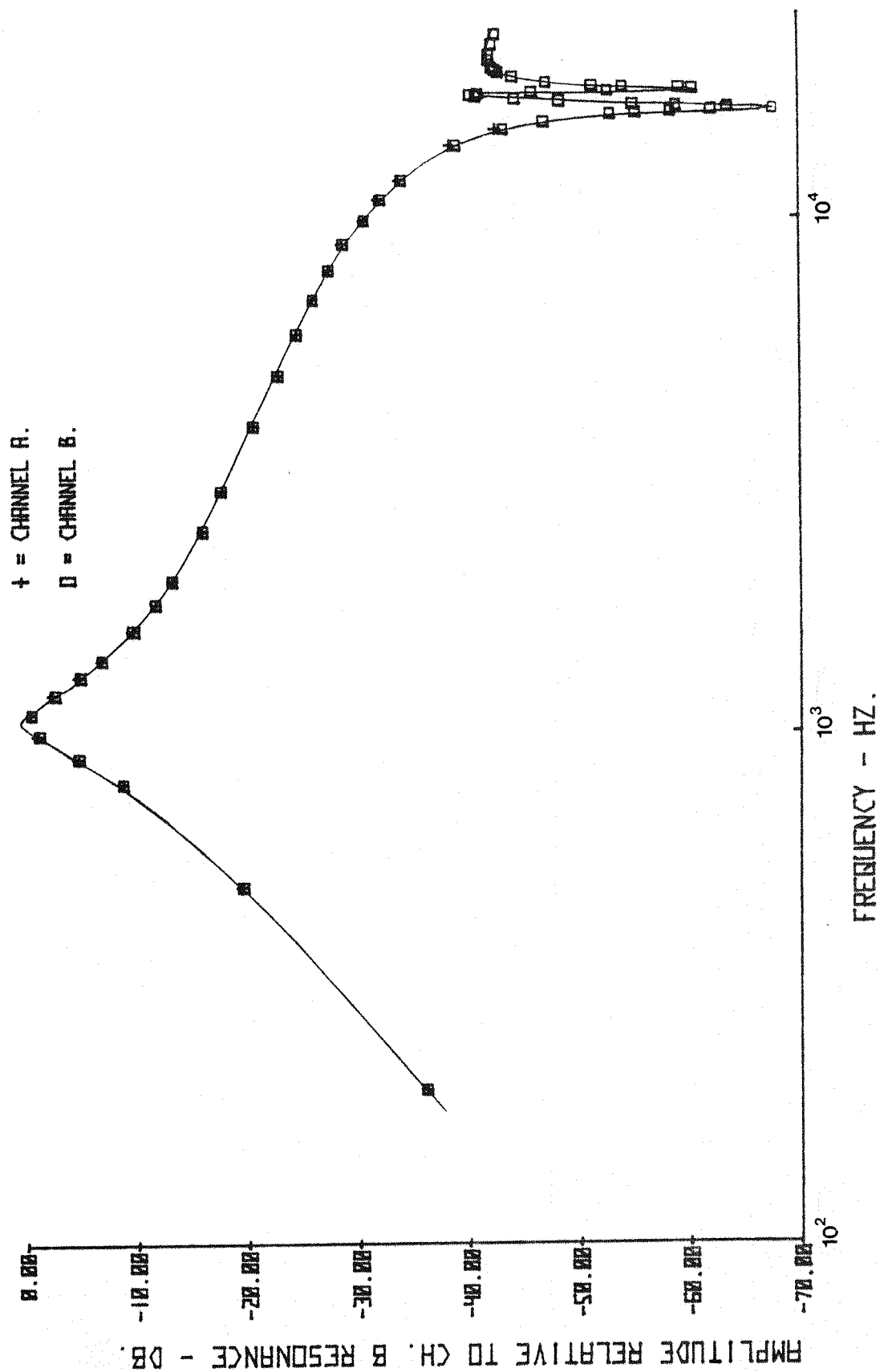


FIG.3.3 PREAMPLIFIER AMPLITUDE RESPONSE.

between the calibration angles and frequency values is inaccurate. This necessarily reduces confidence in the signal bearings derived.

It is consequently necessary to match closely the Q's and resonant frequencies of the preamplifier input transformers since these effectively define the preamplifier amplitude and phase response and thus channel matching.

Matching and preamplifier calibration took place in Southampton, prior to dispatch, however, 'on site' matching and calibration was sometimes necessary as a result of mechanical stresses incurred during transit. Matching to within a $\Delta f_{\text{resonance}}$ of less than 10Hz could easily be obtained. Similar matching of the notch frequencies also took place such that Δf_{notch} was less than 100Hz. In order to check for preamplifier stability the calibration was also repeated at the termination of the experiment.

After completing on site calibration, the preamplifiers were placed inside a thermally insulated container, to increase mechanical and electrical resistance to the extreme Arctic environment. This was placed at the foot of the mast.

It must be pointed out that the high degree of amplitude and phase matching between the two channels makes them particularly susceptible to crosstalk at resonance, via the input transformer. During early experiments (see Chapter 5), the two preamplifier channels were mounted side by side in a common container, the result of which was up to -12dB of crosstalk at resonance. This severely affected the systems ability to provide bearings on signals with frequencies near resonance, i.e. auroral chorus (see Chapter 5). Each preamplifier is currently mounted in a separate container in order to reduce crosstalk between the channels which is now better than -20dB; this being dependent upon their proximity, one to each other.

3.3.5 Attenuators

The maximum allowable signal at the input to the goniometer is approximately 3 volts peak to peak, this varying somewhat from instrument to instrument. Higher amplitude inputs result in the non-linear mixing of different frequency signals. In Scandinavia, the various local high powered VLF transmitters sometimes caused the

preamplifier output to reach .24 volts peak to peak and, as a result, attenuators were required.

Various matched pairs of resistive attenuators, each pair with a different attenuation ratio, were provided for each station. These were specific to each goniometer since they were adjusted to negate any small amplitude differences which existed between the goniometer channels. A ratio was chosen in the field such that the full goniometer dynamic range was utilised without non-linear distortion occurring

3.3.6 The Goniometer

Figure 3.4 shows a block diagram of the goniometer which was a modified version, see section 3.3.4 and below, of that used by Jarvis (1976).

Signals from the appropriate preamplifier attenuator are fed to a high impedance buffer and thence to a Hall Multiplier. Here the signals are modulated at $\sim 27.5\text{Hz}$, the modulation in one channel being in quadrature with that in the other channel. The Hall Multiplier outputs are then summed as required by equation 3.1. The phase reference is provided by a short calibration spike (0.6ms duration) derived from the modulating oscillator.

All stages are now powered via voltage regulators due to the modifications of M. Ogg (private communication, 1976). He investigated the goniometer performance and found that the output was asymmetric about the time axis, and also that the calibration pulse was not in quadrature with respect to the two channels. Ogg concluded that this was due to unbalanced modulation in the Hall Multiplier producing a component at the signal frequency ω , as well as at $\omega + \omega_m$ and $\omega - \omega_m$, where ω_m is the angular modulation frequency. Modifications to reduce this latter error required the introduction of an equal and opposite component at frequency ω to cancel the unbalanced term, this requiring a high stability power supply.

The amplitude response of the goniometer is flat from $\sim 800\text{Hz}$ to 10kHz to better than 0.6 dB peak to peak. The system amplitude and phase variations are thus dominated by the preamplifiers.

3.3.7 Tape Recorder

All goniometered signals were recorded on a Uher 4200 Report Stereo,

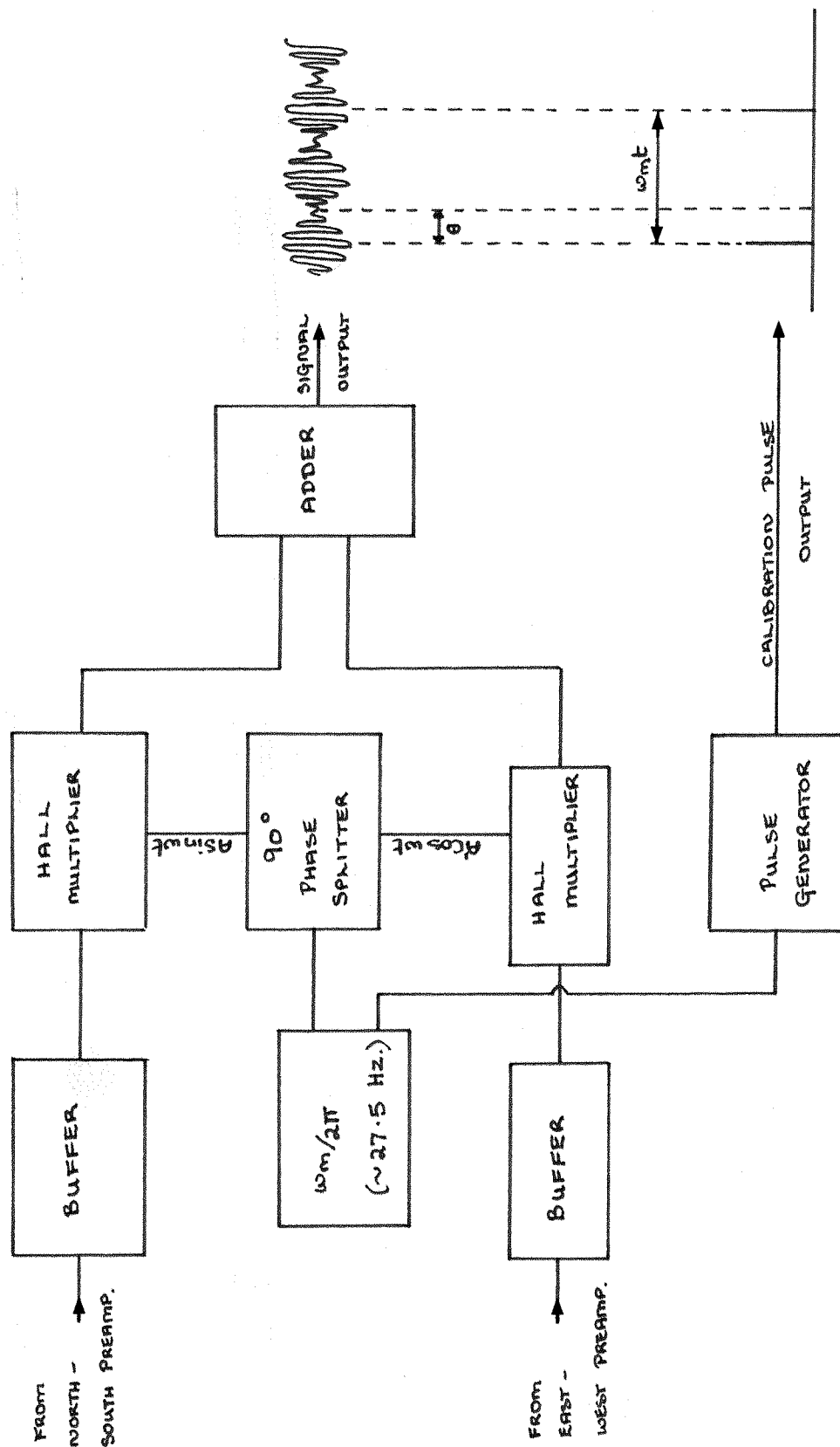


Fig. 3:4 Block Diagram of Goniometer Receiver.

4-track, direct record tape recorder at $3\frac{3}{4}$ " /second. This speed gave adequate quality for signals within the frequency range 0.5kHz to 10kHz.

Recordings were made in stereo, with goniometered ELF/VLF on one channel and calibration pulses, timing information and station keeping information on the other.

3.3.8 Power Supply

Power for the system was provided by 5 Ampere-hour lead acid gel batteries. Constant current chargers designed by Garment (private communication, 1977) were used to charge these batteries between recordings.

3.3.9 The Calibration Coil

Amplitude and azimuthal calibrations were effected using a circular calibration coil and an audio frequency oscillator. The oscillating output from the generator produces a time varying magnetic field perpendicular to the plane of the coil which is equivalent to a linearly polarized wave whose wave normal is in the plane of the antenna.

The calibration coil is mounted at the loop centre with its plane parallel to one loop. Smith and Bullough (1976) equated the voltage induced in the loop antenna due to a current in the coil and the mutual inductance between coil and antenna with the voltage induced by a wave with field B as given by Faradays Law. They showed that for this antenna and coil geometry:

$$i_c = \frac{AB}{M} = \frac{\pi A a B}{\sqrt{2} \mu_0 N_c A_c} \quad \text{equation 3.2}$$

where i_c is the calibration coil current (amps), N_c , the number of turns in the coil, A_c , the average area of the coil (m^2), M the mutual inductance between antenna loop and calibration coil (L), A , the area of the loop antenna (m^2), a , half the length of one side of the loop antenna (m), and B the field strength of the equivalent wave (T).

A knowledge of the coil current determines the equivalent magnetic field and amplitude calibration of each channel can be accomplished. By rotating such a coil it is also possible to simulate waves arriving from various directions, and hence to azimuthally calibrate the system.

The 100 turn coil, of typically $48 \pm 1 \text{ cm}^2$ average area, $1.13 \pm 0.02 \text{ mH}$ inductance and $1.75 \pm 0.05 \text{ ohms}$ resistance was mounted at the loop centre by rigidly attaching it to the mast. A simple mechanical bearing was provided between the bottom fixed mast section and the six sections above which were locked together. A similar bearing was also provided between the seventh section and the top cap, to which the antenna loops and top mast guys were attached. With the addition of slip rings, to which the other guy ropes were attached, it was then possible to rotate the mast, and thus the calibration coil, within the antenna loops. The use of the bearings was a modification to a previous system. In this earlier system, used between February 1977 and October 1978 inclusive, guy rope slip rings were also used, however, the antenna loops were attached to a rotating clamp at the mast base and to a top cap without a bearing. Rotation of the mast thus involved rotation of the whole mast on the base which was adequate in England but tended to "lock up" with ice in Scandinavia.

Rotation of the mast, and thus the coil was effected by pushing a horizontal bar, about one metre in length, which was bolted onto the moving sections of the mast, see figure 3.2.

In order to carry out calibration procedures it was necessary accurately to align the coil at defined angles relative to the loops. Using two cross struts, some 0.3 metres long, mounted behind the coil it was found possible to align the coil in the plane of either loop to better than $\pm 1^\circ$. Other subsequent coil settings involved sighting on the horizontal bar (to better than $\pm 1^\circ$), which was fixed with respect to the coil.

3.4 Azimuthal Calibration

A detailed on site azimuthal bearing calibration, discussed in section 3.3.4.2, was required due to the less than perfect channel matching.

Signals at many different frequencies were injected into the calibration coil, positioned parallel to the north-south loop. The injected signal amplitude was a maximum for each frequency, subject to the proviso that no overloading of the system occurred. At each frequency the goniometer output was recorded for 15 seconds. The following frequencies were used: 0.5, 0.8, 0.9, 1.0, 1.1, 1.2, 1.3,

1.4, 1.5, 1.6, 1.8, 2, 2.5, 3, 4, 5, 6, 7, 8, 9, 10, 11, 12kHz.

Note that around the preamplifier resonance, where channel matching deteriorates, a more detailed calibration was carried out. This procedure was repeated with the plane of the radiating coil at angles of 30° , 60° , 90° , 120° , 150° and 180° to the plane of the N - S antenna at the start of the campaign, and 0° , 15° , 30° , 45° , 60° , 75° , 90° , 105° , 120° , 135° , 150° , 165° and 180° at the campaign end. This limited repetition of the calibration served two purposes. Firstly, it provided some redundancy should human error cause one calibration to be ineffective and, secondly, it provided a check on the electrical stability of the equipment throughout the experiment.

Data analysis following the techniques of section 3.6 enabled a graph of apparent signal bearing as a function of real signal bearing to be plotted for each frequency, see figures 6.10 and 6.11. The apparent bearing of an emission could then be translated into a real bearing using this calibration information.

Jarvis (1976) calibrated his goniometer system by an analytical technique. The laboratory measured quadrature error between the two goniometer modulation signals, and the amplitude and phase difference between the two channels were treated, using a mathematical model of the errors, to give the apparent bearing as a function of the real bearing. On site calibration was, however, deemed preferable for two reasons. Firstly, imperfect modelling of the goniometer response, c.f. section 3.3.6, will introduce errors. Secondly, any variations in the system's electrical performance caused by transportation to and from the field site could invalidate the calibration.

3.5 Data Recording

Recordings were made by each station during prearranged periods, each station changing tapes at approximately the same time. The latter condition was extremely important when rocket associated recordings were being made, see Chapter 5. U.K. associated rockets were never launched within ± 2 minutes of a nominal tape change over time.

The start of each tape side contained the following verbal information: location, date, tape number, tape side, universal time (counted over several seconds from a digital watch which was correct to ± 0.5 seconds).

and an announcement of the instant of tape counter reset. The time of the latter was logged. A time baseline was thus set up and subsequent ELF/VLF emissions were logged with both time and tape count.

A few tapes recorded at Tromsø during October and November 1978, and all tapes recorded at Tromsø during March/April 1979, were coded with timing information from an Omega Locked Clock. This device forms the subject of Chapter 4.

Additionally, calibration fields at 1,3,5,8kHz were applied, via the calibration coil, at the start of each side of tape. Estimation of the field strength of an emission could then be made, via equation 3.2, by a comparison of the emission and calibration signal spectral amplitudes.

3.6 Analysis Equipment

Spectral measurements were performed initially on a Sonogram Analyser. This produces a hard copy representation of the signal with time along the abscissa, frequency along the ordinate and amplitude represented as a greyscale, dark being the stronger. This instrument was subsequently supplemented, and to a large extent superseded, by a Spectral Dynamics, SD 350-6 real time analyser (Spectral Dynamics, 1978). This is a Fast Fourier Transform Analyser with an output capability, in real time up to 80kHz, to either a cathode ray tube (CRT), displaying amplitude - frequency information and/or to a hard copy device. The latter (Spectral Dynamics, 1979) produces an output similar to that of the sonogram.

Goniometer bearings were obtained from the tape recorded signals using the Sheffield University Semi-Automatic Analyser. The analyser displays, on a persistent CRT intensity modulated frequency - time information. On hearing a signal of interest, on playback, the operator can hold two seconds of data on the screen and using a cursor, he can digitise the frequency - time information. To determine the azimuthal bearing these digitised co-ordinates are used to program a bank of bandpass filters each 320 Hz wide, opening each only when the interesting signal occurs in that filter passband. In this manner a signal, even one varying in frequency with time, may be extracted from the background noise. Section 3.2 showed that the phase difference between the calibration pulse and the minima in the modulated signal envelope gives

a measure of the apparent bearing angle. The analyser determines this from the cross correlation function of calibration pulse and filtered signal. The analyser has been described in some detail by Bullough et al (1975) and Smith et al.(1978).

Using this technique the apparent bearing for each of the calibration bearings and frequencies was determined and entered into the analysis computer program developed by A.J. and I.D. Smith of the University of Sheffield. The apparent bearing of a VLF emission was then compared, at the appropriate frequencies, with these calibration data, via the program. This resulted in an average bearing determined over the emission bandwidth, typically 2kHz for a whistler and 500 Hz for a riser element. Madden (1981) describes the adaptation of this program for use on the Southampton Computer Facility.

CHAPTER FOUR

A Battery Powered Time Encoded Clock For Use In A Goniometer ELF/VLF Recording System

4.1 Introduction

This chapter contains a description of a battery operated clock developed for use in the goniometer receiving system described in Chapter 3. During data collection the encoded time is recorded on magnetic tape in parallel with the calibration pulses. On playback the recorded time is decoded and displayed, thus facilitating the analysis.

The time encoded clock contains two subsystems. The first is a digital clock based closely on the design of Blixhavn and Lyngdal (1976). The second is a time encoder/decoder, the detailed design of which is due to E. Friis of the Electronics Laboratory, The Physics Department, Southampton University, in consultation with the author. Circuit diagrams of the complete clock, together with a brief circuit description, are given in Appendix 2.

In the following, the author's design requirements and the solutions considered are given. Details of the clock operation, goniometer system interface, and the Sheffield University Whistler Analyser interface are also provided. The clock performance is evaluated.

4.2 Design Requirements

(i) Analysis generally involves the identification of the same ELF/VLF event, typically 0.5 to 1 second in duration, at different goniometer receiving stations. A digital design with good long term time stability was, therefore, required such that at any instant, during a four week experimental period, the time difference between any two clocks would be less than ≈ 0.2 seconds. Any solution which gave better stability was considered to be a worthwhile bonus since it would provide a more versatile instrument.

(ii) A design which was battery **operated**, for goniometer compatibility, was required.

(iii) A design was required whereby the time could be encoded and

mixed onto either the calibration pulse channel or alternatively the ELF/VLF signal channel, of the stereo data recordings, (see Chapter 3). The former was preferred in order that the ELF/VLF signals were not masked.

(iv) Finally, world-wide operation with the minimum of operator difficulty was required.

4.3 Considered Solutions

Since funds to purchase a commercial instrument were unavailable, all solutions considered involved the design and construction of a clock.

The first solution was to construct a simple, crystal controlled, encoding clock (typical stability 1ppm/°C). This was, however, rejected because the design would require manual starting and it was considered unlikely that the specified relative time difference of better than 0.2 seconds could be met. In addition, nominal oscillator frequency offsets, and variations due to temperature fluctuations, could subsequently enhance this anomaly. (A steady 1 p.p.m. difference in oscillator frequencies results in a 2.5 second error after 28 days).

It follows that in order to meet requirement (i), each clock must be controlled by a common external source, i.e. a radio transmission carrying high stability timing information. Cross (1976) and Giles et al. (1978) have described systems using the M.S.F. 60kHz time encoded signals broadcast from Rugby, England. This system was, however, rejected because it failed to meet requirement (iv), restricting the region of operation to, at best, Europe where the 60kHz field strength is high. The W.W.V. H F transmissions from the Central Radio Propagation Laboratory, National Bureau of Standards, Washington D.C., U.S.A., were also considered. Frequency diversity on 2.5, 5, 10, 15, 20 and 25MHz is employed, providing world-wide coverage during various ionospheric conditions. Unfortunately, since these conditions are non-deterministic the operator or clock is required to constantly monitor the controlling signal field strength, effecting a change in receiver frequency as required. Therefore, this too failed to meet requirement (iv), this time because of operational difficulties.

From the above considerations it was concluded that, for ease of operation and also design, timing information broadcast from a world-wide system, with predictable amplitude propagation characteristics was required.

Candidates considered were a world coverage satellite system, an international LF system such as Loran, or an international VLF system such as Omega. All of these exhibit fairly predictable amplitude characteristics. Cashion et al (1979) describe a satellite timing system using "Transit", the U.S.A. navigation satellite system, which includes timing information in the data stream. Blixhavn and Lyngdal (1976) describe a mains operated, digital, clock (without time code generator/decoder), locked to the "Omega" navigation system (Burgess et al., 1975). Here the timing information is implicit in the operating system. Since the latter design met requirement (i) (giving substantially better synchronisation than required) and requirement (iv) and, additionally, because detailed literature regarding the design was available it was adopted as the baseline solution. Requirement (ii) was met by suitably modifying the design of Blixhavn and Lyngdal. This primarily involved exchanging the LED displays for liquid crystal displays (L.C.D.). The resulting substantial reduction in power gave the option of battery operation. By interfacing to the clock a time code generator/decoder based upon the design of Girling (1977) requirement (iii) was also satisfied.

4.4 Introduction To The Time Encoded Clock

The clock uses the Omega navigation system 10.2kHz signals to update a crystal controlled clock. Each station in the system transmits a pulse once every ten seconds during one of nine time segments (U.S. Naval Observatory, 1979) and these pulses are locked to UT using a caesium beam oscillator (accuracy better than 1 part in 10^9). The clock, providing set to within ± 4 seconds of UT, automatically locks onto a preselected 10.2kHz pulse and displays the correct time, subject to the restrictions given below. Over periods greater than ten seconds, this gives excellent long term stability and extremely close synchronisation between different clocks.

Long term discrepancies between the displayed time and UT are principally determined by the following:

(i) In general the 10.2kHz pulse does not start on an integral number of seconds and there is a systematic shift from UT. When controlled by the Norwegian Omega station at Aldra this error is zero since this always pulses on an integral second (U.S. Naval Observatory, 1979).

(ii) The 5ms synchronisation resolution of the clock circuitry (see Appendix 2).

(iii) Propagation delays between the transmitter and the clock.

The recorded time of any two clocks, using the same Omega transmitter, are offset from each other by an amount determined by:

- (i) The 5ms synchronisation resolution of the clock.
- (ii) The relative propagation delays between the transmitter and the clocks.

Short term stability (≤ 10 seconds) is determined by the crystal oscillator and is thus good to around $1\mu\text{s}$.

The clock time can be fed simultaneously to a nine digit front panel display showing: days, hours, minutes and seconds; to a pen recorder time marker; and also to data tapes in the form of an F.S.K. (Frequency Shift Keyed) serial bit stream containing either days and hours or minutes and seconds information. These F.S.K. Signals (carrier frequencies 5kHz and 10kHz, and modulation frequency 2.5kHz) are mixed with the goniometer calibration information at $\sim 27.5\text{Hz}$ and recorded together.

On playback lowpass and highpass filters separate these. The F.S.K. signals are decoded and the record time displayed, being delayed by 38.4ms, this being the time required to read the F.S.K. serial information. The calibration pulses are used to determine the signal bearing as described in Chapter 3.

4.5 Clock Description and Operation

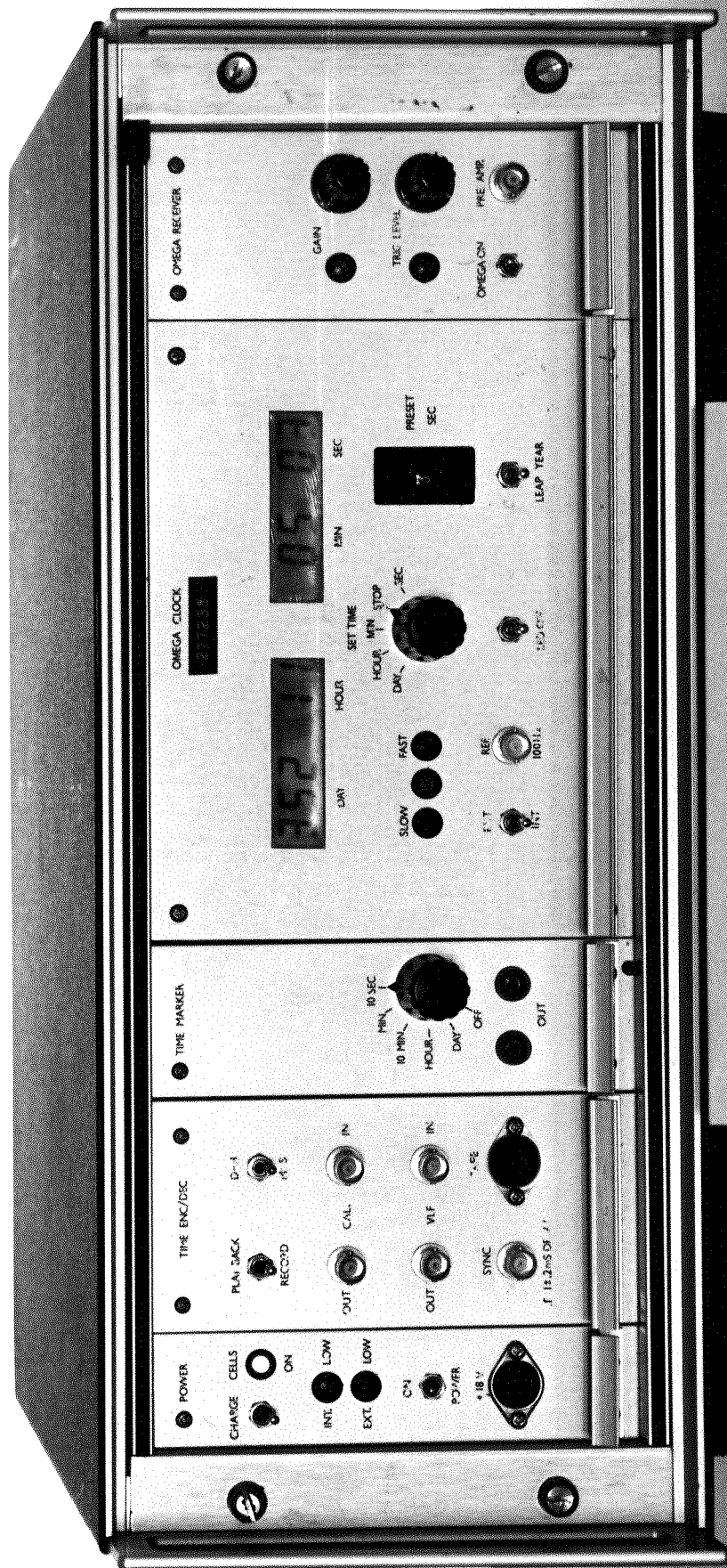
4.5.1 The Preamplifier and Antenna

A tuned preamplifier, (Blixhavn and Lyngdal, 1976), preferentially amplifies 10.2kHz signals. The preamplifier, which is mounted in a small waterproof box, can be placed some distance from the clock itself. It is powered, via the signal feeder lead, from the Omega Receiver (section 4.5.2).

The preamplifier is fed from a simple long wire antenna; ~ 1 metre is sufficient in Norway and ~ 4 metres in England.

4.5.2 Omega Receiver Module (see figure 4.1)

The Omega Receiver further amplifies and filters the 10.2kHz signals. The gain is adjusted using the panel mounted control with the signal amplitude indicated by an LED. Ideally the latter should light brightly for about one second in every ten seconds. A receiver



omega locked clock and
time code generator / decoder

fig 4-1

trigger level control, also mounted on the front panel, defines the signal amplitude required to enable the logic circuitry. This circuitry once triggered, as shown by a lighted LED, will ignore signal peaks for the next eight or nine seconds, giving some immunity against noise.

The module can be connected or disconnected from the clock module using a panel mounted switch.

4.5.3 Omega Clock Module (see figure 4.1)

This contains the crystal controlled clock, phase comparison circuitry, and synchronisation circuitry. A nine digit liquid crystal display gives the time information as: days, hours, minutes and seconds in the record mode and, either days and hours, or alternatively minutes and seconds in the replay mode.

The clock time must be set initially to within ± 4 seconds of UT using the panel mounted control. The clock will then free run without synchronisation signals. The pre-set seconds thumb wheel switch is then set such that it corresponds to the least significant seconds digit at the true start time of the strongest 10.2kHz pulse.

The phase relationship between the Omega pulse and the least significant digit of clock time is given by LED's. These indicate that the clock is either slow, fast, or correct with reference to the Omega signal.

Other controls and facilities include provision to programme a leap year into the clock and an LED control. This switches off all LED's except those in the power module, see section 4.5.6., thus effecting a considerable power saving. The internal 100Hz clocking signal can be overridden, if required, and an external 100Hz frequency standard used.

4.5.4 Time Encode/Decode Module (see figure 4.1)

For tape encoding the playback/record switch is adjusted to record, the goniometer outputs appropriately connected to CALibration_{IN} and VLF_{IN}, and the tape recorder to the standard 5 pin DIN socket. Calibration pulses from the goniometer, see section 4.6, are mixed internally with the FSK signals before being fed to the tape recorder. ELF/VLF signals pass directly to the tape recorder. The record level of the clock/calibration pulse channel is not critical.

Encoding of either the days and hours, or the minutes and seconds is possible and a switch biased to minutes and seconds is provided. Day and hour information is normally recorded at the start of every tape side.

In the playback mode the VLF and calibration pulses are available at VLF_{OUT} and CALibration_{OUT}, the latter having been filtered from the time coding (see section 4.6).

The playback/record switch does not interfere with the clock operation. The 'sync' output provides, in the playback mode only, a clock pulse whose leading edge is delayed by $1.0 \pm 0.2\text{ms}$.

4.5.5 Time Marker Module (see figure 4.1)

This module exactly follows that of Blixhavn and Lyngdal (1976) and produces a time dependent pattern, see Appendix 2, for marking a pen recorder chart. An external power supply is required which should be connected in series with the module and pen recorder. The open circuit voltage must not exceed 55 volts peak to peak and the closed circuit current must be less than 150mA.

4.5.6 Power Module (see figure 4.1)

Clock power is provided by external 3x6V 5-ampere-hour lead acid gel batteries. Current consumption is $\sim 650\text{mA}$. Should this voltage (V_{EXT}) fall below 15 volts all circuitry except that associated with the crystal controlled clock, shuts down, that is no "Omega" synchronisation or time encoding is possible. The crystal clock then operates on an internal 12V 5-ampere-hour battery pack with a considerably reduced power requirement, ($\sim 24\text{mA}$). LED's indicate external and internal batteries low and internal cells on. Internal battery charge is controlled by the charge switch. In the ON condition V_{EXT} charges the internal cells in addition to powering the clock.

4.6 Goniometer Interfacing: Time Encode/Decode Module

Previous practise has been to use a calibration spike (duration $\approx 0.6\text{ms}$), obtained by differentiating a short pulse, as the goniometer reference signal (Jarvis, 1976). When mixed with clock timing information the calibration pulse (duration 0.6ms), rather than the spike, was found

more convenient to deal with.

Figures 4.2 and 4.3 make the mixing and retrieval of the F.S.K. and calibration signals clear. During data collection the F.S.K. is mixed with the calibration pulses which have been slightly filtered to restrict their spectral content. Due to the limited frequency response of the tape recorder, the process of recording smooths the F.S.K. pulse stream to an approximately sinusoidal data stream. On playback the calibration pulses are differentiated by the action of the tape recorder, and these signals, together with the F.S.K. signal, are amplified and then separated by filtering. Both the calibration and F.S.K. signals are then fed to comparators which reconstitute the pulses. In the calibration pulse channel the comparator trigger level is set close to zero volts, subject to the limitation of residual F.S.K. noise (see figure 4.3). Any practical record level will then provide sufficient signal to trigger the comparator. The resultant pulse width is dependent upon the comparator trigger and input voltages. However, providing that the input signal leading edge is sufficiently fast the output leading edge should be approximately independent of the trigger level or the input signal level. This was confirmed, after suitable interfacing had been provided (section 4.7) using the Sheffield University Whistler Analyser (section 3.6). For a 4:1 variation in replay amplitude (no more was possible since the Analyser could not operate with smaller or larger signals) no change in the bearing of a calibration signal could be detected down to a level of $\pm 1^\circ$.

4.7 Whistler Analyser Interface

In order to describe the clock analyser interface it is first necessary to describe, more fully, certain aspects of the Whistler Analyser.

Two Revox tape decks are provided. Data tapes are played on one deck and the stereo output fed to a continuous tape loop on the second. Signals of interest are captured on this two second loop which is repeatedly fed to a high persistence CRT display. To prevent drift of the display across the screen on subsequent sweeps, a sync pulse is recorded on the same channel as the calibration pulse.

In the analysis of the data presented in Chapter 6, the clock was electrically located between these two tape recorders. Before analysis could begin, however, two problems had to be first overcome.

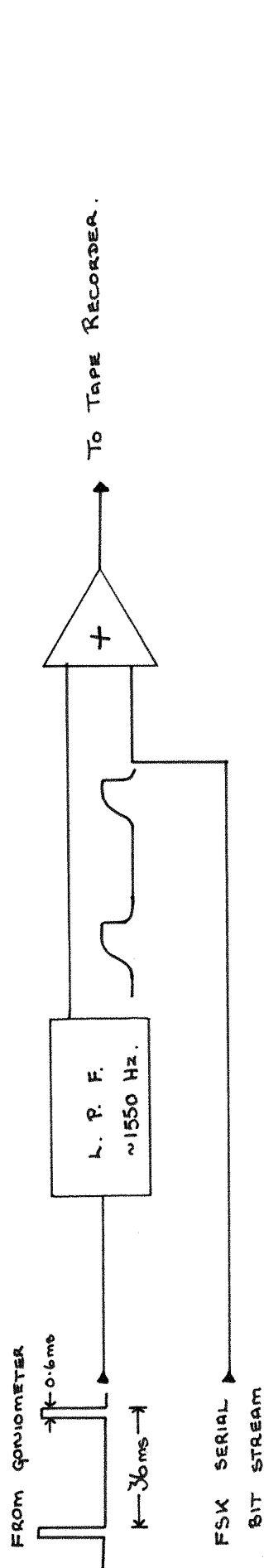


Fig. 4:2 Block Diagram Of Record Mixer Showing Typical Voltage Levels and Waveforms.

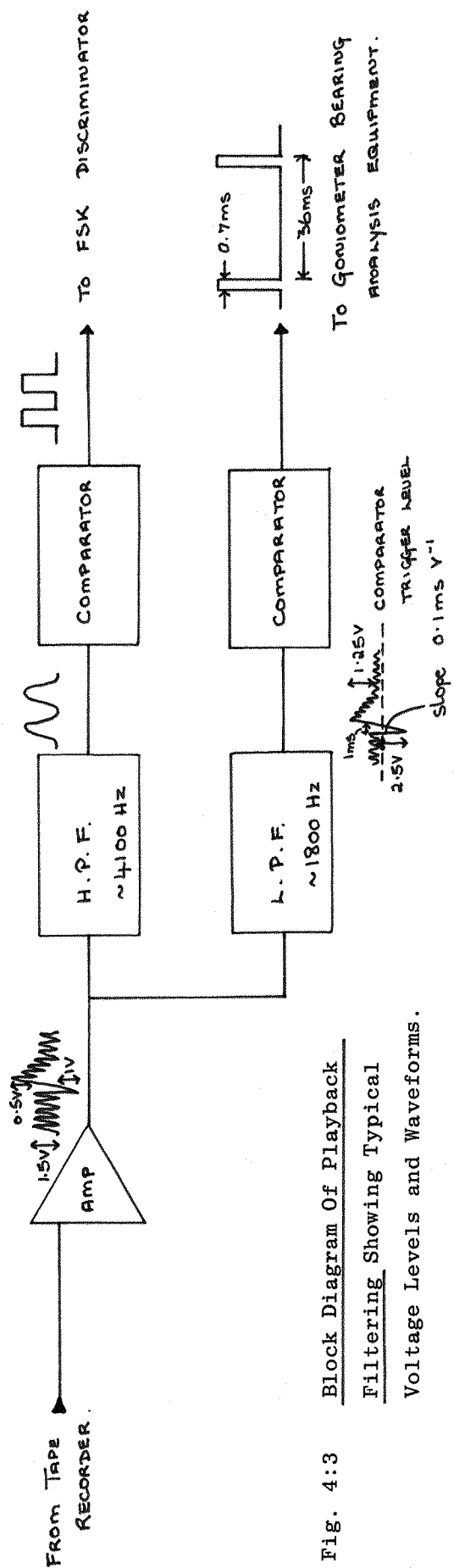


Fig. 4:3 Block Diagram Of Playback Filtering Showing Typical Voltage Levels and Waveforms.

Firstly, the calibration pulse comparator in the clock decoder has been designed to trigger on a negative going edge (see figure 4.3), this being compatible with a Uher 4200 tape recorder. The analyser output derived from Revox tape deck number one is, however, inverted with respect to the Uher. This necessitated the use of an inverter on the clock input (CAL_{IN}) (see figure 4.4a), since otherwise bearings are dependent upon the calibration signal amplitude. Secondly, for correct operation of the Analyser the calibration pulse amplitude (12V) at the clock output must be comparable with the sync pulse amplitude of 1V. Resistive attenuators were unsuccessful because they loaded the sync pulse. Figure 4.4b shows the adopted solution which attenuates the calibration pulse before mixing the two signals. These are then reinverted and fed to the second Revox tape deck.

4.8 Performance

One clock was tested in England and subsequently at Tromsø, Norway, during the campaign of November, 1977. It was introduced into the system during the experiment of March/April, 1979. On all occasions it performed admirably. It has been used extensively in the data analysis presented in Chapter 6.

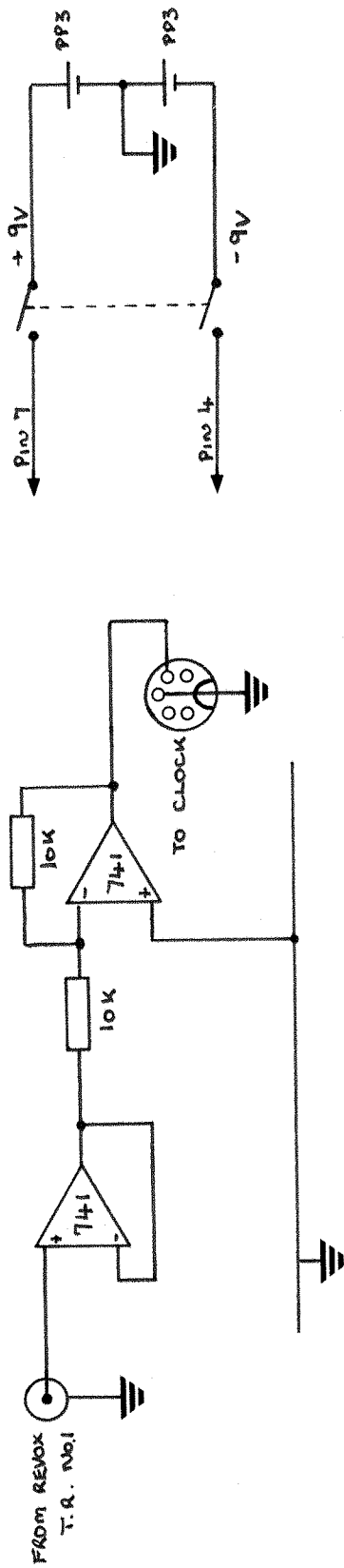


Fig. 4:4a Inverter For Use With Revox Tape Recorder.

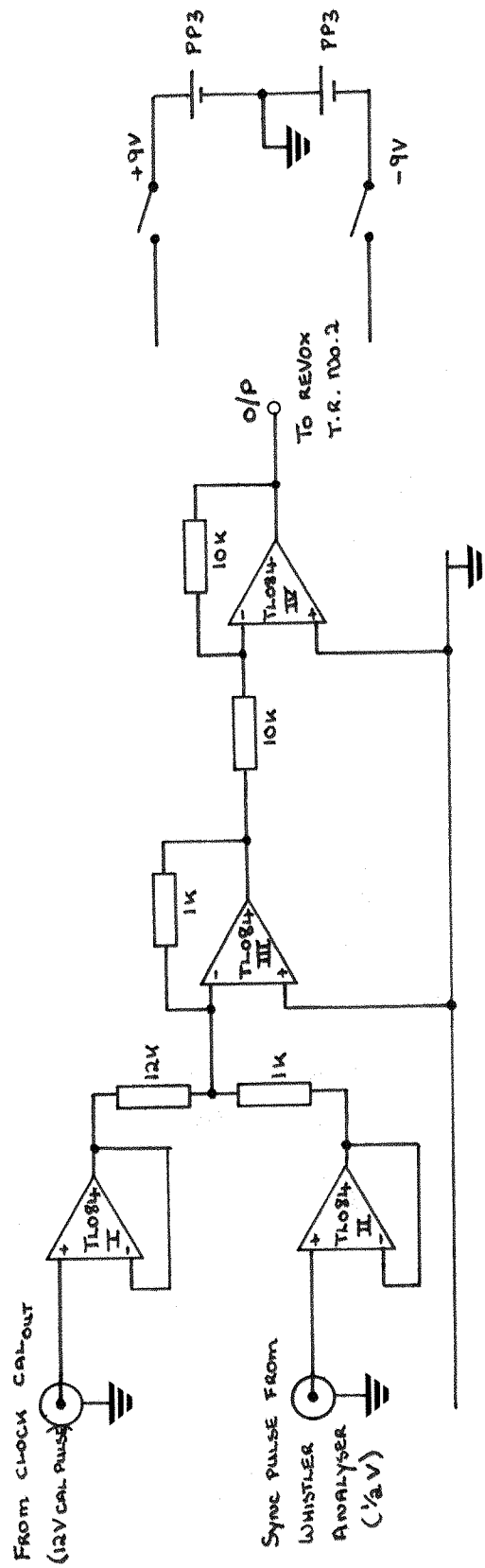


Fig. 4:4b Sync Pulse/Cal Pulse Mixer.

CHAPTER FIVE

Goniometer Experiments During The Period 1977 to 1979

5.1 Introduction

The purpose of this chapter is to review the various multi-station goniometer experiments in which the author has directly participated. Most of these experiments took place in auroral Scandinavia and the locations of the various Scandinavian field sites, together with the Norwegian rocket range near Andenes, Andøya, and the Swedish rocket range "Esrang", near Kiruna, are shown in figure 5.1. The geographic co-ordinates of these locations are shown in table 5.1.

Goniometer experiments were generally associated with other active or passive experiments, provided by groups from various institutions and universities. These invariably involved the release of an ionospheric sounding rocket during certain predetermined meteorological and geophysical conditions. Since many weeks might be spent awaiting the required conditions the opportunity was seized to obtain considerable background data. In the following sections the aim of the various experiments are briefly discussed, the duration of background recording defined, and the results of any analyses indicated. The implications of these results on the design of the goniometer system used in the following experiments is discussed.

A resumé of the ELF/VLF activity, as monitored by the goniometer stations, has been prepared by Madden, University of Southampton (private communication, 1979).

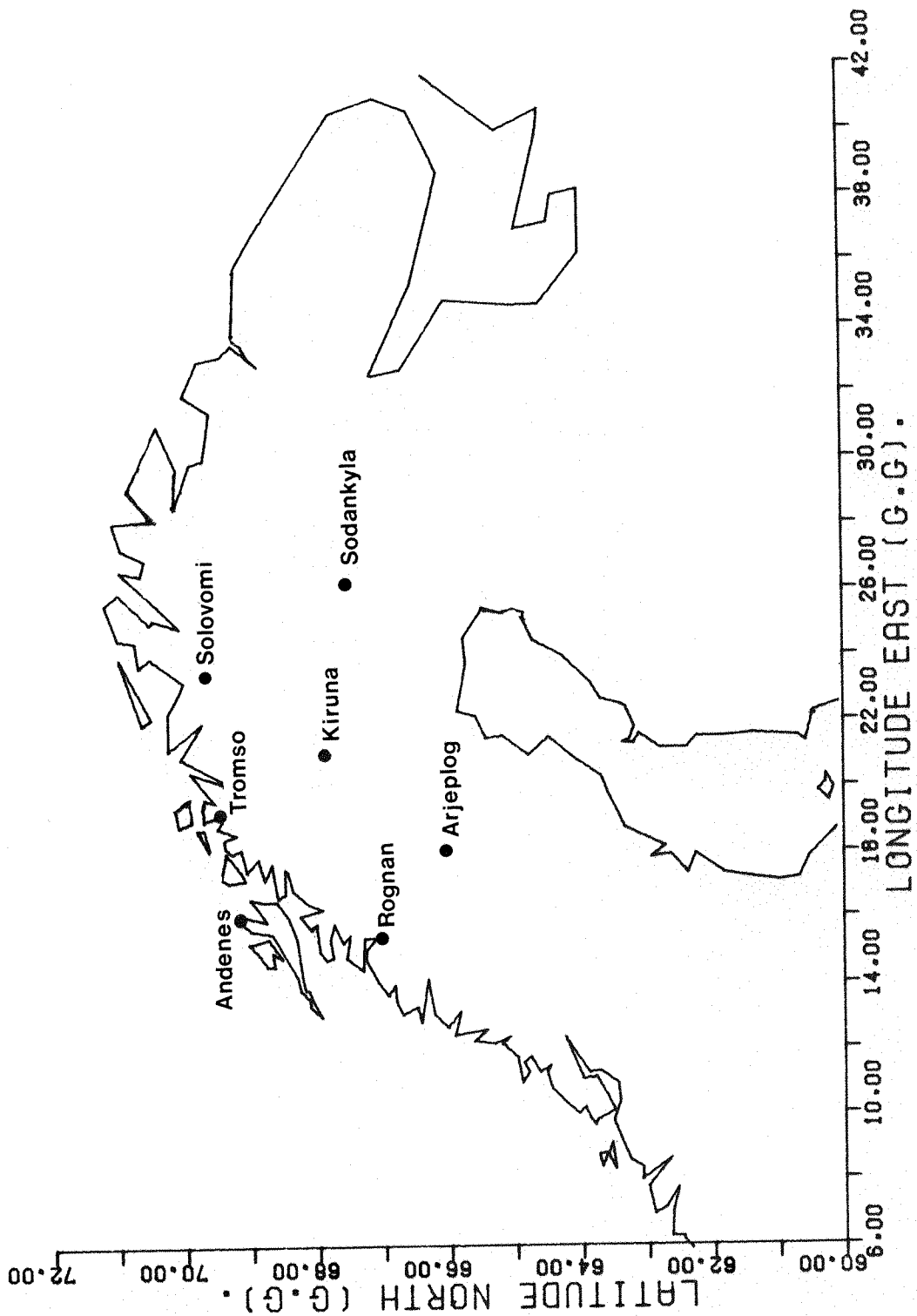


Fig. 5:1 Northern Scandinavia Showing Locations Of Goniometer Stations and Rocket Ranges.

Field Site	Country	Geographic Co-ordinates	L Value At 100Km
Arjeplog	Sweden	66.00°N 18.00°E	4.91
Husafell	Iceland	64.73°N 20.83°W	
Rognan	Norway	67.05°N 15.30°E	
" Siglufjordur	Iceland	66.20°N 19.00°W	5.16
Skaftafell	Iceland	64.00°N 17.00°W	
Sodankyla	Finland	67.51°N 26.25°E	
Solovomi	Norway	69.53°N 23.62°E	6.38
Lavangsdalen Valley near Tromsø	Norway	69.43°N 19.27°E	
Co-ordinates apply to the field sites, not the nearest town by which they are called.			

Table 5.1 Field Sites Used During The Period 1977 to 1979

5.2 Project Trigger

Nominal background recording period:- 7 February to 25 February 1977 from 17 UT to 23 UT.

Goniometer sites were located near Tromsø (Lavangsdalen) Norway, and near Sodankyla, Finland.

Details of Project Trigger, together with some experimental results are presented in Holmgren et al. (1979a) and Holmgren et al. (1979b). On 11 February 1977 a caesium charge was released from a rocket into the ionosphere at a height of 165km where collisional ionization took place. Release took place during quiet auroral conditions.

This goniometer experiment was conducted, as were subsequent barium release associated experiments to follow up on the work of Everhard-Bakker et al. (1976). They reported that $\sim 1\frac{1}{2}$ hours subsequent to a barium release over Alaska short (~ 50 ms) ELF rising and falling elements were detected. They hypothesised that these signals might have been stimulated via the electron cyclotron instability (Brice, 1964) when the barium reached the equatorial plane.

No such emissions were detected during the rocket flight or within two hours of the end of the flight.

5.3 Project Porcupine

Nominal background recording period:- 5 March to 24 March 1977 from 18 UT to 22 UT.

Goniometer stations were located near Tromsø (Lavangsdalen), Norway and Sodankyla, Finland.

Details of Project Porcupine can be found in Haerendel (1976). The Porcupine programme consisted of a series of highly instrumented rockets launched over a period of several years. Each carried electric, magnetic and charged particle sensors on booms (viz Porcupine), a shaped barium injection experiment and several daughter payloads, themselves carrying boom mounted sensors. The Porcupine 2 rocket was launched on 20 March 1977 at 19:22 UT.

Reiger et al. (1979) discuss some results of the flight.

5.4 Iceland Campaign *

Nominal background recording period:- 17 August to 5 September 1977 from 09 UT to 15 UT.

Goniometer stations were located near:- Siglufjörður, Husafell, Skaftafell.

Madden et al. (1978) report the results of preliminary analyses on chorus elements recorded in the morning sector. For the period analysed chorus bearings were obtained and interpreted as resulting from well defined ionospheric exit points, similar to those obtained for whistlers (Jarvis, 1976).

5.5 Second British High Latitude Campaign (H.L.C.)*

Nominal background recording period:- 21 October to 15 December 1977 at various times.

Goniometer stations located near:- Tromsø (University of Southampton), Rognan (University of Sheffield).

The second H.L.C. (Thomas et al, 1975) involved the use of a comprehensive set of ground based, rocket borne and satellite measuring instruments in order to investigate high latitude ionospheric and associated magnetospheric phenomena.

During the above period Skylark rocket SL1421 and Fulmar rocket F1 (November 1977) and Fulmar F4 (5 December 1977) were launched. The latter carried E and B sensors, due to the University of Sheffield. The failure of a tape recorder drive belt near the start of the flight of SL1421 resulted in no goniometer measurements at Tromsø.

Although scheduled for launch during this period SL1424 and F6 were not launched. Both of these rockets, also carrying University of Sheffield E and B field sensors, were rescheduled, see section 5.6.

*The authors participation was limited to technical preparation etc. for these campaigns.

5.6 Second British H.L.C. (Repeat)

Nominal background recording period:- 3 February 1978 to 26 February 1978 from 21 UT to 03 UT.

Goniometer stations were located near:- Tromsø (Lavangsdalen), Norway, Rognan, Norway, Solovomi, Norway.

Rockets to be launched during this period:- SL1424, F6.

Neither rocket was launched. Analyses of certain background data are to be published in Madden (1981).

The Rognan field site, although fairly quiet to mains harmonic interference, did suffer from heavy interference due to the nearby (~ 100 km distant) naval VLF transmitter at Bodø on 16.4kHz, and the nearby (322km distant) Omega transmitter at Aldra (66.42°N , 8.13°E). During certain adverse conditions these caused overloading of the system preamplifier and goniometer (Madden, 1981). As a result in the subsequent H.L.C., section 5.7, the gain of the preamplifier at this station was reduced from ~ 60 dB to ~ 48 dB.

5.7 Second British H.L.C. (Repeat)

Nominal background recording period 21 October 1978 to 15 November 1978 from 21 UT to 03 UT.

Goniometer stations were located:- as defined in section 5.6.

Rockets to be launched during this period:- SL1424, F6.

Skylark SL1424 was launched on 10 November 1978 at 04-14-22 UT when an ELF/VLF chorus event was observed by the Geos II satellite and with a network of ground based receivers. The satellite, above the equator, the rocket, in the ionosphere and the ground based receivers were all approximately in magnetic conjugacy.

5.7.1 General

The period of flight of SL1424 was characterised by discrete ELF risers. These were detected by the rocket E and B field sensors (Cannon et al., 1980) and by the Tromsø and Solovomi ground stations. The goniometer receiver at Rognan, although fully operational received

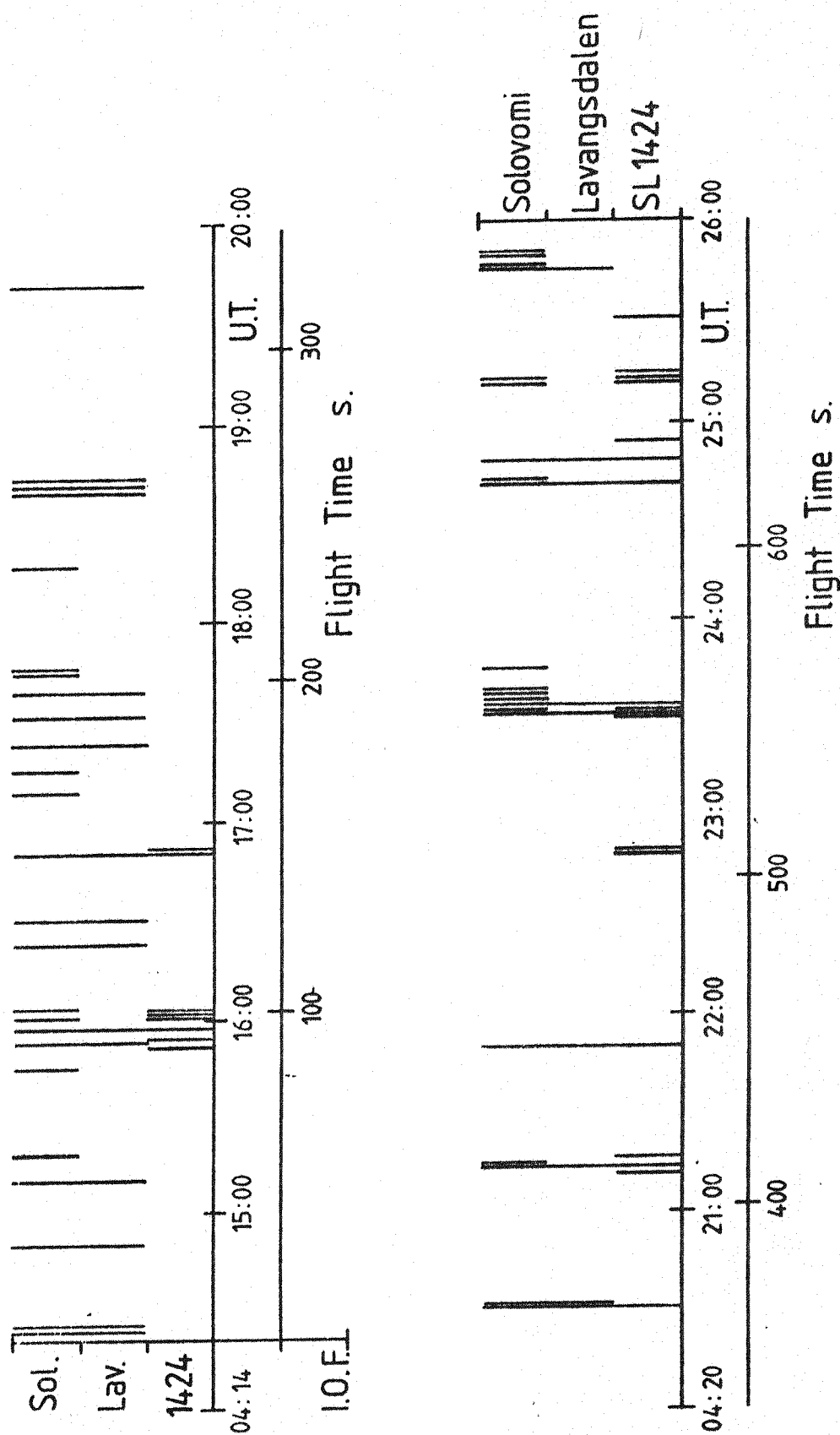


Fig. 5:2 Times Of Risers Recorded During The Flight Of SL1424.

no risers during the flight. It did, however, detect risers over the period 02 to 03 UT. Solovomi and Tromsø detected a steady stream of risers over the period 02 UT to 05.45 UT at which time operation of the stations terminated. Filter bank and high speed quick look data from the Geos II S300 experiment indicates an ELF chorus event from about 00 UT to 05 UT with risers occurring at 60 ± 10 per minute over the rocket flight (Cannon et al., 1980).

5.7.2 Timing

Using the spectrum analyser hard copy output, described in section 3.6, the time of each ground recorded rising element was determined. The Norwegian Omega signals (Burgess and Jones, 1975) were used for timing reference and this resulted in an accuracy of better than ± 0.25 second. Using similar techniques Madahar (private communication, 1979), determined the times of rising elements recorded on SL1424. The results of these analyses are presented in figure 5.2.

Three points should be noted. Firstly, Solovomi received more rising elements than Lavangsdalen (Tromsø). Secondly, the rocket received less risers than Tromsø. (Note that the equipmental noise threshold of the rocket payload is higher than that of the ground stations). Thirdly, there are many common elements, i.e. recorded at both ground stations and on the rocket. Conversely there are many elements specific to just one or two of the three receivers.

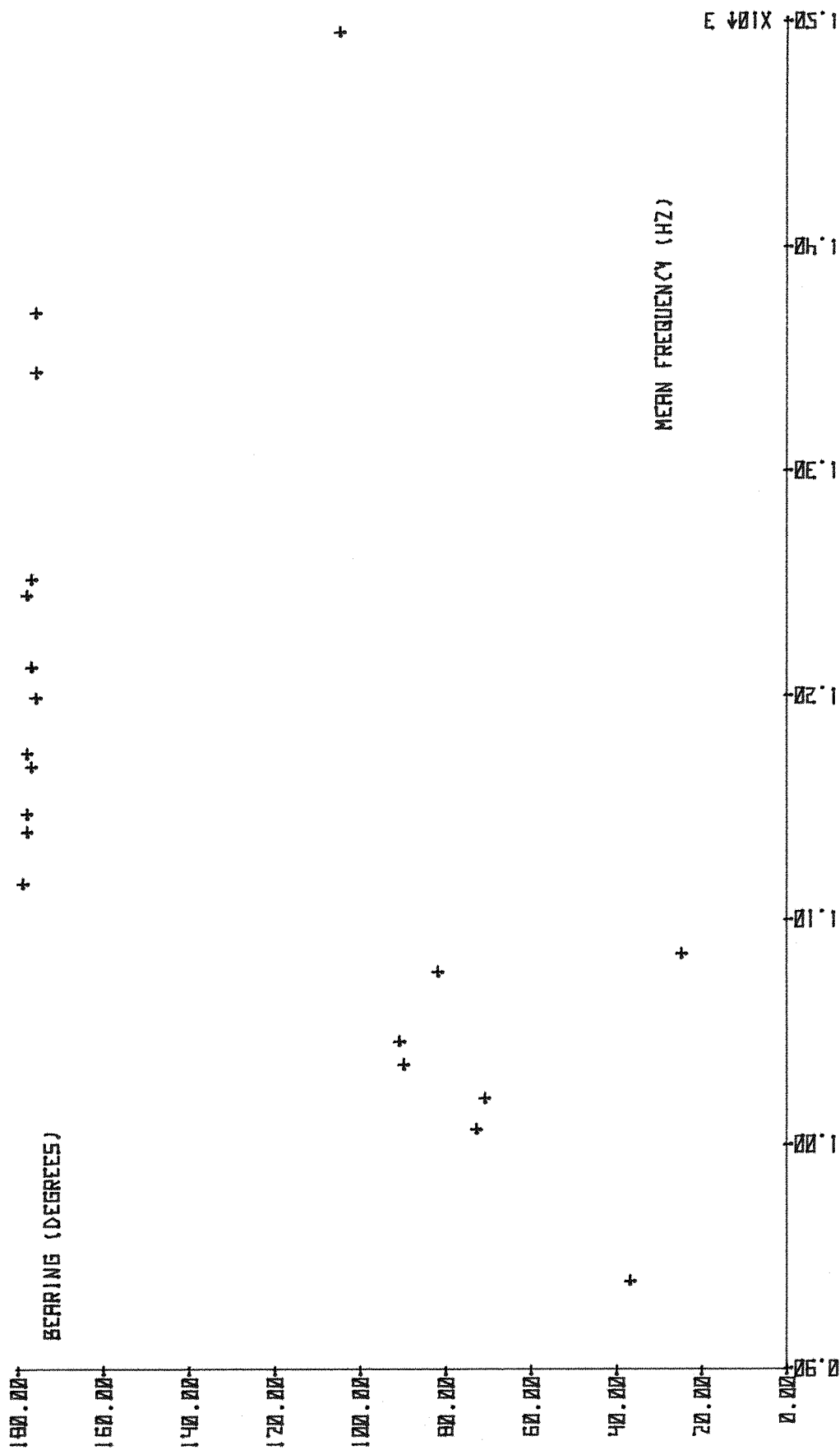
5.7.3 Spectral Analysis

Spectral analysis has revealed that the ground detected risers fall into two frequency bands, approximately defined by $0.9 < f < 1.4$ kHz and $1.4 < f < 1.8$ kHz

5.7.4 Azimuthal Bearing

Using the techniques described in section 3.6, the azimuthal bearings of various rising elements, recorded at Tromsø, were determined.

The analysis technique enables one to sample all, or part, of the risers and this was done in certain cases to check for self consistency in the bearings. The results are presented in figure 5.3, where the bearing is plotted as a function of the centre frequency of the sampled portion of the riser.



BEARING ANGLE VERSUS THE MEAN FREQUENCY OF THE SAMPLED PORTION OF THE RISER.

FIG. 5.3

The bearings divide into two general groups, in two frequency bands. It is believed that those bearings close to 180° (or 0°), which all fall in the higher frequency band, are the result of sampling very strong noise bands. Determination of an emission bearing requires high temporal resolution resulting in low frequency resolution. Consequently, when an emission is sampled all signals, emissions and noise, within the 320 Hz analyser filter bandwidth are fed to the correlator (see section 3.6). Many risers in this study showed a peak in their amplitude spectrum between about 0.9kHz and 1.1kHz and the system amplitude response peaked at approximately 1.13kHz. Thus sampling at the high frequency end of the riser, fed a relatively low amplitude riser signal, together with a relatively high amplitude noise signal, (due to the preamplifier/system resonance peak), to the correlator. This noise is believed to be primarily mains harmonic interference. Although this hypothesis has yet to be verified, by sampling the mains interference, there are two arguments in its favour. Firstly, a bearing of 0° is consistent with the location of the nearest mains source. Secondly, natural signals do not normally provide such consistent bearings. This is especially so near system resonance where the bearings are less reliable than away from resonance.

It is therefore concluded that those bearings not close to 180° (0°) and which all fall in the lower frequency band, represent true estimates of the ionospheric chorus sources. An average bearing of $69^\circ \pm 29^\circ$ was obtained.

5.7.5 Discussion And Conclusions

As previously stated, during the rocket flight Tromsø and Solovomi ground stations received risers but the Rognan ground station did not. This indicates that the ionospheric exit point of the risers was located to the north of Rognan during the flight. Furthermore, assuming that the system sensitivities at Solovomi and Tromsø were the same (identical equipment was used), the higher riser count at Solovomi indicates a source nearer to that station. This is consistent with the bearing of $69^\circ \pm 29^\circ$ since Solovomi subtends a bearing angle of $\sim 92^\circ$ at Tromsø (see section 5.7.4).

If all the risers originated from one source then a corollary of this would be that the rocket, fired north-west from Andenes, see figure 5.1, was directed away from the ionospheric source of the chorus. It should be noted, however, that none of these goniometer analysed risers were recorded on the rocket and it is possible that two or more distinct chorus source regions exist.

5.7.6 Suggestions For Further Work

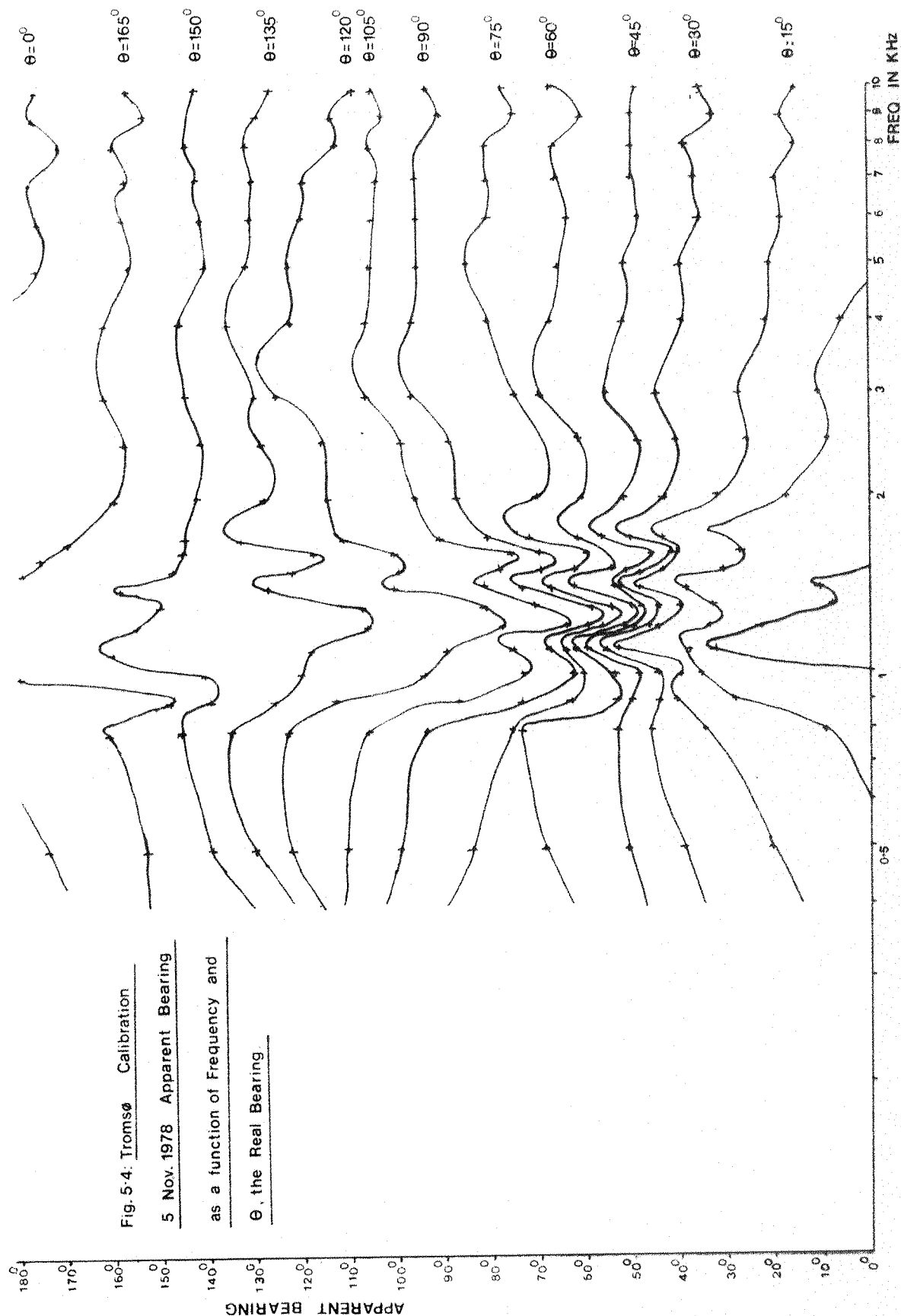
Further goniometer analyses of risers recorded during the rocket flight are required in order to ascertain why such a large spread in bearing angles has been obtained (see section 5.7.7). Data reduction should also examine the possibility of a correlation between bearing angle and the absence or detection of risers aboard the rocket.

Future analyses of goniometer data should attempt to examine the movement, if any, of the ionospheric exit point during the period 02 UT to 03 UT when goniometered risers were recorded at both Rognan and Tromsø. This may help to understand why Rognan received risers over a shorter period that night. One may speculate that the electron distribution involved in the chorus generation has suffered eastward gradient B drift along a constant L-shell. This would move the exit point N.E. away from Rognan and towards Tromsø and Solovomi. A parallel examination of Geos II particle data is required. These studies may also reveal why Geos II detected an ELF chorus event over two hours earlier than the ground stations.

5.7.7. System Implications For Future Campaigns

The variation in bearing angle of $\pm 29^\circ$ can be attributed to one or more of three causes. Firstly, a real scatter in riser exit points. Secondly, a purely statistical variation due to the signals being noisy. Thirdly, badly matched preamplifier channels (section 3.4.2) or other equipmental problems. The latter was investigated in some detail.

Figure 5.4, the result of an azimuthal calibration at Tromsø, shows that the bearing angles 0° (180°) and 90° (270°) did not result in a constant apparent bearing as a function of frequency. This was not expected, since the signals passed through one channel only. As such any amplitude and phase mismatching between channels should have been of no consequence. It was demonstrated that these fluctuations resulted from crosstalk between the preamplifier channels and was remedied, before the next experiment, by physically separating the two preamplifiers, previously mounted in the same container, into two boxes (see also section 3.4.2). Since the fluctuations are most noticeable near the preamplifier resonant frequencies it was deduced that the said coupling took place via the closely matched input transformers. Paradoxically, the better the channel matching, as required by section 3.4.2, the



greater the crosstalk and system degradation.

Crosstalk has similarly degraded the system performance at other azimuthal angles.

5.8 1979 Spring Campaign

Nominal background recording period:- 14 March 1979 to 4 April 1979 primarily from 19 UT to 01 UT.

Goniometer stations located near Tromsø, Norway; Sodankyla, Finland; Arjeplog, Sweden.

Rockets to be launched during this period:- F6, P208A, Barium Geos, two Porcupine payloads.

Rockets Porcupine and F6 have been described in sections 5.3 and 5.5 respectively.

Both these Porcupine rockets were launched successfully, the first on 19 March 1978 at ~23 UT and the second on 31 March 1978 at ~22.30 UT. In both cases, photo-ionization of the injected Barium cloud took place, however, no unusual ELF/VLF emissions were detected.

F6 was launched on 19 March 1978, at 00.34 into a chorus event, however, the second stage failed to ignite.

Petrel P208A (University of Sheffield) carried a payload to measure the wave fields in the ionosphere due to ELF signals from a ground based ELF transmitter. The transmitter due to Koons (1980) was located near Skibotn, Norway (geographic co-ordinates 69°50'N, 29°15'E). The rocket was launched from the Andøya range on 28 March 1979. Unfortunately the telemetry failed early on during the flight. The ELF transmissions were, however, received by the Southampton goniometer stations and the data is at present being analysed by the University of Sheffield, U.K. (Yearby, private communication, 1979).

Barium Geos consisted of a Nike Black Brant VC rocket, to be launched from Esrange, carrying a barium jet experiment together with wave and particle experiments. Due to a low positive correlation between favourable weather and geophysical conditions, the rocket was not launched.

Analyses of background data collected during this campaign forms the basis of Chapter 6 and 7. The "Omega" locked clock, described in Chapter 4, was used at Tromsø throughout this period.

CHAPTER SIX

Radiation Of 1kHz Timing Signals Via The Night-Time

Auroral Ionosphere - Data Analyses And Interpretation

6.1 Introduction

Over the period March 15 to April 4 1979 the Space Radiophysics Group at Southampton University conducted a programme of ELF/VLF goniometer (direction finding) recordings in Northern Scandinavia. It should be pointed out that throughout this period the "Omega" navigation transmitter located at Aldra, Norway was inoperative, significantly increasing the system sensitivity above that obtained during previous, similar experiments.

On certain days it was noted that six pips were occasionally heard, on the hour; these were similar to those broadcast by radio stations for public timing information. A spectrogram of these signals can be seen in figure 6.7. At the time it was a matter of conjecture whether these "pips" were propagating ELF signals or whether they were due to non-linearities in the receiving equipment causing demodulation of a higher frequency wave.

Here evidence is presented from which it is concluded that these pips were, in fact, propagating ELF signals produced by a mechanism in the D-region of the auroral ionosphere.

6.2 The Experiment

Three ELF/VLF goniometer receiving systems (bandwidth 0.5kHz to 16kHz), which have been described in detail in Chapter 3, were operated in Northern Scandinavia. These were located at Lavangsdalen, near Tromsø, Norway, and at Arjeplog, Sweden (operational 15 March to 4 April, 1979) and at Sodankyla, Finland (operational 22 March to 5 April). At this latter station two channel, (non-goniometered), measurements were made during the previous week.

The geographic and geomagnetic co-ordinates of these locations are given in figure 5.1 and table 5.1. The location of the goniometer field sites, rather than those of the appropriate observatories, are given. In addition, the L value at 100km altitude, is shown, calculated from Stassinopoulos (1970).

Due to logistical constraints, it was unfortunately impossible to maintain a 24 hour recording schedule over the above period. The schedule for these stations was prearranged, in conjunction with rocket experiments, to be from 19 UT to 00 UT over the period 15 March to 1 April inclusive, and from 20 UT to 00 UT on April 2,3 and 4. Additionally scheduled recordings were made between 11 UT and 16 UT on 28 March 1979. Outside the above times each station operated independently whenever feasible.

In addition a receiver designed by T. Turunen was operated on 22 March alongside the Southampton Receiver. The former consisted of a long (500m) wire antenna lying on the ground, responding to the electric field of the radio wave, which fed a low noise preamplifier.

Field assessment of a new ELF receiver, see chapters 8, 9 and 10, with a maximum passband of 1 Hz to 1kHz, was also taking place at Tromsø at this time. The receiver was operated with either a mu-metal cored antenna or an air cored antenna; only the latter had a significant sensitivity at 1kHz. This particular antenna was operated intermittently between 31 March and 4 April.

6.3 Identification Of Transmitter(s) Responsible

Sometimes, particularly at Sodankyla it was possible to hear distorted music immediately preceding the pips. More careful investigation of the Sodankyla tapes showed that of the twenty-nine occasions when pips were detected nine occurred within the period 22 UT to 01 UT. On all but one of these nine occasions, distorted music (Midnight in Moscow) was heard. When, however, pips were heard outside the above time period no associated music was detected. With reference to the World Radio and T.V. Handbook (1979), the music was identified as the signature tune of the Russian Internal Service "Second Programme or Channel", known as Mayak or Lighthouse. This is a musical programme/channel intended for all Union coverage and is transmitted on various frequencies, and from many transmitters in the U.S.S.R. The 1kHz time pips are generally transmitted every hour and are preceded by this signature tune. Soviet internal transmissions also include the "First Programme" and various "local programmes". Each of these also has a specific signature tune which is broadcast occasionally. Timing pips are also normally transmitted on each hour, (Meacham, private communication, 1979) on these other services.

Using the above publication the Soviet internal schedules were studied over the frequency range 155kHz to 12.005MHz. On two frequencies only, 173kHz and 657kHz, it was discovered that the U.S.S.R. broadcasts its "First Programme" from 02 UT to 22 UT and its "Second Programme" from 22 UT to 02 UT. This agrees well with the presence or absence of the "Second Programme" signature tune outlined above. It would thus seem likely that the transmitter, or transmitters, responsible for this effect operate on either one or both of these frequencies; however, contributions from other transmitters on other frequencies cannot be ruled out. This subject is revisited in section 7.2.5.

Table 6.1 lists the transmitters operational on 173kHz and 657kHz, together with the most powerful of the Soviet transmitters on other frequencies, that are within a 1500km radius of Sodankyla. Maximum output powers permitted by the Geneva Plan of 1975 are given together with transmitter locations (also shown in figure 6.1). This information was obtained from the above handbook, from The Finnish Broadcasting Co. Ltd., (1979), and from the European Broadcasting Union (1979a).

Figure 6.2 shows the transmission schedules of these various transmitters.

LF Transmitter Location	Geographic Co-ordinates of Transmitter	Power (kW)	Frequency (kHz)
Kaliningrad	54° 45' N 20° 30' E	1000kW	173kHz
Moscow	55° 45' N 37° 38' E	500kW	173kHz
Syktvykar *	61° 41' N 50° 31' E	300kW	173kHz
Leningrad	59° 59' N 30° 21' E	1000kW	236kHz
Moscow	55° 45' N 37° 38' E	2000kW	263kHz
Minsk	53° 54' N 27° 34' E	500kW	281kHz
Minsk	53° 54' N 27° 34' E	1000kW	549kHz
Murmansk	68° 58' N 33° 56' E	50kW	657kHz
* operation unconfirmed by E.B.U.			

Table 6.1 Candidate Transmitters

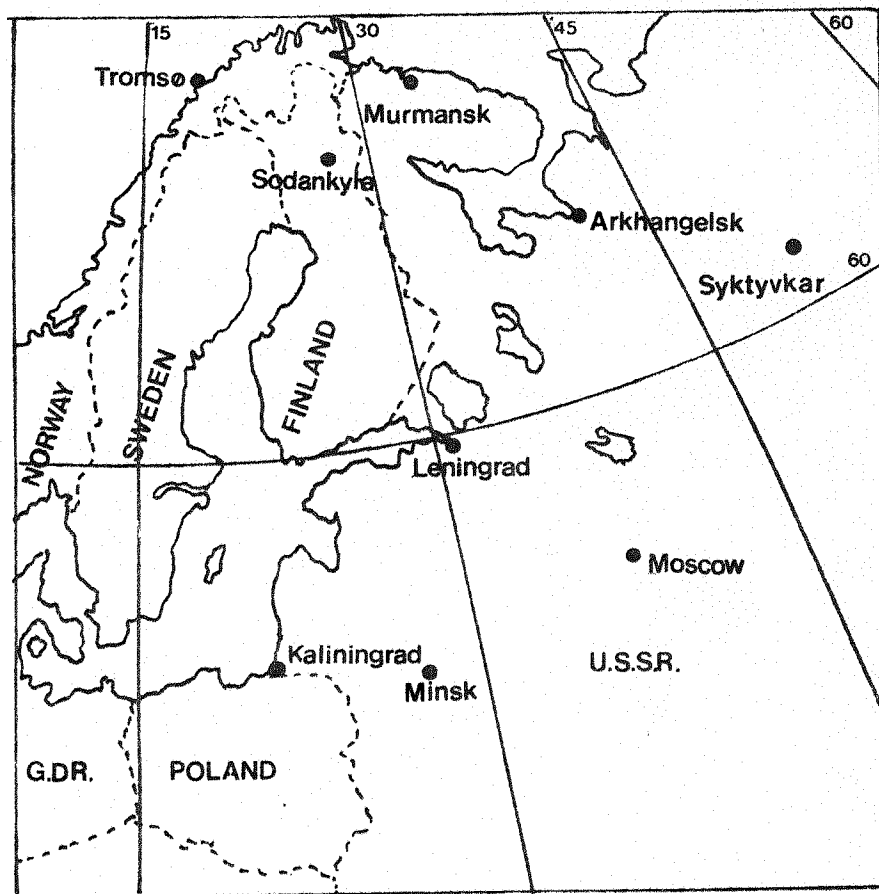


Fig. 6:1 Mercator Projection of Scandinavia and North Western USSR showing the major Soviet high power LF and MF broadcast stations within 1500 km of Sodankyla.

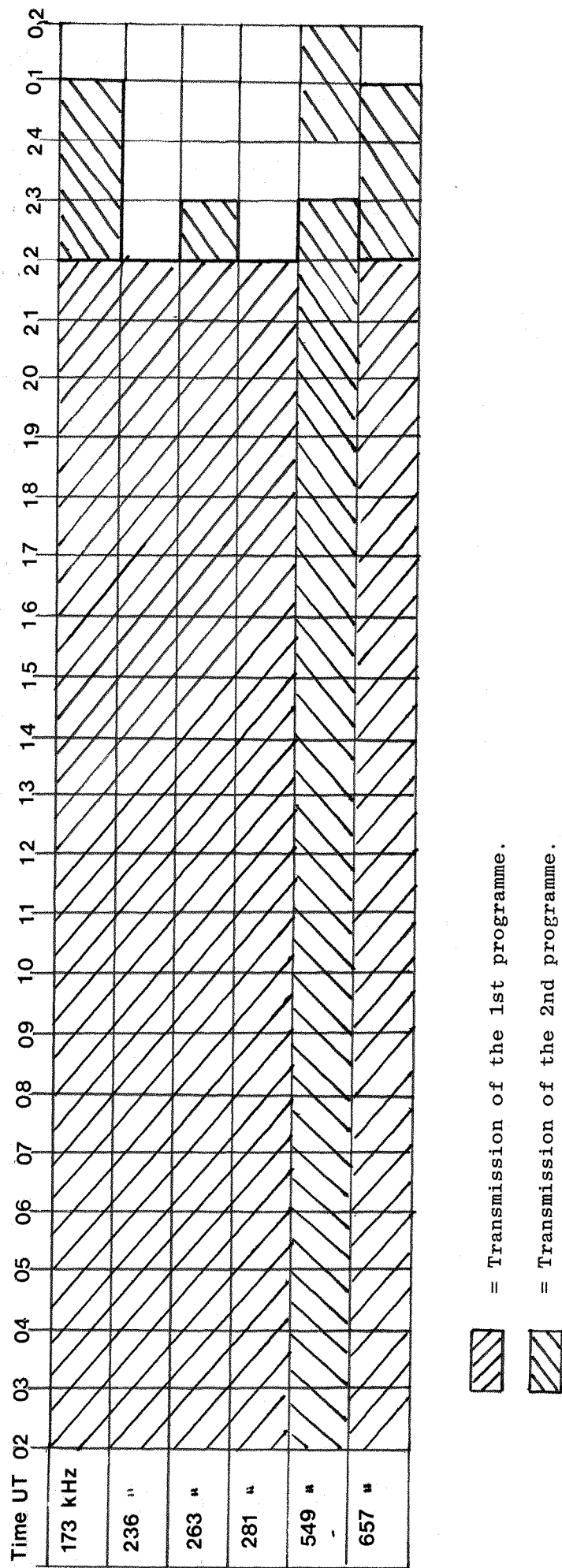


Fig. 6:2 Schedules of the Principal Soviet LF Transmitters within 1500 km of Sodankyla.

6.4 VLF Goniometer System Tests

6.4.1 Introduction

It is clearly of the utmost importance to establish without question that the ELF pips were not the result of demodulation of LF/MF signals within the goniometer or ELF receiving equipment.

Two investigative paths were pursued. The first was an investigation into the amplitude response of various system elements, up to 1MHz, in order to check for an enhanced signal response at LF or MF. The second was the injection of signals, at the suspected transmission frequencies modulated at 1kHz, the modulation frequency of the pips (see section 6.1), into various components of the system. This was to check for demodulation products caused by system non-linearities.

The goniometer system was the principal receiving system used in this work and only this was examined in detail.

6.4.2 Amplitude Response

The goniometer system can be subdivided into aerial, preamplifier, and goniometer receiver itself. Each will now be considered.

6.4.2.1 Aerial

The aerial (see section 3.3.3) used for the goniometer measurements is a magnetic field sensor consisting of a diamond loop aerial, 58 square metres in area, mounted in a vertical plane and constructed from heavy duty coaxial cable. The inner core is used as the aerial. The outer sheath has two purposes. The first is as an electrostatic screen and the second is to bandlimit the aerial response. The latter is effected by breaking the outer screen at the aerial apex (see figure 2.1) and inserting a 0.1 μ f capacitor across the gap, (Smith and Bullough, 1976). Figure 6.3a, reproduced from Smith (1970), shows the equivalent circuit of the aerial and screen, and figure 6.3b, reproduced from Smith and Bullough (1976), shows a schematic of the aerial's frequency response. The response divides into three regions. Firstly, a low frequency region where the output voltage obeys Faraday's Law and is proportional to the angular frequency - ω . Secondly, a resonance region, around 65kHz. This is a result of the screen resonance, due to its

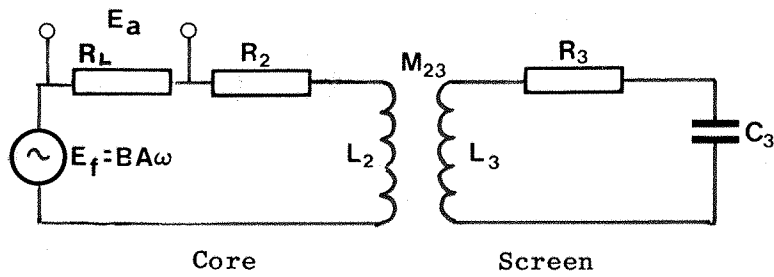


Fig. 6:3a Equivalent Circuit Of Goniometer Aerial

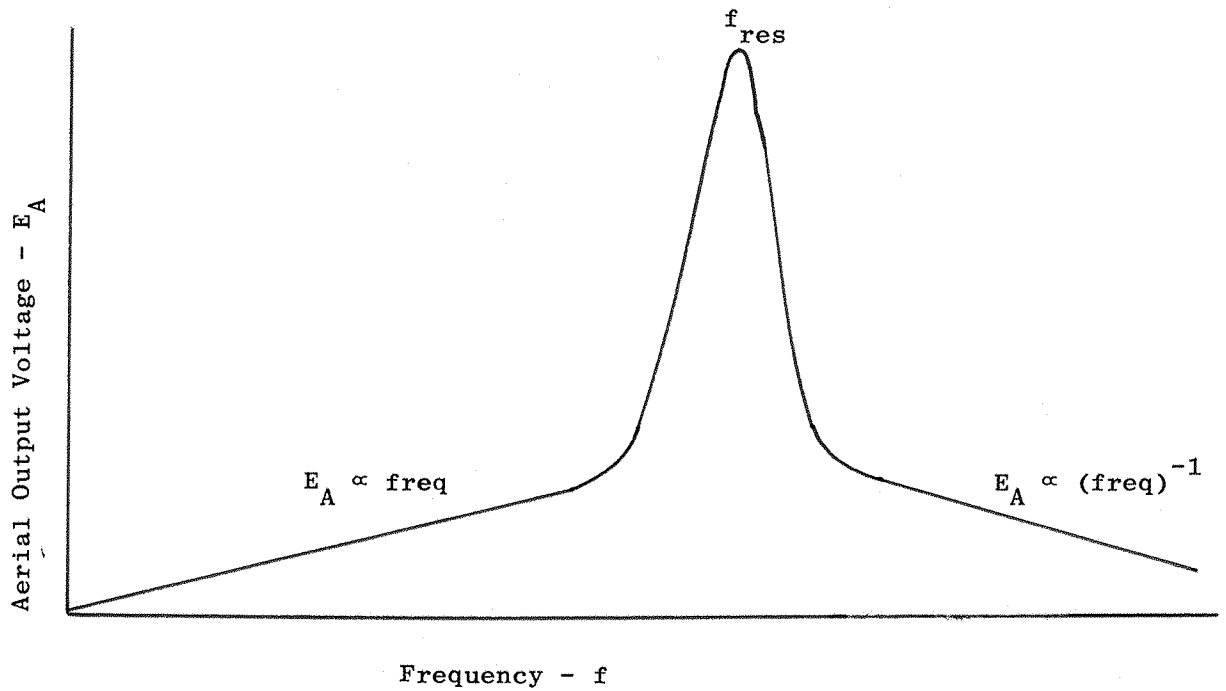


Fig. 6:3b Idealised Amplitude Response Of The Goniometer Aerial.

$$L_2 = 66\mu\text{H}$$

$$R_2 = 0.5\Omega$$

$$L_3 = 50\mu\text{H}$$

$$R_3 = 0.3\Omega$$

$$M_{23} = 50\mu\text{H}$$

$$Q \approx f_{\text{res}} \text{ in KHz}$$

$$C_3 = 0.1\mu\text{F}$$

Table 6:2 Goniometer Aerial Characteristics.

series capacitance and inductance, being reflected through the screen to core transformer. Thirdly, a high frequency region where the output voltage is inversely proportional to the angular frequency. At these frequencies the screen acts as a shorted turn in the magnetic circuit between core and screen. The aerial is consequently bandlimited for frequencies above resonance. Smith (1970) has experimentally determined the inductance of the core, the screen, and the mutual inductance between core and screen. His values, together with other pertinent parameters, are given in table 6.2. In particular, note that the Q of the resonance peak is ~ 65 (i.e. the 3dB bandwidth ≈ 1 kHz). Therefore in practice the aerial is bandlimited for all frequencies above about 70 kHz.

6.4.2.2 Preamplifier Plus Aerial Response

It was necessary to test the preamplifier response in association with either the aerial itself or a dummy aerial which modelled the electrical characteristics of the aerial.

Ideally field site amplitude response measurements should have been made using a known input field with the preamplifier output amplitude being measured on a spectrum analyser. The latter would have been used as a variable band pass filter to reject the background (manmade) noise, prevalent at any European field site. Such measurements must be made on site and not subsequently from tape recordings, because above ~ 20 kHz even the best conventional (direct record) tape recorders become inoperative. Unfortunately no suitable field site, with a mains source, (required for the spectrum analyser), was available near Southampton. Chilbolton, a field site used by previous research workers in Southampton, was no longer available for ELF/VLF measurements due to an increase in local mains interference to levels which caused preamplifier saturation. This was deemed to be due to the 24 hour operation of the S.R.C. Chilbolton Radio Telescope, and also, due to the construction of a new housing estate in the nearby village.

Another measurement technique considered was the use of a dummy aerial which correctly modelled the electrical characteristic of the aerial up to 1 MHz. Smith and Bullough (1976) have described the construction of a dummy aerial to model the low frequency, (Faraday Law), response of the aerial. This does not, however, simulate the effects of the aerial screen plus series capacitance. Figure 6.4

depicts the configuration adopted to rectify this situation. The secondaries (2 and 3) electrically represent the core and the sheath of the goniometer aerial respectively. The sheath secondary resistance has been omitted from the model since it has negligible impact for $500 \text{ Hz} < F < 1\text{MHz}$, except close to resonance. The modelled core resistance has been neglected, being small compared with that of the load. The values of inductance and mutual inductance obtained for, and between the secondaries are given in table 6.3b and should be compared with measurements on a real aerial, (Smith, 1970), see table 6.2. The agreement is to within 2%.

We wish to derive a relationship between the input voltage to the dummy aerial and an equivalent wave field. The voltage, E_d appearing at the dummy aerial output (figure 6.4) for a sinusoidal input signal E_s with angular frequency ω , from a source impedance $\ll R_L$, can be calculated by the application of Kirchhoff's Law to each mesh.

Mesh 1

$$E_s = (R_1 + j\omega L_1) I_1 - j\omega(M_{12} I_2 + M_{13} I_3)$$

Mesh 2

$$0 = (R_L + j\omega L_2) I_2 - j\omega(M_{12} I_1 + M_{23} I_3) \quad \text{equations 6.1}$$

Mesh 3

$$0 = (j\omega L_3 + \frac{1}{j\omega c_3}) I_3 - j\omega(M_{31} I_1 + M_{23} I_2)$$

Substituting for I_1 and I_3 gives I_2 and since $E_d = R_L I_2$

$$E_d = \frac{E_s R_L}{\left(R_1 + j\omega L_1 + \frac{\omega^2 M_{13}^2}{j(\omega L_3 - \frac{1}{\omega c_3})} \right) \left(R_L + j\omega L_2 + \frac{\omega^2 M_{23}^2}{j(\omega L_3 - \frac{1}{\omega c_3})} \right) - j \left(\frac{\omega^2 M_{13} M_{23} + \omega M_{12}}{(\omega L_3 - \frac{1}{\omega c_3})} \right) - j \left(\frac{\omega^2 M_{13} M_{23}}{(\omega L_3 - \frac{1}{\omega c_3})} + \omega M_{12} \right)} \quad \text{equation 6.2}$$

The corresponding voltage E_a , at the antenna output is the 'Faraday Law' induced voltage modified by the sheath. Application of Kirchhoff's Law to the two meshes of figure 6.3a gives:

$$E_a = I_2 R_L = \frac{R_L A B \omega}{R_L + j\omega L_2 + \omega^2 \frac{M_{23}^2}{j(\omega L_3 - \frac{1}{\omega c_3})}} \quad \text{equation 6.3}$$

where A is the aerial loop area and B is the wave field. Providing

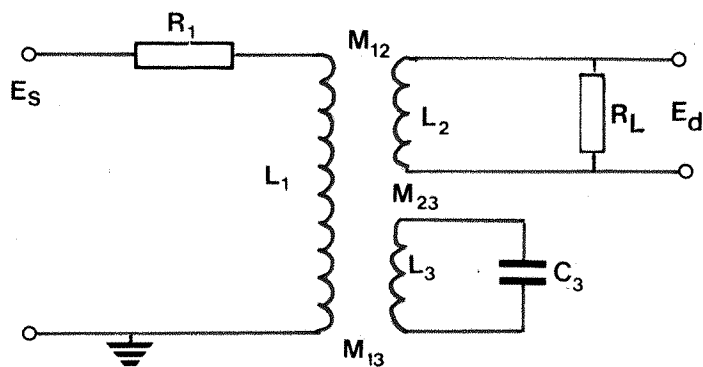


Fig. 6:4 New Style Dummy Aerial Circuit.

L_1 = 2 turns of 24 s.w.g. wire.
 L_2 = 12 turns of 36 s.w.g. wire.
 L_3 = 12 turns of 34 s.w.g. wire.
 Ferrite core : LA2400
 C_3 = 0.1 μ F

Table 6:3a Constructional Details.

L_2 = 67 μ H
 L_3 = 51 μ H
 M_{23} = 49 μ H

Table 6:3b Dummy Aerial Inductance Values.

$$R_1 \gg \omega L_1, R_1 \gg \frac{\omega^2 M_{13}^2}{(\omega L_3 - \frac{1}{\omega C_3})} \quad \text{and} \quad M_{12} \gg \frac{\omega M_{13} M_{23}}{(\omega L_3 - \frac{1}{\omega C_3})}$$

it is simple to show, by equating 6.2 and 6.3 that:

$$E_s = \frac{ABR_1}{M_{12}}$$

which for perfect coupling between windings 1 and 2 reduces to:

$$E_s = \frac{ABNR_1}{L_2} \quad \text{equation 6.4}$$

where N is the winding one to winding two turns ratio. This frequency independent relationship is identical to that derived by Smith and Bullough (1976) for their low frequency dummy aerial.

Of the above approximations the first is met for $500 < f < 1\text{MHz}$ as is the second, except within a few kilohertz of resonance. The third condition is also met for this frequency range except near resonance. In this instance, however, the regime of nonconformity is larger. In figure 6.5, which shows the response determined using this dummy aerial, this region is shown dotted. For comparison the response using the Faraday Law dummy aerial is also shown. It can be seen that the gain of the aerial plus preamplifier decreases with increasing frequency with no tendency to instability or high gain. This fall-off is a result of both the aerial bandlimiting and the $\sim 1\text{kHz}$ preamplifier input transformer resonance, see section 3.3.4 and figure 3.3.

The input signal is, from equation 6.4., calculated to be equivalent to a field of 4.5pT, or assuming a plane polarised wave propagating in free space, 1.3mV/m.

6.4.2.3 The Goniometer Amplitude Response

The goniometer response has also been determined by applying a signal of 2V peak to peak to the input. This is approximately 75% of the maximum permissible input. The measured response is depicted in figure 6.6 and it is interesting to note that it shows a peak near 145kHz. The frequency of this resonance was found to be constant to within

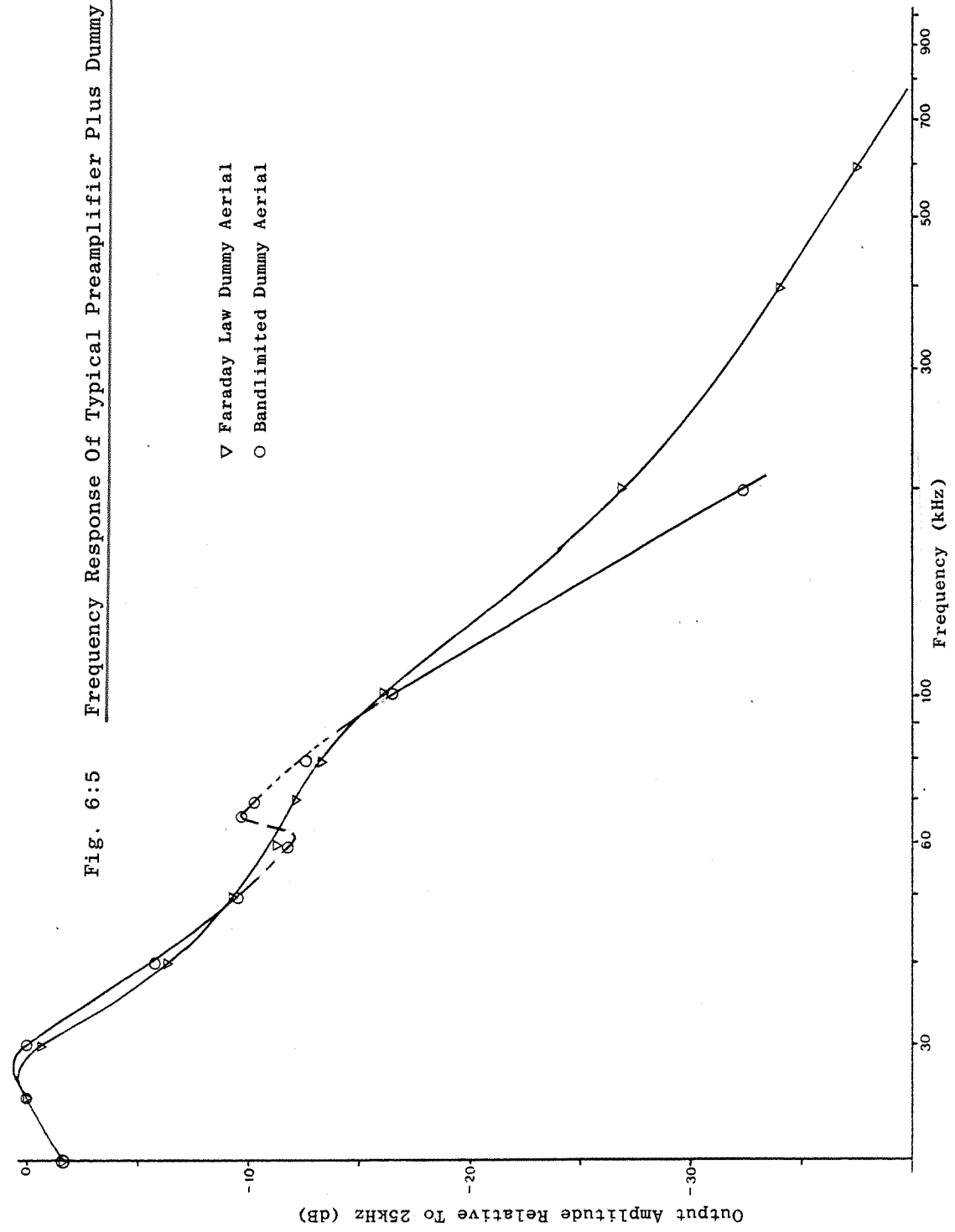


Fig. 6:5 Frequency Response Of Typical Preamplifier Plus Dummy Aerial

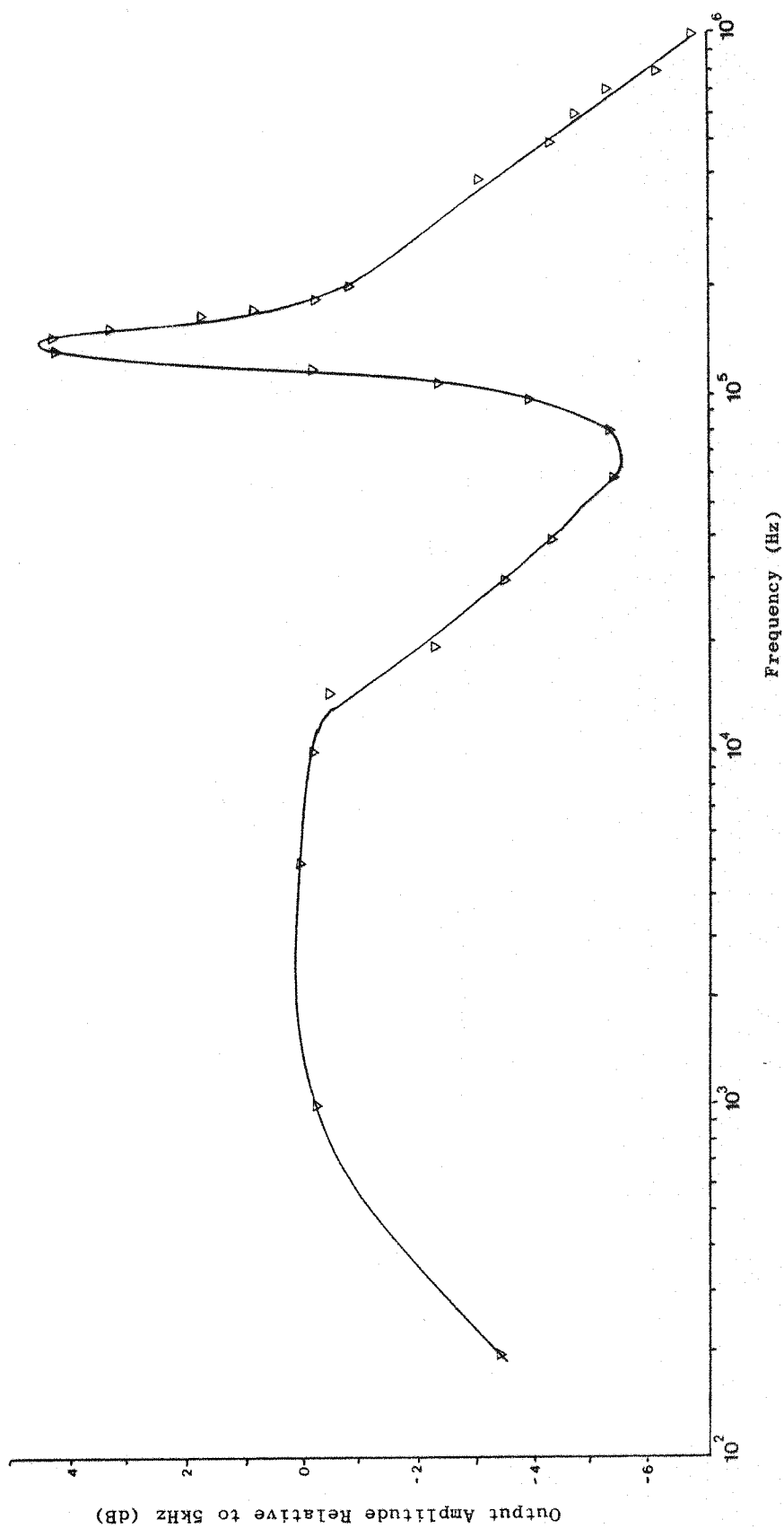


Fig. 6:6 Response Of Typical Goniometer Receiver

$\pm 5\%$ from channel to channel and goniometer receiver to goniometer receiver. This goniometer channel shows a gain of + 2dB, (relative to 5kHz) at 173kHz, one of the possible transmitter frequencies; this measurement obviously warranted further investigation.

More careful examination of the goniometer output signal at LF frequencies showed that for input signals above 100kHz the output signal showed no modulation due to the internal goniometer oscillator. Figure 6.7, however, shows the pips to be strongly modulated, (shown here by the splitting of the signals into two sidebands). It was therefore concluded that if this amplitude resonance was indicative of receiver demodulation, then it must have taken place in the buffer stage, prior to the multiplier, in order for there to be a 1kHz modulated signal at the goniometer output. This was further investigated, see section 6.4.2.5.

6.4.2.4 Preamplifier Non Linearities

The preamplifier linearity was investigated by applying, via the dummy aerial, signals at 173kHz and 657kHz, amplitude modulated to 75% at 1kHz. The object of the exercise was to simulate reception of an LF wave of high field strength. No information could be obtained on the modulation depth of the Russian transmitters. The value adopted (75%) is similar to that used by the B.B.C. The signal applied was equivalent to a field of 1.4×10^{-1} nT or 42mV/m. Sivusaami (private communication, 1979), of the Finnish Monitoring Service, reports that the daytime field strength of transmissions on 173kHz, measured at Sodankyla on 3 April, 1979, was 112 μ V/m. Belrose (1968) considered that the field strength at night, (when most of the ELF pips were detected) could be up to four times greater than that measured during the day. He also reported that LF field strengths are variable during nighttime auroral activity but generally not higher than during quiet time conditions. We may therefore conclude that the field strengths applied in this linearity test were approaching 40dB (i.e. $\frac{1}{4} \times \frac{42\text{mV}}{112\mu\text{V}}$) larger than the 173kHz nighttime field strength at Sodankyla, the station nearest to the Soviet border.

The output voltage at 1kHz was measured using the SD350-6 spectrum analyser (Spectral Dynamics, 1978) with a 5Hz bandwidth. No output signal was observed at the level determined by noise in the laboratory. This was itself at least 40dB less than the output expected from

natural atmospheric noise at the preamplifier output for a frequency of 1 kHz.

Thus had demodulation taken place in the equipment the 1kHz signal would have been so weak that it would never have been discovered.

6.4.2.5 Goniometer Non-Linearities

Similar measurements were conducted on the goniometer using a 2V peak to peak input voltage. No signal at 1kHz could be detected down to the -112 dB level relative to 1 volt. This is > 60dB down on the expected atmospheric noise output at any receiving station.

Tests were also conducted at 145kHz, i.e. on the goniometer resonant peak, and again no output signal was detected.

Additionally the output from the goniometer was recorded by the same model tape recorder as used on site and the recorded signal tested for non-linearities.

Similar negative results were obtained.

These measurements substantiate the view that the existence of the resonant peak is inconsequential in this regard.

6.4.2.6 Conclusions

All these measurements indicate that the "pips" recorded at 1kHz were due to propagating ELF signals rather than due to the demodulation of LF/MF radio signals by the equipment.

This view is further corroborated in the following sections where the observations are best interpreted in terms of a propagating ELF signal.

6.5 Analysis Equipment

Most spectral measurements of the pips were made using a Spectral Dynamics SD 350-6 real time analyser (Spectral Dynamics, 1978).

Goniometric bearings were obtained from the tape recorded signals using the Sheffield University Semi-Automatic Whistler Analyser.

Both of these instruments have been described in Chapter 3.

6.6 Investigation of the Pips

6.6.1 Introduction

A thorough examination of recordings made by the Southampton Group at Tromsø, Arjeplog, and Sodankyla was undertaken. Although all three stations received the pips, Arjeplog was unfortunately subjected to high mains harmonic interference at 1kHz. This made positive identification of weak signals difficult, and amplitude and directional measurements impossible. The data from this station have therefore not been examined in detail.

Pips were also recorded several times on the Turunen ELF/VLF receiver, in parallel with Southampton measurements. Additionally, on one occasion the ELF system received the music which sometimes precedes the pips. This was at a time outside the scheduled recording hours, i.e. when the goniometer system was not in operation. At other times when the ELF system was operating in a mode suitable for the reception of pips, (that is with a bandwidth up to 1kHz, see section 6.2), no pips (or music) were recorded on either the ELF receiver or, when also operational, the goniometer receivers.

6.6.2 Description Of Pips

The pips recorded at the Scandinavian field sites were, on return to England, found to have a frequency of $1\text{kHz} \pm 0.5\text{ Hz}$ and each pip was found to be $105 \pm 8\text{ms}$ in duration. The pips fell in groups of six, occurring one per second, with the onset of the last of the six being on the hour.

Figure 6.7 shows the dynamic spectra of the six pips in hard copy form. Each pip has been split into two because of the goniometer modulation at approximately 27.5 Hz. No similar signals were identified at 2kHz or higher harmonics, at any recording station.

6.6.3 Correlation Of Pip Occurrence With Magnetic Activity - Daily Variation

The number of occasions that pips were detected within one day, over a specified time period, at either Tromsø or Sodankyla, were

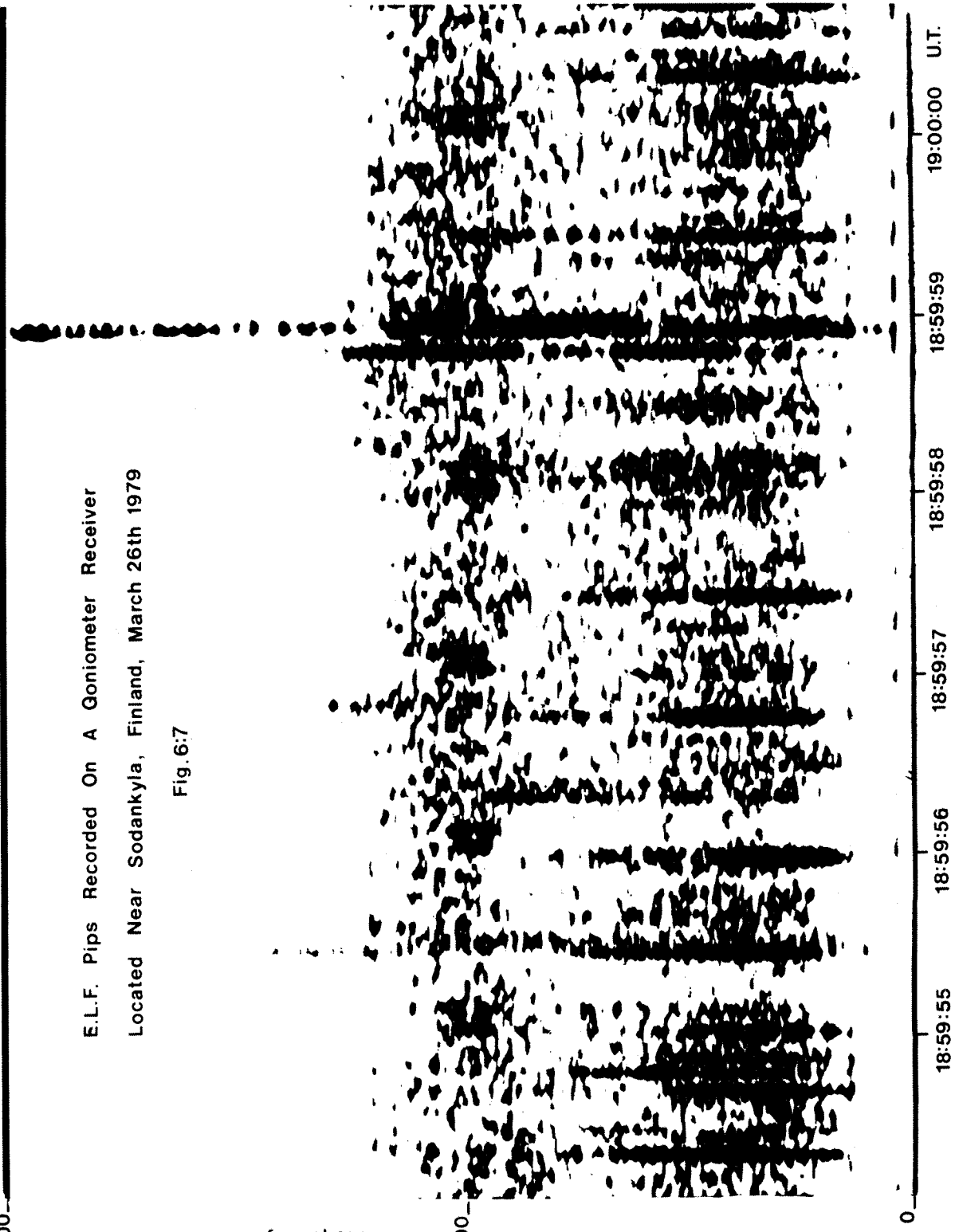
2000

E.L.F. Pips Recorded On A Goniometer Receiver
Located Near Sodankyla, Finland, March 26th 1979

Fig. 6:7

Frequency in Hz.

1000



plotted as a bar chart, see figure 6.8a. These specified periods were given in section 6.2. When pips were heard between 23:59:55 UT and 24:00:00 UT they were assigned a value of $\frac{1}{2}$ to the present day and $\frac{1}{2}$ to the following day. The shaded areas indicate that data were lost for one or more hours during that day's schedule and show the maximum number of times that pips might have been detected. Note that in order to confirm that pips were indeed transmitted every hour during this period a copy of the Soviet "Radio/TV Times" was obtained. This was unfortunately, for the period March 11 to March 17 1979, the week previous to that of interest; however, Meacham (private communication, 1979) reports that programming remains fairly constant from week to week. On the basis that pips were broadcast when the programmes changed on the hour and not when the programmes ran across the hour, it was inferred that pips were broadcast every hour except at 08 UT and 11 UT on Thursdays and at 18 UT on Sundays. No recordings were made at these times and so the data set is unaffected.

Figure 6.8b shows the daily sum of the eight Sodankyla magnetic indices, K_{HDZ} , (Rostoker, 1972) over the period of interest. (The index K gives, on a logarithmic scale of 0 to 9, a measure of the local geomagnetic activity over a three hour period).

We see that this period was characterised by little geomagnetic activity from March 14 to March 21, and strong activity thereafter.

Comparison of the two charts shows that, apart from March 28 and April 1, there is a broad positive correlation between the detection of pips and geomagnetic activity. In particular a threshold of magnetic activity exists ($K_{HDZ} \cong 18$) below which the pips were not received.

6.6.4 Dirurnal Variations

Figure 6.9 shows the number of times that recordings were made, on each hour, at either Sodankyla or Tromsø over the period March 22 to April 4, 1979. Also shown are the number of times that pips were detected. The period March 15 to March 21 has not been included in the data set, because at no time were pips detected. Again no corrections, of the type discussed in section 6.6.3, had to be applied to the data set.

It can be seen that the number of samples in the evening/midnight sector is comparable with the number of days being considered. In the

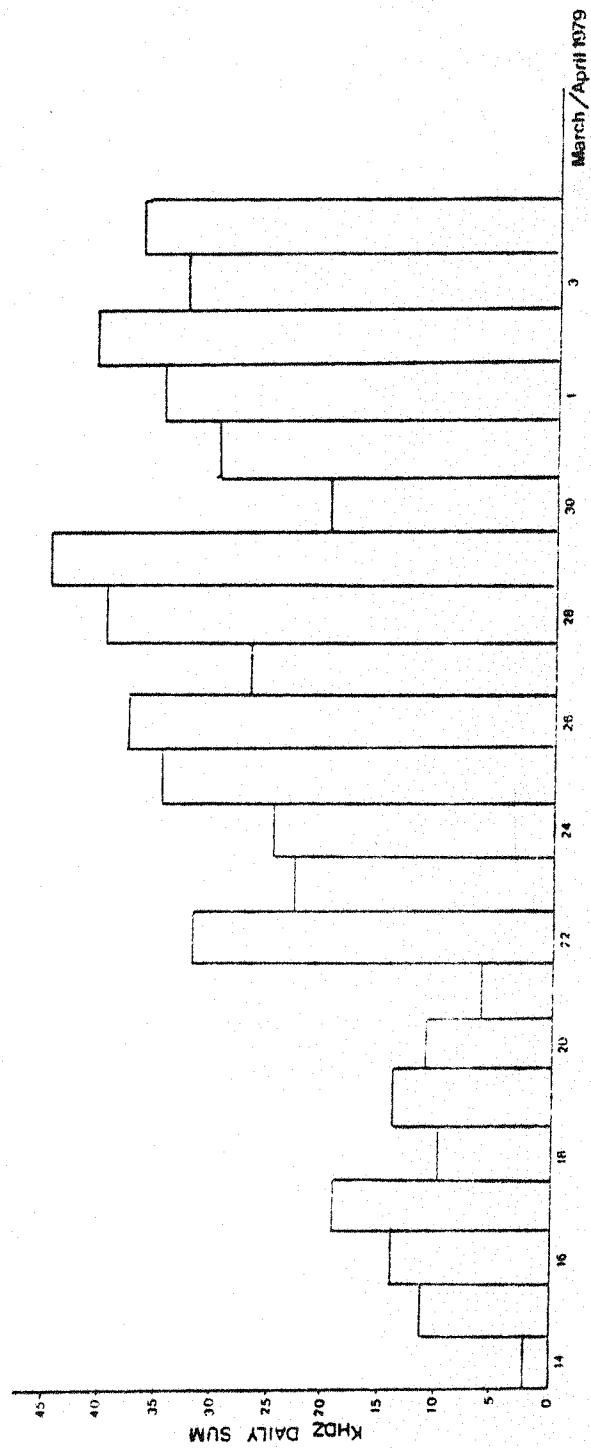
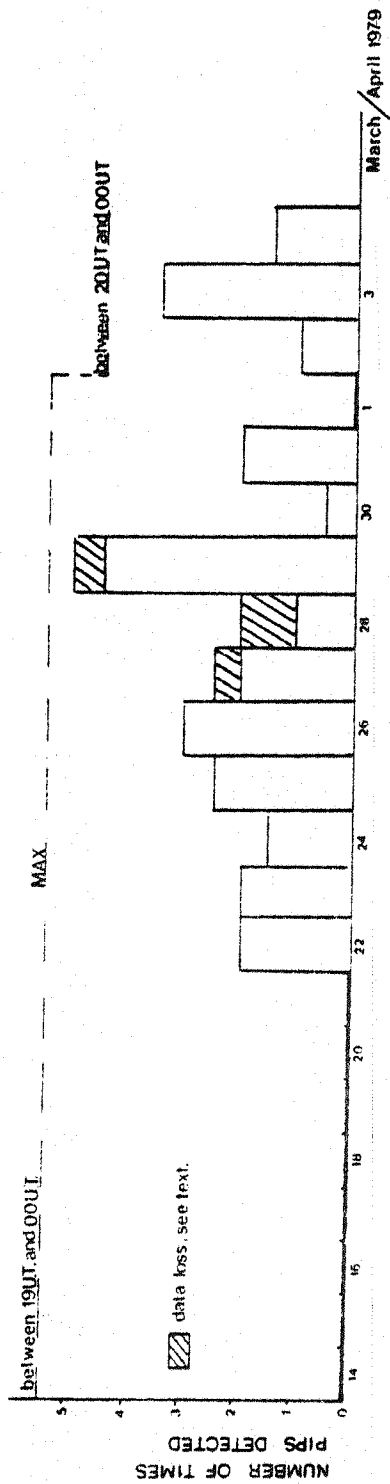


Fig. 6:8a (top) Daily Variation Of Pip Occurrence
 Fig. 6:8b (below) Daily Geomagnetic Activity At Sodankyla

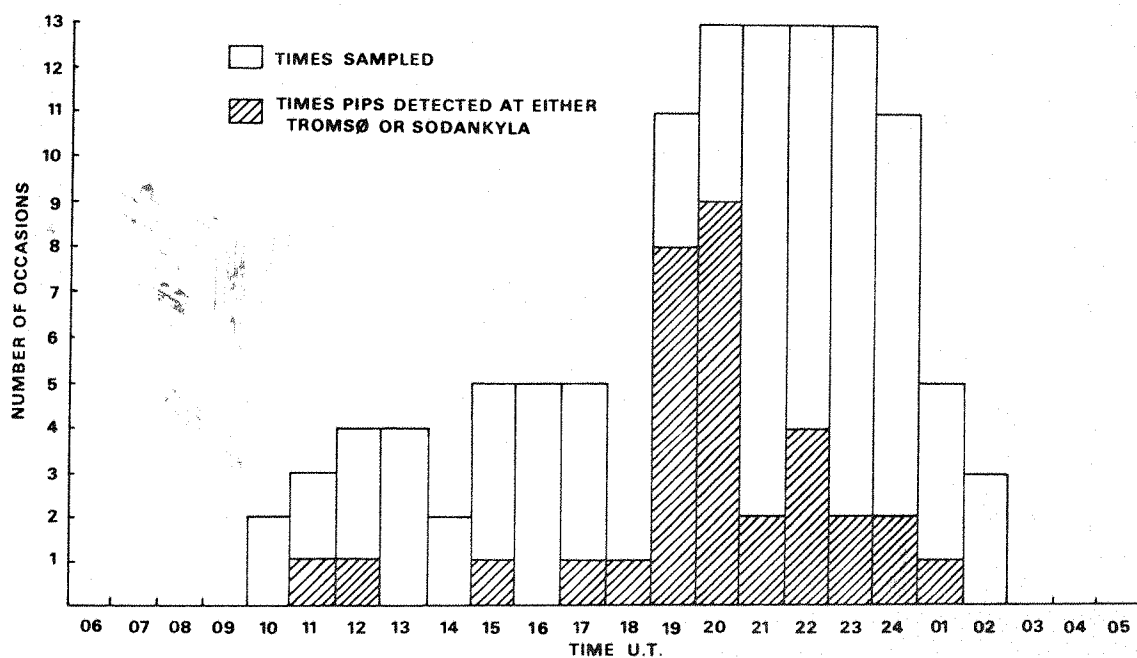


Fig. 6:9 Diurnal Variation Of Pip Detection.

afternoon sector the number of samples is low, and in the morning sector, zero.

Two points should be recognised.

Firstly, the probability of hearing pips is greatest during the evening sector. (The time of magnetic midnight at Sodankyla, for the March equinox, has been determined as 21:32 UT, using the method of Montbriand (1970)).

Secondly, although the afternoon sector statistics are less reliable than those of the evening/midnight sector, it is interesting to note that the pips detected at 15 UT and 17 UT (on March 22), and 11 UT and 12 UT (on March 28), show a strong positive correlation with 500Y, or greater, positive magnetic bays recorded at Sodankyla. Over the whole experimental period, these afternoons exhibited the strongest afternoon magnetic activity. The positive bay is interpreted as being indicative of a strong eastward flowing electrojet. This particular result agrees well with general conclusions drawn from an analysis of the STARE data, see section 6.6.6.

6.6.5 Bearings

Using the Sheffield University Semi-Automatic Whistler Analyser, a calibration curve of apparent azimuthal arrival angle against real azimuthal arrival angle was obtained for the 1kHz calibration at both Tromsø and Sodankyla. Two azimuthal calibrations, see section 3.4 were executed at both stations, one at the start and one at the end of the campaign. This was to provide redundancy and, in addition, a check of the equipment stability throughout the experimental campaign.

Figure 6.10 depicts the 1kHz calibration curve for Sodankyla. Since, for the angles 0°E to 90°E the apparent bearings obtained from both calibrations were within $\pm 1^{\circ}$ of each other, only one curve is shown. This error may readily be accounted for as misalignment of the calibration coil by the operator. For the remaining angles, it was impossible to obtain bearings from the second calibration due to the reception of strong chorus at 1kHz. The close agreement over the angles 0°E to 90°E indicates, however, that the equipment functioned in a stable manner during the entire campaign.

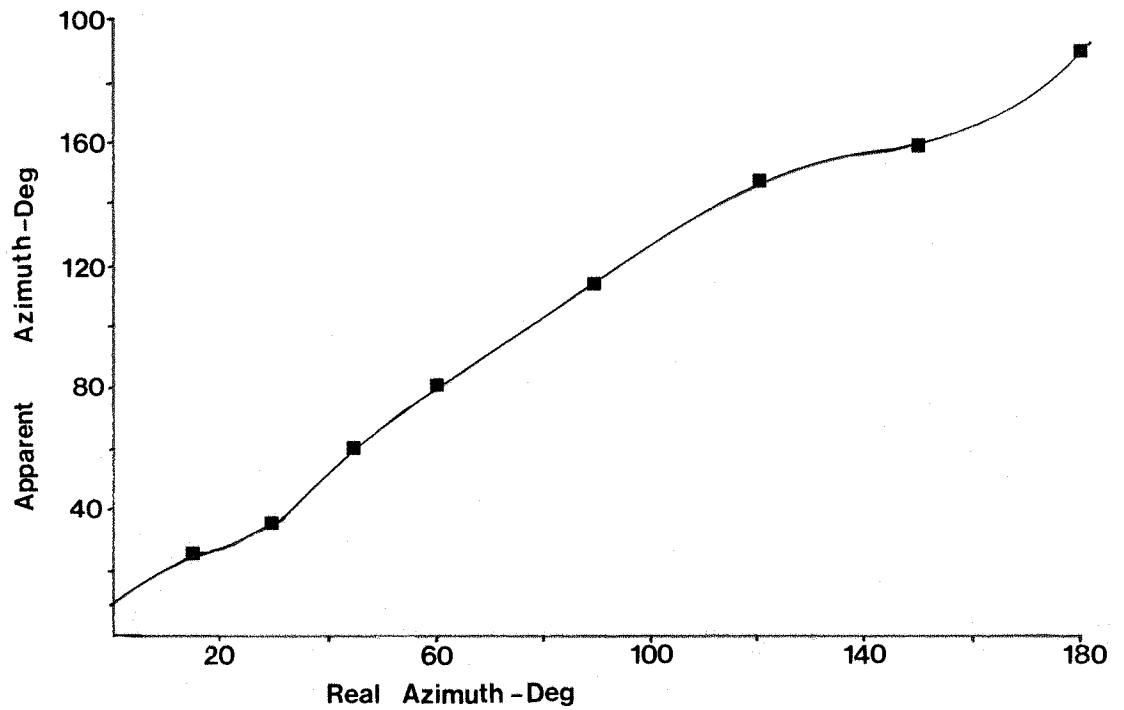


Fig. 6:10 Graph Of Apparent Azimuth Against Real Azimuth
At 1kHz For Sodankyla

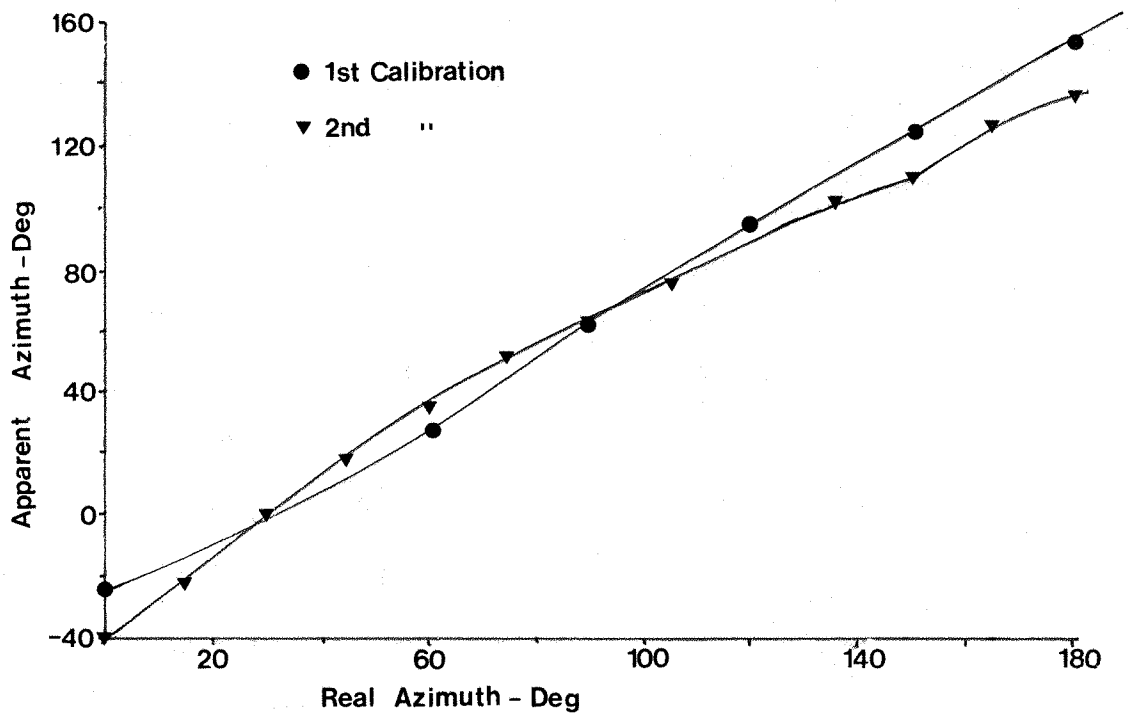


Fig. 6:11 Graph Of Apparent Azimuth Against Real Azimuth
At 1kHz For Tromsø

Figure 6.11 depicts similar 1kHz calibration curves for Tromsø. The variation of apparent bearing between the two calibration curves cannot be accounted for by errors in calibration coil alignment. A variation in the N/S loop preamplifier response, between the start and the end of the campaign, also indicated that the two azimuthal calibrations should be treated separately.

Measurements on the pips involved obtaining the apparent bearing for each of the six pips in the set and averaging these values. Due to the pips short duration, "reliable" cross correlograms between signal and calibration pulse, were only obtained for the strongest pips at each station. The real azimuthal bearing angle was obtained from the apparent bearing by using the appropriate calibration curve, (figure 6.10 and 6.11).

For each set of pips the "noise" between the pips was sampled at 1kHz, and cross-correlated with the calibration pulse, to verify that no source existed, locally or otherwise, which could give an erroneous result. On all occasions the correlogram, which was generally poor (indicative of general background noise with various azimuthal arrival angles), gave a bearing greater than 20° from the bearing obtained for the pips.

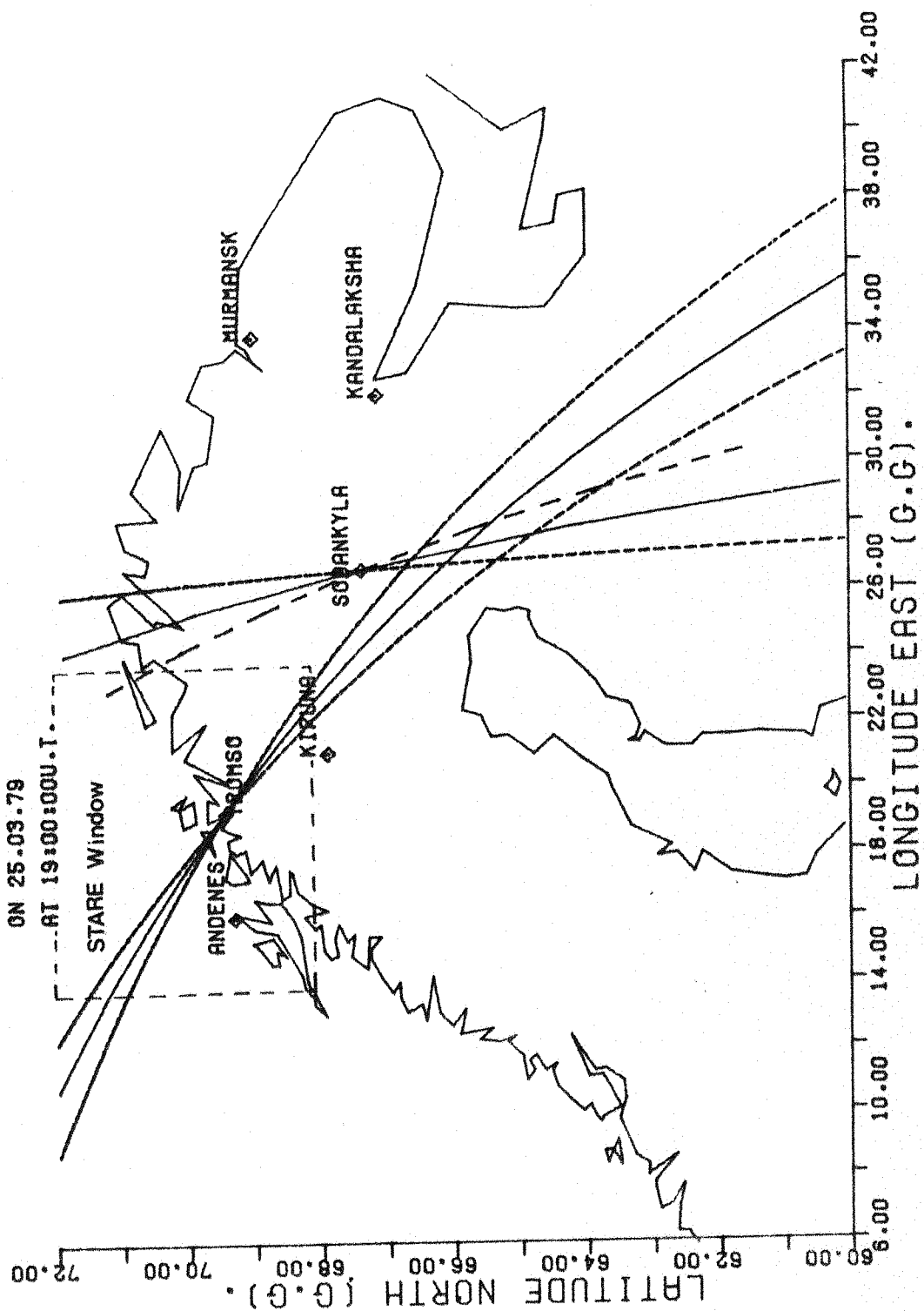
Table 6.4 lists the average bearings obtained from Sodankylä and Tromsø. As expected from signal strength considerations (see section 6.6.10), and signal to noise ratio considerations, the number of reliable bearings obtained from Sodankylä was higher than from Tromsø. Bearings from the latter were obtained by associating the apparent bearing of the first pip set with the first calibration curve and the remainder with the second calibration curve. It can be seen that by doing so a fairly consistent set of bearings, throughout the experiment, was obtained.

In cases where two bearings were available the source of the proposed ELF signal was determined using the computer program of Jarvis (1976). The geographic co-ordinates obtained from the program, are shown in table 6.4. Additionally the bearings have been plotted as great circle paths on cartesian maps of Northern Scandinavia, and North-West Russia. A map program based upon the north American program of Dr. Strangeways and modified for Scandinavian use by the author, was used for this purpose. A typical example is shown in figure 6.12. In this presentation the signal source is shown as the intersection of the two solid lines, and the bearing angle errors are represented

Date	Time (UT)	Bearing From Södankyla	Bearing From Tromsø	Crossing Pt. Lat Long		Distance From Södankyla	Distance From Tromsø
22.3.79	19	167° ± 8°	135° ± 4°	66.08°	27.07°	138 km	418 km
25.3.79	19	5° ± 4°					
26.3.79	19	170° ± 7°	136° ± 5°	66.04°	26.89°	140 km	417 km
27.3.79	19	29° ± 8°					
27.3.79	20	165° ± 4°	132° ± 7°	66.49°	26.93°	98 km	385 km
29.3.79	21	14° ± 4°					
29.3.79	22	129° ± 4°	133° ± 8°	69.21°	19.94°	270 km	31 km
31.3.79	19	167° ± 4°	138° ± 10°	65.48°	27.38°	195 km	470 km
31.3.79	20	164° ± 7°	128° ± 8°	67.03°	26.60°	47 km	340 km

Table 6.4 Average Goniometer Bearings

FIG. 6-12
 IONOSPHERIC SOURCE OF SIGNAL OBTAINED FROM GONIOMETER V.L.F. RECEIVERS.



as dashed lines. The latter constructs a so called error diamond around the source location. Figure 6.13 shows the location of all the triangulated sources together with the worst case envelope of standard errors.

The distance of the ELF pip sources from Tromsø and Sodankylä has been calculated, and is also given in table 6.4.

Strangeways (1977) has shown that, for a 1kHz signal, with the ionospheric source located at such distances from the receiver, a systematic bearing angle error of up to twenty degrees can be associated with polarisation and multipath effects. Strangeways work, however, involved idealised situations with assumed values of the ground conductivity and ionospheric parameters. Evidently in an experimental situation we have no knowledge of these parameters, nor are they constant over the propagation path. The bearing errors given in table 6.4 and figures 6.12 and 6.13, do not, therefore, include these systematic errors, and show purely the random measurement errors. The remaining bearings, from Sodankylä only, do not fall close to 165° but around 10° to 20° (or 190° to 200° , due to the 180° ambiguity in the goniometer technique). It is not known whether these represent valid bearings since they were generally obtained from lower field strength signals, than those discussed in previous paragraphs.

6.6.6. Hourly Determination Of The Direction Of Ionospheric Electrojet Currents

6.6.6.1 Introduction to STARE

The Scandinavian Twin Auroral Radar Experiment, or STARE is a radar system designed to study electrostatic ion waves or irregularities (Buneman, 1963; Farley, 1963; Rogister and D'Angelo, 1970) in the E region of the Scandinavian auroral ionosphere. Such irregularities occur in the region of the auroral electrojet.

The facility consists of two pulsed bistatic radars located in Norway and Finland, operating on 140.0 MHz and 143.8 MHz, respectively. Each transmitting antenna illuminates a large common area of the ionosphere stretching from 68°N to 72°N , and from 14°E to 23°E . Using a multiple, narrow beam, phased receiving antenna it is possible for each receiver to measure simultaneously the mean Doppler velocity of these auroral irregularities at 50 different radar ranges, along eight different lobes. A combination of Doppler data from both receivers

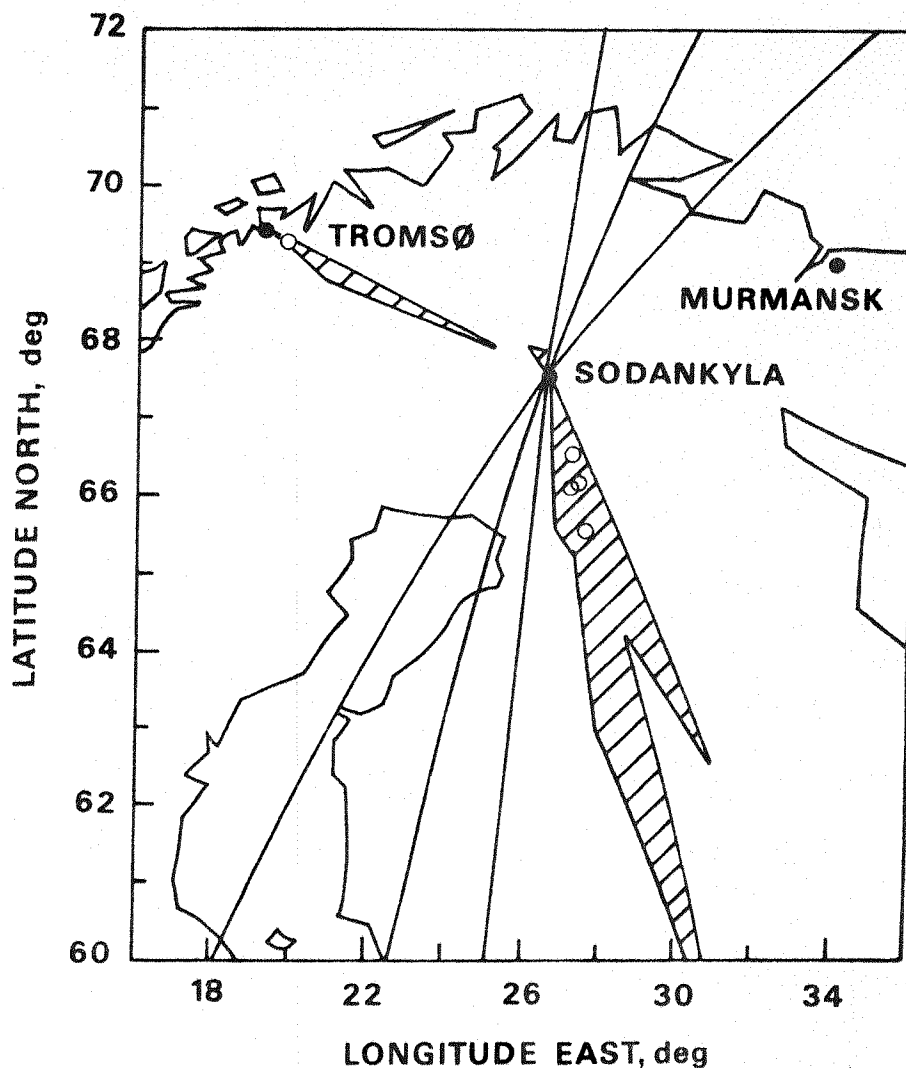


Fig. 6:13 Cartesian projection of Northern Scandinavia showing the positions (O) of the sources in the ionosphere of the 1kHz pips, with the worst case error envelopes (hatched area). Additionally, three bearings with 180° ambiguity and a typical error of $\pm 6^\circ$ are shown from Sodankylä.

enables the mean velocity of the irregularities to be determined. The system has been described in detail by Greenwald et al. (1978).

By making certain assumptions, discussed by Greenwald et al. (1978), it is possible to determine certain ionospheric parameters from these measurements. It has been demonstrated by Ecklund et al. (1977) that this mean velocity is approximately equal to the electron drift velocity, which in the E-region of the auroral ionosphere is given by:

$$\underline{V}_0 = \underline{E} \times \underline{B}/B^2$$

\underline{V}_0 being the mean irregularity drift velocity. The direction of the auroral electrojet current is opposite to that of the electron drift velocity. Additionally, since the radar measurements are made in a plane perpendicular to the geomagnetic field, the horizontal ionospheric electric fields can also be determined from \underline{V}_0 , via the above equation.

Cahill et al. (1978) have reported close agreement between electric fields derived from the STARE data and electric fields obtained from rocket borne payloads. However, a word of warning is appropriate. Siren et al. (1977), have compared measurements from the Chatanika Incoherent Scatter Radar, described by Balsley et al. (1973), and measurements from a 50 MHz backscatter radar, situated at Anchorage, Alaska. They found a difference between the electron drift velocities obtained from Chatanika and Anchorage. Additionally, they demonstrated that the Chatanika results agreed well with ground based magnetometer data. It was consequently concluded that the mean drift velocities, determined from the Auroral Radar, were suspect. Since the E region electric field is derived directly from the mean drift velocity it too must be treated with care. Siren (1977) concluded, however, that STARE is a valuable tool for locating the auroral electrojet, and determining its sense (direction). In this work we are primarily interested in the latter.

Figure 6.14 shows some typical STARE results obtained during the period of interest. The direction of the vector, integrated over 20 seconds, shows the direction of motion of the irregularities. Note that within one hour the mean irregularity drift velocity vectors have changed from a predominately westward to a predominately eastward direction, consistent with a change from an eastward to a westward flowing electrojet. Using the assumptions outlined above the electric field may be obtained by rotating the velocity vectors 90° clockwise and setting 1000 ms^{-1} to be equivalent to 50 mV/m (Greenwald et al. 1978).

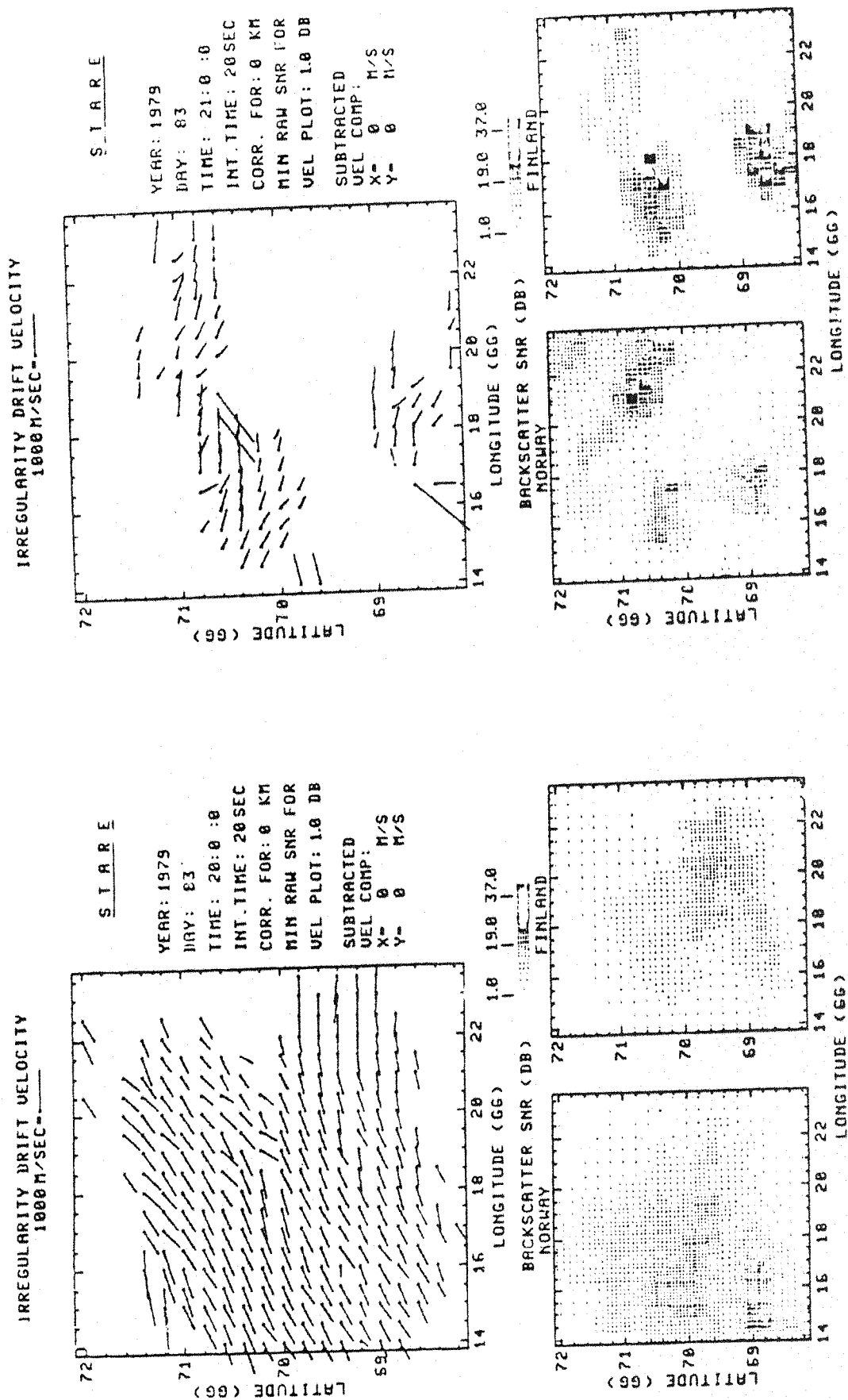


Fig. 6:14 Typical STARE Data

The lower plots show the location and strength, on a grey scale, of the radar echoes from each station. These have been included for completeness but have no relevance to this study.

6.6.6.2 Results

Due to the inoperation of the Finnish STARE facility over part of the period of interest, Doppler maps could only be obtained for a limited number of hours and days. Figure 6.15 shows the times when both radars were operational and also whether or not pips were detected. In figure 6.16 the absence or detection of pips has been plotted, on a compass projection, as a function of electrojet direction within the STARE viewing window. Each point is the result of a visual average of the STARE velocity vectors. An attempt has also been made to indicate the variation of vector direction within the window. The radial distance of each point from the intersection of the axes should not be interpreted as an indication of the electric field strength which was, subject to the provisos of section 6.6.6.1, always approximately 25 mV/m.

It can be seen from figure 6.16 that the occurrence of the pips shows a high positive correlation with an eastward flowing electrojet. Conversely, the absence of pips shows a similar correlation with a westward flowing electrojet. Note that the absence of a recorded pip does not necessarily indicate that no ELF signal was generated. High ionospheric absorption could have taken place en route from the source.

Note also that the STARE viewing window does not coincide with source of the pips determined from goniometer measurements, see figure 6.13. The geomagnetic time difference between the pip generation region and the window is however, only ~ 20 minutes and as such STARE may still be a valid diagnostic tool in this context.

6.6.7 Magnetometer Data

Consideration was given to establishing the electrojet position and direction, using data from the Finnish meridian magnetometer chain, following the methods described by Kisabeth et al. (1973). This method involves, however, many assumptions (which are not necessarily valid), expertise, and time, and was consequently not pursued.

Magnetometer analysis was restricted to examining data from Sodankyla. Positive bays were interpreted due to a nearby eastward

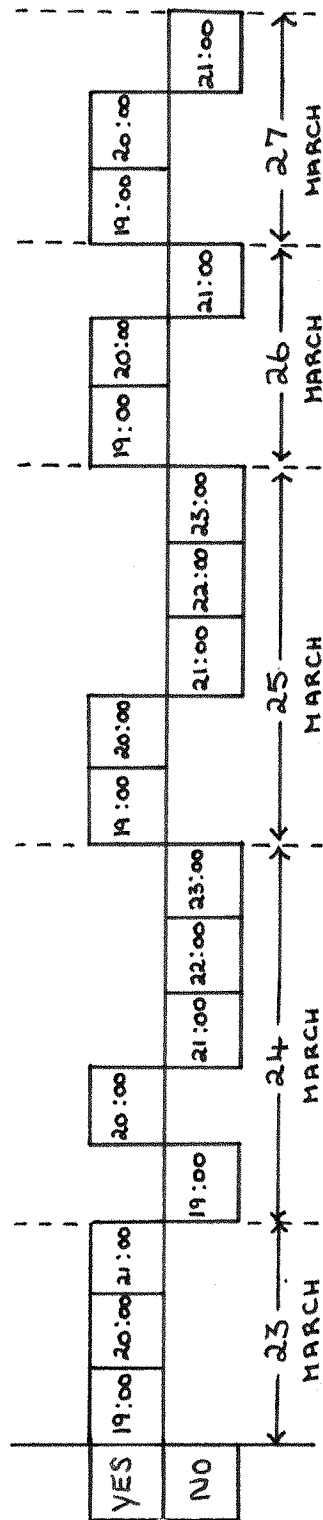


Fig. 6:15 Diagram illustrating availability of full hourly STARE data.
The boxes indicate the time (UT) and whether or not pips were recorded at Tromsø or Sodankylä.

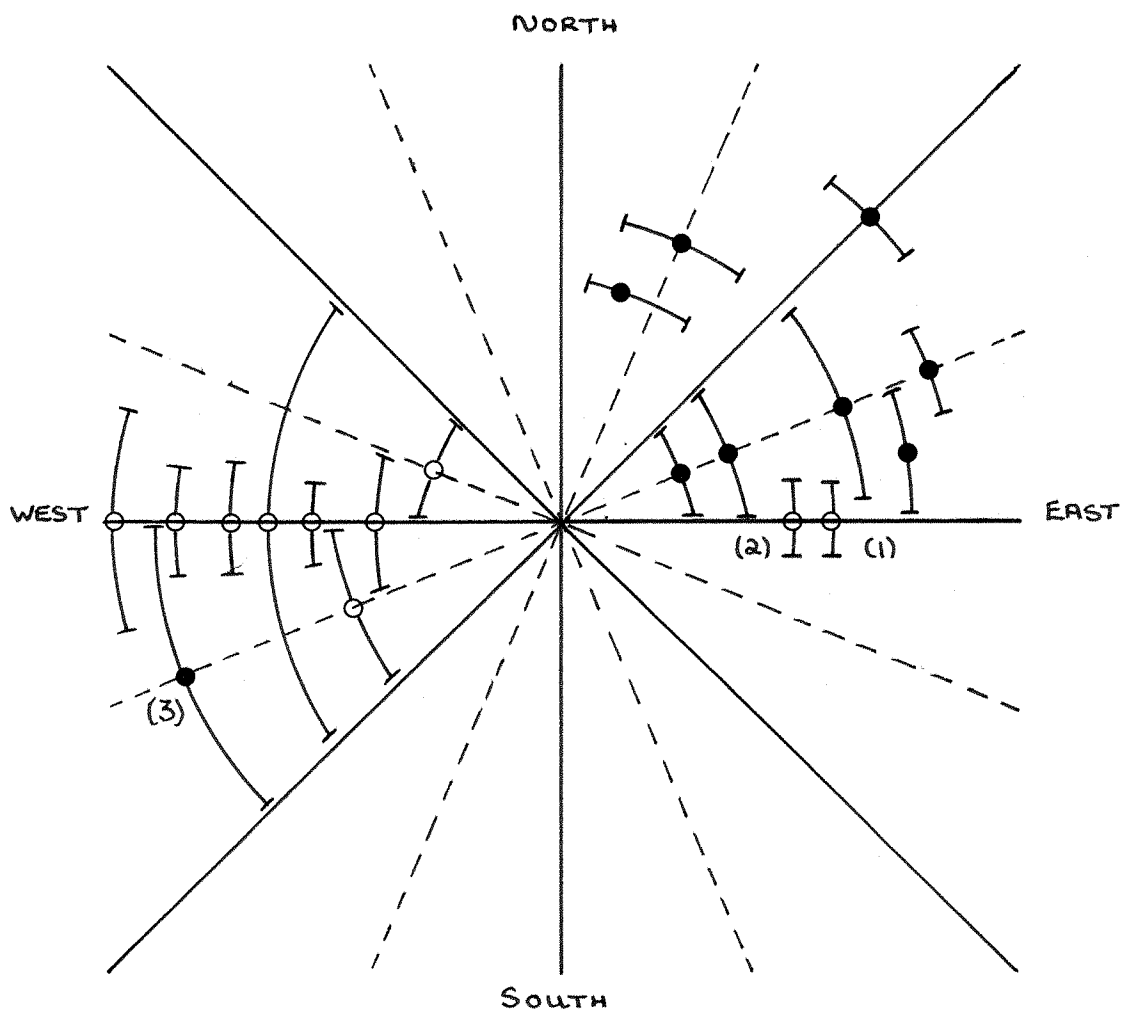


Fig. 6:16 Absence or detection of pips, as a function of the average electrojet direction within the STARE viewing window. (Geographic Coordinates).

● = pips detected

○ = pips not detected

1 - low backscatter

2 - 23 March 1979 at 21 UT

3 - 27 March 1979 at 20 UT

electrojet system and negative bays due to a westward system. Pips were found to occur during both positive and negative bays which failed to corroborate the findings of the STARE analysis. It was, however, clear that pips were only received when an active auroral zone current system existed nearby.

6.6.8 Riometer Data

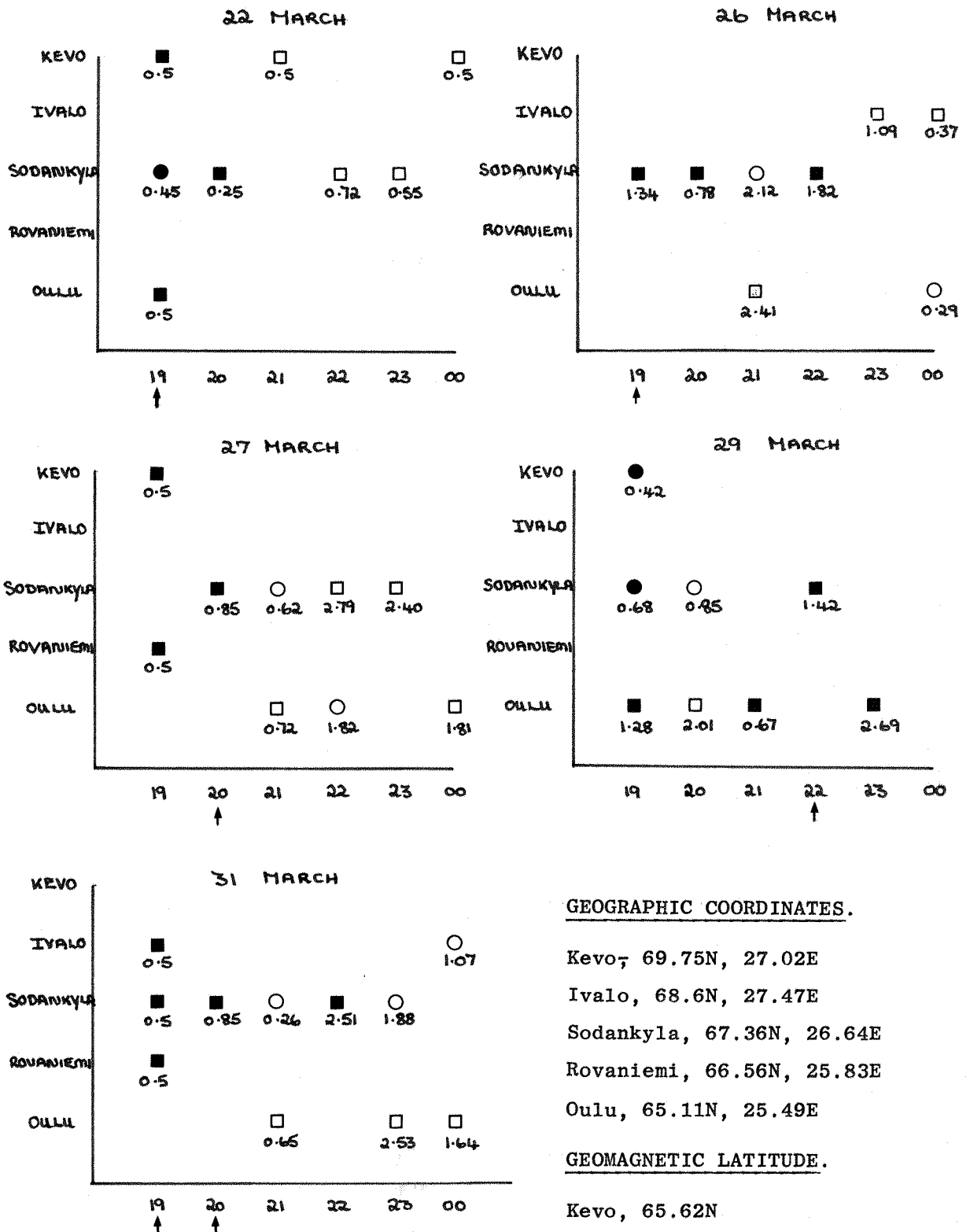
Riometer absorption data from the northern section of the Finnish meridional riometer network were examined. Kamide and Akasofu (1975) report that the westward electrojet is coincident with the diffuse aurora (Akasofu, 1974) in the midnight sector and the westward travelling surge in the evening sector. Similarly Potemra (1979) reports that in the evening sector the eastward electrojet is also associated with the diffuse aurora. Hartz and Brice (1967) have shown that the quasi-circular region of diffuse aurora is associated with drizzle type precipitation of $> 10\text{keV}$ electrons which cause D-region absorption (Heikkila, 1972). Thus, the latitudinal position of the maximum riometer absorption was interpreted as indicating the electrojet position.

Figure 6.17 shows the location, in latitude, of the riometer absorption maximum, for each hour, on the nights that at least one triangulated pip source was determined. The dark symbols show when pips were detected on each hour; arrows show when the source could be determined.

It can be seen that, when ELF pips are known to be generated just to the south of Sodankyla the electrojet is also located above, or somewhat south of Sodankyla. This provides yet further evidence for the close association between pip generation and the electrojet.

Figure 6.17 also shows that, as the electrojet moves southward, pips are sometimes detected and sometimes not. On other occasions, when the maximum riometer absorption is located near Sodankyla, but when there is also heavy absorption to the south, no pips are received. It is believed that this results from absorption of a northward propagating causative signal before it can attain electrojet altitudes and/or the interaction latitude.

Figure 6.18 shows a similar plot, but this time as a function of day for various times. The maximum riometer absorption generally moves southward from 20 UT to 21 UT only to return north again at 22 UT. At



GEOGRAPHIC COORDINATES.

Kevo, 69.75N, 27.02E

Ivalo, 68.6N, 27.47E

Sodankylä, 67.36N, 26.64E

Rovaniemi, 66.56N, 25.83E

Oulu, 65.11N, 25.49E

GEOMAGNETIC LATITUDE.

Kevo, 65.62N

Ivalo, 64.52N

Sodankylä, 63.55N

Rovaniemi, 63.68N

Oulu, 61.70N

The numbers by each symbol show the riometer absorption in dB.

Fig. 6:17 The Location Of The Riometer Absorption Maxima.

(Hourly Variation)

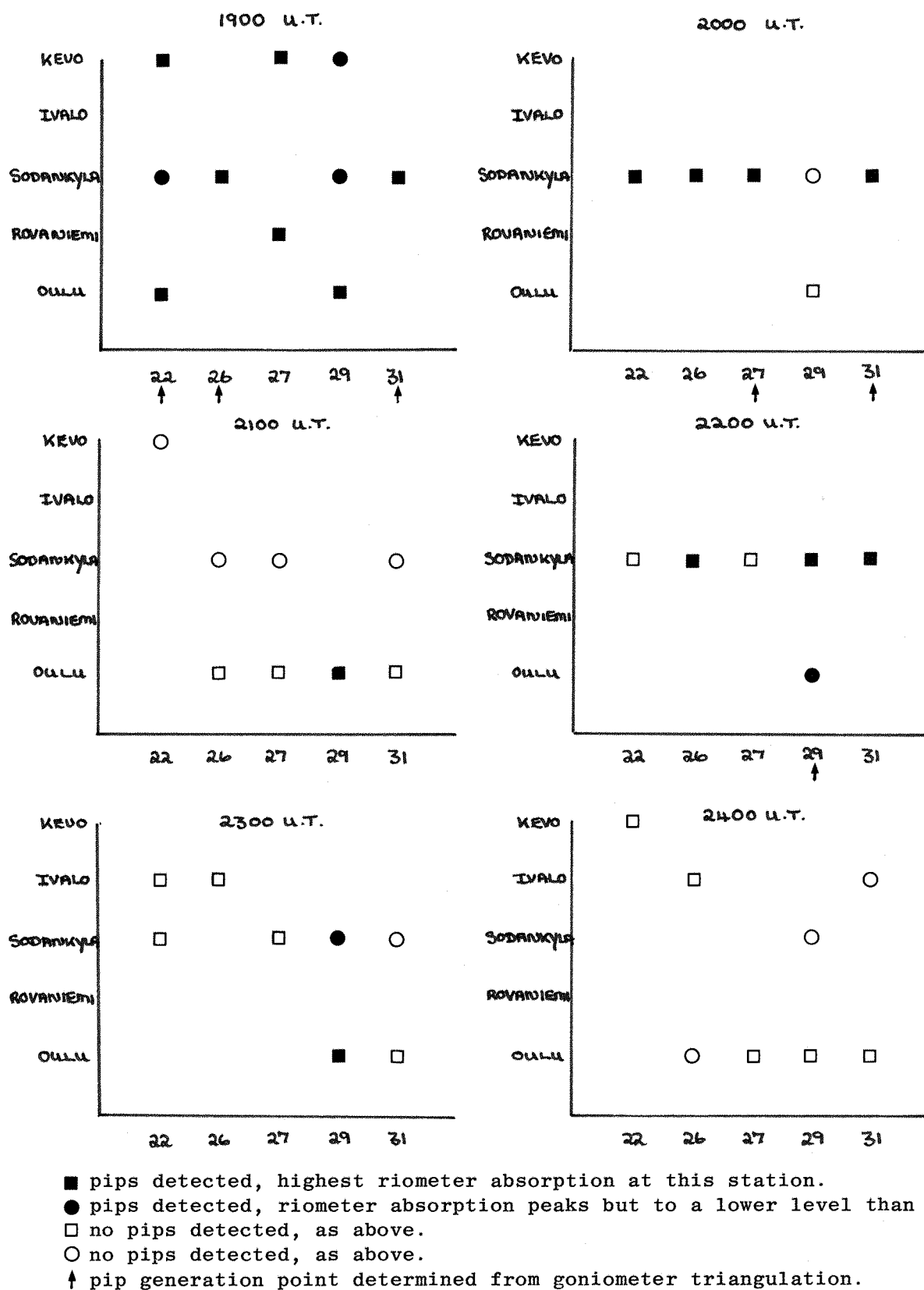


Fig. 6:18 The Location Of The Riometer Absorption Maxima
(Daily Variation)

21 UT few pips were detected, see figure 6.9, from which we conclude that there is some special significance in the electrojet position being near or just to the south of Sodankyla.

6.6.9 Defense Meteorological Photographs (DMSP)

Kamide and Akasofu (1975) and Wallis et al. (1976) found that the electrojet was confined to a latitudinal region within the diffuse auroral emission zone, just equatorward of the region of bright discrete aurora.

In order to pursue the findings that the occurrence of pips was correlated with the auroral electrojet (section 6.6.3, 4, 6, 7 and 8) DMSP data were examined. The objective was to relate the occurrence, or otherwise, of pips with the diffuse aurora location. The limited temporal resolution of the photographs resulted in the study being aborted.

6.6.10 Pip Amplitude Measurements

It is well known that the minimum time, T_{\min} , during which a spectrum analyser must acquire information in order to make a valid amplitude estimate is:

$$T_w \geq T_{\min} = 1/B$$

where B is the resolution of the analyser and where T_w is the analyser time window (Bendat and Piersol, 1971). For a pip duration of ~ 0.1 seconds (section 6.2) $B \geq 10$ Hz. The selected resolution of 10 Hz enables the 27.5 Hz goniometer modulation to be easily identified and amplitude measurements were consequently made on each sideband.

Several measurement techniques were considered. A linear average, at (1000 ± 5) Hz, over the six pips, including the intervening periods was rejected because the pips last for only 0.5 seconds in 5.1 seconds; this would have given a low signal to noise ratio in the presence of atmospherics and further signals at 1kHz.

It was, therefore, necessary to measure the amplitude of each pip separately, subsequently averaging these values. The technique adopted was to utilise the "peak" facility of the analyser which stores the peak amplitude occurring in each frequency bin whilst the averager is

in operation. With practise and with use of a digital time code clock (chapter 4) it was possible to switch on the averager for < 0.3 seconds over each pip. Using this method the maximum amplitude of the pip plus noise was measured, rather than the time average of the noise and pip. (The signal to noise ratio at Tromsø was typically 6dB and at Sodankyla, 12 dB). The peak amplitudes of both the upper and lower sidebands were measured, where possible, on all six pips. (For about 20% of the pip sets analysed, one or more such measurements were rejected from the data because they fell concurrently with a loud spheric, producing an unrepresentative peak value). From up to twelve of these values, the average amplitude was calculated for each hourly timing pip set.

In order to convert the pip amplitude, in arbitrary units, into a field strength it was compared to the amplitude of a calibration signal which corresponded to a known field strength. Such 1kHz signals were recorded at the start of each side of tape, chapter 3. With due allowance for any change in background noise, normally caused by the onset, or end, of a chorus event the absolute field strength of the pip signal was readily calculated. This correction for noise variation was obtained by computing a linear average preceding and directly after both the pips and calibration tones and subtracting these, in an R.S.S. ^(root sum square) sense, from the signal and calibration signal amplitudes.

The resulting mean pip field strengths, are shown, for both Sodankyla and Tromsø, in figure 6.1 9. Field strengths at Sodankyla are higher than those at Tromsø; in agreement with the goniometer measurements which show a favoured source location close to Sodankyla. In general, on one night, variations at one station are mimicked by the others.

6.7 Summary Of Major Results And Initial Conclusions

Section 6.4 has established that the ELF pips recorded during this period were not the result of non-linear demodulation of a strong broadcast service radio signal in any part of the equipment. It is consequently proposed that these ELF pips, strength $\sim 0.1\mu T$, were produced by non-linear ionospheric demodulation of signals from one or more transmitters on these frequencies. Since all candidate transmission frequencies are < 700 kHz such an interaction would take place in the D region or lower E region.

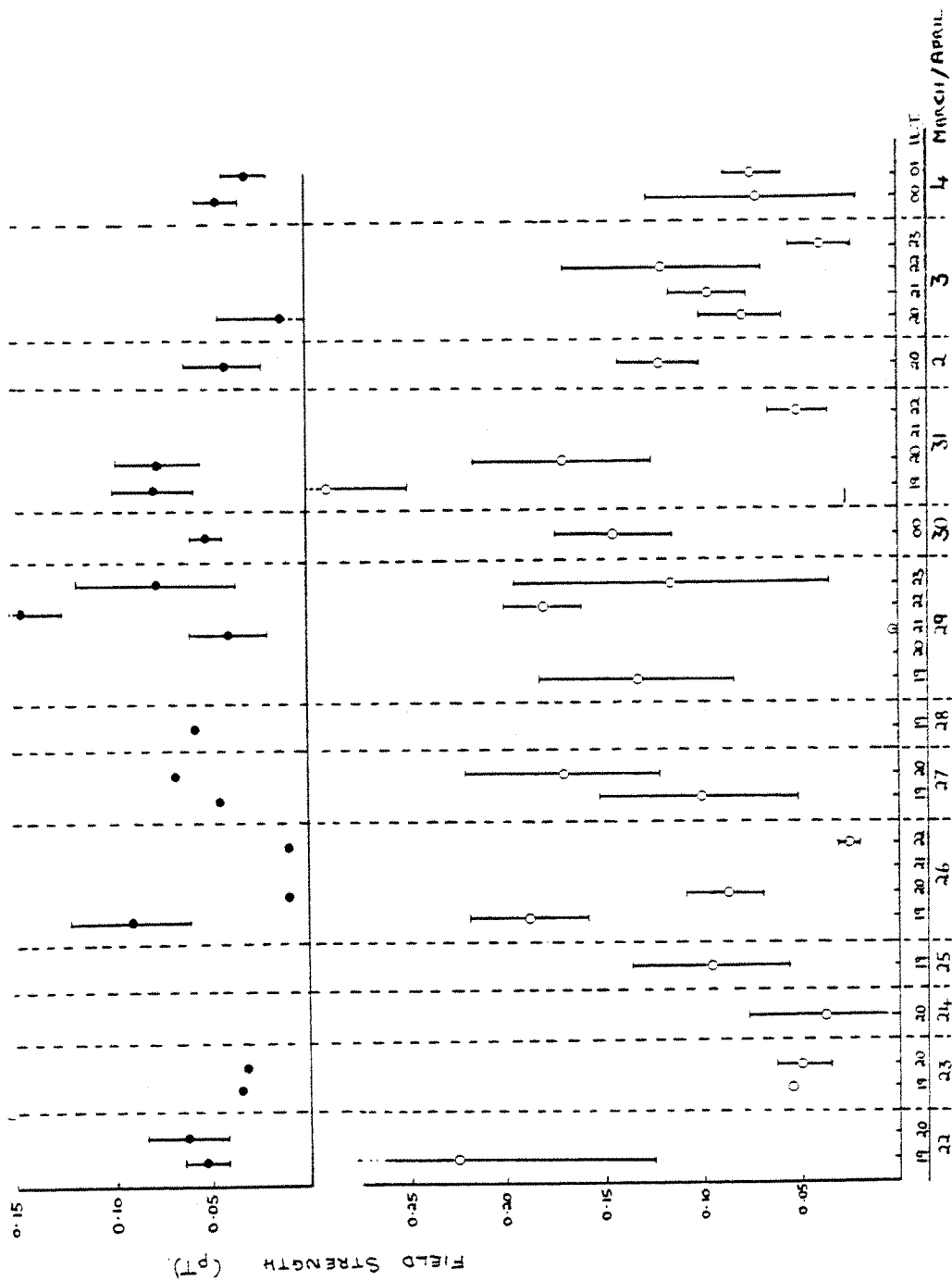


Fig. 6:19 ELF Pip Field Strengths At Tromso (●) And Sodankyla (○)



Controlled experiments, on non-linear ionospheric processes, usually involve E or F region interactions, see chapter 2. D-region effects are not, however, unprecedented; indeed, the Luxembourg effect itself (Tellegen, 1933) is a result of non-linear cross modulation in the D-region. The Finnish Broadcasting Co. Ltd., (1979) give a summary of such cross modulation effects monitored near Helsinki, Finland. It is interesting to note that many of the candidate frequencies defined in section 6.3 are reported to be associated with such non-linear effects.

The period of the experiment was characterised by two different levels of local geomagnetic activity, see section 6.6.3. From 14 March to 21 March, when no pips were recorded, the daily sum of K_{HDZ} indices, measured at the Sodankyla Geophysical Observatory, varied between two and twenty. From 22 March to 4 April, the corresponding values varied between twenty and forty-five and, with the exception of the 1 April, pips were recorded at least once each day. It is concluded that pips were only recorded when the daily magnetic activity was high. At high latitudes such activity is primarily a function of the auroral ionospheric current intensity and consequently a corollary of the above is that pips only occur when the ionospheric currents are strong. This is in agreement with the HF demodulation experiments of Kapustin (1977).

Inspection of STARE data and magnetograms from Sodankyla and Kiruna showed that there was always an active auroral zone current system nearby during the times of pip occurrence. Within the STARE viewing window the direction of the electrojet current was generally eastward when pips were recorded and westward when they were not, see figure 6.16.

The probability of pips occurring was greatest in the local evening, at 19 and 20 UT (around 22 magnetic local time). Only one measurement was, however, available at 18 UT and thus a high probability of occurrence at this time should not be ruled out.

On six occasions the signal to noise ratio was high enough to allow the determination of the azimuthal bearing on the 1kHz signal source from both Sodankyla and Tromsø. On five occasions the sources were approximately the same. On three more occasions a bearing angle, with 180° ambiguity, was obtained from Sodankyla which did not coincide with the direction of the five cases having roughly the same source location.

This situation is depicted in figure 6.13.

Examination of riometer data from the meridinal Finnish chain showed that, within the latitudinal range of the stations analysed, the maximum region of absorption occurred near, or somewhat south of, Sodankyla on the five occasions described above. The riometer absorption maximum, interpreted as indicating the electrojet position, approximately coincides, latitudinally, with the triangulated generation region, see section 6.6.5.

Measurement of the pip duration, section 6.6.2, showed that there was considerable variation in ELF pip duration. The average pip duration was found to be 105 ± 8 ms. Turunen (private communication, 1980) states that the transmission duration of each pip is, however, only 100 ms.

CHAPTER SEVEN

ELF Pip Generation Mechanisms

7.1 Introduction

Section 6.7 has summarised the results obtained and has demonstrated a close relationship between strong local ionospheric current systems and the generation of ELF pips.

In the following sections possible ionospheric pip generation mechanisms are outlined. These mechanisms are based upon the theories outlined in chapter 2 for an isotropic plasma whereby modulated RF energy incident upon a localised region of the ionosphere causes, in the steady state, both time independent and time dependent variations of electron temperature. These time dependent variations, at the modulation frequency Ω and also 2Ω , cause a like variation in the ionospheric electron-neutral collision frequency which in turn causes a similar variation in the conductivity. Any ambient D.C. current is consequently modulated and acts as a large transmitting antenna in the lower ionosphere. Evidently, the auroral ionosphere, where the D.C. current of the auroral electrojet is extremely strong, will be particularly effective in this respect.

7.2 The Location Of The Generation Region

Previous (Utlaut, 1975) or proposed (Stubbe and Kopka, 1977) HF ionospheric heating experiments utilise a vertically incident wave from a high gain antenna in order to produce a localised "hot spot" overhead. The cause of the effect reported here has, however, been identified as LF and/or MF transmitters located several hundred kilometres distant from the generation region in the ionosphere. In addition, although no specific information regarding the transmitter antenna design and performance could be obtained (Zhulin, private communication, 1980) it is reasonable to suppose that the antennae are low gain capacitively loaded verticals (Blake, 1966). The radiation pattern is expected to be omnidirectional in azimuth with a maximum at 10° or 20° elevation (Belrose et al. 1959). Such an antenna is vertically polarised (Belrose et al. 1959).

As a consequence of these facts it is perhaps puzzling why one

region of the ionosphere should be heated preferentially to all others. In addition it is of interest to enquire why, within the limit of the triangulation error diamonds, five pip sources were colocated. Various mechanisms by which a localised heating region could be formed are discussed below.

7.2.1 Mechanism One

Consider a "heating" LF/MF wave propagating from either the south or north of the auroral zone and incident directly (no reflections) upon the ionosphere. (Figure 6.1 shows that most candidate transmitters are south of the auroral zone). For an omnidirectional high latitude antenna a circularly expanding LF/MF wave pattern(planar geometry) will result, which could cut the electrojet, considered here to be flowing east-west. Demodulation might then occur, by a manner such as described in chapter 2, within either the southerly or northerly edges of the electrojet region. Here there will be adequate current flow but low radio wave absorption, thus allowing the incident wave to attain electrojet altitudes.

Further consideration, however, shows that the effect of both the electrojet and the absorption is, primarily, to localise the pip generation region in geomagnetic latitude. Localisation in a longitudinal direction is less efficient, being provided by the inverse law decay of field with distance and, to some extent, by absorption. Additionally, the distance from the transmitter to each element of the electrojet is different from that of neighbouring elements. Consequently, each element will not be heated in phase with its neighbour.

It is thus difficult to visualise how a localised, and coherent ionospheric radiator could be formed.

7.2.2 Mechanism Two

In the second mechanism, illustrated in figure 7.1, a single transmitter is also considered but the possibility of waves multiply reflected from the ionosphere and ground is addressed. In certain regions the periodic heating effect of a wave having suffered m collisions may be in phase with the periodic heating from a wave having suffered n collisions ($n \neq m$). If the phase changes on reflection are the same for both waves this occurs when:

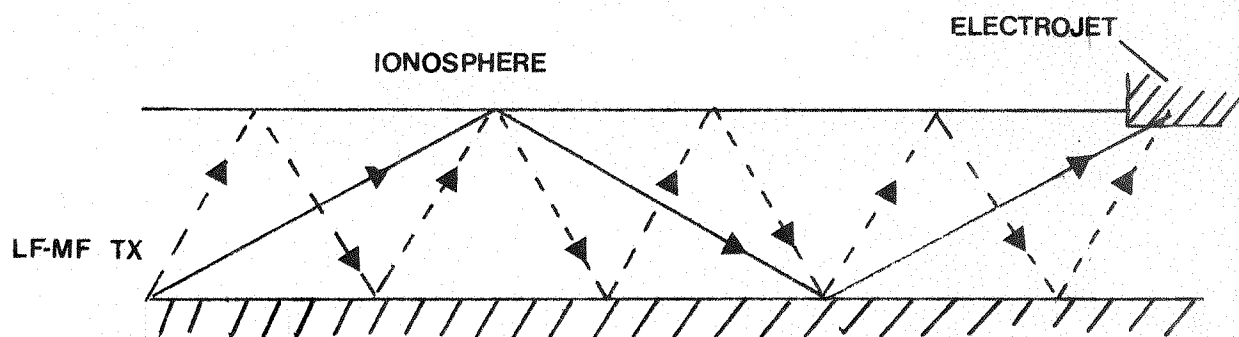


Fig. 7:1 Mechanism 2, employing multiply reflected waves.

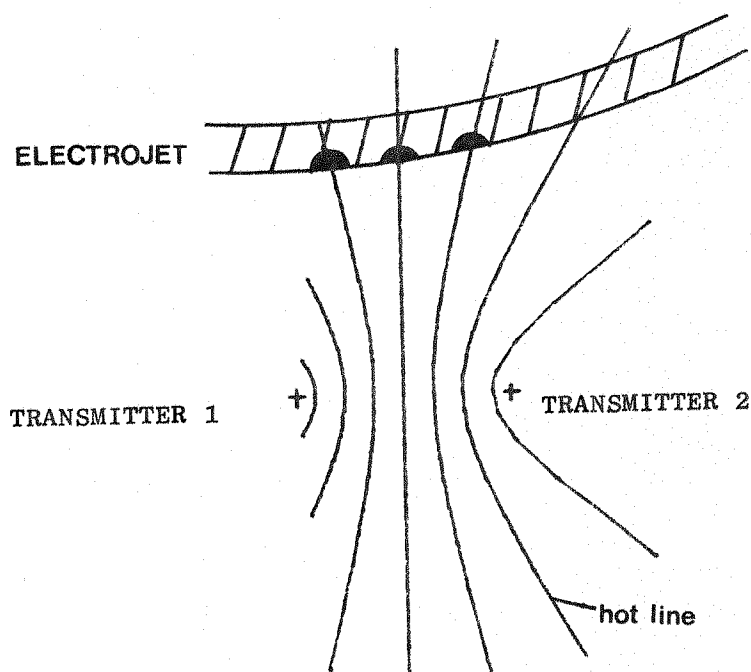


Fig. 7:2 Mechanism 3. Ionospheric demodulation occurs in a region (denoted \bullet) centred on the intersection of a hyperbola, defining the locus of equiphase modulation signals, and the auroral electrojet.

$$p \frac{\lambda_m}{2} = L_n - L_m$$

is satisfied, where p is a positive integer, L_n and L_m represent the effective path lengths and λ_m is the modulation wave length. In planar geometry a stationary pattern of periodically heated rings ("hot" rings) concentric with the transmitter would result in the ionosphere. Stationary "cold" rings corresponding to antiphase modulated signals would occur between the hot rings.

A localised demodulation region would be expected to occur where the electrojet and the hot ring overlap. Demodulation would be forbidden within a cold ring.

7.2.3 Mechanism Three

For the third mechanism, see figure 7.2, consider two transmitters accurately controlled in such a way that the modulated information (but not necessarily the carrier information) is broadcast with some constant phase difference (which could be zero). Consider, for convenience, only the direct waves incident upon the ionosphere. These will result, in planar geometry, in a set of hyperbolae defining lines of equiphase where the ionosphere is periodically heated. Along the base line joining the two transmitters these hot strips will be separated by $\lambda_m/2$ where λ_m is the modulation wavelength. Strips of periodically heated ionospheric plasma may be envisaged, centred upon these in phase hyperbolae. Along the baseline, between the two stations, the hot strips will be $\lambda_m/4$ in width, and separated from each other by corresponding cold strips.

A localised demodulation region will exist where a hot strip overlaps that region of the ionosphere carrying an adequate D.C. electrojet current.

7.2.4 Mechanism Four

Consider now the case of three, or more, stably phased transmitters each pair of which gives rise to a set of hot strips. At the intersection of two or more of these a specially hot region will occur. This is depicted in figure 7.3 for the case of three transmitters.

A fixed demodulation region is now defined by the crossing of one

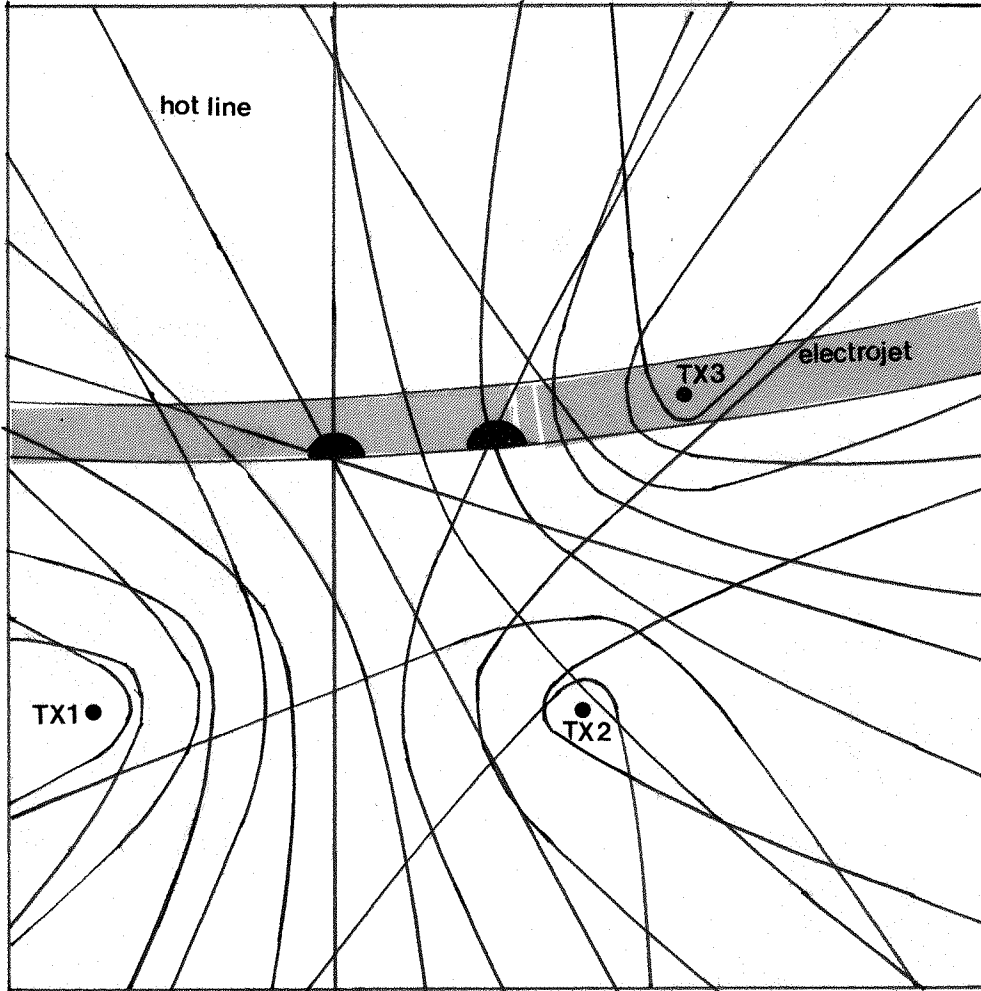



Fig. 7:3 Mechanism 4. Ionospheric demodulation occurs where the electrojet flows through a fixed hot region (denoted ) defined by the intersection of > 2 hyperbolae of equiphase modulation signals.

of these hot regions by the electrojet. It is important to realise that a finite number of such demodulation regions is now possible, unlike mechanisms two or three which give rise to an infinite number of such regions.

7.2.5 Some Comments On Mechanisms Three and Four

Mechanisms three and four do not require that the transmitters use the same carrier frequency. The above arguments still hold providing that the interaction (reflection) heights are similar, i.e. that the transmitted frequencies are similar. More importantly, the modulation frequencies should be the same with the transmitters stably phased. Turunen (private communication, 1980) reports that the second pip broadcast at 12 UT carries information for transmitter time synchronisation, and frequency synchronisation purposes. The Finnish Broadcasting Co. Ltd., (1979) have tabulated the known characteristics of the Soviet LF/MF transmitters and have shown that, within most frequency groups, transmissions are synchronised. Turunen (private communication, 1980) has confirmed this for 173kHz, 236kHz and 612kHz. Confirmation that all LF/MF time pip transmissions, from the European region of the U.S.S.R., are synchronised could not be obtained (Zhulin, private communication, 1980; Turunen, private communication, 1980). It would appear reasonable, however, to assume that the pips are synchronised, particularly since certain transmitters, on different frequencies, are located on the same site.

Table 7.1 shows the mean distance of each generation region from each of the principal Soviet transmitters within a 1500 km radius of Sodankyla; such a distance represents about three hundred kilometres more than the radio horizon at these frequencies (Belrose, 1968). The table also gives the mean generation region to transmitter distances for each transmitter; denoted d_1 to d_6 inclusive, together with the standard deviation in the mean.

Evidently $d_1 \approx d_2 \approx d_3 \approx d_6$. Since one of the possible generation regions of mechanisms three and four is located equidistant from two or more synchronised transmitters this approximate equality was further investigated.

The analysis of variance and Fisher's F distribution (Runyon and Haber, 1971) were used to determine the probability with which the

TRANSMITTER		KALININGRAD	MOSCOW	MINSK	LENINGRAD	MURMANSK	SYKTYVKAR
TRANSMITTER FREQUENCIES AND POWERS		173kHz 1000 kW	173kHz 500 kW	281kHz 500 kW 549kHz 1000 kW	236kHz 1000 kW	657kHz 150 kW	173kHz 300 kW
			263kHz 2000 kW				
DATE	UT TIME	MEAN DISTANCE FROM TRANSMITTER TO CROSSING POINT, ON EACH DAY (km)					
22.3.79	19	1309	1279	1351	697	409	1238
26.3.79	19	1302	1280	1347	695	418	1245
27.3.79	20	1350	1321	1397	743	377	1256
29.3.79*	22	1608	1736	1743	1136	521	1616
31.3.79	19	1260	1214	1284	630	458	1212
31.3.79	20	1403	1380	1457	805	345	1284
MEAN DISTANCE TO EACH TRANSMITTER		$d_1 = 1325$ ± 24	$d_2 = 1295$ ± 27	$d_3 = 1367$ ± 29	$d_4 = 714$ ± 29	$d_5 = 401$ ± 23	$d_6 = 1247$ ± 12

* Omitted in the determination of each mean.

Table 7.1 Transmitter to Generation Region Distance Statistics

various mean transmitter to generation region distances could be considered samples of the same population, i.e. represent estimates of the same mean distance. For the two transmitter case such a test is equivalent to the better known Student's t test (Runyon and Haber, 1971).

The test was applied to the 173kHz transmitters at Kaliningrad and Moscow, which exactly fit the scheduling data. This showed that as large a difference as 30km ($d_1 - d_2$) would occur with a probability of 0.44. We thus conclude that the discrepancy between d_1 and d_2 is hardly significant, lending support to mechanism three.

Although the data set described in section 6.3, does fit with the programme scheduling of transmitters on 173kHz and 657kHz, this does not preclude contributions to ELF pip generation from other correctly phased signals. Here we restrict ourselves to Soviet transmissions, although a chance phasing between a Soviet transmitter and one located in another country is possible. Minsk (281kHz) transmits the 'First Programme' 02 to 22 UT and Moscow (263kHz) transmits the 'First Programme' 02 to 22 UT followed by the 'Second Programme' for one hour. Both of these transmitters can contribute to the ionospheric heating without conflict with the data described in section 6.3. Minsk (549kHz), which transmits the 'Second Programme', with its associated jingle, most of the day could also contribute to the heating and reradiation of pips. Since it is the only one of the major, in this context, transmitters radiating the 'Second Programme' prior to 22 UT reradiation of the jingle should be low, or non existent depending on the mechanism, and only its contribution to the coherent radiation of the ELF pips will be detected. Between 22 UT and 02 UT it will contribute to the general reradiation of the jingle and pips, see figure 6.2.

Inclusion of the very high power 2MW Moscow (263kHz) transmitter, which is approximately colocated with the Moscow 173kHz transmitter increases the available heating power but has no other impact.

When the 500kW Minsk (281kHz) and the 1MW Minsk (549kHz) transmitters are included a type four mechanism could result. Application of the variance analysis shows that the probability of the means d_1 , d_2 and d_3 taking the values given in table 7.1 and being estimates of the same population mean is ~ 0.2 .

We conclude that a type four mechanism is less probable than a

type three mechanism; however, its probability is far from insignificant. Attention must also be drawn to the Syktyvkar (173kHz) transmitter which is also $\sim 1300\text{km}$ from the generation region. Variance analysis again gives a probability of ~ 0.2 that Syktyvkar is equidistant, together with the Kaliningrad and Moscow transmitters, from the generation region. Confirmation of its operational status could not be obtained and therefore the transmitter has not been included in later calculations. Figure 6.1 shows, however, that Minsk, Kaliningrad, and Moscow lie between the south-south-west and south-east of the favoured pip generation region. These result in a mechanism four generation region which is somewhat larger in the north-south direction than in the east-west direction. Inclusion of the transmitter at Syktyvkar would, by giving a much better geometrical situation, reduce the north-south dimensions of the region.

The Leningrad (236kHz) transmitter is also interesting. The transmitter is not one of those stations approximately equidistant from the favoured generation region. For synchronised transmissions, however, signals from it, and signals from other stations satisfying mechanisms three and four could heat the ionosphere in phase providing:

$$\frac{n \lambda_m}{2} + d_4 = d_1 = d_2 (= d_3) (= d_6)$$

where n is an integer, λ_m is the modulation wavelength, and the parentheses indicate the condition required for a type four mechanism. For $n = 4$ this condition is well satisfied, table 7.1. Since this transmitter closes down at 22 UT its contribution to the heating effect might manifest itself by a drop in ELF pip field strength subsequent to this time. No such change was found, figure 6.19, and consequently it too has not been included in later calculations. Any sudden variations in field strength at 22 UT may be masked, however, by systematic movements of the electrojet away from a hot spot (mechanism four) or changes in the local electrojet strength, mechanisms three and four.

Finally, mechanisms three and four give rise to several hot strips, or regions, with the possibility of ELF radiation taking place from any of them, providing that they overlap the electrojet. Figure 6.13 shows three instances when source directions, which are only available from Sodankyla, do not pass through the worst case standard error region. These results can thus be explained via mechanisms three or four.

7.3 Heating Effects From Each Transmitter

Section 2.5.2 showed that the temperature rise ΔT , in an isotropic plasma, due to an incident wave, is proportional to $\left(E_o/E_p\right)^2$ where E_o is the incident field and E_p is the so called plasma field (Gurevich, 1978). We wish to evaluate both of these parameters for the transmission frequencies under consideration.

The ionospheric wave fields due to each of the transmitters defined in table 7.2 were determined at an altitude of 90km; this a typical night time (when most pips were detected) midlatitude reflection height (Belrose, 1968). The demodulation and reradiation is believed to take place near the reflection height, within the steep electron density ledge, of the bottom side nighttime ionosphere. Such a reflection height is probably somewhat high at these auroral latitudes; Belrose (1968) adopts a value of 85km for a high latitude path. A prodigious quantity of data applicable to later calculations is available, however, at 90km.

Adapting the LF/MF propagation equations of Belrose (1968) the RMS ionospheric field, E_I , (mV/m) at distance, L , (km) from an electrically short radiator is given by:

$$E_I = \frac{E_o}{\sqrt{2}} = \frac{E_u}{L} \cos \psi F_T \quad \text{equation 7.1}$$

Here E_u is the field 1km from the antenna which, for a short vertical radiator is given by:

$$E_u = 9.36 P_r^{\frac{1}{2}} \quad (\text{mV/m}) \quad \text{equation 7.2}$$

where P_r is the radiated power (watts) and ψ is the launching angle (degrees) necessary to attain the required altitude at a distance L away. This was determined from the curves presented by Belrose (1968). ψ can take negative angles in which case the wave is diffracted some distance around the surface of the earth. F_T is a factor <1 introduced because of the finite ground conductivity in the vicinity of the transmitting antenna (Jordan and Balmain, 1968). Belrose (1968) presents graphs of F_T as a function of ψ for local ground conductivities. The value of F_T , derived from the theoretical analyses of Wait and Conda (1958), who describe it as the antenna cut-back factor, is small for low launching angles (i.e. long skip distances), particularly when

the local ground conductivity is low, see table 7.2. Watt et al. (1959) have compared experimental Arctic LF field strength measurements with theoretically calculated values, and obtained good agreement when the antenna cut back factor was included. Propagation from the transmitter to the ionosphere is assumed to be direct. For the group of transmitters ~ 1300km distant from the favoured generation regions this requires a negative launch angle with a correspondingly high loss (via F_T). The ground conductivity was estimated from the ice cover which was itself estimated from March/April mean temperatures given by Salt (1976). Wave absorption at sub-electrojet altitudes is considered negligible for this predominantly night time effect.

Table 7.2 shows the results of evaluating equation 7.1. We see that the field (E_T) due to each of the approximately equidistant transmitters is exceeded by the field due to the transmitter located at Murmansk, which is itself exceeded by the field due to the powerful Leningrad transmitter.

That any resulting non-linear effect must in fact be small can be seen by examining the ratio of wave electric field energy density, U_E , to particle energy density, U_p :

$$\frac{U_E}{U_p} = \frac{\epsilon_0 E_T^2}{2 N_e \kappa T_e}$$

where T_e is the electron temperature (K), N_e is the electron number density (m^{-3}) and κ is Boltzman's constant. For $E_T = 1mV/m$, $10^7 m^{-3} < N_e < 10^{10} m^{-3}$ for the D region and $T_e = 200K$ $U_E/U_p \leq 1 \times 10^{-4}$; i.e. the electric field energy density is much much lower than the particle energy density.

The plasma field E_p , given by equation 2.11 i.e.

$$E_p = 4.2 \times 10^{-5} \left[\delta T_e (\omega^2 + \nu_{en}) \right]^{\frac{1}{2}} \text{ mV/m}$$

was also evaluated at each candidate frequency, table 7.2. Identical interaction heights have been assumed at all frequencies for this predominantly night time effect. The effective collision frequency, ν_{en} , (Davis, 1969), at 90km altitude, was derived from the expression given by Gurevich (1978):

$$\nu_{en} = 5.8 \times 10^{-17} N_m T_e^{5/6} (s^{-1}) \text{ for } T_e \leq 10^4 K \quad \text{equation 7.3}$$

Transmitter Location	Kaliningrad	Moscow	Moscow	Moscow	Minsk	Minsk	Leningrad	Murmansk
Average distance from generation region (km)	1325	1295	1295	1295	1367	1367	714	401
Frequency (kHz)	173	173	263	263	281	549	236	657
Radiated Power (kW)	1000	500	2000	2000	500	1000	1000	150
Launch Angle (ψ) (degrees)	-2	-2	-2	-2	-2	-2	+2	+10
(1) Mean Ground Temperature ($^{\circ}\text{C}$)	(2)10	6	6	6	? (~ 8)	? (~ 8)	2.5	≤ 0
Estimated local ground conductivity (mhos/m)	5×10^{-3}	5×10^{-3}	5×10^{-3}	5×10^{-3}	5×10^{-3}	5×10^{-3}	2×10^{-3}	0.5×10^{-7} (ice)
F_T	0.25	0.25	0.175	0.175	0.175	0.06	0.35	0.3
E_I (mV/m)	1.8	1.3	1.8	1.8	0.9	0.4	4.6	2.7
E_p (mV/m)	40.2	40.2	60.8	60.8	64.9	126	54.6	151.3
$\left(\frac{E_o}{E_p}\right)^2$	4×10^{-3}	2.1×10^{-3}	1.7×10^{-3}	1.7×10^{-3}	3.8×10^{-4}	2×10^{-5}	1.4×10^{-2}	16.2×10^{-4}
$\left(\frac{E_o}{E_p}\right)^2$ SUM	8.2×10^{-3}							

(1) - from Salt (1976) (2) - estimated as per Copenhagen

Table 7.2 Transmitter Heating Effects

where N_m is the neutral gas number density (m^{-3}), T_e is the electron temperature (K), and δ is the average fractional energy lost per electron neutral collision (s^{-1}). N_m , T_e and δ were obtained from the atmospheric model also given by Gurevich (1978), see table 7.3. The values of E_p so obtained show that the lower frequency signals are more efficient at heating the ionosphere than the higher frequency signals.

In order to assess the relative heating effects of each transmitter, these values of E_I and E_p were combined in table 7.2 to give $\left[E_o/E_p\right]^2$; ($E_o = \sqrt{2}E_I$). We now see that the Leningrad transmitter has the largest heating effect, followed by certain of the transmitters ~ 1300 km distant followed by transmissions from Murmansk. Generation of ELF pips via mechanisms three or four, however, uses the combined heating effect from two or more transmitters. Thus a more valid comparison may be between Leningrad, the summed effect of the groups ~ 1300 km distant, and Murmansk. This too is shown in table 7.2.

On the basis of the heating effect only we conclude that Leningrad (236kHz) is the most likely cause of the ELF pips.

7.4 Conclusions - The Generation Mechanism

Various mechanisms which can result in a localised generation region, consistent with the observations, have been discussed.

If the generation mechanism were due to a single transmitter, via mechanism two, consideration of the ratio $\left(E_o/E_p\right)^2$ indicates that signals from the relatively nearby Murmansk (657kHz) transmitter will have a smaller heating effect than those from the more distant, but lower frequency transmitters. Of the latter, signals from Leningrad (236kHz) dominate, even over the sum of the transmitters about 1300km distant. Leningrad does not, however, transmit between 22 UT and 01 UT and since pips were heard several times during this period the effect cannot be accredited simply to this one transmitter. The next most effective individual transmitter is located at Kaliningrad (173kHz) and is a member of the group 1300km distant. One possibility is that the pips were caused by the Leningrad transmitter prior to 22 UT and the Kaliningrad transmitter subsequent to this time.

In favour of a multi-transmitter mechanism (three or four) is the statistical evidence that most of the pip generation regions are

Parameter	Value	Comments
ν_{en}	$1.6 \times 10^5 \text{ s}^{-1}$	Determined from equation 7.3
ν_{in}	$2.0 \times 10^4 \text{ s}^{-1}$	Obtained from Gurevich (1978). Agreement is to within 5% of Chapman (1959).
Mean molar mass	28 A.M.U.	
ω_{Be}	$8.9 \times 10^6 \text{ rad s}^{-1}$	Calculated using a value of the magnetic field for 90km altitude determined from Stassinopoulos (1966)
ω_{Bi}	164 rad s^{-1}	
T_e	200K	Given by Walker (1966)
N_m	$3.9 \times 10^{19} \text{ m}^{-3}$	Determined from Gurevich (1978)
δ	4×10^{-3}	Determined from Gurevich (1978)

Table 7.3 Auroral Ionospheric Parameters at 90km Altitude

equidistant from several of the tabulated transmitters. At least two of these were operational at any time (three if Syktyvkar was operational) between 02 UT and 01 UT.

Due to the strong evidence in favour of a multi-transmitter effect it is proposed that the ELF pips result from heating of the ionosphere via either mechanism three or four. There are arguments in favour of both mechanisms.

Table 7.2 shows the principal contributing equidistant transmitter to be: Kaliningrad (173kHz), Moscow (173kHz) and Moscow (263kHz). Since two of these transmitters are approximately colocated this would represent a type three effect. A type four effect would result by also including Minsk (281kHz and/or 549kHz) in the set of contributing transmitters. However, not only are the heating effects of these transmitters lower than the previously mentioned transmitters, but there is less, although not insignificant, statistical evidence in favour of their inclusion. On the basis of these discussions a type three mechanism might be considered the favourite candidate for explaining the observations.

Both mechanisms are compliant with the requirement to explain the approximate colocation of several generation regions. In this respect, however, mechanism four is most attractive since colocation of the generation regions is implicit in the mechanism description. Mechanism three satisfies this requirement only because the electrojet flows (during the evening UT) most often at a particular latitude. Goniometer derived generation regions consequently will be biased towards this latitude.

Two other transmitters cannot be completely ruled out. The first is Syktyvkar, also 1300 km from several generation regions. Confirmation of its operational status would result in almost ideal geometry for a type four effect. The second is Leningrad whose signals could be $4\lambda_m$ out of phase at the generation region, with signals from the transmitters cited above. This would result in additional coherent heating.

In summary statistical evidence argues in favour of a multi-transmitter effect but the data are unable to distinguish between the proposed mechanisms or their variants.

7.5 Physical Plausibility Of ELF Pip Generation By LF/MF

Modulation Of The Electrojet

7.5.1 Introduction

It has been proposed that certain transmitters, equidistant from the favoured generation region, are the most likely cause of ELF pips. The following demonstrates the plausibility of this hypothesis. The effects of the LF/MF transmitters on the auroral ionosphere, and the resulting ground ELF field strengths are estimated and compared to the experimental ELF pip field strengths given in figure 6.19.

7.5.2 The Problem

We wish to determine the value of ΔJ , the modulated component of the electrojet current density, due to the incident modulated wave.

Consider first the D.C. ionospheric current flowing due to an external field \underline{E} . This situation is depicted simplistically in figure 7.4

$$\underline{J} = \underline{\sigma} \underline{E} \quad \text{equation 7.5}$$

where \underline{E} is the external, constant electric field driving the auroral electrojet, \underline{J} is the D.C. ionospheric current density, and $\underline{\sigma}$ is the ionospheric conductivity tensor.

Now consider the A.C. (1kHz) perturbation to this current (ΔJ) due to perturbations of the conductivity $\Delta \underline{\sigma}$

$$\Delta \underline{J} = \Delta \underline{\sigma} \underline{E} \quad \text{equation 7.6}$$

Writing these equations in terms of their Hall and Pedersen components and dividing gives:

$$\frac{\Delta J_H}{J_H} = \frac{\Delta \sigma_H}{\sigma_H} \quad \text{and} \quad \frac{\Delta J_P}{J_P} = \frac{\Delta \sigma_P}{\sigma_P} \quad \text{equation 7.7}$$

7.5.3 The Ambient Ionospheric Conductivity (σ)

Following Rishbeth and Garriott (1969), we write the ionospheric Hall and Pedersen conductivities σ_H and σ_P in terms of their electron and ion components:

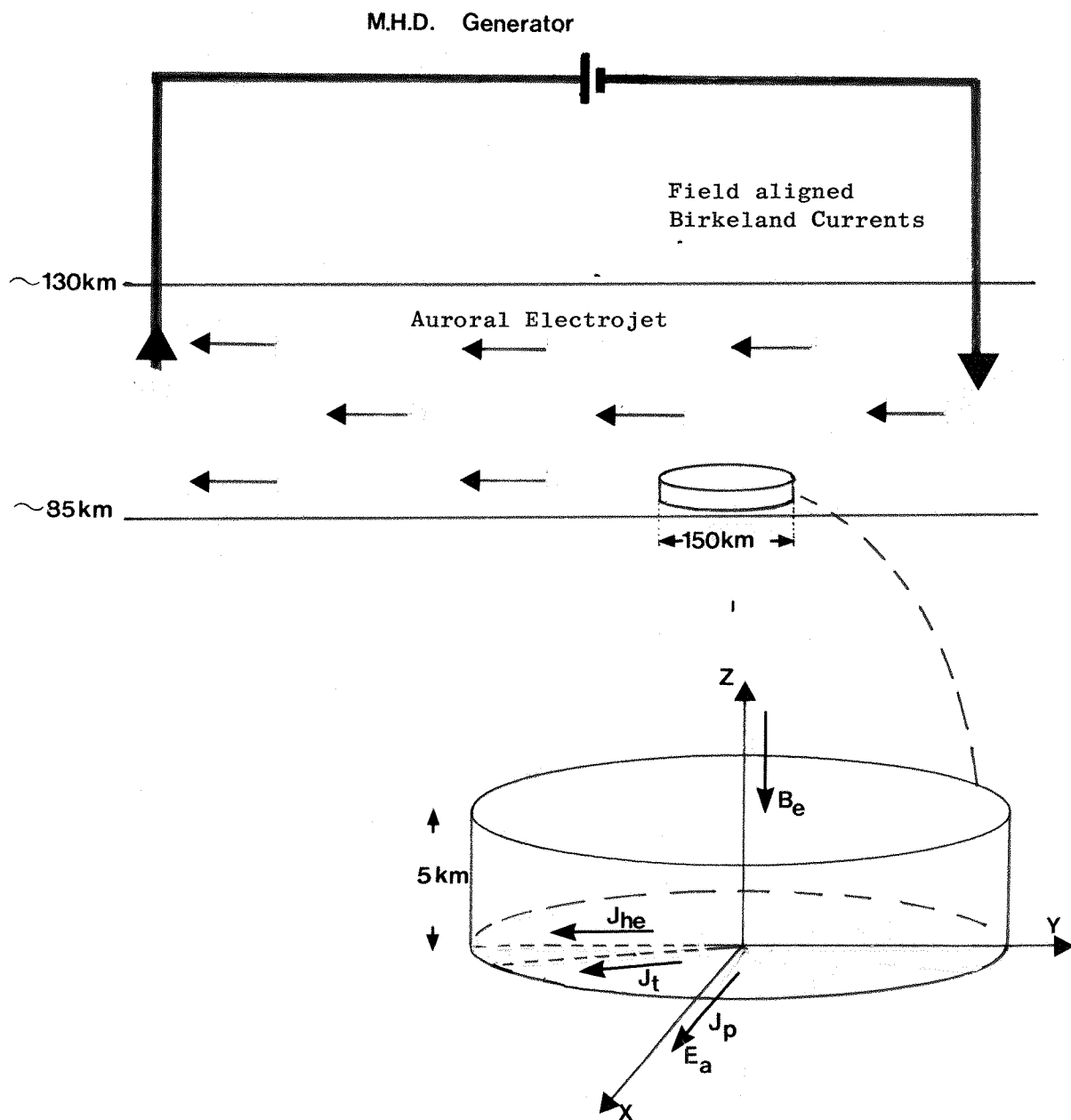


Fig. 7:4 Auroral Electrojet Modulation - Illustration Of
The Adopted Model And Coordinate System.

The ambient ionospheric electric field vector E_A is assumed to be orientated southward and perpendicular to the geomagnetic field B_E . J_t which represents the unresolved current vector flows approximately westward

$$\sigma_H = \frac{Ne^2}{m_e} \left(\frac{\omega_{Be}}{\omega_{Be}^2 + \nu_{en}^2} \right) \quad \text{equation 7.8}$$

$$\sigma_p = \frac{Ne^2}{m_e} \left(\frac{\nu_{en}}{\omega_{Be}^2 + \nu_{en}^2} \right) + \frac{Ne^2}{m_i} \left(\frac{\nu_{in}}{\omega_{Bi}^2 + \nu_{in}^2} \right) \quad \text{equation 7.9}$$

Here N is the electron or ion concentration (m^{-3}), ν_{en} and ν_{in} are the effective electron-neutral, and ion-neutral collision frequencies (s^{-1}), ω_{Be} and ω_{Bi} the electron and average ion gyrofrequencies ($rad\ s^{-1}$), and m_e and m_i the masses of the electron and average positive ion (Kg).

Rishbeth and Garriott (1969) have shown that the ionic component of the Hall conductivity is everywhere negligible in the ionosphere and it has consequently been neglected. Additionally, the effects of negative ions have been neglected since the ratio of negative ion number density to electron number density is less than 10^{-3} above 80km and at night (Turco and Sechrist, 1972).

σ_H and the two terms of σ_p , termed σ_{pe} and σ_{pi} respectively, were evaluated using the values for an altitude of 90km given in table 7.3. This resulted in:

$$\frac{\sigma_H}{\sigma_p} \sim 3.6 \quad \text{equation 7.10}$$

$$\text{and } \frac{\sigma_{pe}}{\sigma_{pi}} \sim 2.2 \quad \text{equation 7.11}$$

7.5.4 The Ambient D.C. Current Density (J)

Br kke and Rino (1978) have determined the horizontally flowing auroral ionospheric current density, during a fairly active period, using the Chatanika Incoherent Scatter Facility. In the midnight sector, and over the height range 85km to 95km, they give an integrated current density of $\sim 5\mu A/m^2$, a value which has been adopted in the following analyses.

By direct proportion it follows that the different current density components may be expressed as:

$$J_p \simeq \frac{5}{37} \mu A/m^2 \quad \text{equation 7.12}$$

$$J_{pe} \simeq \frac{5}{37} \times \frac{2.2}{3.2} \mu A/m^2$$

$$\text{i.e. } J_{pe} = 9.3 \times 10^{-2} \mu A/m^2 \quad \text{equation 7.13}$$

$$J_H \simeq 5 \times \frac{36}{37}$$

$$\text{i.e. } J_{He} = 4.9 \mu A/m^2 \quad \text{equation 7.14}$$

7.5.5 The Variation In Conductivity ($\Delta \sigma$)

Only variations in the electron component of the conductivity, $\Delta \sigma_e$, will occur due to the propagation of the LF/MF wave through the plasma.

$\Delta \sigma_e$ may be determined by evaluating the following equation for both the Hall and Pedersen conductivities (Gurevich, 1978):

$$\Delta \sigma_e = \frac{\partial \sigma_e}{\partial v_{en}} \frac{d v_{en}}{dT_e} \Delta \Omega T_e \quad \text{equation 7.15}$$

$\Delta \Omega T_e$ is the modulated component of the change in electron temperature due to the incident wave and may be obtained from equation 2.15. Any time independent temperature rise ΔT_e will be given by equation 2.14. Both are repeated here for convenience.

$$\frac{\Delta \Omega T_e}{T_e} = \left[\frac{E_o}{E_p} \right]^2 2M \left\{ \frac{1}{(\Omega^2 + \delta^2 v_{en}^2)} \left[\delta^2 v_{en}^2 \cos \Omega t + \Omega \delta v_{en} \sin \Omega t \right] \right. \quad \text{equation 7.16}$$

$$\left. + \frac{M}{4(4\Omega^2 + \delta^2 v_{en}^2)} \left[\delta^2 v_{en}^2 \cos 2\Omega t + 2\Omega \delta v_{en} \sin 2\Omega t \right] \right\}$$

$$\frac{\Delta T_e}{T_e} = \left[\frac{E_o}{E_p} \right]^2 \left(1 + \frac{M^2}{2} \right) \quad \text{equation 7.17}$$

Here M is the modulation index, T_e the ambient electron temperature, Ω the modulation frequency and v_{en} the effective electron-neutral collision frequency.

Both equations 7.16 and 7.17 assume both an isotropic ionosphere and insignificant LF/MF wave absorption at sub electrojet altitudes. In an anisotropic plasma the above heating equations are multiplied by ϕ_p , a polarisation factor < 1 (Gurevich, 1978). This is unity when the wave electric field, E , lies parallel to the imposed geomagnetic field B_E . For a vertically polarised wave originating $\sim 1300\text{km}$ distant, and incident upon the auroral ionosphere, the wave E vector subtends an angle $\sim 5^\circ$ to the B_E field and $\phi_p \sim 1$. The isotropic approximation is consequently valid.

$\left(\frac{\partial \sigma}{\partial \nu_{en}} \right)_{H_e}$, $\left(\frac{\partial \sigma}{\partial \nu_{en}} \right)_{p_e}$ and $\frac{d\nu_{en}}{dT_e}$ may be derived from equations 7.8, 7.9 and table 7.3 i.e.:

$$\left(\frac{\partial \sigma}{\partial \nu_{en}} \right)_{H_e} = \frac{-2 N_e^2 \nu_{en} \omega_{Be}}{m_e (\omega_{Be}^2 + \nu_{en}^2)^2} \quad \text{equation 7.18}$$

$$\left(\frac{\partial \sigma}{\partial \nu_{en}} \right)_{p_e} = \frac{N_e^2}{m_e} \frac{(\omega_{Be}^2 - \nu_{en}^2)}{(\omega_{Be}^2 + \nu_{en}^2)^2} \quad \text{equation 7.19}$$

$$\frac{d\nu_{en}}{dT_e} = 4.8 \times 10^{-17} N_m T_e^{-1/6} \text{ (s}^{-1} \text{ K}^{-1}) \quad \text{equation 7.20}$$

7.5.6 Determination of ΔJ , ΔT_e and $\Delta_\Omega T_e$

Using equations 7.7, 7.15 and 7.18

$$\Delta J_{He} = - J_{He} \left[\frac{2 \nu_{en}}{(\omega_{Be}^2 + \nu_{en}^2)} \right] \frac{d\nu_{en}}{dT_e} \Delta_\Omega T_e \quad \text{equation 7.21a}$$

which at 90km approximates to:

$$\Delta J_{He} = - J_{He} \left[\frac{2 \nu_{en}}{\omega_{Be}^2} \right] \frac{d\nu_{en}}{dT_e} \Delta_\Omega T_e \quad \text{equation 7.21b}$$

and using equations 7.7, 7.15 and 7.19

$$\Delta J_{pe} = \frac{J_{pe}}{\nu_{en}} \left[\frac{(\omega_{Be}^2 - \nu_{en}^2)}{(\omega_{Be}^2 + \nu_{en}^2)} \right] \frac{d\nu_{en}}{dT_e} \Delta_\Omega T_e \quad \text{equation 7.22a}$$

which at 90km approximates to:

$$\Delta J_{pe} = \frac{J_{pe}}{v_{en}} \frac{dv_{en}}{dT_e} \Delta_\Omega T_e \quad \text{equation 7.22b}$$

7.5.7 Evaluation

Equations 7.16 and 7.17 were evaluated for a wave of modulation index 75% and a composite $(E_o/E_p)^2$ of 8.2×10^{-3} , see table 7.2, giving a predicted temperature change of:

ΔT_e , the increase in ambient electron temperature due to the wave, $\simeq 2K$ (i.e. an increase of $\sim 1\%$ over ambient) and $\Delta_\Omega T_e$, the modulated variation in electron temperature due to the wave, $\simeq 0.5K$ peak to peak (i.e. a variation of $\sim 0.25\%$ in the ambient temperature).

Using this value of $\Delta_\Omega T_e$ and values of other parameters given in table 7.3 equations 7.21 and 7.22 were evaluated giving predicted A.C. electrojet components of:

$\Delta J_{He} \simeq -2.5 \times 10^{-12} \text{ Am}^{-2}$ (R.M.S.), (i.e. $5 \times 10^{-5}\%$ of the ambient Hall current) and $\Delta J_{pe} \simeq 8 \times 10^{-11} \text{ Am}^{-2}$ (R.M.S.), (i.e. $\sim 8 \times 10^{-2}\%$ of the ambient Pedersen current).

Interestingly at this height, the Pedersen current density variation due to the incident waves is ~ 30 times larger than the Hall current density variation. This applies though the electrojet flows predominantly as a Hall current.

We conclude that ELF pip radiation from the auroral electrojet will occur primarily from the Pedersen currents.

7.5.8 Estimation of Ground Field Strength

Using this prediction of the current variations due to the 1kHz pip modulation a zeroth order estimate of the ground measured field strength can be made. It is convenient to consider a cylindrical region of perturbed plasma in the lower ionosphere, figure 7.4, and to calculate the field density directly below the cylinder.

In the near zone the magnetic vector potential is quasi-static

and given, at some point r_1 , by :

$$A(r_1) = \frac{\mu_o}{4\pi} \frac{1}{r} \int_V J_o(r) d^3 r \quad \text{equation 7.23}$$

With the approximation that the resulting field is due to the Pedersen current variations on intergration the resulting magnetic field directly below the cylinder is given by:

$$\Delta B_y = (\nabla \times A)_y = \frac{\mu_o}{4\pi} \frac{1}{Z^2} V J_p \quad \text{equation 7.24}$$

where V is the cylinder volume and Z is the mean altitude of the cylinder.

A volume 5km high and 150km in diameter is assumed. An interaction volume height of 5km was selected because of the steep electron density gradient on the bottom side nighttime ionosphere (when most pips were received). 150km represents $\lambda_m/2$. For $Z = 90\text{km}$:

$$\Delta B \simeq 0.09\text{pT} \quad \text{equation 7.25}$$

which is in good agreement with the ELF pip field strength measurements (typically 0.05pT to 0.2pT) made at Sodankyla, figure 6.19.

7.5.9 Conclusions

A simple theoretical approach to determine the ionospheric temperature variations, auroral electrojet current density variation, and the corresponding magnetic field variations, due to the modulated component of the incident LF/MF waves has been developed.

The 1kHz timing pip modulation due to the combined heating effects of the transmitters defined in table 7.2 produce a 2K rise in electron temperature over ambient, with a superimposed alternating component of $\sim 0.5\text{K}$. The corresponding modulated change in Pedersen current density is higher than the Hall variations by a factor of ~ 30 . Using the derived Pedersen current density variation of $\Delta J_{pe} = 8 \times 10^{-11} \text{Am}^{-2}$, and an idealized heated ionospheric volume, the magnetic field variation measured on the ground, directly below the volume is calculated to be 0.09pT. This is in good agreement with the experimental field strengths determined from the Sodankyla data, shown in figure 6.19.

We conclude that it is indeed plausible that the aforementioned LF/MF transmitters caused modulation of the auroral electrojet.

7.6 Final Summary And Conclusions

A new non-linear ionospheric effect has been discovered by analysing ELF and VLF radio signal data collected in auroral Scandinavia during March and April 1979. This effect involved demodulation, in the auroral ionosphere of the six hourly timing pips from certain Soviet LF and/or MF broadcast transmitters. The resulting ELF pips, each of duration (105 ± 8) ms, and frequency $1\text{kHz} \pm 0.5\text{ Hz}$ were received by five receivers at three locations in auroral Scandinavia. A detailed study has shown that demodulation could not have taken place in the goniometer equipment.

The demodulation only occurred during periods of enhanced magnetic activity, and only when the daily sum of the index K_{HDZ} (daily sum) for Sodankyla exceeded ~ 18 . Magnetometer data showed that pips were only received when there was an active electrojet current system nearby. Within the STARE viewing window (over Northern Norway) there was a high correlation between pip occurrence and an eastward flowing electrojet.

The probability of pips occurring was greatest at 19 UT and 20 UT, although, since few data were available at 18 UT a high probability of occurrence at this time should not be ruled out.

On six occasions the goniometer technique was used to locate the generation region. On five occasions these were approximately the same, being about $\sim 150\text{km}$ south of Sodankyla and $\sim 400\text{km}$ south-east of Tromsø. At these times the position of maximum riometer absorption, interpreted as indicating the electrojet position, lay at this same latitude.

A close association between the generation of ELF pips and both the strength and position of the auroral electrojet current system was clearly demonstrated. As a result it was proposed that the RF energy from a modulated LF/MF wave caused time dependent variations of the electron temperature at the modulation frequency. A like variation in the ionospheric electron-neutral collision frequency then resulted causing a similar variation in the conductivity which in turn modulated the electrojet current system. The latter acted as a large ionospheric ELF antenna.

Eight LF/MF transmitters were identified, within a 1500km radius of the generation region, which might give rise to these ELF pips. Four possible generation mechanisms were proposed. Of these, mechanisms two, three and four described how a localised, coherent source could be produced many kilometres from any of the transmitters. Each also explained why several source locations were approximately the same. Mechanism two, a single transmitter mechanism, proposed that generation could occur within stationary circles of preferentially heated plasma (hot rings) where the modulation on two waves which had suffered an unequal number of ionospheric and ground reflections were in phase. These would be separated from each other by similar cold rings. The third mechanism proposed that generation would occur anywhere along hyperbolae defining the loci of equiphase modulation from two transmitters. The fourth mechanism suggested that generation occurred at the intersection of two or more of these hyperbolae, resulting from three or more transmitters.

The data argued strongly in favour of mechanism three or four, but were unable to resolve between the two. A study of the mean generation region to transmitter distances showed that a type three mechanism involving Kaliningrad (173kHz) and Moscow (173kHz and 263kHz) was the more probable ($p = 0.44$). The probability of a type four mechanism involving additional transmitters at Minsk (281kHz and 549kHz) (and/or Syktyvkar (173kHz) - operational status unconfirmed) was less than for mechanism three but was still far from insignificant ($p \sim 0.2$). Additionally, since the generation regions were fixed under mechanism four this explained better the colocation of several generation regions. The colocation was explained for generation via a type three mechanism by the statistical preference of the electrojet for a certain latitude at any local time.

Using theoretical results adapted from Hibberd (1955) and Gurevich (1978), an alternating electron temperature variation, at the pip modulation frequency of ~ 0.5 K peak to peak, superimposed upon a steady electron temperature rise of 2K over ambient, was predicted from the combined heating effect of Kaliningrad (173kHz), Moscow (173kHz, 263kHz) and Minsk (281kHz, 549kHz). The corresponding Pedersen conductivity variation, for an interaction height of 90km, was shown to be $8 \times 10^{-11} \text{ Am}^{-2}$; larger than the Hall conductivity variation. Using a zeroth order approximation a corresponding magnetic field variation of ~ 0.09 pT was predicted on the ground, directly below the source.

This was in good agreement with the experimental field strengths measured at Sodankyla (~ 0.05 pT to ~ 0.2 pT). The plausibility of the premise that ELF pip generation occurred in the auroral electrojet due to ionospheric heating by Soviet LF and MF transmitters was therefore confirmed.

CHAPTER EIGHT

An ELF Receiver For The Frequency Range 0.3 Hz to 700 Hz

8.1 Introduction

The ELF receiver described in this chapter has been designed as a many faceted instrument. Its dual channels can independently process the signals from two orthogonal antennae, feeding each output separately to an FM tape recorder. Care has been taken in the design to obtain good amplitude and phase matching between the two channels in order that it may be later developed into a direction finding (goniometer) receiver. Chapter 3 describes the requirements placed upon such an instrument. The receiver has a maximum flat response over the frequency range ~ 0.3 Hz to ~ 700 Hz; however, two other optional bandwidths are provided within this range viz, 0.3 Hz to 40 Hz and ~ 200 Hz to ~ 700 Hz. This is to suit experimental interests and/or noisy (high interference) recording locations, section 8.3.

It must be emphasized that the receiver has been designed to be used primarily at remote locations in Europe or North America, c.f. section 3.3.2. As such it has been recognised that, although operated some distance from the nearest mains supply, the limiting noise source for such a receiver will probably be radiated mains fundamental and harmonic interference together with other man made interference. (In the remainder of this chapter mains interference is taken to include both fundamental and harmonic signals). It is extremely unlikely that equipmental noise will ever limit the system sensitivity. To this end sophisticated mains harmonic and other filtering has been provided. The effects of the equipmental noise have, however, not been ignored.

It is envisaged that the receiver will be used in conjunction with many different types of antenna and preamplifier, optimised for different frequency ranges within the overall receiver passband. Using techniques described in Appendix 3 the receiver gains can be adjusted such that they are compatible with various input signal levels. Chapter 9 describes one such antenna and preamplifier used.

8.2 Design Constraints

In 1976, after several experiments using equipment similar to that described in chapter 3, a decision was made to broaden the research

interests of the Space Radio Physics Group at Southampton, U.K. To this end a field site, two channel receiver with a 0.5 Hz to 1kHz passband was specified, this to lie between the bandwidth of magnetometers (Ness, 1970) and that of the goniometer receiver which has a passband between ~ 800 Hz and 16kHz. Amongst others, this receiver should be sensitive to high frequency PCl micropulsations (e.g. Orr, 1973); Schumann resonances (e.g. Rycroft, 1963); and auroral and polar chorus (e.g. Cannon et al., 1980). Additional specifications were that the receiver should be battery operated, and also transportable to remote field sites.

8.3 System Overview

Figure 8.1 depicts one channel of the two channel receiver. Each channel is essentially identical and, therefore, only one will be described below.

The signal from a low noise preamplifier, see for example chapter 9, is fed to a low noise non-inverting amplifier with a max. gain of 20dB. This is adjusted, using a trimmer potentiometer on the front panel, to present the maximum permissible signal to the following stages. This level is determined by high Q active notch filters and/or a mains comb filter.

The signal next feeds either a mains comb filter, or a buffer stage. The former configuration is used at locations with extremely high mains noise where, without early filtering, saturation of the following stages would occur. In regions where mains interference is less severe the latter configuration is adopted and the comb filter is switched to later in the receiver. Where possible this latter configuration should be utilised since the filter introduces noise which will be considerably amplified in the former. It is convenient to note at this juncture that in order to monitor signal levels panel mounted test points have been provided, after the first stage of amplification, prior to the notch filters, and after the last stage of amplification.

The mains comb filter is a high Q notch filter which attenuates 50 Hz (60 Hz) by 48 dB and, the first 31 harmonics to progressively lesser extents. It has a bandwidth of ~ 2 Hz at 50 Hz. The notch frequency is controlled by the output of a phased locked loop (P.L.L.), locked to the local mains frequency or to a high stability internal crystal oscillator signal at 50 Hz. Note that the mains comb frequencies are identical for

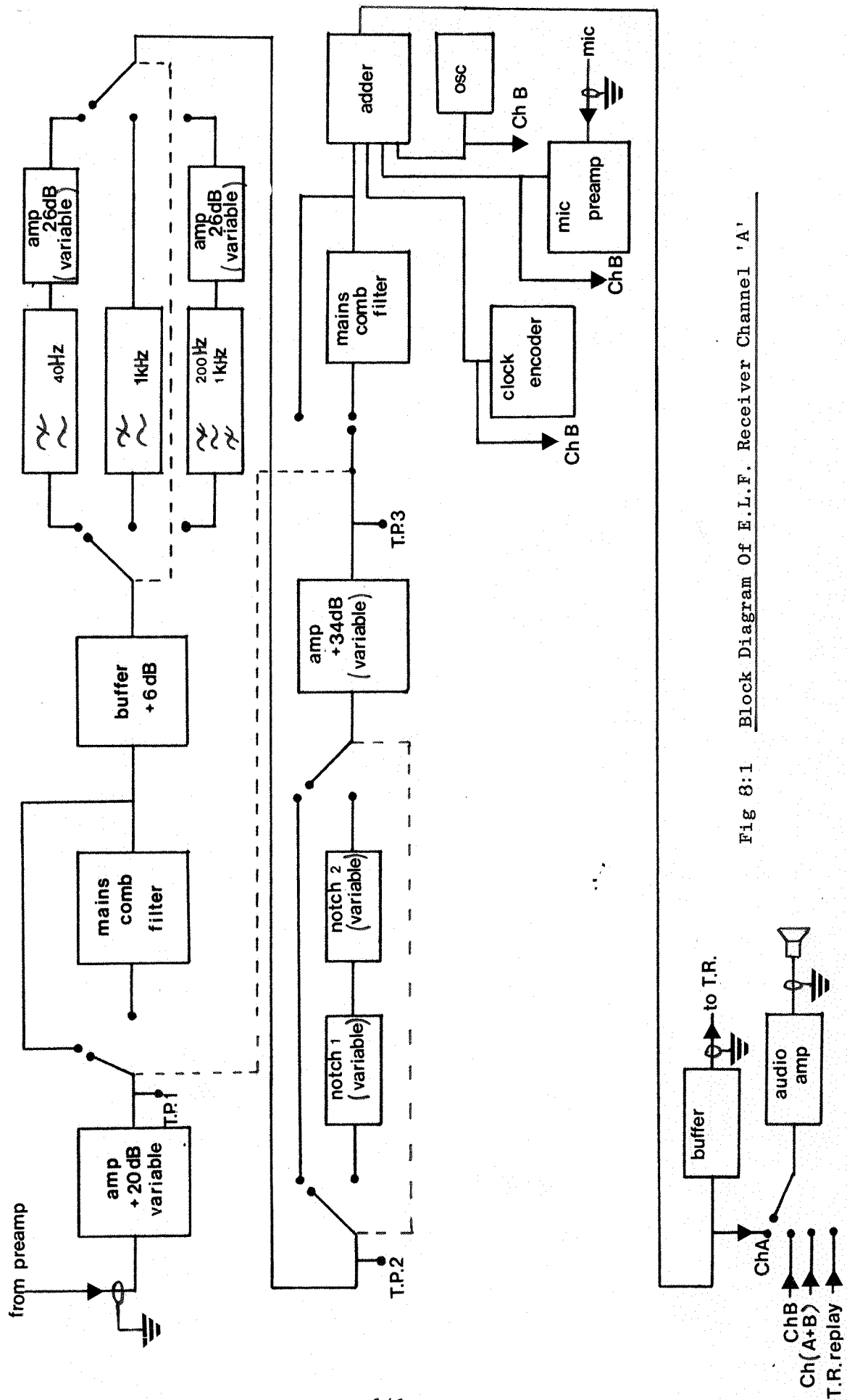


Fig 8:1 Block Diagram Of E.L.F. Receiver Channel 'A'

both channels since they are controlled by the same source. The channels are consequently better matched than they would be if conventional passive or active filters were used. The filter is regarded as the centre piece of the receiver since a receiver with a passband over the mains fundamental and lower harmonic frequencies, and operated in Europe or North America, will almost always be limited in sensitivity by mains interference.

Figure 8.1 shows that the signal may next take one of three paths; the prime route is through a low pass 4 pole Bessel filter with a gain of 5.6 dB and a 3 dB point at ~ 1 kHz. The second path is through a low pass 4 pole Bessel filter with a 3 dB point at ~ 40 Hz and thence to a stage of variable gain, maximum 26 dB. The third path feeds the signal through the low pass 1 kHz filter and thence through a 200 Hz 2 pole high pass filter. This bandlimited signal then passes to another stage of variable gain; maximum 26 dB. Three separate filter routes were included to suit specific experimental requirements. Gain, (adjustable via front panel mounted trimmer potentiometers), is provided on the two secondary channels in order to bring the voltage at the output of these channels up to that of the prime channel. Consequently, once the receiver has been set up for a particular receiving location any of the three modes can be used without substantially affecting the output amplitude; that is tape recorder settings. Bessel filters have been chosen because they exhibit no overshoot on impulsive signals. In addition to the above filtering considerable high frequency cut off is provided by the comb filter low pass filtering; see section 8.6.7.

The next stage consists of two optional, and independent, two pole pair notch filters with a Q of 20, and variable between 40 Hz and 400 Hz using a calibrated slow motion drive. These notch filters can be used to attenuate interfering signals specific to a particular receiving location. If necessary they may also be used to further reduce mains interference.

The signal passes to the mains comb filter, as already described, and/or to a summing amplifier. The latter is used to mix, where necessary, timing information from an external clock, verbal announcements from an amplified microphone signal and 0.5 second bursts from a 160 Hz marker oscillator onto the ELF channel. The restricted

frequency response of an FM tape recorder, when operating at slow speeds, makes voice announcements impossible. 160 Hz falls within the passband of the lowest speed and serves to "announce" the start and end of recordings.

The final signal stage is an output buffer. In parallel with this the signal is fed to an audio amplifier for monitoring purposes. A front panel switch facilitates the monitoring of channel A, or channel B (or channel (A + B) when developed further into a goniometer receiver). In addition, where the tape recorder has no internal replay monitoring facility its output may be fed to the receiver audio amplifier.

8.4 Amplifiers: Offsets, Noise and Device Selection

8.4.1 Introduction

The design of a sensitive receiver to operate at the high end of the specified frequency range (0.5 Hz to 1kHz) presents little difficulty when operational amplifiers are used as the basic building blocks. Problems do, however, arise at the lower end where care must be taken to ensure adequate noise performance, due to the onset of $1/f$ noise (Motchenbacher and Fitchen, 1973). D.C. offsets and D.C. drifts may also present difficulties depending upon the design.

8.4.2 Offsets and Offset Drifts

When designing a receiver to operate down to 0.5 Hz D.C. coupling between operational amplifiers is an obvious design approach. As such D.C. offsets and offset drifts with time, primarily due to temperature variations, would be a major factor governing the choice of front end integrated circuits since subsequent amplification of these offsets could cause saturation of the following stages. The subject of offsets and offset drifts has been reviewed by Clayton (1971).

In this application, however, A.C. coupling is almost obligatory. Any antenna will be subjected to varying degrees of vibration which will cause induced currents as the antenna cuts the earth's magnetic field. Rycroft (1965) has experienced such problems. The magnitude of the induced signals will be a function of any damping introduced by the antenna mounting but could, conceivably, cause saturation in later stages of the receiver. A.C. coupling reduces the possibility of this happening from low frequency vibrational signals.

The result of such A.C. coupling is that D.C. offset temperature drifts, at frequencies substantially below the break frequency, will also be blocked. Typical temperature drifts are of the order of 1K per minute or per hour rather than per second. We therefore conclude that if a design philosophy of A.C. coupling is employed the device D.C. offset and D.C. drift performances have little consequence on the choice of operational amplifier.

8.4.3 Noise

In the design of a sensitive receiver noise constraints often determine the amplifier configuration and the type of device employed. It is extremely important to study the noise performance at the front end, because this noise is amplified by later stages.

A non-inverting configuration has been employed throughout the receiver, in amplification and buffer stages. An inverting configuration would necessitate the use of high valued coupling capacitors and series input resistors in order to obtain a suitably low break point. The former would be a disadvantage in terms of bulk, the latter in terms of the high noise associated with the large valued resistor. The non-inverting configuration can, however, employ a high valued parallel input resistor, see figure 8.2, and it is shown below that the input referred noise is minimised by the use of such a resistor.

8.4.4. Input Referred Noise For A Non-Inverting A.C. Coupled Operational Amplifier

Figure 8.2 depicts an A.C. coupled non-inverting, (series voltage feedback), operational amplifier with its corresponding noise circuit shown in figure 8.3. Note that the feedback resistors R_E and R_F have been included in the noise calculation. Feedback itself does not change the equivalent input noise of the amplifier; however, the feedback resistors may themselves add noise via their thermal noise and via the input referred voltage and current terms (Motchenbacher and Fitchen, 1973).

If E_{ns} = noise associated with previous stage
 Z_s = sensor impedance
 i_p = noise associated with R_p , $\left[\frac{4kTB}{R_p} \right]$
 i_n = input referred current noise of the amplifier

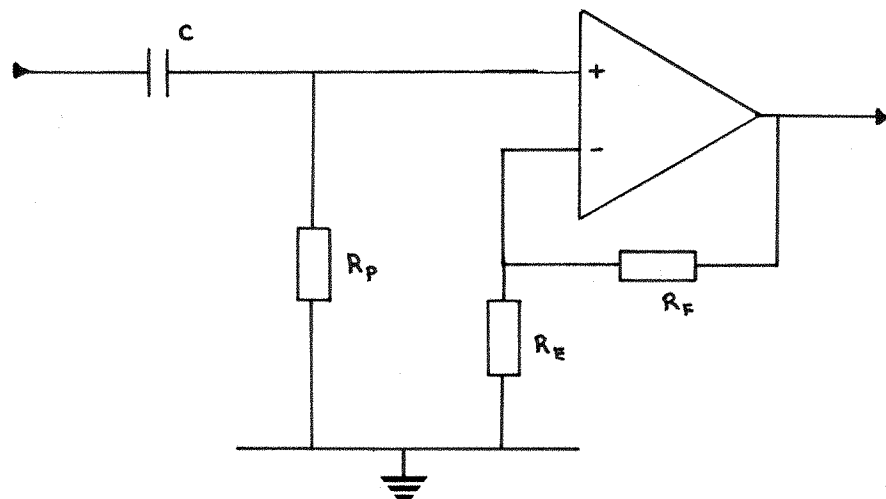
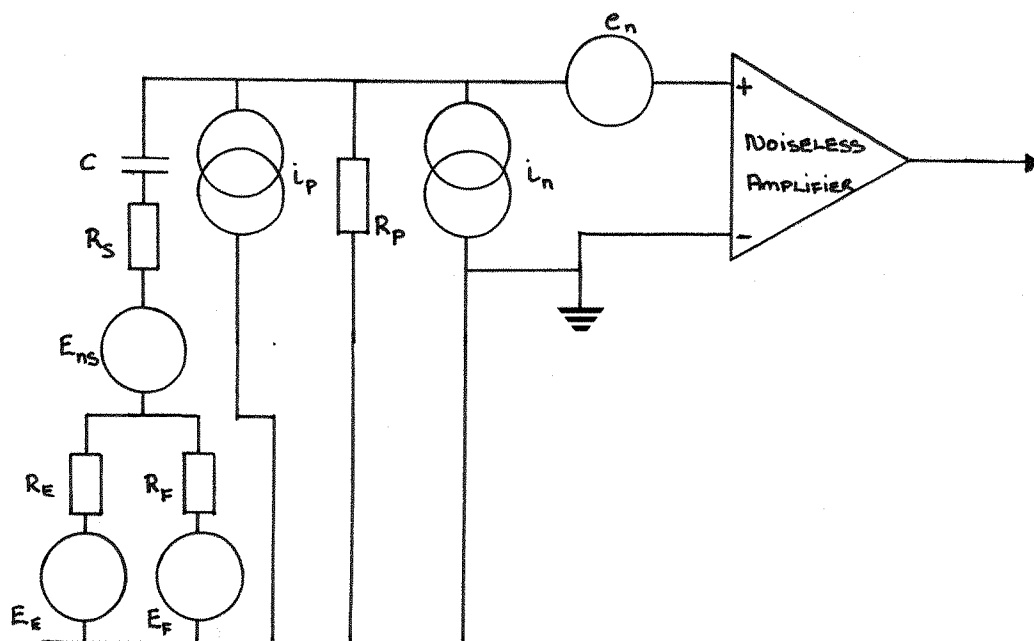


Fig. 8:2 A.C. Coupled Non-Inverting Amplifier.

Fig. 8:3 Noise Circuit For A.C. Coupled Non-Inverting Amplifier.



e_n = input referred voltage noise of the amplifier
 E_E = thermal noise associated with resistor R_E
 E_F = thermal noise associated with resistor R_F
 κ = Boltzmann's constant
 B = Bandwidth considered

and in addition defining:

E_{no} = total output noise of amplifier plus sensor
 E_{ni} = total input referred of amplifier plus sensor
 K_t = transfer function of the input circuit
 $//$ = parallel combination of circuit elements

We have:

$$\begin{aligned}
 E_{no}^2 &= E_{ns}^2 \left[\frac{R_p}{R_p + Z_s + R_E // R_F} \right]^2 + e_n^2 + (i_p + i_n) \left[(R_E // R_F + Z_s) // R_p \right] \\
 &+ E_E^2 \left[\left(\frac{R_F}{R_E + R_F} \right) \left(\frac{R_p}{Z_s + R_p} \right) \right]^2 + E_F^2 \left[\left(\frac{R_E}{R_F + R_E} \right) \left(\frac{R_p}{Z_s + R_p} \right) \right]^2 \\
 K_t^2 &= \left[\frac{R_p}{Z_s + R_p + R_E // R_F} \right]^2
 \end{aligned}$$

Since $E_{ni}^2 = E_{no}^2 / K_t^2$ we have after considerable manipulation:

$$\begin{aligned}
 E_{ni}^2 &= E_{ns}^2 + \frac{e_n^2}{R_p^2} \left[\left(\frac{R_E R_F}{R_E + R_p} + R_p \right)^2 + \frac{1}{\omega^2 C^2} \right] \\
 &+ \underbrace{i_n^2 + i_p^2}_{\text{term T}} \left[\left(\frac{R_E R_F}{R_E + R_F} + R_s \right)^2 + \frac{1}{\omega^2 C^2} \right] \\
 &+ E_E^2 \left\{ \underbrace{\left[\frac{R_F}{R_E + R_F} + \frac{R_F^2 R_E R_p}{(R_F + R_E)^2 \left(\frac{1}{\omega^2 C^2} + R_p^2 \right)} \right]^2}_{\text{term U}} + \underbrace{\left[\frac{R_F^2 R_E}{\omega C (R_F + R_E)^2 \left(R_p^2 + \frac{1}{\omega^2 C^2} \right)} \right]}_{\text{term V}} \right\} \\
 &+ E_F^2 \left\{ \underbrace{\left[\frac{R_E}{R_F + R_E} + \frac{R_E^2 R_F R_p}{(R_F + R_E)^2 \left(\frac{1}{\omega^2 C^2} + R_p^2 \right)} \right]^2}_{\text{term W}} + \underbrace{\left[\frac{R_E^2 R_F}{\omega C (R_F + R_E)^2 \left(R_p^2 + \frac{1}{\omega^2 C^2} \right)} \right]}_{\text{term X}} \right\}
 \end{aligned}$$

where the source impedance is assumed resistive and $R_s < R_p$ which is true when one operational amplifier is fed by another.

We conclude that terms T,U,V,W,X may be minimised by using a high value of R_p . (The first, (term T) is dependent on i_p which is itself inversely proportional to R_p). Quite evidently, however, the relative magnitude of each term is a function of many other variables and minimisation of the expression is a complicated matter.

8.4.5 Device Selection

Section 8.4.4 has demonstrated the importance of i_n and e_n on the choice of operational amplifier and additionally the importance of choosing a suitable value of R_p .

A self imposed noise limit of 10^{-13} V²/Hz over the whole operating temperature range was defined. Such a value does not degrade signals fed from a low noise preamplifier, using some of the best semiconductor devices currently available, providing that the preamplifier gain is greater than ~ 40 dB. A typical example of such a preamplifier is that described by Cantarano and Pallotino (1970), see section 3.3.4.

Many devices were reviewed, some (e.g. the 741) being dismissed because they were obviously too noisy, some because they were expensive, and some because they were not readily available.

The selected device was a TL081AC bifet (bipolar-FET) operational amplifier which was both cheap, (~ 1) and readily available. Noise characteristics were obtained from Texas Instruments (1977) which gave e_n and i_n power spectra curves down to 10 Hz. These curves were extrapolated back to 0.5 Hz.

Equation 8.1 was evaluated using the following component values: $R_p = 100\text{K}\Omega$, $C = 4.7\mu\text{F}$, $R_F = 100\text{K}\Omega$, and $R_E = 100\text{K}\Omega$. The various terms in equation 8.1, together with the total, are plotted in figure 8.4 which shows that the device meets the noise requirements over the total bandwidth albeit with little margin at low frequencies. The dominant noise terms are evidently S (via e_n) and U/W (via R_p) from which we conclude that some improvement could be found, if required, by increasing the value of R_p .

It should be noted that the TL081AC is not particularly special

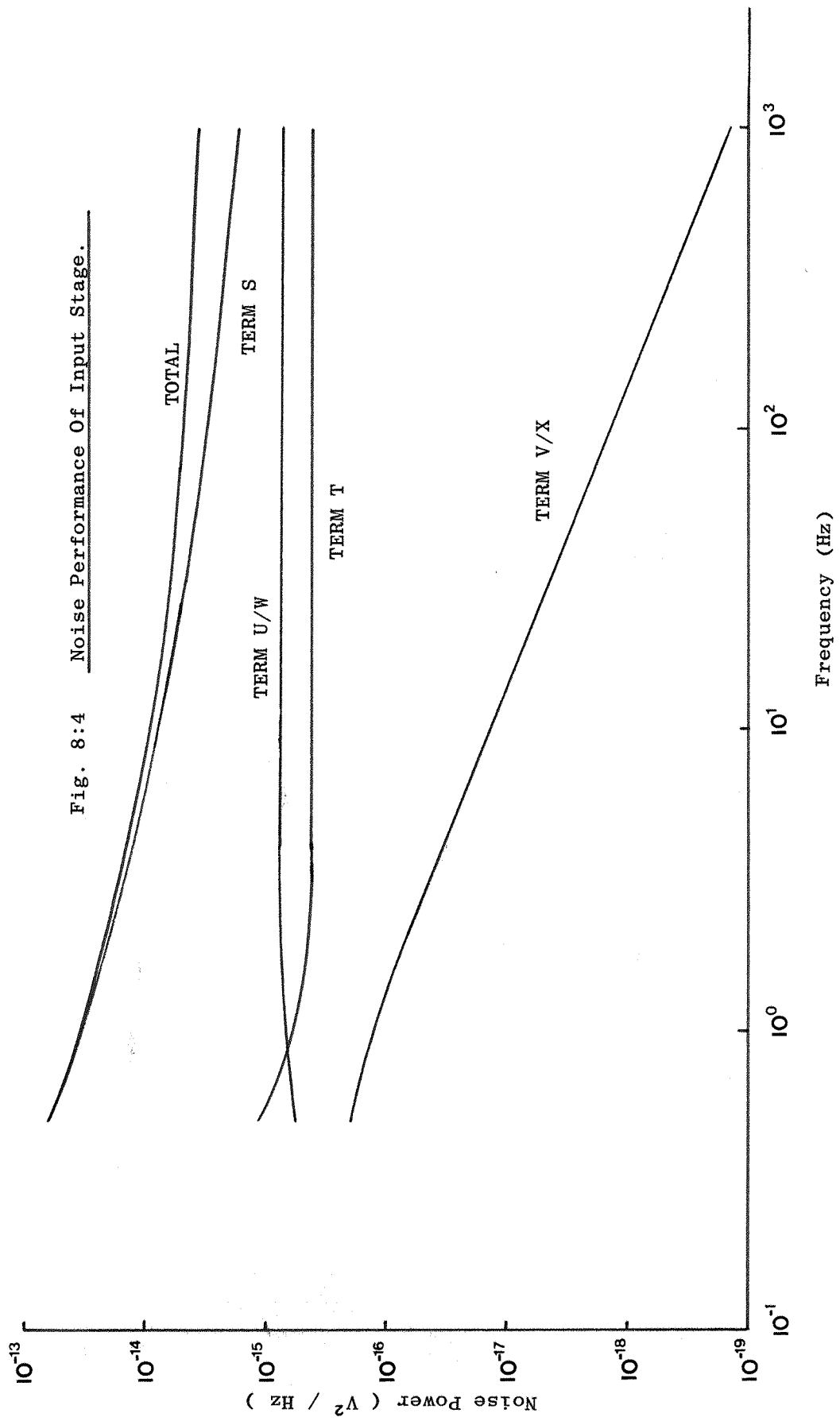


Fig. 8:4 Noise Performance Of Input Stage.

within the class of low noise operational amplifiers and many other devices exist which could have fulfilled the role. It is the design of the circuit which is all important in this context.

8.5 Receiver Circuitry

8.5.1 Introduction

The receiver is a field site instrument and, since it is also to be periodically shipped abroad, a high standard of mechanical construction has been adopted. The receiver has been built in modular form in a 19" rack unit, figure 8.5.

High stability ($\pm 2\%$) metal oxide resistors, and high quality ($<\pm 10\%$) capacitors have been utilised throughout. This is necessary, particularly in filter stages, in order to match the two channels.

To conserve space TL083AC and TL084AC integrated circuits have been used in place of the TL081 discussed in section 8.4.5. These devices contain three and four TL081 circuits per package respectively. Sections 8.5.2, 8.5.3, and 8.5.4 give a description of the receiver circuitry with the exception of the comb filter, which is treated separately in section 8.6.

8.5.2 Power Supply Figure 8.6 IC1 to IC4 inclusive

Figure 8.6 is a schematic diagram of the receiver $\pm 15V$ and $\pm 5V$ regulated supplies for analogue circuits and CMOS logic circuits.

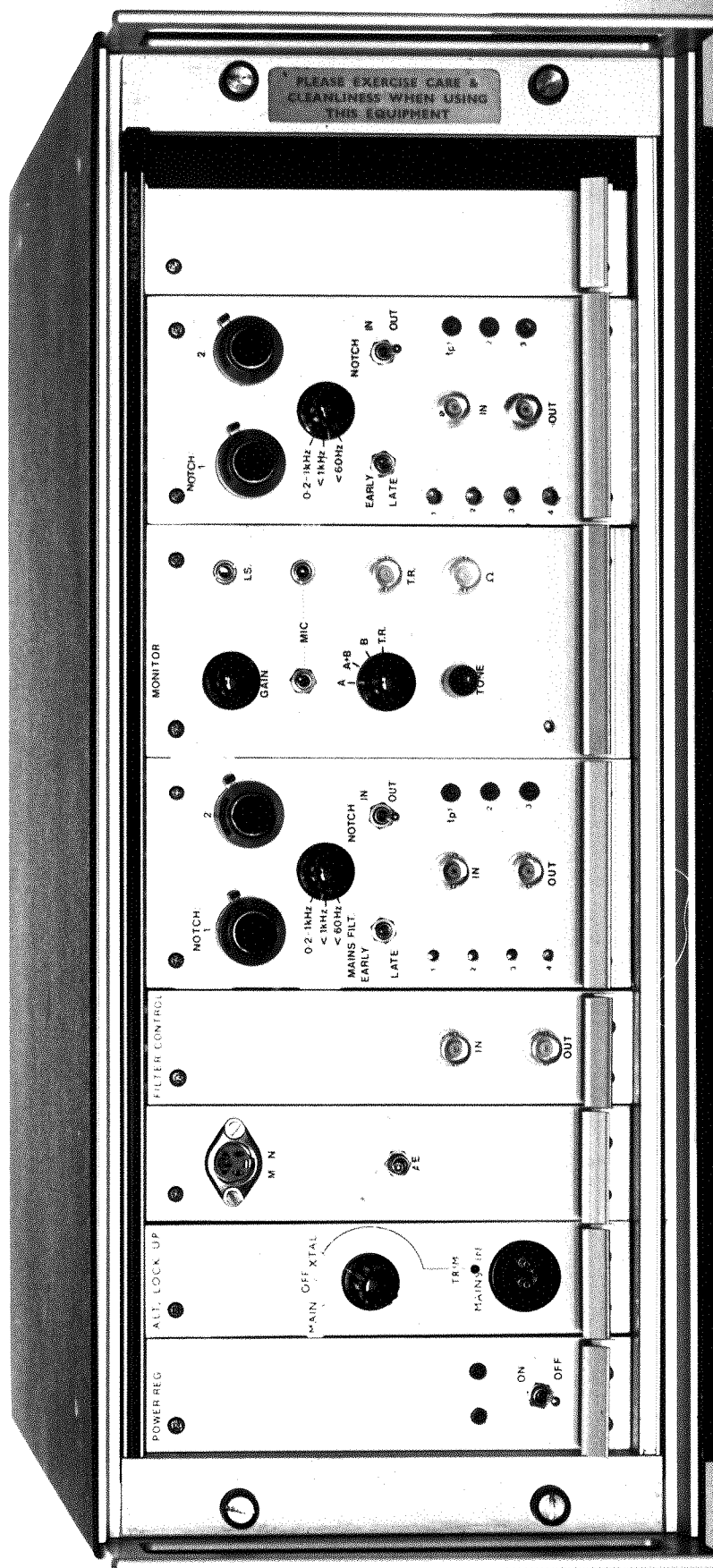
The current drawn by the receiver is 150mA, positive supply and 120mA negative supply.

IC5 and IC6

IC5 and IC6 provide an oscillating voltage, at approximately 1 Hz and with a duty cycle of about 10%, to drive two front panel mounted LEDs. Failure of these LEDs to flash on and off indicates loss of the appropriate power rail. LED power consumption is negligible.

8.5.3 Amplification and Filtering Figure 8.7 IC4

Integrated circuits 7a and 7b are A.C. coupled and give a maximum



E.L.F. RECEIVER FIG85

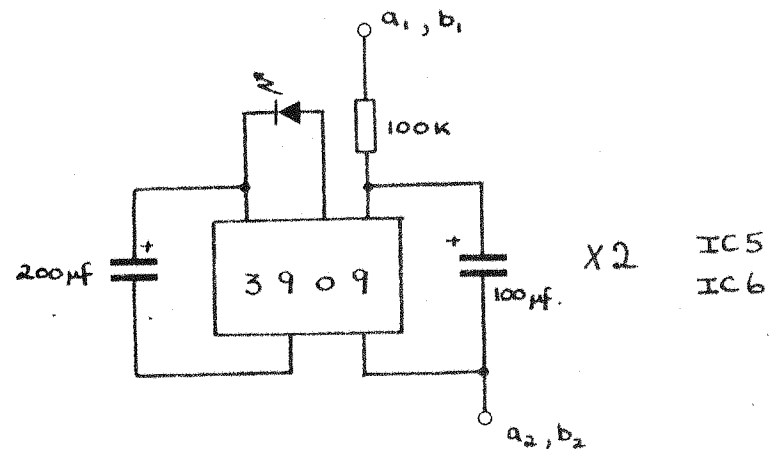
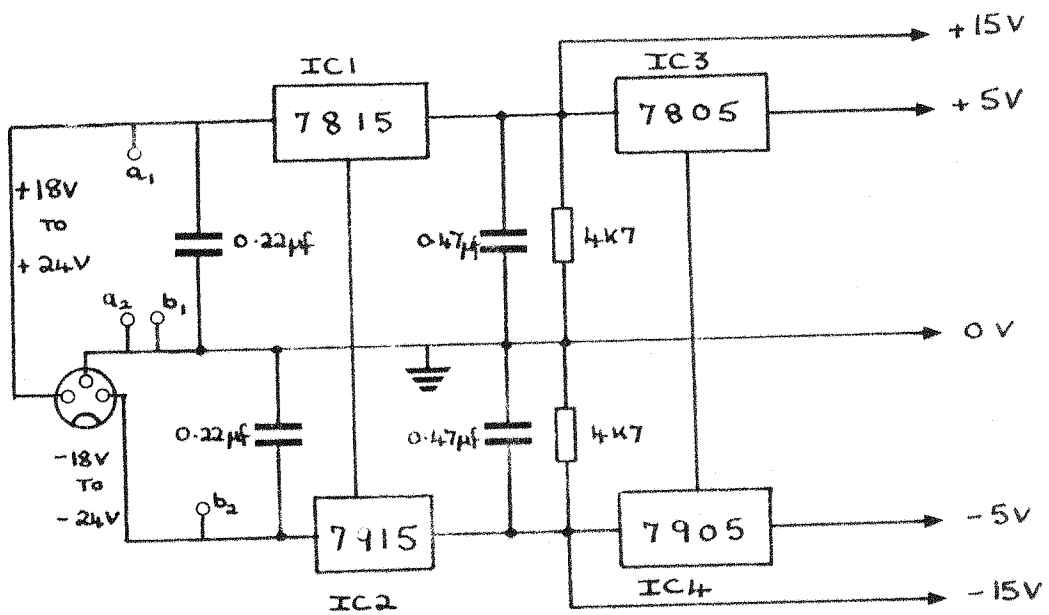
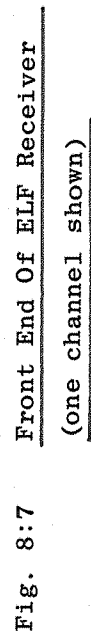


Fig. 8:6 Power Supply.



of 20 dB and 6 dB gain respectively with a lower 3 dB point of 0.34 Hz.

SW1 routes the signal to either the comb filter, see section 8.6, and thence to the response tailoring circuitry or alternatively directly to the latter.

IC8, IC9, IC10

IC8a and IC8b make up a four pole Bessel low pass active filter (Orr, 1977) with an upper 3 dB point at 1kHz. IC9a and IC9b similarly make up a four pole Bessel low pass active filter with a 3 dB point at 40 Hz. IC9c provides variable gain up to a maximum of 26 dB. IC10a provides a 2 pole Bessel high pass filter with a 3 dB point at 200 Hz and IC10b variable gain up to a maximum of 26 dB. Switch SW2 enables either IC8, receiver passband 0.3Hz to 1kHz; IC9, receiver passband 0.3Hz to 40Hz; IC8 plus IC10, receiver 3 dB passband 200 Hz to 1kHz.

8.5.4 Further Amplification and Filtering Figure 8.8 IC11 and IC12

IC11 and 12 are the optional 2 pole pair notch filters with Q of 20 and a passband gain of 0 dB. SW3 switches the filters in and out of circuit as demanded.

There are several approaches to the design of notch filters, i.e. the active twin T configuration, the phase subtraction configuration, and the state variable approach (Tobey and Graeme, 1978). The latter technique was adopted for several reasons. Firstly, it is the most stable active filter configuration, enabling the construction of a high Q notch filter. Secondly, easy tuning of the notch filter over a wide frequency range is achieved most easily using the state variable approach. Thirdly, it may be arranged that the notch Q is unaffected by varying its frequency.

A Q of 20 was chosen as a practical compromise between a wish for a narrow response and the necessity to be able to tune the filter easily onto the required frequency. With this value, the maximum peak to peak input to the notch filter is 1.5 volts for a supply voltage of $\pm 15V$. Note also that a higher Q would imply greater gain reducing the maximum input voltage to the filter, and consequently front end amplification.

The state variable filters were constructed from Burr Brown UAF41,

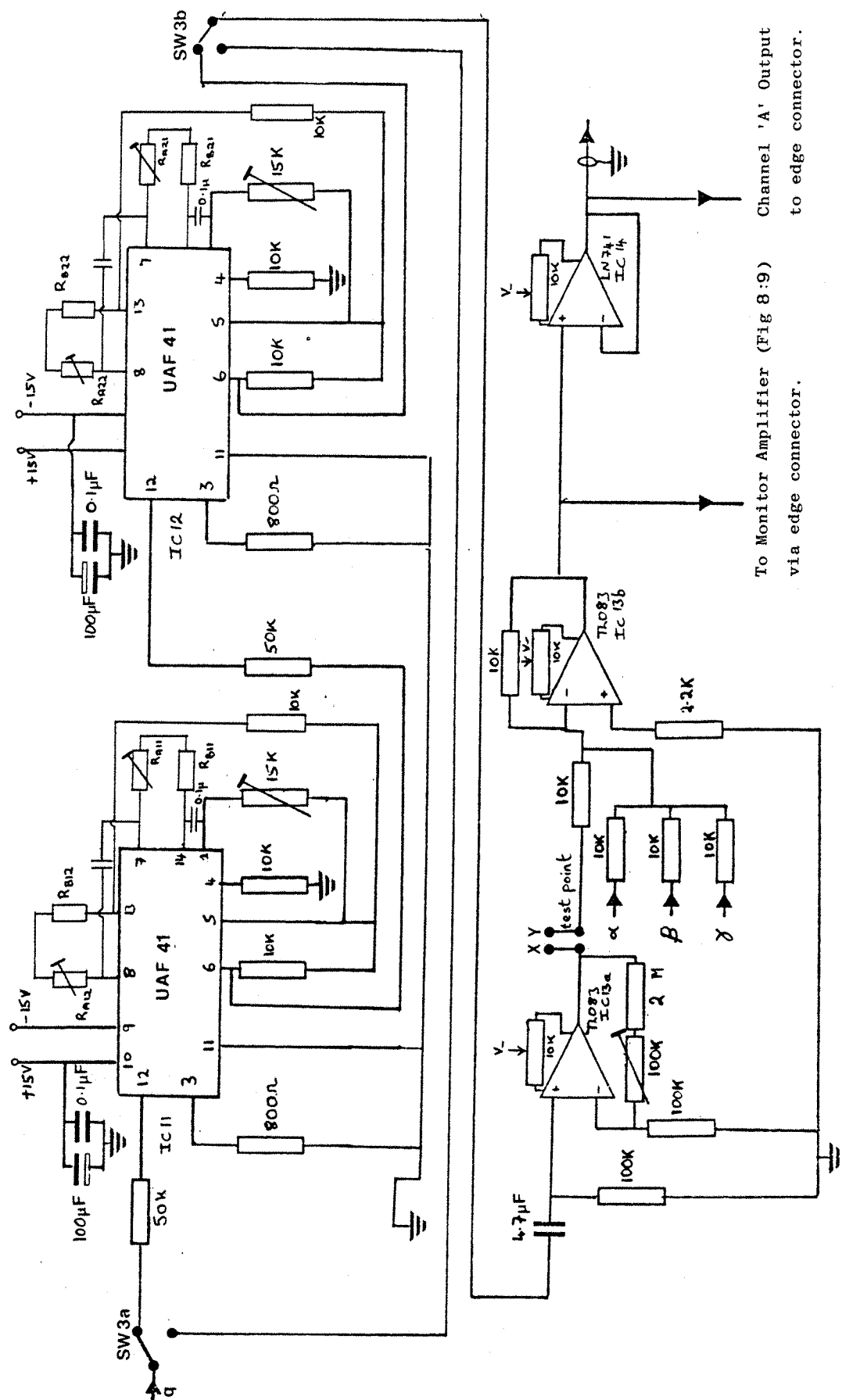


Fig. 8:8 Further Amplification And Filtering

Universal Active Filter integrated circuits because they enabled reproducible notch filters to be constructed with ease. Details of the design equations may be found in Burr Brown (1976), together with specifications. At this point in the circuit noise performance is not critical.

IC13

IC13a is another stage of variable gain, (maximum 34 dB). The signal is then fed via SW1, the comb filter switch to a conventional D.C. coupled mixer, IC13b. The various inputs to this mixer have been described in section 8.3. To reduce pick up the clock input is shorted to earth whilst not in use.

IC14

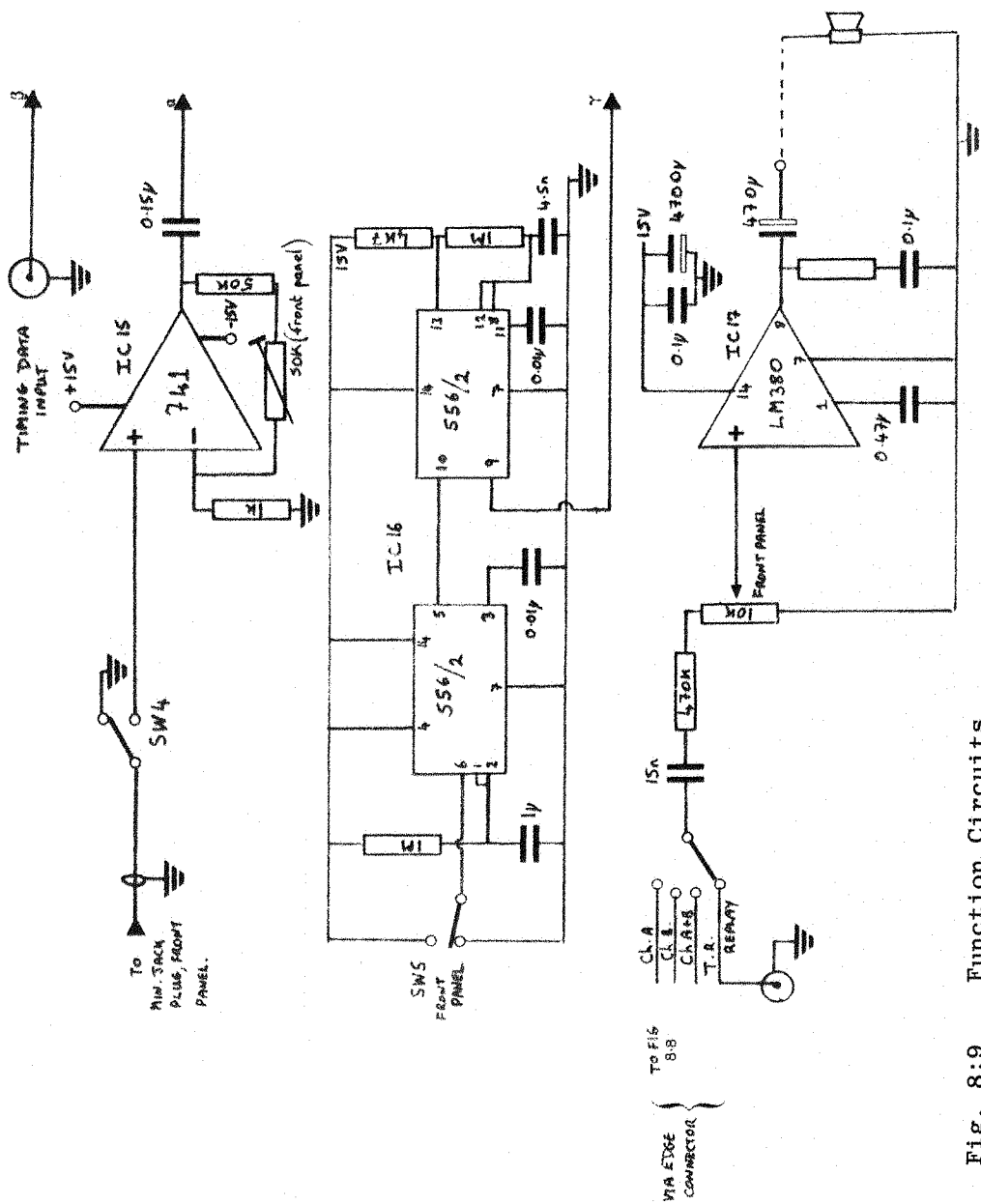
IC14 forms an output buffer. A 741 was found preferable to a TL081 as its lower bandwidth (Texas Instruments, 1977) gives the stage more stability. The output from the buffer is fed to a BNC output on the front panel and, in addition, to the edge connector. This is in order that at a further stage of development it may be used as an input to a goniometer multiplier stage, see section 3.2.

8.5.5 Function Circuits Figure 8.9. IC15

IC15 is a simple crystal microphone amplifier whose gain may be adjusted to a suitable value via the front panel mounted trimmer potentiometer. The microphone signal to the mixer should be comparable to the ELF signal. Whilst not in use the amplifier input is shorted to earth by a biased switch in order to prevent injection of noise into the receiver.

IC16

IC16 is a dual 555 timer operated as a monostable and astable. A negative pulse on the trigger input of the monostable, caused by the momentary depression of a button on the front panel, enables the monostable causing a high at its output, pin 5. This is used to reset the astable and cause it to run at 160 Hz for 0.5 second. Whilst in operation it is impossible to enable the oscillator again to extend the pulse length.



IC17

IC17 is a LM380 audio amplifier which may be used in various modes as described in section 8.3. It delivers 2 watts maximum into an 8Ω speaker. The input to the amplifier is considerably attenuated by the 470K input resistor. The 15nF input capacitor provides a low frequency break point at 30 Hz to maintain circuit stability.

8.6 A Comb Bandstop Filter For Use In An ELF Receiver

8.6.1 Introduction

A commutating comb filter is a highly stable, high Q, bandstop (notch) filter which is capable of attenuating a fundamental frequency, in this case 50 Hz (mains frequency Europe) or 60 Hz (mains frequency North America) and a number of harmonics. This number is dependent upon the number of capacitors in the commutation network. The filter may be viewed as a digital filter, where the highest attenuated harmonic is limited by the Nyquist frequency. This filter provides > 48 dB attenuation at 50 Hz, with progressively less attenuation at higher harmonics up to, and including, 1600 Hz.

8.6.2 Theory

The theory of such filters has been discussed by Broeker (1970) and Knott and Unsworth (1974).

Consider a signal, frequency f , applied to figure 8.10 where each of the N capacitors, of identical value C , are switched sequentially to earth at a frequency Nf_m , the commutation frequency. If $f = nf_m$, where n is an integer, each capacitor is switched into circuit at an identical point in the wave cycle, every cycle. Providing that there is a high discharge time constant relative to Nf_m , each capacitor will, after several cycles, charge to a value corresponding to the instantaneous amplitude of the input waveform. The differential voltage across the input resistor is consequently zero. Conversely, if $f \neq nf_m$ each capacitor charges to a different voltage each and every cycle and the voltage across each capacitor averages to zero. Hence, the differential voltage across the input resistor is that of the input signal.

The bandwidth of each notch is given by:

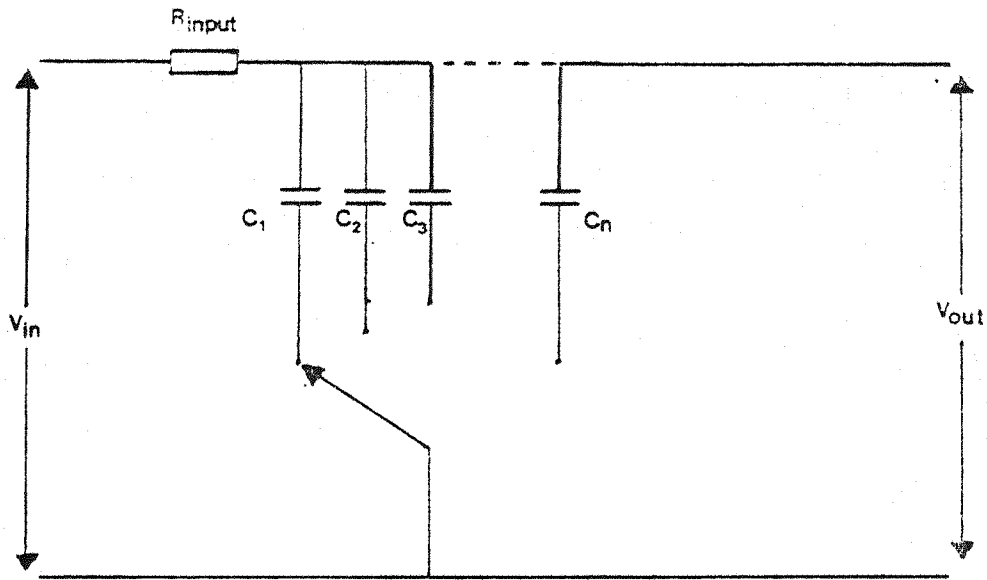


Fig. 8:10 Commutating C.R. Network

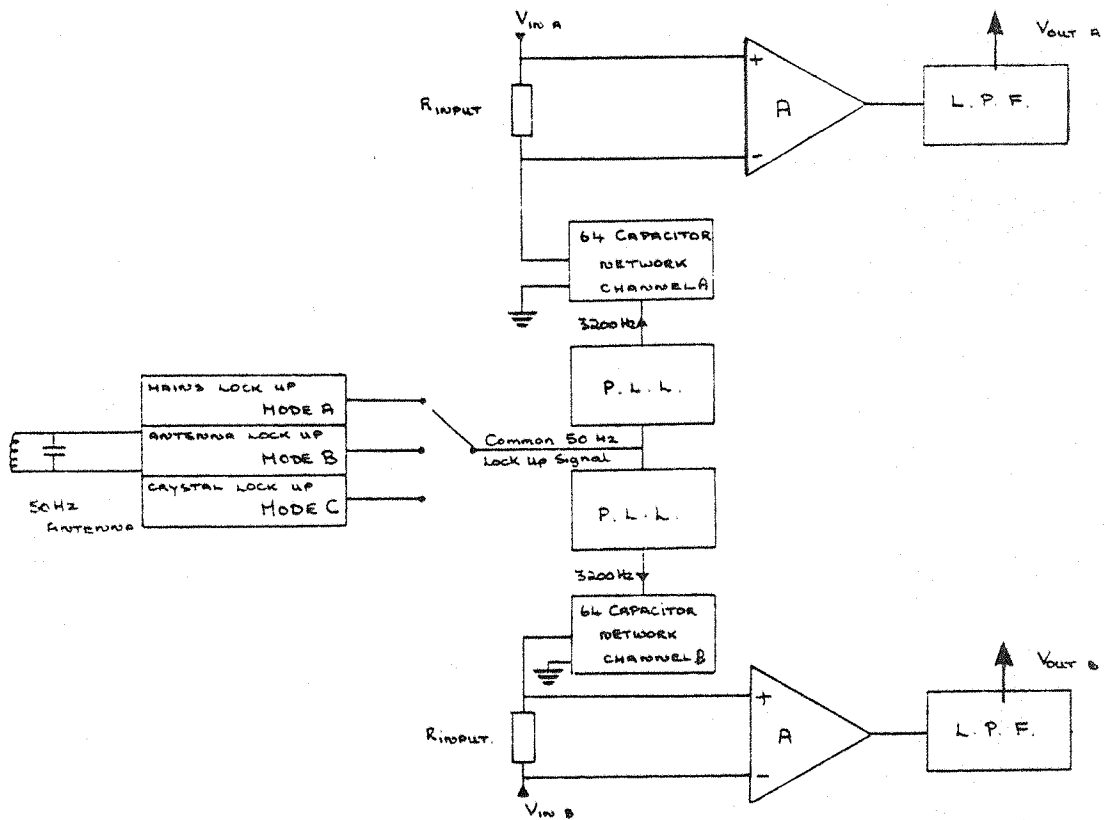


Fig. 8:11 Block Diagram Of Comb Filter

$$\text{Bandwidth} = \frac{2}{N} \left[\frac{1}{2\pi C R_{\text{INPUT}}} \right] = \frac{1}{\pi N C R_{\text{INPUT}}} \quad \text{equation 8.3}$$

where N arises because the time constant is increased by N over a normal RC filter, and the two arises because the switching causes reflection of the low pass response about the centre frequency (Knott and Unsworth, 1974).

8.6.3 Rejection

The theoretical rejection, at each frequency, may be calculated by Fourier analysis techniques (Knott and Unsworth, 1974). In practise, however, the rejection is limited by implementation noise, section 8.6.

8.6.4 Switching Noise

The comb filter introduces switching noise at the commutating frequency and its harmonics; this may be reduced by strong low pass filtering. One possible configuration is shown in figure 8.11.

8.6.5 Tracking

The filter described in this chapter has been designed as a tracking filter by using a phase locked loop, (P.L.L.) to control the commutation frequency. This tracking is required because the statutory mains frequency limits in the U.K. are between 49.5 Hz and 50.5 Hz (Knott and Unsworth, 1974). Consequently, a high Q notch filter could easily become ineffective without this facility. A similar but worse situation pertains in regions not served by a grid system, but by local generators, for example arctic Scandinavia.

8.6.6 Choice of R_{INPUT} and C

The receiver described here was operated primarily at Lavangsdalen near Tromsø, Norway where the mains interference was found to have a complex frequency structure. This interference resulted not only from the distant Norwegian grid system but also from a nearby private generator; generally running at a different frequency. Tracking in this instance was evidently impossible. It was consequently necessary to employ a wider notch than had been originally anticipated (< 1 Hz).

A bandwidth of 2 Hz was found suitable which gave for $C = 0.1\mu F$ a value of $R_{IN} = 23.5K\Omega$, equation 8.3.

8.6.7 Description Of The Comb Filter

Figure 8.11 depicts a block diagram of the two amplitude and phase matched comb filters, one for each receiver channel, and it can be seen that each divides into four common sections.

A common lock-up circuit provides a signal at f_m (~ 50 Hz or ~ 60 Hz) the fundamental notch frequency. This signal controls the frequency of a P.L.L. (Signetics, 1974) which in turn controls the switching rate of the capacitor network, see below. The signal may be derived from one of three selectable sources, that chosen being dependent upon the operational location of the receiver. Mode A is used in a laboratory environment where the locking signal is derived from the output of a step down transformer. At present this mode may only be used in regions where 220V/240V (50 Hz) is available. Mode B is for use in noisy field locations where a stable locking signal can be obtained from the amplified output of a low Q resonated coil. Finally mode C is for use in quiet field locations where a "noise free" locking signal is unavailable by either of the above methods. In this mode a signal is obtained, after suitable division, from an internal screened crystal source. The latter two modes may be used where the mains frequency is 50 Hz or 60 Hz.

The signal is fed to a P.L.L. with a free running voltage controlled oscillator (V.C.O) at approximately Nf_m Hz. An internal phase comparator adjusts the V.C.O. frequency to an integral multiple of the locking signal frequency and consequently variations in this frequency are tracked by the V.C.O. in the P.L.L. Hence, when the source of the locking signal is the mains supply or the antenna, the filter notch frequencies track the interference signal fundamental and harmonic frequencies. When the crystal controlled lock up signal is used no such tracking of the interference signal frequency occurs. Operation of the receiver in mode C implies, however, a low interference level and consequently high attenuation is less critical.

The P.L.L. output is utilised, via synchronous logic circuitry, to **earth sequentially** the N capacitors to which the raw signal has been applied.

Finally, in order to filter the out of band switching noise, referred to in section 8.6.4, the differential signal across the input

resistor is fed to a low pass filter with a 3 dB point at 700 Hz and a roll off of 48 dB/octave.

8.6.8 Circuit Description

Since it was desired that the receiver should be capable of being used in North America (60 Hz interference), and Europe (50 Hz interference), the circuit was designed to function adequately in either location without the need for major circuit modification. Figure 8.12 depicts a schematic of the lock up circuitry.

Mode A shows a simple step down transformer.

In mode B the output of a resonated coil antenna consisting of 100,000 turns of 38 s.w.g. wire with average diameter 6 cm, width 7cm, and resonated to 55 Hz with a 0.1 μ F capacitor is connected across M.N. The Q of the coil is low (\sim 0.4) facilitating adequate operation at both 50 Hz and 60 Hz. A resonated pick up coil, rather than a long wire antenna, was chosen for two reasons. Firstly, it reduces the noise on the locking signal which could cause the filter to "lose lock". Secondly it attenuates mains harmonics, which are prevalent in ill regulated mains supplies, and onto which the filter might lock. The signal is amplified by 20 dB using a high input impedance FET bandlimited amplifier, IC18. The signal then passes through IC19, a bandpass filter (Q = 4) centred on 55 Hz, which again reduces the effects of noise and higher mains harmonics. The signal is further amplified by 40 dB using a 741, IC20. This mode is fully compatible with 50 Hz or 60 Hz operation.

In mode C a crystal oscillator at 3.2768MHz, and buffered by IC22, provides after division by 2^{16} a highly stable 50 Hz signal. Operation of the filter in North America, using this mode, requires recrystallisation at 3.9322MHz.

The 50 Hz lock up signal from any mode is fed to a comparator, IC21, with logic levels \pm 5V. This is compatible with the CMOS logic levels of the following circuitry. The comparator is A.C. coupled at the input to reject D.C. offsets from the previous stages which would affect operation of the comparator on low amplitude signals. A TL081AC (Texas Instruments, 1977) FET input integrated circuit with low input bias currents is used in order to reduce offsets at the comparator output caused by the 1M Ω resistor.

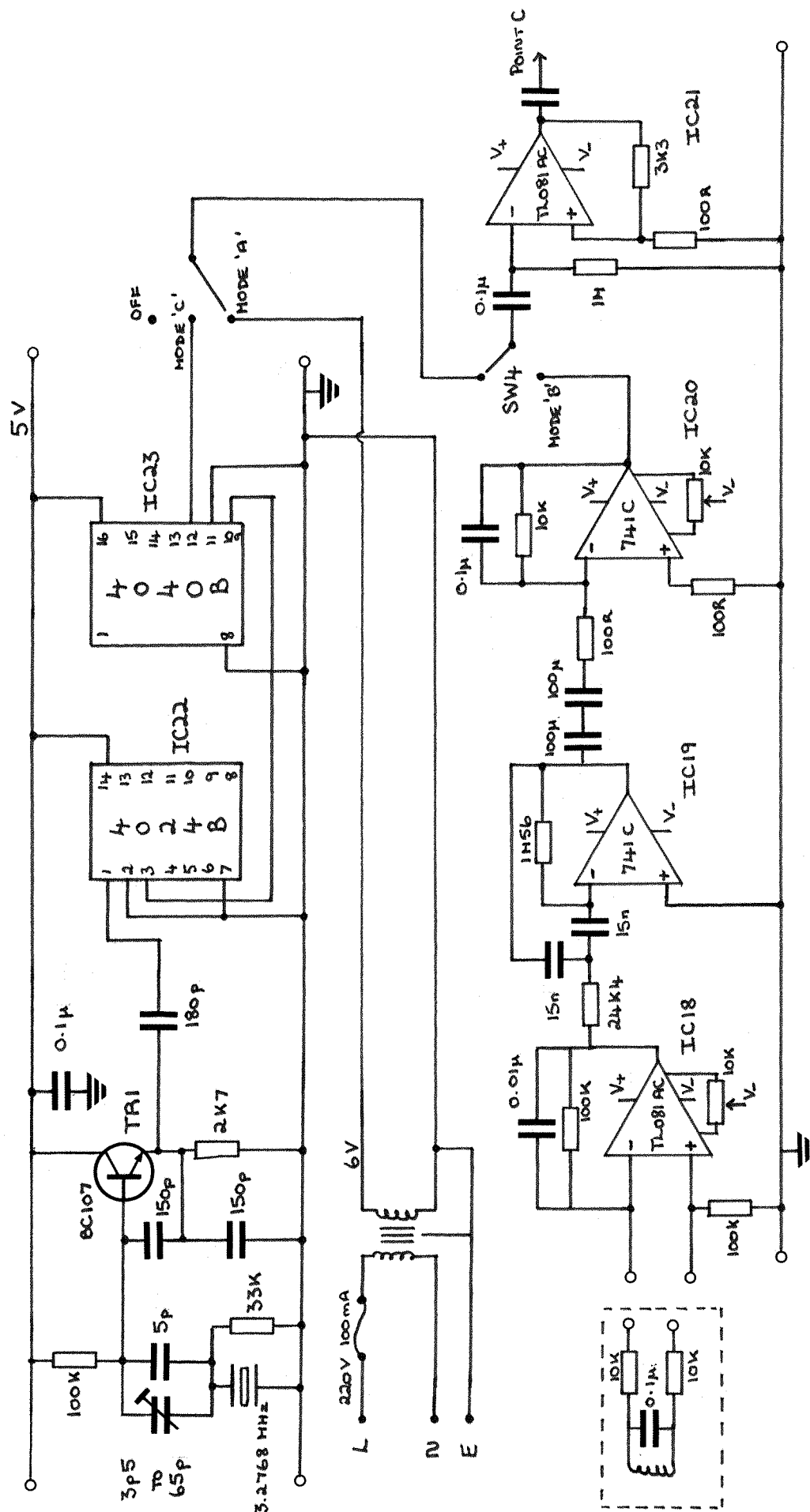


Figure 8.13 shows the mains derived or crystal derived comparator output fed to the phase comparator input of IC24, a CD4046B, CMOS phase locked loop. This has a free running V.C.O. frequency of approximately 3520 Hz (55 Hz x 64). The output from the V.C.O. is divided by 64 using IC25 a CD4520B, dual up-counter and fed back to the P.L.L. phase comparator. The phase, (frequency), difference between these two signals creates an error voltage within the P.L.L. which is used to correct the internal V.C.O. free running frequency to exactly 64 x the local mains or crystal frequency (Signetics, 1974). This locked and tracking V.C.O. is used to short the 64 capacitors sequentially to earth. The P.L.L. will capture and remain locked to signals within ± 10 Hz of 55 Hz (R.C.A., 1977).

Commutation is accomplished by using the logic outputs from 8 CD4015B dual 4-stage static shift registers, (IC27 to IC34 inclusive), which enable the CD4066B analogue switches, (IC35 to IC50). A data pulse is entered into the shift registers from IC26, a CD4068B 8 input AND gate. The output of this gate is only true once every ~ 20 ms, i.e. once every 64 clock pulses and is clocked through the shift registers at a frequency determined by the V.C.O. output of the P.L.L.

The CD4066B contains four independent quad bilateral switches where the resistance of the analogue input to output path is governed by the digital control terminal voltage. They have an on resistance of 120Ω , an off resistance of $10M\Omega$ with distortion quoted typically at 0.4%. The variation in on resistance between any two of four switches is typically $\pm 10\Omega$ (R.C.A., 1977). Note that as required by section 8.6.2 the capacitor discharge time constant in the off condition is large compared to the commutation period. A CD4066B was used in preference to the pin compatible CD4016B because the former has a lower on resistance.

It is important to note the synchronous nature of this circuit. Following the design of Cannon (1976) which used a 16 capacitor network an attempt was made to scale this asynchronous TTL design to a 64 capacitor CMOS network. Due to the increased switching speed, however, race hazards inherent in that design became significant causing high noise spikes at the filter output. This has resulted in a complete redesign of the switching circuitry together with redesign of the filtering and lock-up circuitry. The differential amplification and filtering is shown schematically in figure 8.14.

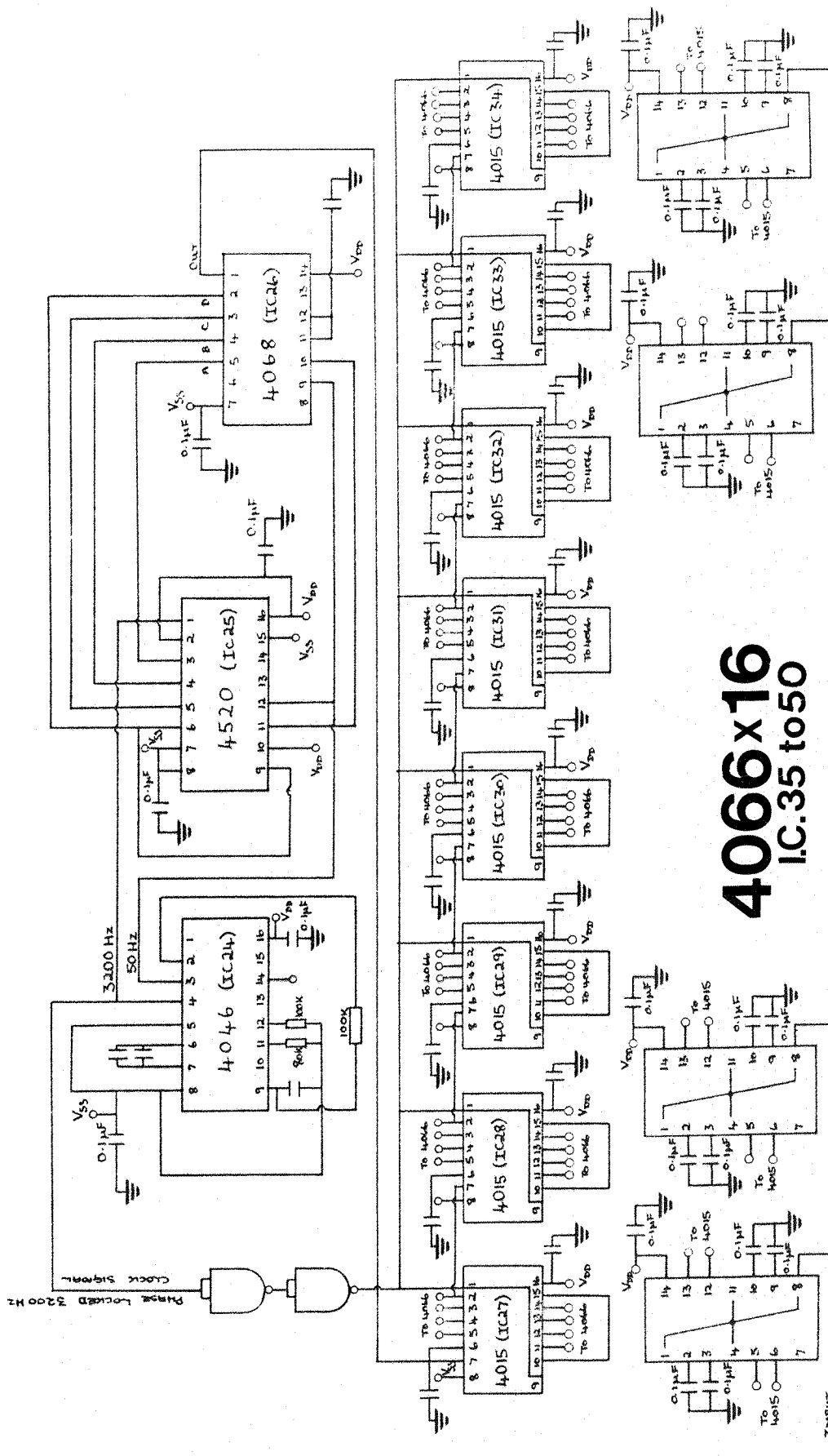
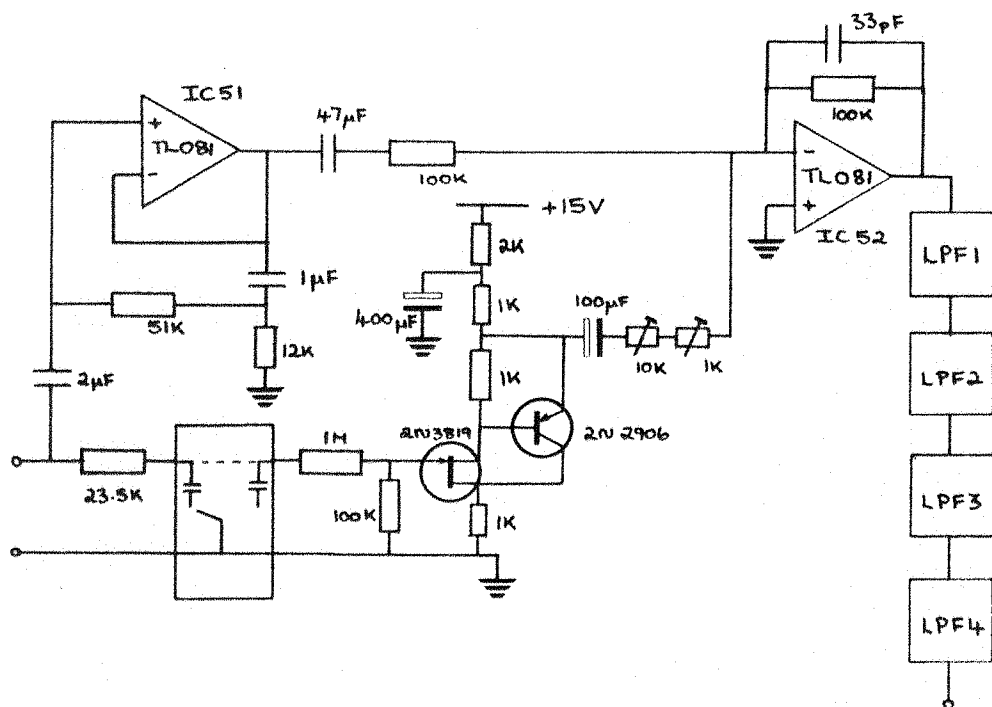


Fig. 8:13 Phase Locked Loop and Commutator



LPF (Low Pass Filters)

LPF1	$R_{F1} = R_{F2} = 89K$
	$R_G = 50K$
	$R_Q = 96.53K$
LPF2	$R_{F1} = R_{F2} = 86.75K$
	$R_G = 50K$
	$R_Q = 73.65K$
LPF3	$R_{F1} = R_{F2} = 81.37K$
	$R_G = 50K$
	$R_Q = 44.14K$
LPF4	$R_{F1} = R_{F2} = 72.61K$
	$R_G = 50K$
	$R_Q = 13.59K$

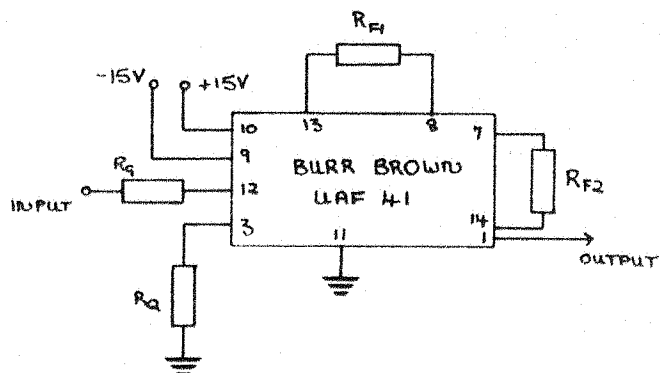


Fig. 8:14 Differential Amplification and Switching Noise Filter

The former follows the design of Knott (1974). The input signal to the comb filter is fed, via an A.C. coupled TL081 buffer (IC51) to a TL081 adder (IC52), whilst the switched signal is fed via an inverting FET buffer to the adder. A variable multi-turn trimmer is provided between the FET and adder to balance the gain of the two paths such that the output voltage from IC52 gives the differential voltage across the input resistor. Note that the FET input buffer limits the input peak to peak voltage to $\sim 5V$, it exhibiting a non-linear response for higher amplitude input signals.

The output from IC52 feeds 4 Burr Brown UAF41 filters (Burr Brown, 1976) configured as an eight pole low pass Bessel filter with 0 dB gain and a 3 dB point at 700 Hz. The filter reduces switching noise and also helps to bandlimit the receiver.

8.7 Performance

Figure 8.15 depicts the wide band (0.3Hz to 700Hz) frequency response of channel A, (no notch filters). This response is applicable to data gathered during March/April 1979, see chapter 10. In addition the figure also shows the gain difference between channels A and B and the output phase difference as a function of frequency. The response of the receiver shows a 3 dB bandwidth of ~ 700 Hz, somewhat less than the planned value of 1kHz. This was due to an error in calculating the switching noise filter 3 dB break point. The amplitude matching between the two channels is better than 1.25 dB over this bandwidth and the phase matching is better than 10° .

Figure 8.16 and 8.17 show similar graphs for the 0.3Hz to 40Hz and 200 Hz to 700 Hz passbands. For clarity the comb response is not shown.

Experience with the goniometer system described in chapter 3 indicates that this degree of matching is perfectly adequate for future development into a goniometer receiver providing that it is azimuthally calibrated at various frequencies within the passband.

The output noise power spectrum was determined, using a Saicor SAI51B time compression spectrum analyser, and referred to the input (figure 8.18). The experimental values are some seven times higher than the theoretically predicted values (equation 8.1). This anomaly is believed due to pick up of noise from the output circuitry via SW1 (figure 8.7); now believed to be redundant, section 8.8. The noise peaks

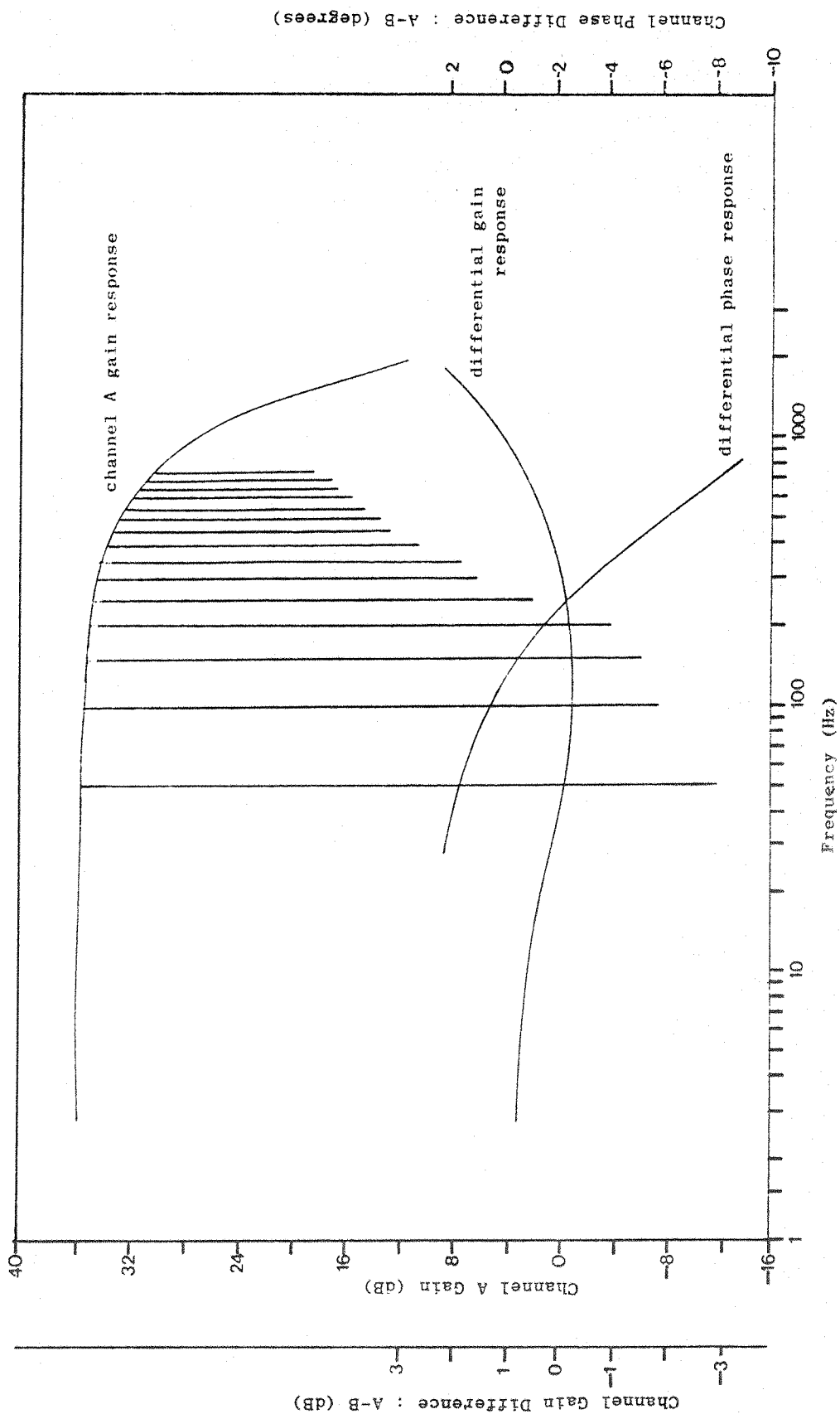


Fig. 8:15 Response Of The 1Hz to 700Hz Passband

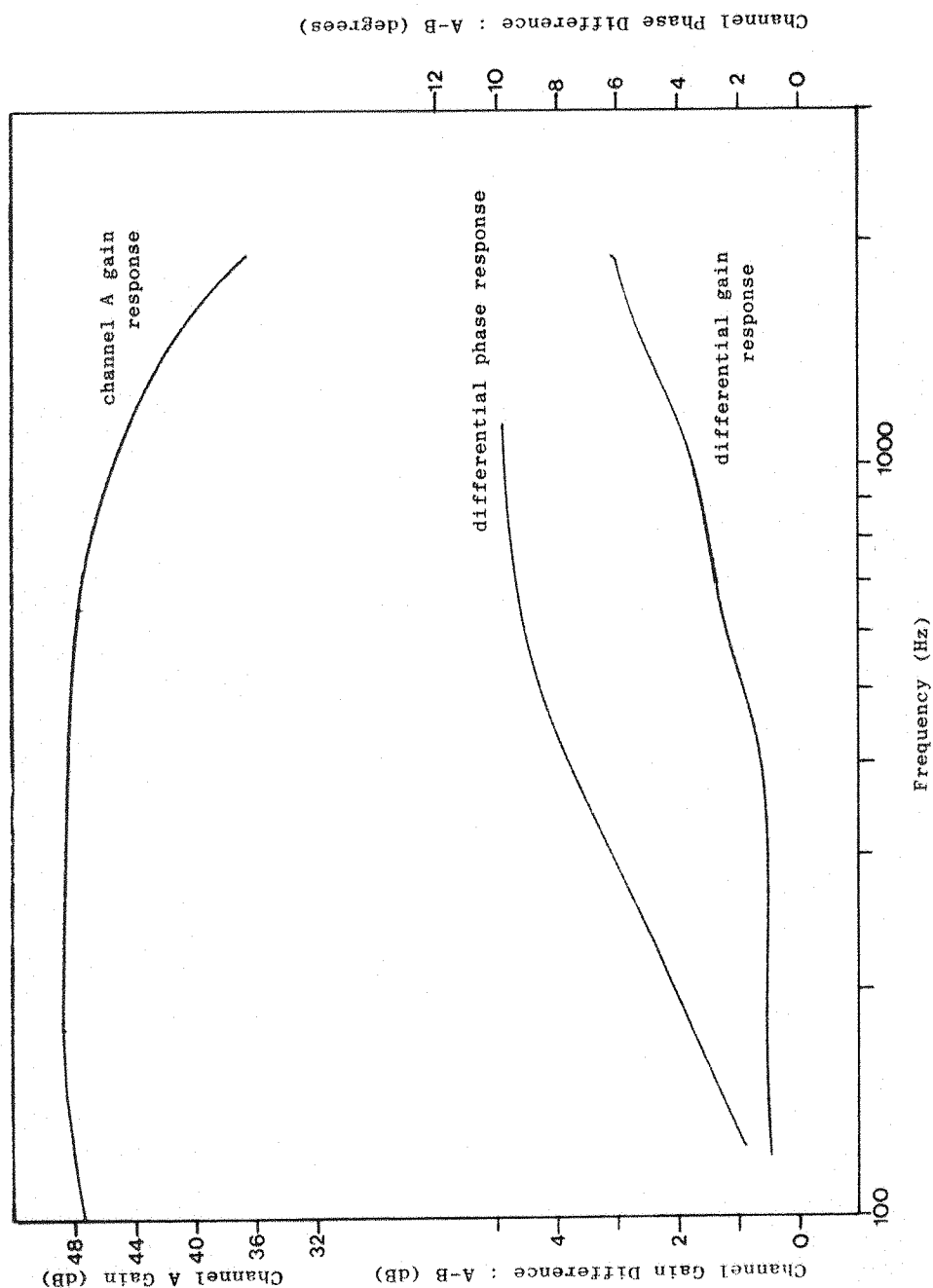


Fig. 8:17 Response Of The 200Hz to 700Hz Passband

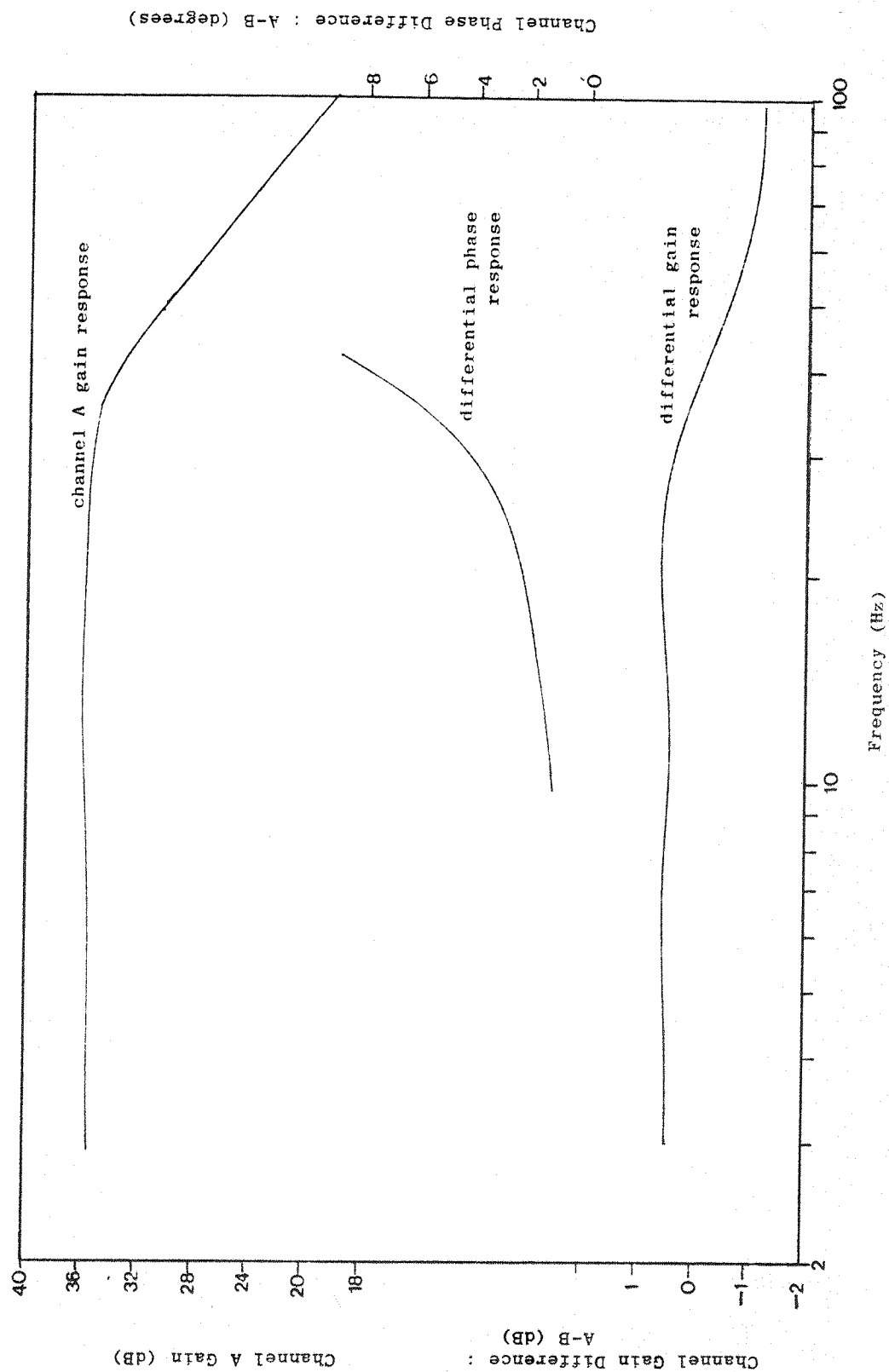
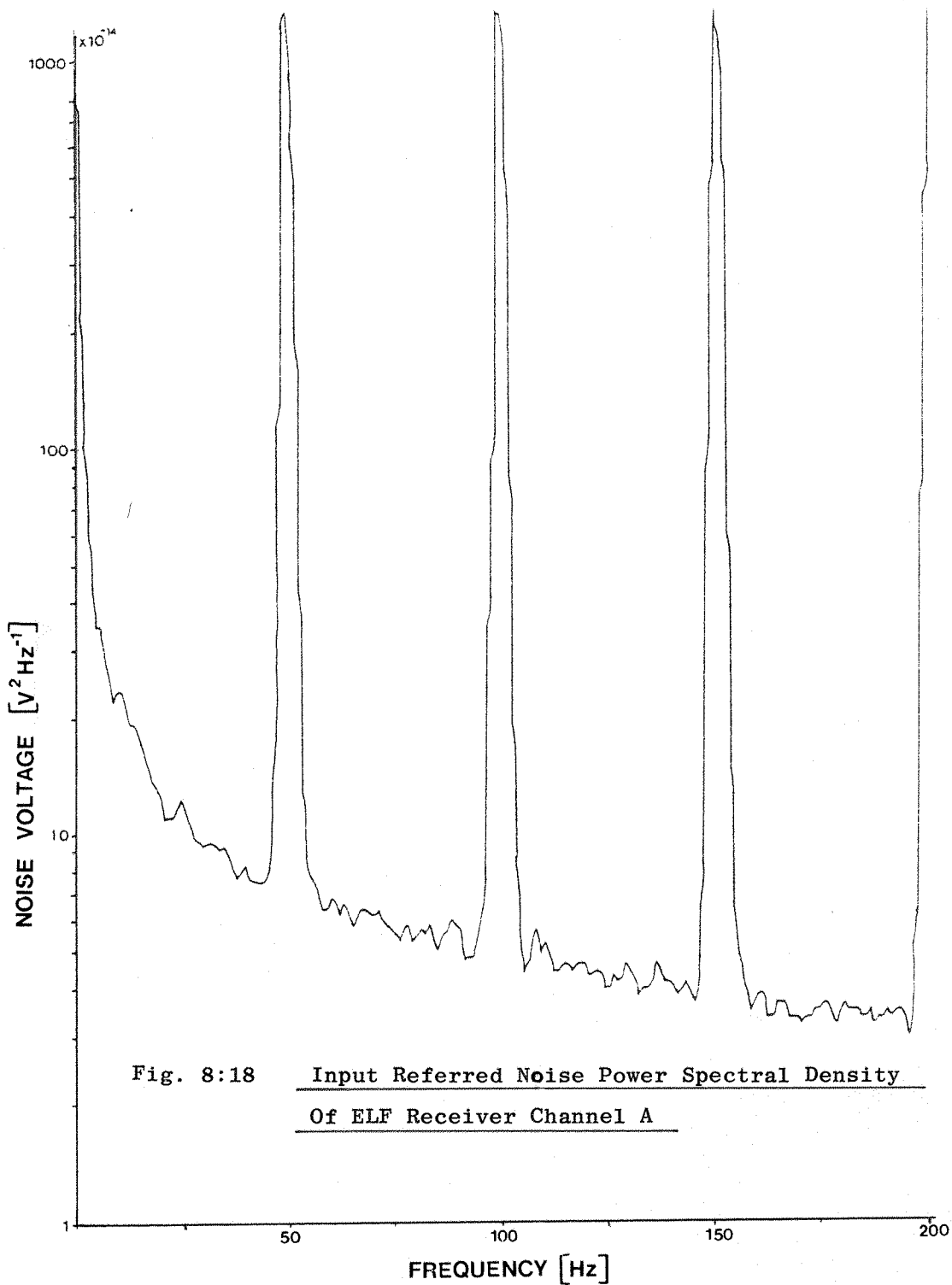


Fig. 8:16 Response Of The 1Hz to 40Hz Passband



are due to 50 Hz and harmonic switching noise from the commutating filter. Although theory only predicts switching noise at the commutating frequency (3200 Hz), and above, noise is, in practise also introduced at lower frequencies. This is due to slight variations in the CMOS switch characteristics, variations in the period of the logic circuitry enabling pulses, and mismatched network capacitors. For a 2V maximum output signal the dynamic range is, however, still greater than 70 dB at mains and harmonic frequencies. Hence, because this is far greater than the 48 dB ascribed to a good FM tape recorder we conclude that the system sensitivity is tape recorder limited.

The inter-channel crosstalk is better than -60 dB.

Current consumption is +150mA and -120mA at moderate monitoring levels.

8.8 Future Work

1) Field sites which are sufficiently quiet, (i.e. low mains interference) to give adequate sensitivity are also quiet enough for the comb filter to be placed subsequent to IC13 (late in circuit) and not after IC7 (early in circuit). Thus the design could be simplified by the removal of SW1 (figure 8.6); this should also improve the noise performance.

2) The non-linearity associated with overdriving the comb filter differential amplifier (section 8.6.8) is a danger to the inexperienced operator and this section of the circuit could benefit from being redesigned.

3) The monitoring amplifier, figure 8.8, does not provide sufficient power for ready monitoring of previously recorded signals; the circuit should be modified to remedy this.

8.9 Assessment

Experience gained from the goniometer system, described in chapter 3, has shown that in Europe its sensitivity is almost always limited by mains harmonic and/or VLF transmitter interference (frequencies > 10kHz) rather than by noise from the receiver electronics. The limitation by the former occurs because the tape recorder dynamic range is less than that of the receiver. Due to the heavy top cut filtering and the use of a mains interference comb filter these problems are substantially reduced in this receiver design.

The successful completion of this receiver and the results presented in chapter 10 clearly demonstrate the usefulness of the comb filter approach to mains harmonic interference in ELF/VLF radio research.

CHAPTER NINE

A Mu-metal Cored Antenna And Its Associated Preamplifier

9.1 Introduction

The sensitivity of an ELF receiving system is, providing that man made interfering signals are ignored, dependent upon the noise performance of the antenna and preamplifier. Since the noise performance of the latter is dependent upon the impedance of the former they are inextricably linked in considerations of system sensitivity. Note that in this application it is particularly difficult to obtain a good noise performance at the low end of the band where amplifier $1/f$ noise can be substantial.

This chapter describes a portable mu-metal cored, multi-turn antenna which gives adequate sensitivity (see figure 9.12) over the frequency range 1Hz to several hundred Hertz. Cannon (1976) gives both a design approach for multi-turn mu-metal antennae on which this design is based, and also a description of the mu-metal core used here.

A coil antenna was selected because it offered high mechanical stability compared with a long wire antenna. This is an important consideration at low frequencies where movement of the antenna in the terrestrial magnetic field, possibly due to the wind, can simulate a real signal (Rycroft, 1965). Additionally the effects of man made noise, so often electrostatic in nature, can be reduced by screening of the coil.

9.2 The Use Of A High Magnetic Permeability Core

By using a ferromagnetic core increased antenna sensitivity can be achieved because the output voltage increases without an increase in thermal noise. When using an air cored antenna loop an increased output voltage can only be achieved by increasing the diameter or the turns number, with a corresponding increase in resistive noise. Keefe et al. (1972) show that as a result the signal to noise ratio of the antenna only increases as $N^{\frac{1}{2}}$ and $r^{1.5}$ where N and r are the turns number and the average radius respectively.

One disadvantage of such an approach is that theoretical estimates of the antenna's electrical characteristics are fraught with difficulties

(Cannon, 1976; Morgan, 1976). Empirical design techniques are thus adopted. In addition the high inductance associated with a coil wound on such a core can result in a degraded noise performance resulting from the preamplifier current noise and parallel resistor current noise generators. This is discussed in detail in later sections.

9.3 The Antenna Gain Factor

The high permeability core will determine both the antenna output voltage for an incident field, and the inductance of the antenna, and consequently its resonant frequency.

For small amplitude signals, and providing that no flux loss occurs between core and coil, the use of a mu-metal core increases the coil flux density, relative to the free space value, in proportion to the incremental permeability μ_{inc} . This is given by $(dB/dH)^1/\mu_0$, measured at the DC operating point on the B-H curve of the material. In this context this is defined by the local strength of the earth's magnetic field. For open magnetic circuits, such as found in a mu-metal rod, the determination of this operating point is a complicated function of the demagnetisation field set up in the core which is itself a function of the core geometry. Morgan (1976) investigated the problems involved with such a calculation. He concluded that for a square sectioned rod, used in this case for manufacturing convenience, these problems were almost insurmountable; although a crude approximation to the analytically tractable long prolate spheroid (Stoner, 1945) could be made. As such the demagnetisation field is minimised for a long thin rod.

Cannon (1976) points out, however, that such analytical approaches are doomed to failure since various design constraints can result in an antenna with considerable flux leakage. Principally, in order to maintain a high resonant frequency, which section 9.8.3 shows to be a prerequisite for a good noise performance over a wide frequency range, the coil capacitance should be kept to a minimum. Keefe et al. (1972) shows that this occurs for a high b:a ratio, see figure 9.1 and table 9.2. With this condition satisfied there will be considerable flux leakage.

Both Cannon (1976) and Morgan (1976) conclude that an empirical design approach is necessary. The approach adopted in this work is to define a dimensionless quantity G_c , the antenna gain factor. As such

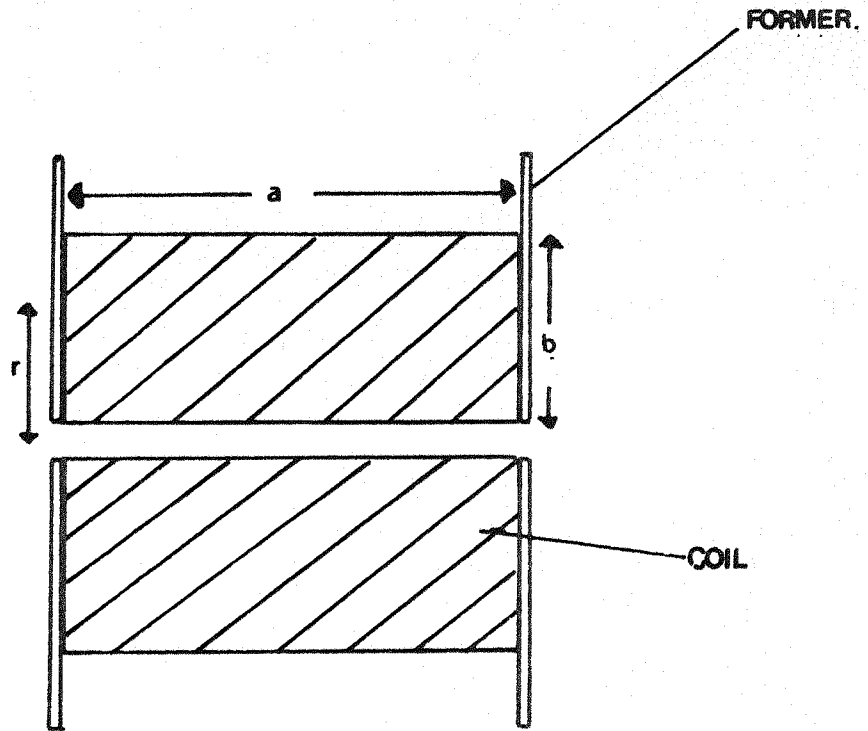


Fig. 9:1 Diagram Illustrating Coil Geometry.

$$a = 7.3 \text{ cm}$$

$$b = 3.1 \text{ cm}$$

$$r = 2.15 \text{ cm}$$

$$\text{Average cross-sectional area} = 14.52 \text{ cm}^2$$

Table 9:1 Physical Characteristics.

the induced voltage is given by a modified Faraday's Law viz:

$$V_s = - G_c N A \frac{d}{dt} (\mu_o H) \quad (\text{volts}) \quad \text{equation 9.1}$$

The antenna inductance will be similarly modified from its free space value, by the multiplicative factor G_c , making prediction of this parameter difficult.

9.4 Physical Description And Construction Of The Mu-Metal Cored Antenna

The antenna core was constructed from 50,000 turns of 38 s.w.g. enamelled copper wire wound on a perspex former 1cm square. The width of the coil, a , the depth of the windings, b , and the radius corresponding to the mean coil area, r , are defined in figure 9.1 and table 9.1. The depth, b , was limited by the coil winding facilities.

The core consists of a 75cm long (limited by the core production facilities (Telcon, 1975)), 1cm square section (limited by a requirement for mechanic strength) mu-metal bar constructed from a stack of laminated, 0.1mm thick foils. The laminations reduce eddy current losses providing constant permeability from DC to 250 Hz (Telcon, 1975).

For mechanical rigidity the circular cross section coil end plates were themselves supported by teflon plates 1.75cm thick. Similar plates were also provided to support the mu-metal bar; this is illustrated in figure 9.2.

The whole was then mounted inside a rolled aluminium, earthed, electrostatic screen to which the teflon plates were screwed. The screen was broken, in a length wise sense, in order that it did not present a shorted turn to the antenna. The resulting cylindrical antenna was supported during transportation, and during measurement periods, in a wooden box lined with expanded foam in order to absorb vibrations. Figure 9.4 shows the antenna so mounted.

9.5 The Electrical Characteristics Of The Antenna

9.5.1 Introduction

In order to define the electrical characteristics of the antenna fully, it is necessary to determine theoretically, or experimentally, several parameters. These are, the DC resistance, the antenna

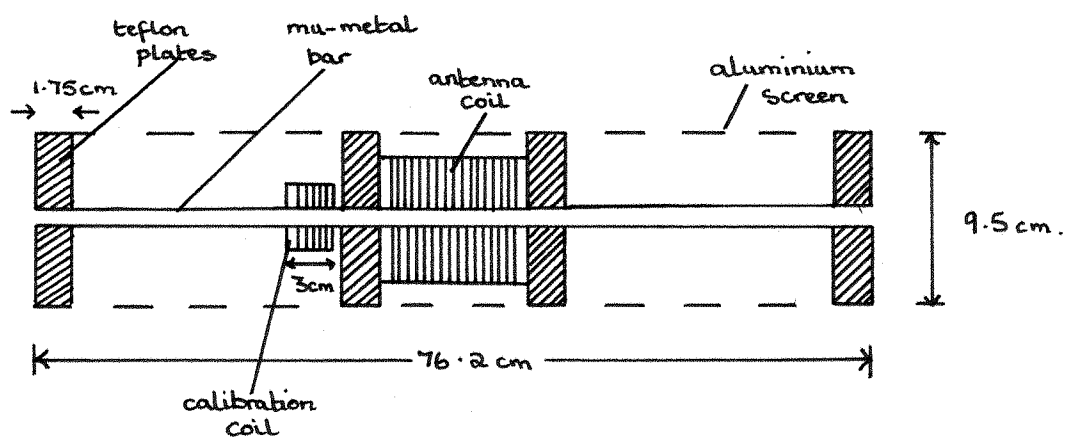


Fig. 9:2 Coil and Mu-Metal Bar Mounting Arrangement.

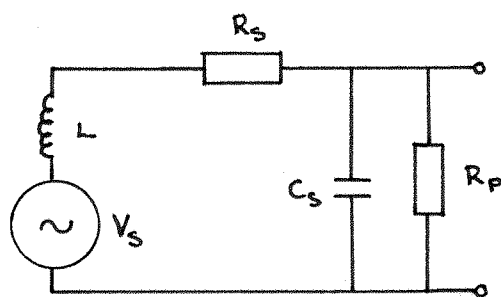
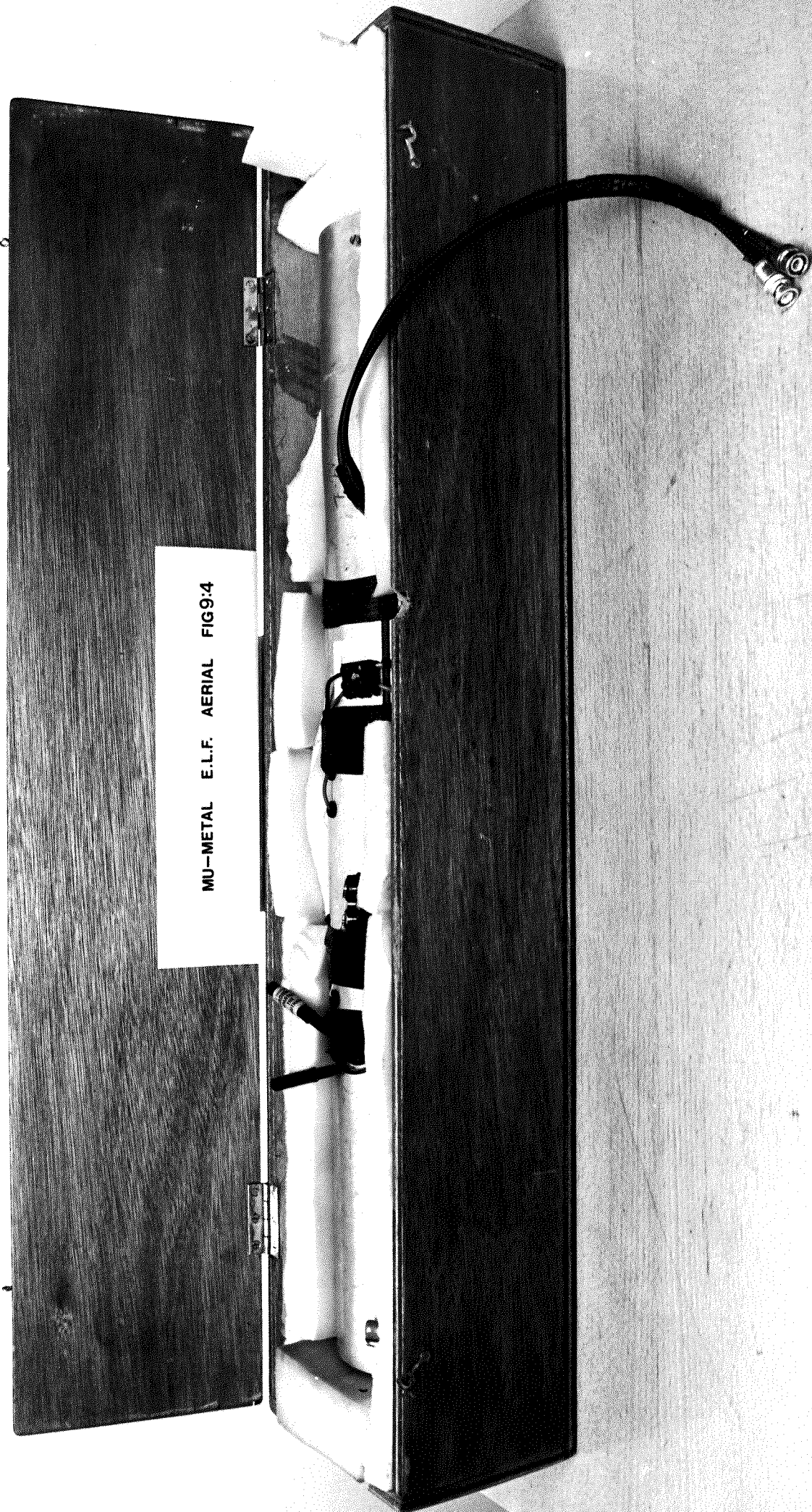


Fig. 9:3 Equivalent Circuit Of The Antenna.



inductance, the distributed coil capacitance and the parallel loss resistance associated with eddy and hysteresis losses in the core, and the self capacitance. This distributed self capacitance arises from the interwinding capacitance and capacitance between the windings and the mount. Figure 9.3 shows a lumped circuit element model of the antenna, used in these analyses, which is probably the simplest that could be used. Evidently such a model must be an approximation to the real antenna where the inductance, resistance and capacitance are all distributed throughout the coil. The success of such a model can only be judged by its ability to give a self-consistent set of experimental results and close agreement between theoretically predicted and experimental values.

The theoretical evaluation of the above quantities has been discussed by Terman (1943), Keefe et al. (1972), Morgan (1976), and Cannon (1976). Generalising, an adequate analytical determination of the DC resistance and distributed capacitance is shown to be possible. For a mu-metal cored antenna the theoretical determination of the gain factor, the inductance (as previously discussed), and the parallel loss resistance is, however, shown to be difficult.

The remainder of this section describes techniques employed to determine these quantities experimentally and their effects on the antenna performance.

9.5.2 Experimental Determination Of Inductance, Capacitance And Loss Resistance

The determination of the coil inductance using a bridge technique is made difficult by the strong mains pick up. The direct determination of the capacitance by this method is impossible due to its distributed and lossy nature. We must consequently resort to other techniques.

Terman (1943) describes a method for the determination of both the coil inductance, and its distributed capacitance, C_D . The technique involves resonating the antenna at several frequencies by placing various capacitors, C_{ADD} , in parallel with C_D , see figure 9.3. Providing that the voltage resonance, measured across C_D , occurs at an angular frequency ω_{RES} , corresponding to a simple LC circuit and, given by $(LC_T)^{-\frac{1}{2}}$, a graph of ω_{RES}^{-2} against C_{ADD} gives a straight line. The slope of this line is then proportional to the inductance, and the negative intercept on

the capacitance axis gives the distributed capacitance. In general, however, ω_{RES} is not given by this simple expression.

$$\text{Writing } K = \frac{V_{\text{OUT}}}{V_{\text{IN}}} = \frac{R_p // C_T}{R_p // C_T + R_s + L} \quad \text{equation 9.2}$$

where $//$ indicates a parallel combination of circuit elements and C_T is the total parallel capacitance. It is simple to show that:

$$\frac{V_{\text{OUT}}}{V_{\text{IN}}} = \frac{R_p}{\left[(R_p + R_s - \omega^2 LC_T R_p)^2 + \omega^2 (C_T R_p R_s + L)^2 \right]^{1/2}}$$

and differentiating to obtain the resonant frequency gives:

$$\omega_{\text{RES}} = \frac{1}{LC_T} + \frac{1}{LC} \frac{R_s}{R_p} \frac{(C R_s R_p + L)^2}{2 L^2 C_T^2 R_p^2} \text{ rad s}^{-1}$$

which in this application approximates to:

$$\omega_{\text{RES}}^2 = \frac{1}{LC_T} - \frac{1}{2 R_p^2 C_T^2} \text{ rad s}^{-1} \quad \text{equation 9.3}$$

Equation 9.3 shows that, providing $\frac{1}{LC_T} \gg \frac{1}{2 R_p^2 C_T^2}$,

the method outlined above will be valid.

Telcon (1975) and Morgan (1976) have addressed the possibility of determining R_p (typically $> 1\text{M}\Omega$) and have shown that providing $\frac{L}{C_T R_p} \gg R_s$ and $\frac{1}{LC_T} \gg \frac{1}{C_T^2 R_p^2}$, the Q at resonance can be written

$$\text{as } Q_{\text{RES}} = \frac{R_p}{\omega_{\text{RES}} L} \quad \text{equation 9.4}$$

The technique for finding R_p involves shunting the antenna output with a resistance R_{EXT} ($\text{M}\Omega$), preferably of a value close to that estimated for R_p . Providing that the above conditions are still true, there will be no change of resonant frequency and we may write:

$$R_p = R_{\text{EXT}} \frac{(Q_{\text{OLD}} - 1)}{Q_{\text{NEW}}} \text{ (M}\Omega\text{)} \quad \text{equation 9.5}$$

where Q_{OLD} and Q_{NEW} are the Q factors before and after the addition of R_{EXT} . Note that, if $R_p \approx 1\text{M}\Omega$, compensation for the measuring instrument

input impedance must be made. The Q was determined by evaluating the ratio of the voltage across the output capacitor to the injected voltage (Terman, 1943).

Using such techniques a value of $R_p \gtrsim 25M\Omega$ was obtained at 195 Hz and as such $\omega^2_{RES} = \frac{1}{LC_T}$ may be considered a good approximation when $C_T \ll 1nF$.

The coil inductance and capacitance were subsequently evaluated using the method outlined above. In order to minimise loading of the antenna by the signal, source signals were injected into the antenna using a Helmholtz coil system developed by the author, see appendix 4. Using values of C_{ADD} between ~ 250 pF and ~ 600 pF the antenna output was monitored. A least squares linear regression of f^{-2} versus C_{ADD} resulted in value of $L = (740 \pm 10)$ H and $C_D = 32 \pm 5$ pF. It is simple to show that with these values of L , C_T , and R_p the previously stated approximations are met over the frequency range of these measurements.

The validity of equation 9.3 was checked by loading the antenna with various values of R_p and C_{ADD} and comparing the experimentally determined, and theoretically predicted, resonant frequencies. Agreement to $\pm 1\%$ was obtained.

9.5.3 Gain Factor

The gain factor was determined, in the laboratory, by measuring the coil inductance with and without the core. A direct comparison gave $G_c = 16.4 \pm 1.6$.

9.5.4 Laboratory Amplitude Response

A laboratory calibration of the frequency response of the antenna was carried out using the Helmholtz coil system. The antenna output was buffered during these measurements by a high input impedance ($> 10M\Omega$) unity gain amplifier. In order to reduce the effects of mains interference the signals were fed to the comb filter, chapter 8, and additionally the measurements were carried out at night when the mains interference was relatively low. The output amplitude was measured using a D.V.M.

Figure 9.6 shows the results of the calibration. That shown is

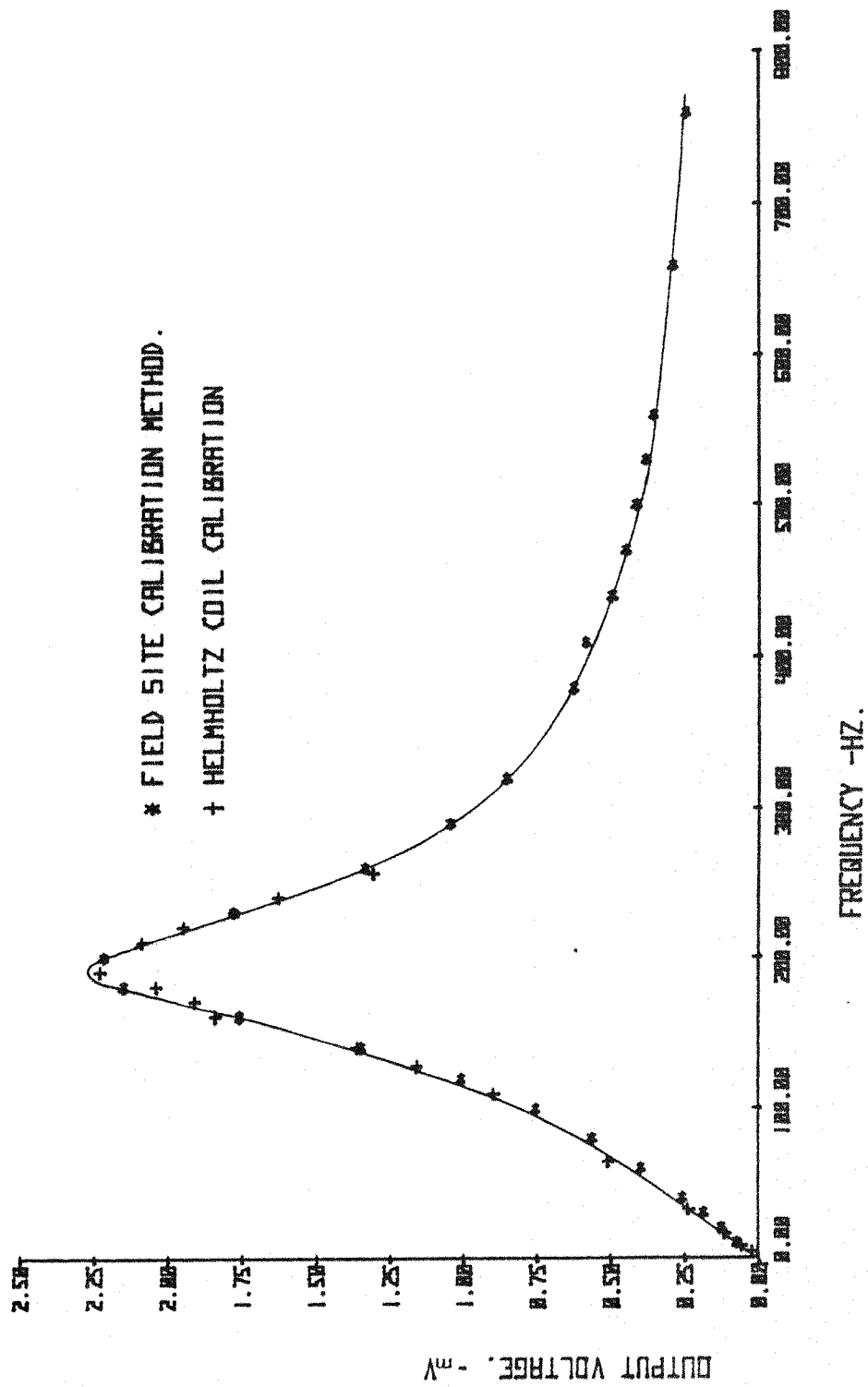


Fig. 9:5 Amplitude Response Of The Mu-Metal Antenna - Input Signal 10^3 pT

for the antenna with a 780 pF high stability silver mica capacitance in parallel with the distributed capacitance of the coil, it being the configuration adopted for the measurements described in chapter 10. This gave a resonant frequency at ~ 200 Hz, resulting in good sensitivity over the required frequency range. The calibration has been normalised to an input field of 10^3 pT.

9.5.5 Summary

Table 9.2 summarises the electrical performance of the antenna, as discussed so far, together with parameters to be discussed in later sections.

9.6 Field Calibration

9.6.1 Introduction

In order to facilitate calibration of the antenna and system in the field an integrated calibration coil has been incorporated into the antenna, see figure 9.2. The coil, length ~ 3 cm, and consisting of 2000 turns of 28 s.w.g. enamelled copper wire wound on a paxolin former is located adjacent to the antenna coil, figure 9.2. As such it maximises the magnetic coupling.

9.6.2 Theory

The voltage E_A induced in the antenna by a current flowing in a nearby coil is given by:

$$E_A = \frac{M dI_c}{dt} \quad (\text{volts}) \quad \text{equation 9.6}$$

where M is the mutual inductance between antenna and coil and where I_c is the current in the calibration coil.

Additionally we may write, from Faraday's Law, that the voltage, E_F , induced in the antenna by an ELF signal with its magnetic vector lying perpendicular to the antenna is given by equation 9.1.

Integrating and equating we have:

$$B = \frac{M I_c}{NA G_c} \quad (\text{Teslas}) \quad \text{equation 9.7}$$

<u>Parameter</u>	<u>Experimental Value</u>	<u>Predicted Value</u>
Series resistance	7K2	(1) 6K3
Loss resistance	> 25M	
Inductance of antenna	$(740 \pm 10)\text{H}$	(2)
Distributed capacitance	$(32 \pm 5)\text{ pF}$	30pF
External parallel capacitance	780pF	
Inductance of coil (no core)	$(45 \pm 0.5)\text{H}$	
Mutual inductance between calibration coil and antenna	$(30.5 \pm 3)\text{H}$	
Preamplifier input capacitance	< 3pF	

(1) Predicted resistance = $2\pi rN\eta$, where η is the resistance per unit length (Keefe et al., 1972).

(2) Predicted interwinding capacitance = $\epsilon_0\epsilon_r \frac{2\sqrt{\pi}}{d} \frac{a}{b} \sqrt{\frac{\pi r^2 ab}{N}}$

where ϵ_0 is the permittivity of free space, ϵ_r the relative permittivity of the wire enamel (3), and d is twice the enamel thickness ($6 \times 10^{-5}\text{m}$) (Keefe et al. 1972).

Table 9.2 Mu-metal antenna electrical characteristics

The mutual inductance was determined by measuring the inductance of the antenna and coil in series, L_A , and then by measuring the inductance of the antenna and coil after reversing the connections of the latter to give L_B . Duffin (1965) shows that the mutual inductance between the antenna and the calibration coil is then given by:

$$M = \frac{L_A - L_B}{4} \quad (\text{Henries}) \quad \text{equation 9.8}$$

Using this technique a value of $M = (30.5 \pm 3.5) \text{ H}$ was obtained. I_c was constrained, for convenience, to be approximately constant with frequency over the band of interest by feeding the coil through a high valued resistor. A total coil resistance of $(2.280 \pm 0.005) \text{ M}\Omega$ was found to be suitable. Such a high series resistance also prevents loading of the antenna.

Using these values of M and I_c and values of N , A and G_c from tables 9.1 and 2, equation 9.7 reduces to:

$$B = 1.14 \times 10^{-8} V_{IN} \quad (\text{Tesla}) \quad \text{equation 9.9}$$

where V_{IN} is the signal generator output voltage (with 600Ω output impedance).

9.6.3 Performance

The antenna response was measured again (in the laboratory) using the calibration coil and it too is shown in figure 9.5. Similar buffering of the antenna was employed during these measurements to that employed during the Helmholtz coil calibration.

It is gratifying to note the close agreement between the calibration technique and the Helmholtz coil laboratory technique. Agreement is at all times to within 5%. It is concluded that field calibrations using this technique will give valid results. The close correspondance also demonstrates the self consistency of the measured parameters M , A , and L (via G_c), together with the lumped circuit model on which the electrical measurements were based. By implication the high value of R_p assigned in section 9.2.4.2 must also be correct since otherwise the value of L obtained from the approximation $\omega_{RES}^2 = \frac{1}{LC_T}$ would have been in error.

9.7 The Preamplifier

9.7.1 Introduction

The preamplifier will limit the overall system sensitivity if it contributes more noise than that introduced by the thermal noise of the antenna. The choice of the correct preamplifier design is consequently of extreme importance.

The design of a low noise preamplifier, using discrete components requires considerable effort and it was consequently concluded that a proven discrete or alternatively an integrated circuit design should be adopted.

9.7.2 General Considerations

In a similar fashion to the analysis outlined in section 8.4.4, the noise introduced by the preamplifier can be expressed in terms of two uncorrelated input referred noise sources; i_n ($A\ Hz^{-\frac{1}{2}}$), the input referred current noise, and e_n ($V\ Hz^{-\frac{1}{2}}$), the input referred voltage noise. It is well known (Motchenbacher and Fitchen, 1972) that the noise introduced via the former is highly dependent upon the source impedance whereas the latter is only weakly dependent upon it.

Generalising, an FET input preamplifier has a low i_n and a high e_n ; for a bipolar these parameters are vice-versa. Since the impedance of the mu-metal antenna is several hundred $K\Omega$ at 100 Hz, it can be shown that in this case an FET input preamplifier will give a better performance than a bipolar (Cannon, 1976). The choice of an FET is further enhanced because, in general, the so called $1/f$ noise breaks in, as the frequency is decreased, at lower frequencies for FET devices than for bipolars. Note also that an input noise matching transformer cannot be used in this application since its efficiency will be too low at the LF end of the passband.

9.7.3 A Discrete Preamplifier

Cannon (1976) discussed the modification of a preamplifier due to Cantarano and Pallotino (1970) in order that its low frequency 3 dB point be reduced from 10 Hz to 1 Hz. Unfortunately, although stable on its own the preamplifier had a tendency to oscillate, at the antenna resonant frequency, when used in conjunction with this antenna.

9.7.4 An Integrated Preamplifier

The possibility of using an integrated device was also examined. A literature search revealed the model AD606 instrumentation amplifier (Analog Devices, 1974) as a possible contender. It has a specified input referred voltage noise of $10 \text{ nV Hz}^{-\frac{1}{2}}$ between 10 Hz and 1kHz. Below 10 Hz the noise rises linearly to $30 \text{ nV Hz}^{-\frac{1}{2}}$ at 1 Hz. These values apply to a gain of 60 dB, with slightly inferior figures being expected at lower gains. The common mode rejection ratio (CMRR) is specified to be 90 dB, giving good protection against electrostatic pick up of man-made signals.

The circuit diagram of the preamplifier used in this work is shown in figure 9.6. The input, $1\text{M}\Omega$, resistors provide a path to earth for the amplifier input currents and are required by the manufacturer. Gain is variable from ~ 10 dB to 60 dB using the 4K7 20 turn trimmer. A.C. coupling is employed between the 606 and the TL081 buffer to reduce vibrational signals, block DC offsets and reduce $1/f$ noise, see chapter 8. The noise characteristics and a noise model which can be directly adapted to the high input impedance/low output impedance buffer circuit have also been discussed in chapter 8. The preamplifier is mounted in a die-cast box, see figure 9.7. Power to the preamplifier is provided by a separate regulated power supply, see figure 9.7 and 9.8.

The response of the preamplifier (only) was measured to be flat to better than 0.2 dB peak to peak from 0.5 Hz to 10kHz. A gain of ~ 45 dB (specifically 44.5 dB for the measurements described in chapter 10) was found adequate for use with the mu-metal antenna described in this chapter and the receiver described in chapter 7. The CMRR was measured and found to be > 65 dB.

9.8 Noise Performance Of The Mu-Metal Antenna And Preamplifier

9.8.1 Introduction

Cannon (1976) developed an expression for the determination of the source referred noise due to a mu-metal cored antenna and the, then proposed, preamplifier. Due to the introduction of an alternative preamplifier this expression must be revised. The new equation will be used to evaluate the various noise terms, the total system noise and the system sensitivity by employing the values of L , C_T , R_s , R_p etc. determined earlier in this chapter.

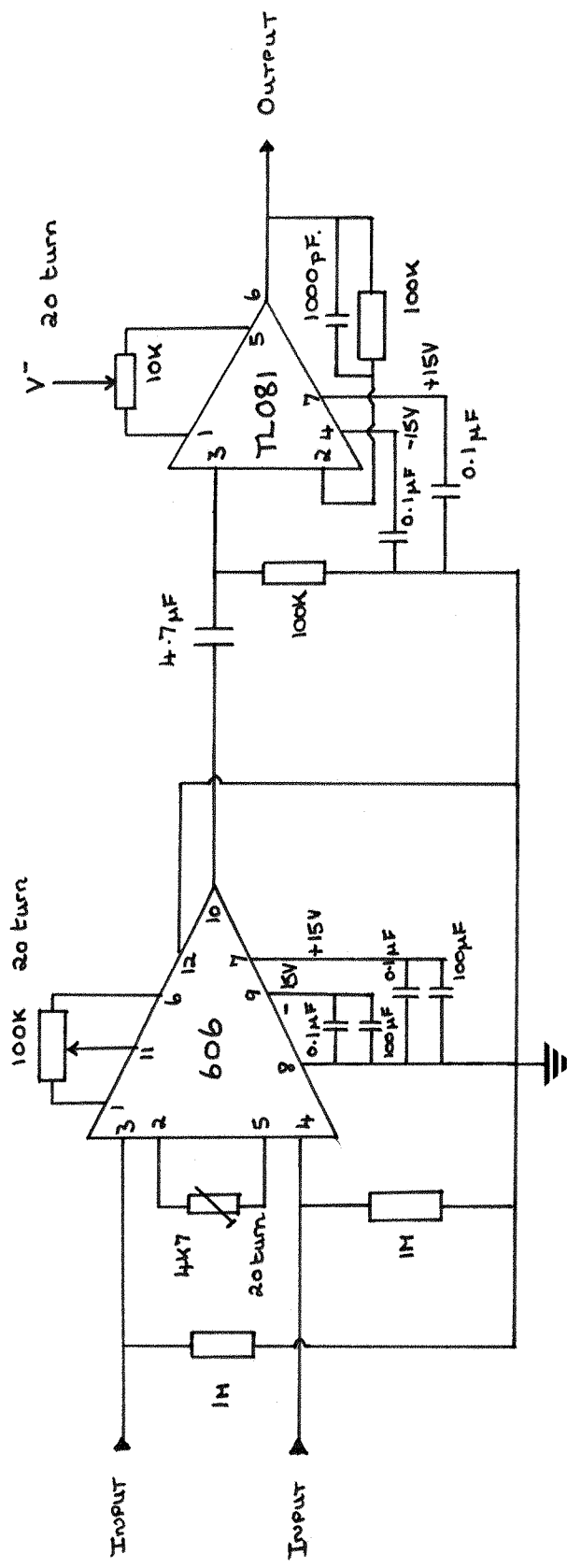


Fig. 9:6 Model 606 ELF Preamplifier.

FIG 9.7A

ELF PREAMPLIFIER

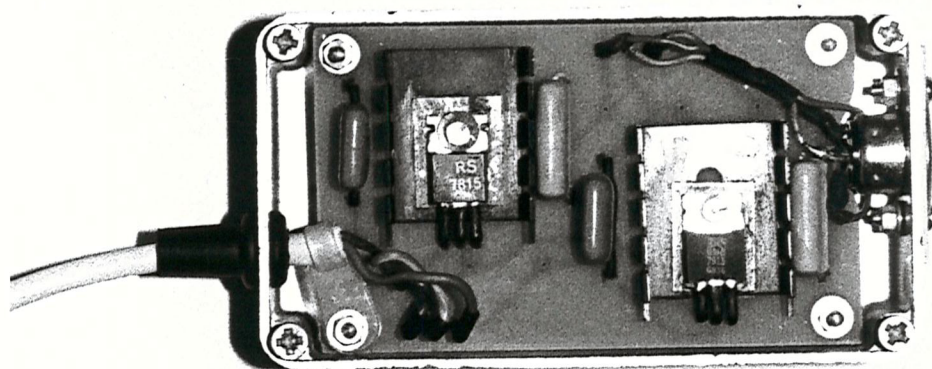
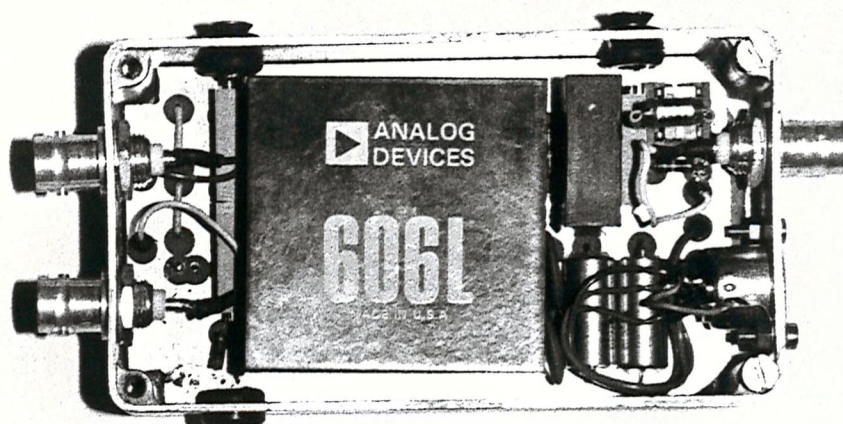


FIG 9.7B

REGULATED POWER SUPPLY

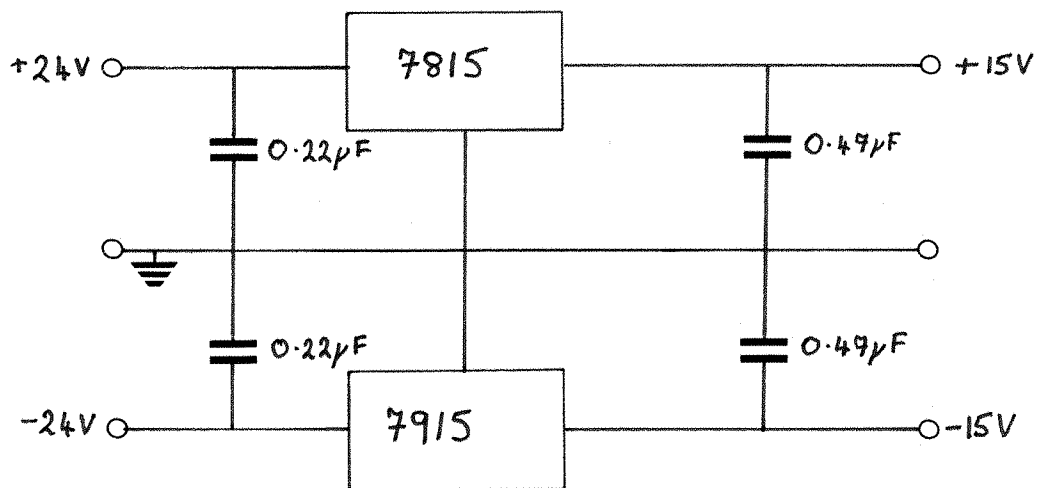


Fig. 9:8 Preamplifier Regulated Power Supply

9.8.2 Noise Analysis

Figure 9.9a shows the lumped circuit model of the antenna together with C_{ADD} , comprising the 780 pf parallel capacitance plus any antenna to preamplifier lead capacitance. C_{IN} represents the preamplifier input capacitance, and $R_N/2$ are the two $1M\Omega$ resistors required by the manufacturer between input and earth, see figure 9.6. In fact only one of these resistors is required; however, two were used to maintain a balanced circuit and good CMRR performance. Figure 9.9b shows 9.9a simplified such that $C_T = C_D // C_{ADD} // C_{IN}$.

In figure 9.9c this circuit has been translated into an equivalent noise circuit. No noise generator is required for R_p since it has no thermal noise associated with it.

We define:

i_p = current noise associated with the resistance $\frac{R_N}{2}$ (A Hz^{-1/2})

i_n = current noise associated with the amplifier (A Hz^{-1/2})

e_s = voltage noise associated with the source resistance R_s (V Hz^{-1/2})

e_n = voltage noise associated with the amplifier (V Hz^{-1/2})

and

E_{ni} = total input referred noise

E_{no} = total output referred noise

$$R_T = R_N // R_p$$

The total output noise from the system is then given by:-

$$E_{no}^2 = e_n^2 + i_n^2 \left[j\omega(L + R_s) // \frac{1}{j\omega C} // R_T \right]^2 + e_s^2 \left[\frac{R_T // \frac{1}{j\omega C}}{R_T // \frac{1}{j\omega C} + R_s + j\omega L} \right]^2 + 2 i_p^2 \left[\frac{0.5 R_N ((j\omega L + R_s) // \frac{1}{j\omega C} // R_p)}{R_N + ((j\omega L + R_s) // \frac{1}{j\omega C} // R_p)} \right]^2$$

equation 9.10

Using the system transfer function, equation 9.2, this can be translated back to the input (i.e. V_s) to give the input or source referred noise, i.e. $E_{ni}^2 = \frac{E_{no}^2}{K^2}$

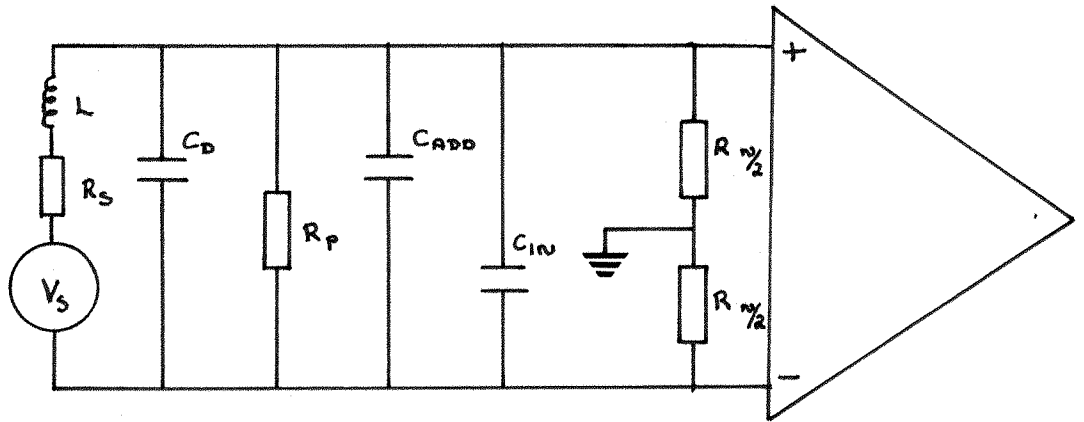


Fig. 9:9a Antenna+Coupling Network (Lumped Circuit Model).

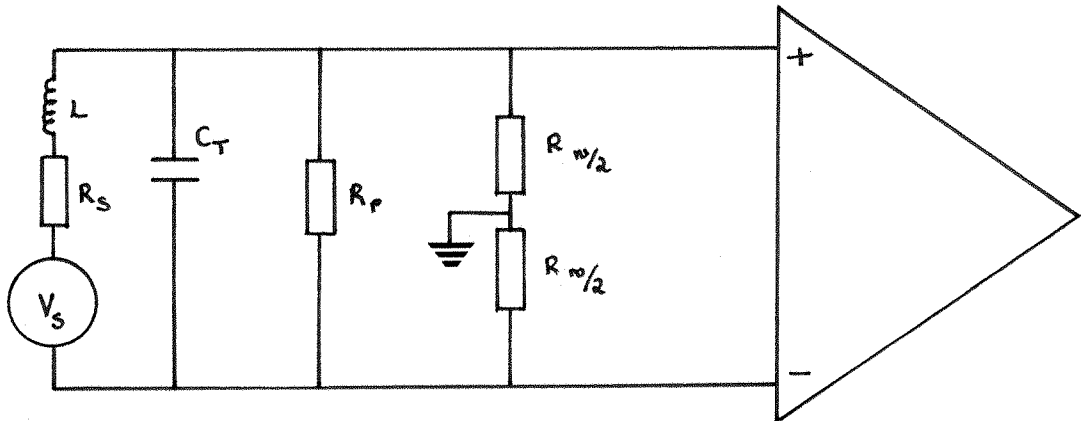


Fig. 9:9b Simplified 9:9a.

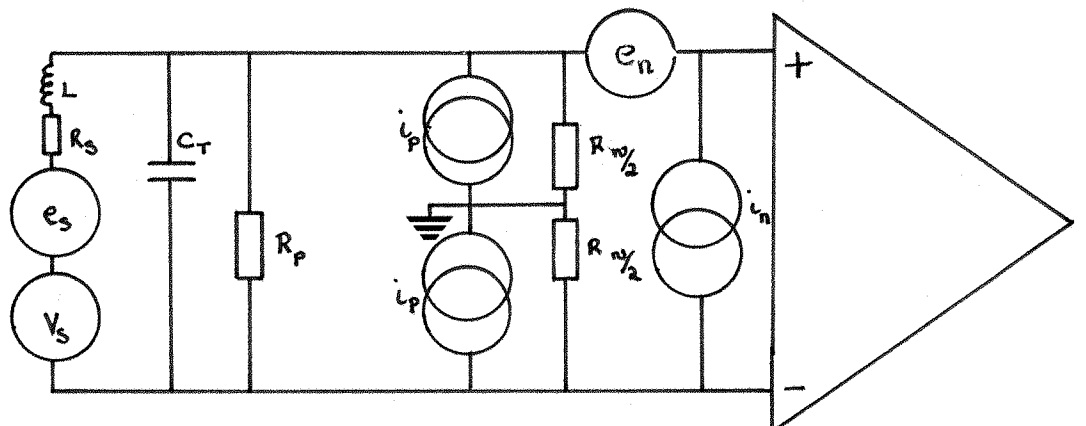


Fig. 9:9c Noise Circuit Corresponding To Figs. 9:9a/b.

$$\begin{aligned}
E_{ni}^2 &= \underbrace{e_s^2}_{\text{Term A}} + \underbrace{i_n^2 (R_s^2 + \omega^2 L^2)}_{\text{Term B}} + \underbrace{e_n^2 (1 + R_s/R_T - \omega^2 LC_T)}_{\text{Term C}} + \underbrace{\omega^2 (R_s C_T + \frac{L}{R_T})^2}_{\text{Term D}} \\
&+ \frac{2 i_p^2 \left\{ (1 - \omega^2 C_T L) \left[R_s (1 - \omega^2 C_T L) + \frac{L^2 \omega^2}{R_p} \right] + \frac{\omega^2 L^2 R_s}{R_N^2} \right\}^2}{\left\{ (1 - \omega^2 C_T L)^2 + \omega^2 (L/R_p + L/R_N)^2 \right\}^2} \\
&+ \frac{2 i_p^2 \left\{ \omega L (1 - \omega^2 C_T L)^2 + \frac{\omega L}{R_N} \left[\frac{\omega^2 L^2}{R_N} + \frac{\omega^2 L^2}{R_p} + \frac{R_s^2}{R_p} \right] \right\}^2}{\left\{ (1 - \omega^2 C_T L)^2 + \omega^2 (L/R_p + L/R_N)^2 \right\}^2} \\
&\quad \text{Term E} \qquad \qquad \qquad \text{Term F}
\end{aligned}$$

equation 9.11

Terms A, B, C and D are exact. In the derivation of terms E and F several approximations have, however, been made to simplify the final expression, these being

$$R_s/R_N \ll 1, CR_s \ll L/R_N, \text{ and } R_s/R_p \ll R_s/R_N.$$

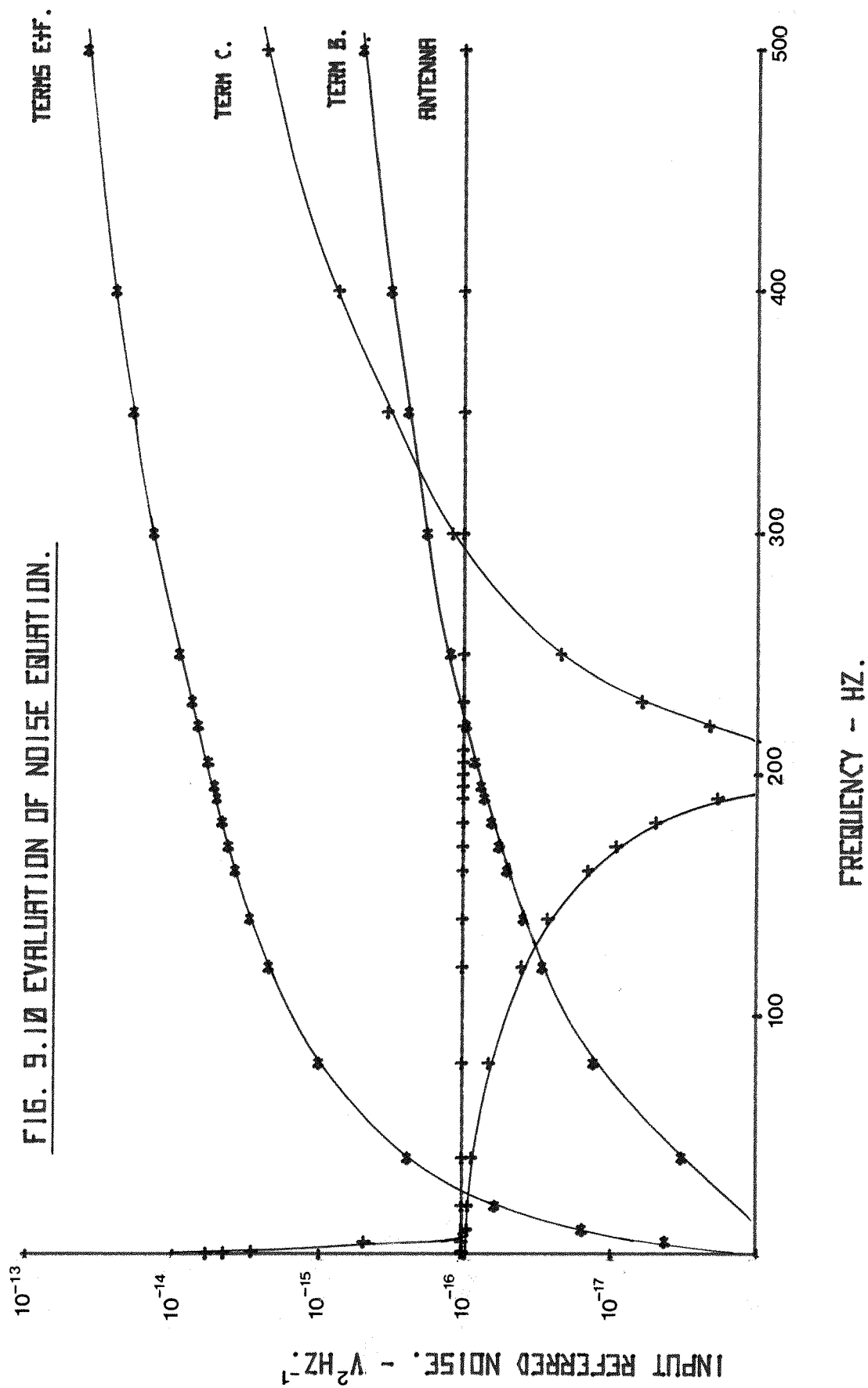
9.8.3 Evaluation

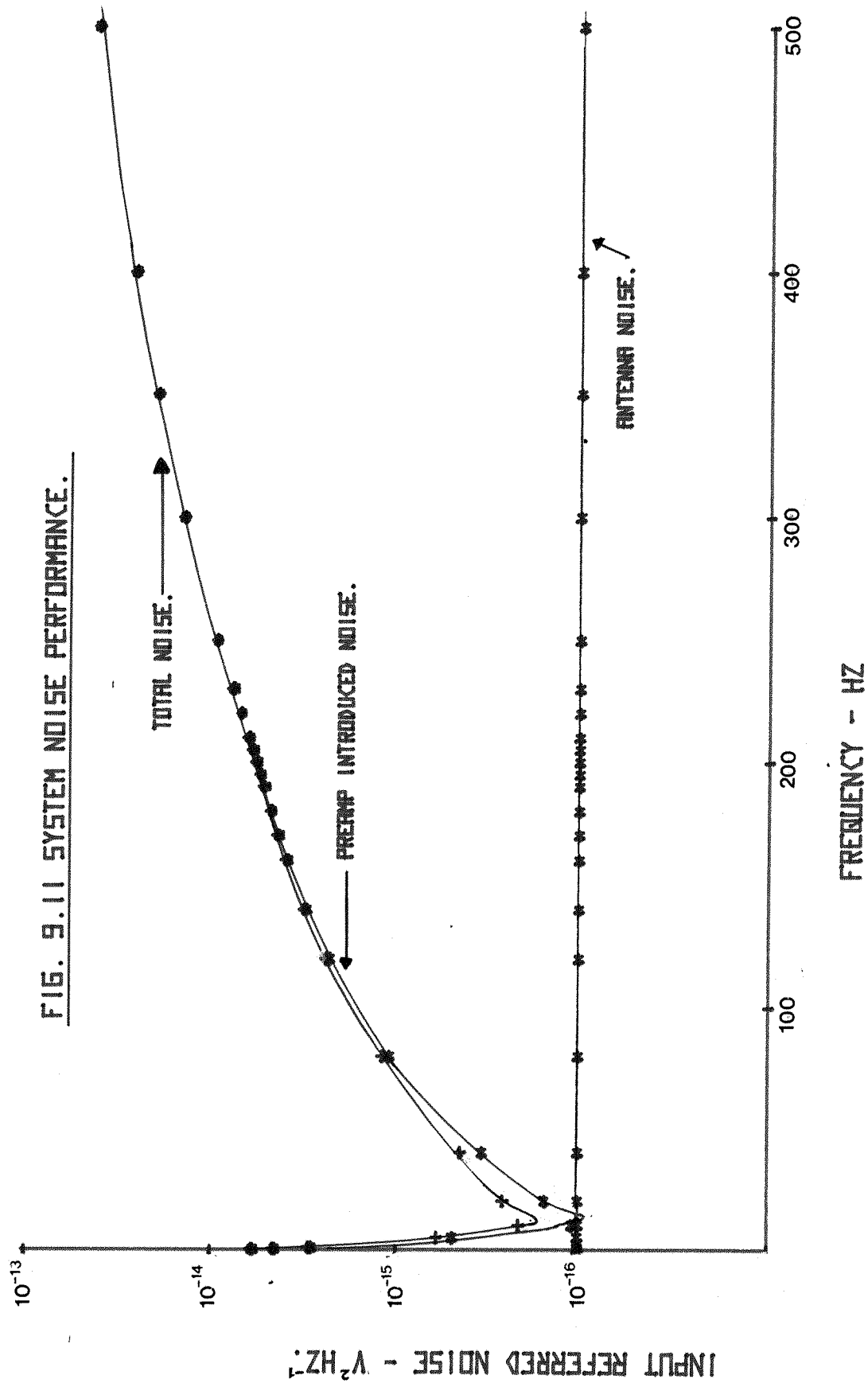
Each of the terms in equation 9.11 has been evaluated and the more important are plotted in figure 9.10. For clarity the sum of the preamplifier noise components and the antenna thermal noise are plotted separately in figure 9.11.

Term A is the antenna thermal noise component given by $e_s^2 = 4kTR_s$ ($V^2 \text{ Hz}^{-1}$).

Term B results from the amplifier parallel current noise generator. This is not quoted in the amplifier specifications; however, a value of $i_n \sim 10^{-14} \text{ A Hz}^{-1}$ is typical for an FET input device.

Terms C and D are associated with the input referred voltage noise of the amplifier. Term D (not plotted) is always small in this application. Term C is more interesting, going to zero at a frequency $\omega = (1/LC (1 + R_s/R_T))^{1/2} \text{ rad s}^{-1}$. This is approximately equal to the





output voltage resonance if $\frac{1}{LC_T} \gg \frac{1}{2 R_P^2 C_T^2}$ and $\frac{R_s}{R_T} \ll 1$; a

condition met in this instance. Thus, in narrow band applications, providing that this noise source dominates, the resonance peak may be utilised to provide enhanced sensitivity over a narrow frequency band. Above this frequency, the noise power increases with increasing frequency at 12 dB per octave, more rapidly than any other term, and consequently it will eventually limit the useful system bandwidth.

Terms E and F, resulting from the two parallel resistor current generators, with magnitude $(4kT/R)^{\frac{1}{2}}$ are rather complicated. Figure 9.10 shows them to be the dominant noise sources for $30 \text{ Hz} < f < 500 \text{ Hz}$, with term C being dominant below this frequency. Since, however, E + F only degrades at $\sim 6 \text{ dB}$ per octave term C will again dominate at higher frequencies. Extrapolation shows that this occurs at $\sim 1700 \text{ Hz}$.

9.9 System Sensitivity

By referring the noise of the antenna back to the input it is a simple matter to evaluate the system sensitivity by equating the noise power to the signal power:

$$B = \left(\frac{\text{Noise Power}}{\omega N A G_c} \right)^{\frac{1}{2}} T \text{ Hz}^{-\frac{1}{2}} \quad \text{equation 9.12}$$

Figure 9.12 shows the result of evaluating equation 9.12 at various frequencies. A shallow sensitivity maximum is evident at resonance.

Figure 9.12 also shows the effect of varying the parallel capacitance. We see that an increase in capacitance from 815 pf to 3200 pf reduces the frequency at which the sensitivity maximum occurs, possibly a useful feature for high harmonic studies of the Schumann resonances ($\sim 80 \text{ Hz}$). Unfortunately, as would be expected, it reduces the sensitivity at higher frequencies. The use of a lower parallel capacitance results in the opposite effect. Since, as stated in chapter 8, it was hoped that this system might complement the goniometer system between 1 Hz and 800 Hz, 810 pf was chosen as a compromise value.

9.10 Conclusions And Further Work

A small and mechanically robust antenna has been built, tested and shown to give an adequate performance between 1 Hz and 500 Hz.

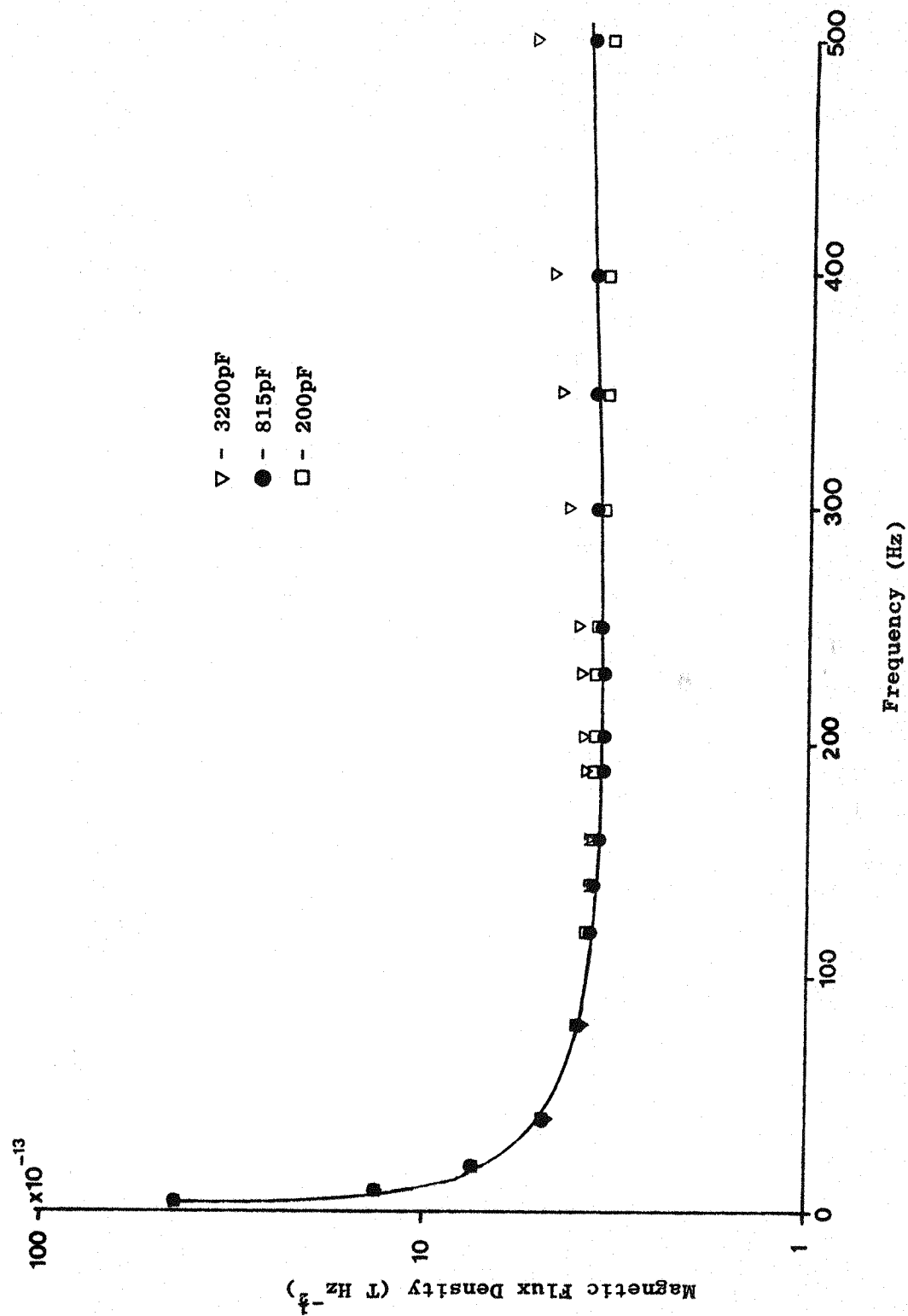


Fig. 9:12 Minimum Detectable Signal As A Function Of Frequency

The antenna has been characterised using a lumped circuit element model. This has given consistent results; it is therefore concluded that the model adequately describes the antenna behaviour. A method of field calibrating such an antenna has been developed which gives results in close agreement with a laboratory Helmholtz coil calibration.

It is useful to compare the sensitivity of this antenna with antenna designs, by other authors, for similar purposes. Morgan (1976) examined mu-metal cored antennae with turns numbers varying between 1000 and 40,000. By selecting the best of these (16,000 turns) he obtained a system sensitivity of $3.1 \times 10^{-14} \text{ T Hz}^{-\frac{1}{2}}$ at 1kHz. This is, albeit at a higher frequency, approximately one order of magnitude better than the design described in this chapter. Keefe et al. (1974) report the design of a bulky 2 metre multi-turn air cored antenna claiming a performance slightly better ($\sim 5 \times 10^{-13} \text{ T Hz}^{-\frac{1}{2}}$) over 1 Hz to 30 Hz. There is, however, an anomaly between this sensitivity and the thermal noise calculated from the quoted coil resistance. This would infer a substantially inferior performance.

With the knowledge and experience gained from this exercise the next step in the design of such an antenna can be considered. The system sensitivity at low frequencies (1 to 30 Hz) is adequate for Schumann resonance studies (field strengths $\sim 10^{-10} \text{ T Hz}^{-\frac{1}{2}}$ at 8 Hz (Rycroft, 1965)). An improved performance at higher frequencies, where reports of signals detected using ground based instrumentation are rare, would, however, be welcome.

Such an increase in sensitivity could be obtained by reducing term E + F (equation 9.11) such that it becomes less than, or at least comparable to, term C. The most obvious way to expedite this is to use a preamplifier with a higher input impedance (since term E + F is proportional to i_n^2 i.e. $1/R_N^2$).

Should a further increase in system sensitivity be required it is suggested that a reduction in turns number would be profitable. This would result in a reduction in antenna noise and noise from terms B and E + F at low frequencies. At higher frequencies (above resonance) the situation is not so simple. The inductance (proportional to N^2) would be expected to decrease as N were decreased resulting in a reduction in terms B and E + F. There is however, also likely to be a variation in G_c dependant upon the coil geometry. Assuming that this factor remained constant, a reduction in term B proportional to

L^2 , and $E + F$ approximately proportional to L^2 would be expected. Of course the effect of this reduction in turns number will be a decrease in V_s (equation 9.1) and as a consequence the turns number should only be reduced until the preamplifier contributed noise is comparable to the antenna generated noise.

CHAPTER TEN

Some Results From The ELF Receiver

10.1 Introduction

Over the period 27 March 1979 to 5 April 1979 the ELF system described in Chapters 8 and 9 was operated at Lavangsdalen, Norway.

The analysis of data collected during this period fell into two categories involving first, an assessment of the general equipment performance and then a more detailed investigation of a limited period of data. Power spectra, presented below, were produced using a Saicor SAI51B time compression spectrum analyser (Honeywell, 1970). Spectrograms were produced using the Spectral Dynamics SD 350-6 analyser and the associated hard copy facility (Spectral Dynamics, 1978; 1979).

10.2 Power Spectra Reduction Of ELF Data

A convenient ELF data analysis approach is to examine the signal power spectrum (Bendat and Piersol, 1971), particularly since a low strength, stationary signal can often be extracted from the background noise by averaging contiguous, or overlapping spectra.

For long integration periods (> 10 minutes) it is often prudent, in order to facilitate the data reduction, to analyse FM data recordings at a speed greater than that used during the recordings.

The Saicor SAI51B analyser is a 200 line instrument with frequency resolution, Δf , given by:

$$\Delta f = \frac{B}{200}$$

where B is the bandwidth in Hz.

It is convenient to define a playback factor, m, equal to the ratio of playback to record tape speed. The real time frequency resolution, Δf_r , is then modified to:

$$\Delta f_r = \frac{B}{200m}$$

equation 10.1

Now the average power spectral density (PSD), $P(f)$, can be written as:

$$P(f) = \frac{1}{T} \sum_{i=1}^N P_i(f) \quad \text{equation 10.2}$$

where $P_i(f)$ represents each of N , PSD calculations and T is the period of integration.

For $m = 1$, $T = N\Delta T$ (Honeywell, 1970), where N is the number of averages. ΔT , the time for each spectral estimate, is given by:

$$\Delta T = \frac{200}{B} \quad \text{equation 10.3}$$

It follows that:

$$T = \frac{200N}{B} = \frac{N}{\Delta f} \quad \text{equation 10.4}$$

which for $m \neq 1$ gives a real time integration period of:

$$T_r = \frac{Nm}{\Delta f} \quad \text{equation 10.5}$$

It is important to assess the spectral confidence in each averaged spectrum. Blackman and Tukey (1958) show that, providing the background noise amplitude distribution can be assumed Gaussian, the confidence in each spectral estimate is given by:

$$\sigma = \left(\frac{2}{3 \Delta f_r T_r} \right)^{\frac{1}{2}} \quad \text{equation 10.6}$$

Table 10.1 shows the result of evaluating these equations for the integration times and playback factors used here.

10.3 Equipment Performance

Representative selections of the data were made and analysed in order to assess the equipment performance. Some typical examples are given.

Figure 10.1 shows a spectrogram of the recorded signal when analysed over a 312.5 Hz bandwidth. Figure 10.2 shows a power spectrum (averaged over 1.7 minutes) for a similar section of data. Neither figure has been corrected for the amplitude response of the antenna. After correction the mean signal power spectral density is approximately

m	f_{rm} (Hz)	Δf_r (Hz)	T_r for 128 averages	T_r for 256 averages	T_r for 512 averages
			$\sigma = 7.2\%$	$\sigma = 5.1\%$	$\sigma = 3.6\%$
1	1000	5	25.6 s	51.2 s	1.71 mins
2	500	2.5	51.2 s	1.71 mins	3.41 mins
16	62.5	0.313	6.83 mins	13.65 mins	27.3 mins
32	31.25	0.156	13.65 mins	27.3 mins	54.6 mins

m = playback factor

f_{rm} = real time maximum bandwidth

Δf_r = real time resolution

T_r = real time integration time.

Table 10.1 Analysis Parameters Using A Saicor SAI51B

The selected SAI51B analysis range is 1kHz.

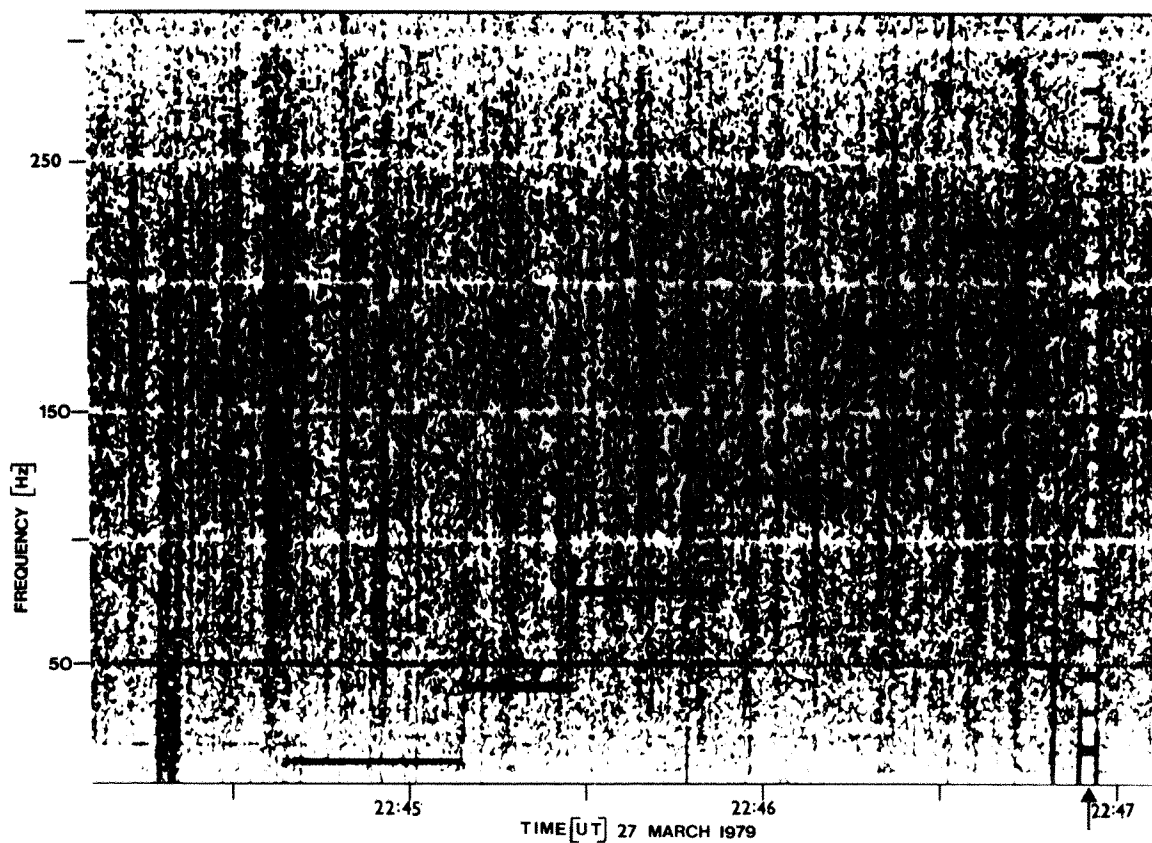


Fig. 10:1 Spectrogram showing the ELF receiver plus mu-metal antenna response over a 312.5Hz bandwidth. Also shown are various calibration signals and the marker tone (arrowed).

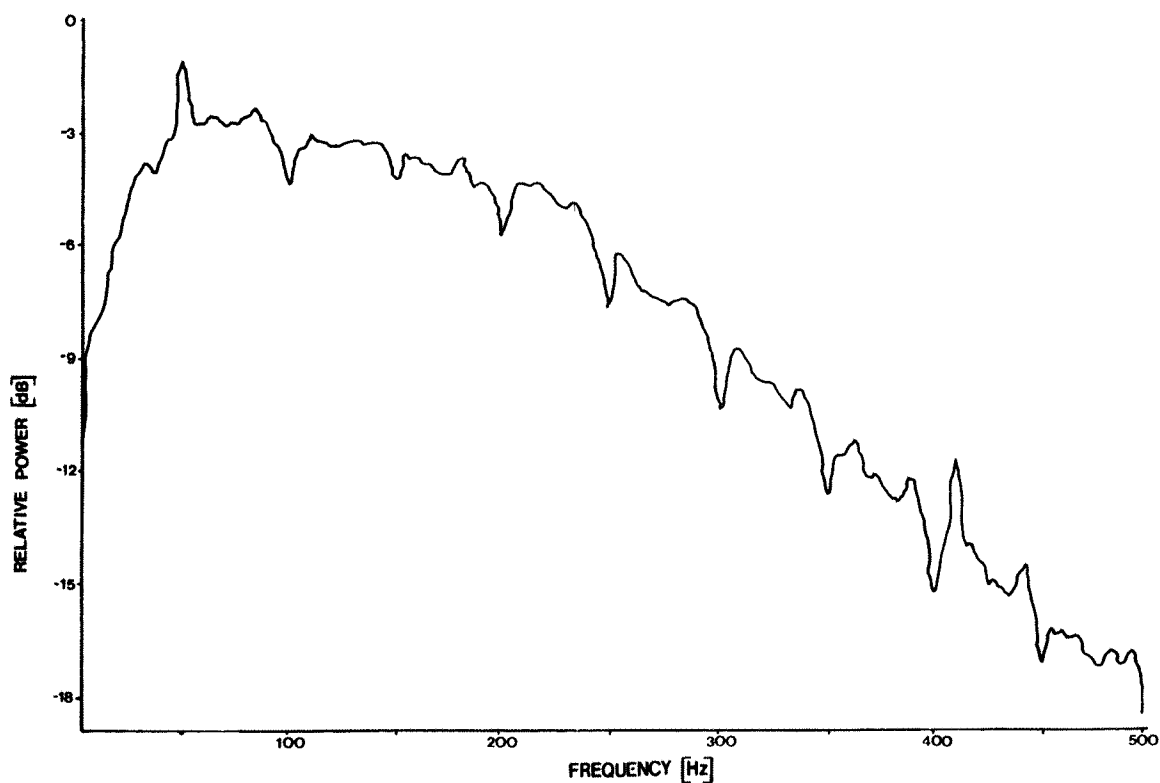


Fig. 10:2 Power Spectrogram Of ELF Data Recorded At Tromsø, Norway On 28 March 1979- resolution 2.5Hz, integration period 1.71 minutes.

flat between 250 Hz and 500 Hz. The effectiveness of the mains harmonic comb filter can be seen in both figures. In these latter two examples the optional notch filters were not in use. Figure 10.3 shows a similar spectrogram of data recorded with these filters tuned to 50 Hz and 100 Hz in order to supplement the comb filtering. The amplitude peaks, slightly LF of 50 Hz and 100 Hz, are the result of badly adjusted filters (figure 8.8, IC's 11 and 12).

Figures 10.4 and 10.5 show a spectrogram and power spectra (averaged over ~ 27 minutes) of data analysed over a 62.5 Hz bandwidth. Figure 10.4 shows Schumann resonance modes up to 2nd order and figure 10.5 shows peaks up to 7th order. The peak marked with an arrow (figure 10.5) falls at $\sim 16 \frac{1}{3}$ Hz; a mains sub-harmonic. System noise measurements showed no indication of the peak and consequently it is not receiver generated. Figure 10.5 shows a power increase of approximately 3dB, over a period of ~ 3 hours, for frequencies > 10 Hz.

The above spectra, and others like them, demonstrate that the receiver was operating adequately over this experimental period.

Some measurements were also carried out using a 300 turn air cored antenna with an average radius of ~ 0.5 m. The antenna of resistance 9.4Ω , inductance 116 mH, and resonated to ~ 815 Hz using an added capacitance of $0.22\mu\text{F}$ was mounted in an electrostatically screened container. It fed directly, without matching transformer, to the preamplifier described in Chapter 9. This antenna provided a better system performance than the mu-metal cored antenna for frequencies greater than ~ 500 Hz. Chorus and also the music preceding the ELF pips (chapter 6) were detected using this air cored antenna.

10.4 An Investigation Of High Latitude Schumman Resonance Frequency Variations On 28 March 1979

10.4.1 Introduction

Many authors have studied the diurnal variation of Schumann resonance frequencies using measurements separated from each other by periods $\gtrsim 1$ hour (e.g. Balser and Wagner, 1962b; Benoit et al., 1967). In contrast to this, Balser and Wagner (1963) have presented the mode 1 (~ 8 Hz) frequency variations with a temporal resolution of ~ 15 minutes before, during, and after a high altitude nuclear

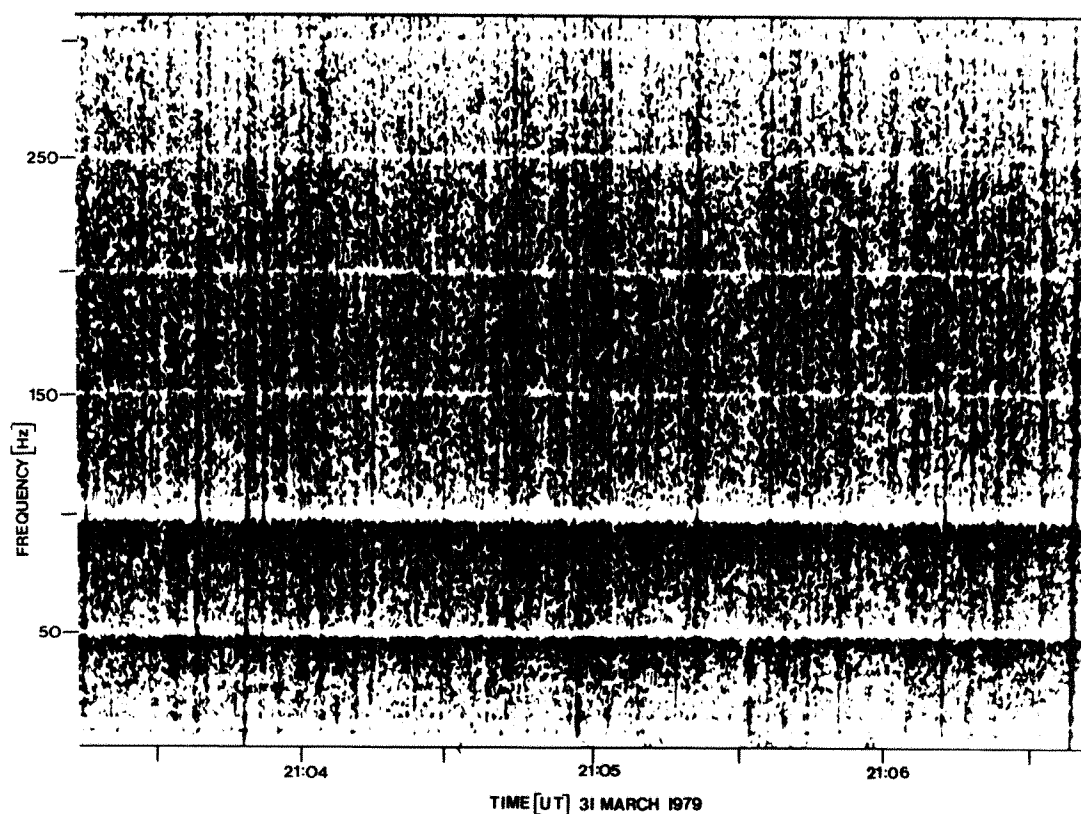


Fig. 10:3 Spectrogram showing the ELF receiver plus mu-metal antenna response over a 312.5Hz bandwidth when the additional notch filters are in use at 50Hz and 100Hz.

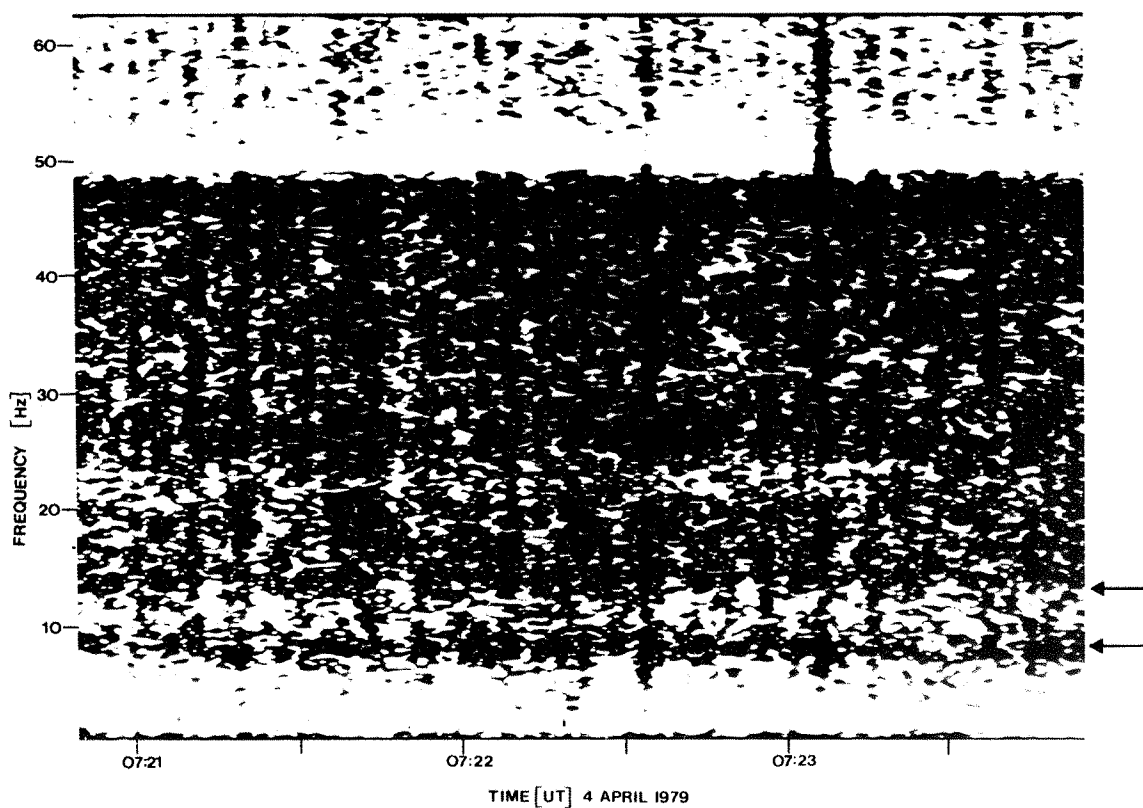
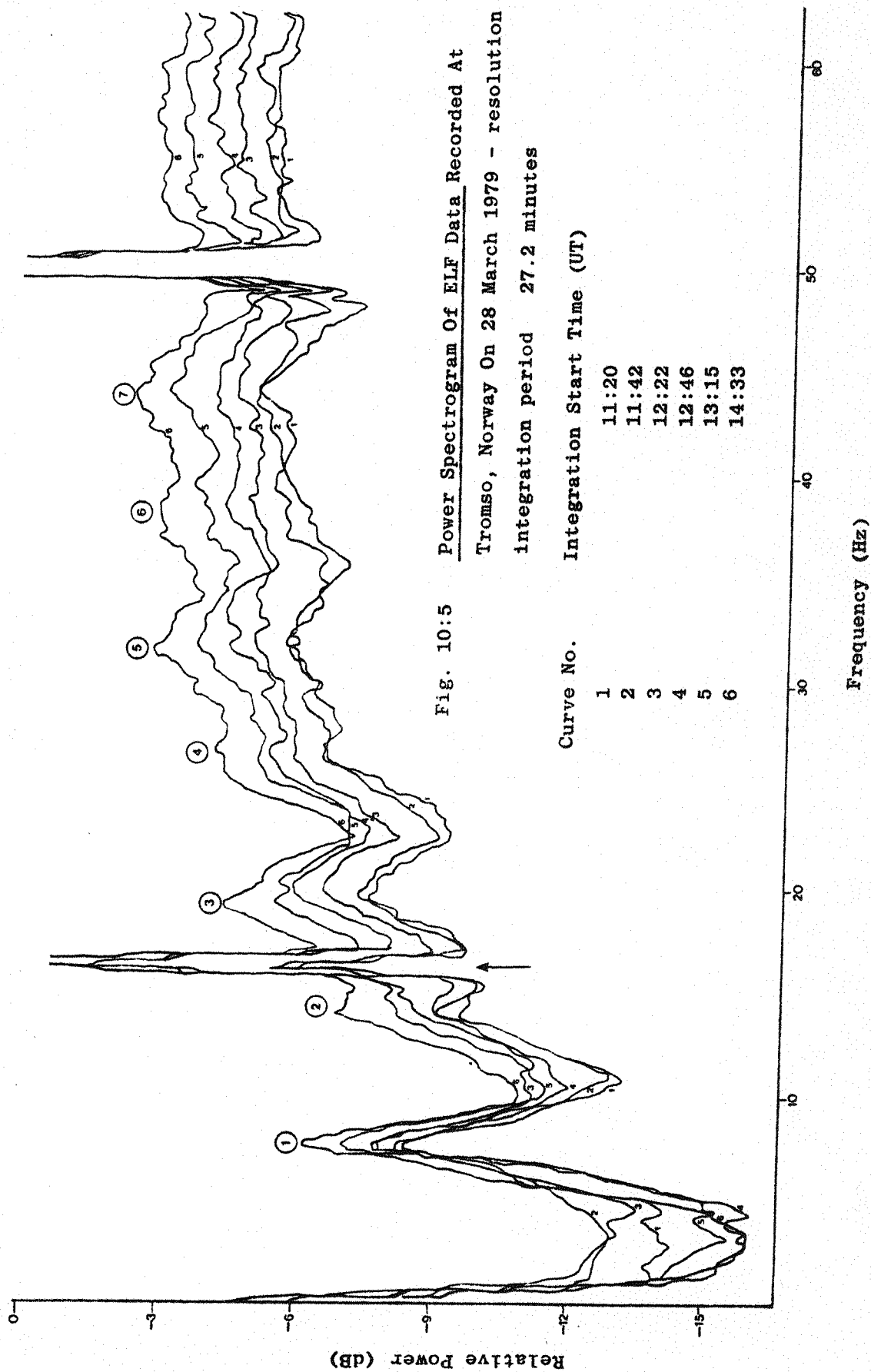


Fig. 10:4 Spectrogram showing the first two Schumann Resonance Modes (marked by arrows)



explosion. They reported a sudden drop (~ 0.5 Hz) in the mode 1 resonant frequency at the time of the explosion. This was in agreement with the theoretically predicted variations of Madden and Thompson (1965) who have investigated in some detail the frequency variations resulting from various D region disturbances. They have also briefly examined the effects of modifying the E region.

The purpose of this analysis is to examine, with good temporal resolution, the frequency variations of the first five modes and to correlate these with various geophysical events.

The ELF system (Chapters 8 and 9) was operated on 28 March 1979 between ~ 11.45 UT and ~ 1600 UT and ~ 1900 UT and ~ 2400 UT. During this time the mu-metal antenna was orientated such that it was sensitive to a north-south propagating wave.

10.4.2 Geophysical Conditions

The 28 March 1979 was a geophysically active day exhibiting periods of high magnetic activity interspersed by periods of moderate activity. As such any anomalous frequency variations should stand out from the diurnal frequency variations (Balser and Wagner, 1962b).

A sudden commencement occurred in the morning hours (UT) and several sudden ionospheric disturbance events were reported (N.O.A.A., 1979a). These various events together with the times of H α flares for part of the period of interest (N.O.A.A., 1979b) and the three hourly magnetic index K_p are presented in table 10.2. Figure 10.6 shows the Kiruna magnetogram for that day.

10.4.3 Analysis

The frequency variations of mode 1 signals were obtained using an integration time of 13.6 minutes and a real time resolution of 0.156 Hz, table 10.1. The resonance peak was determined using an "eye-ball" curve fit through the spectral points, taking into account the standard error in each estimate.

Analysis of the higher order (lower strength) modes was made using an identical integration time but with a 0.3 13Hz real time resolution, table 10.1. The increased spectral confidence (equation 10.6) resulted

Table 10.2a Sudden Commencements

Sudden commencement 0827 UT

Table 10.2b Sudden Ionospheric Disturbances

Start (UT)	End (UT)	Maximum (UT)	Wide Spread (1) Index
0652	0703	0656	3
1001	1052	1025	5
1100	1145	1105	5
1118	1224	1126	1
1247	(2)	1300	3
1631	1710	1644	1
2040	2140	2105	1
2100	2145	2125	1

- (1) Gives a measure of the world wide significance:- scale 0 to 5
 (2) End time unknown

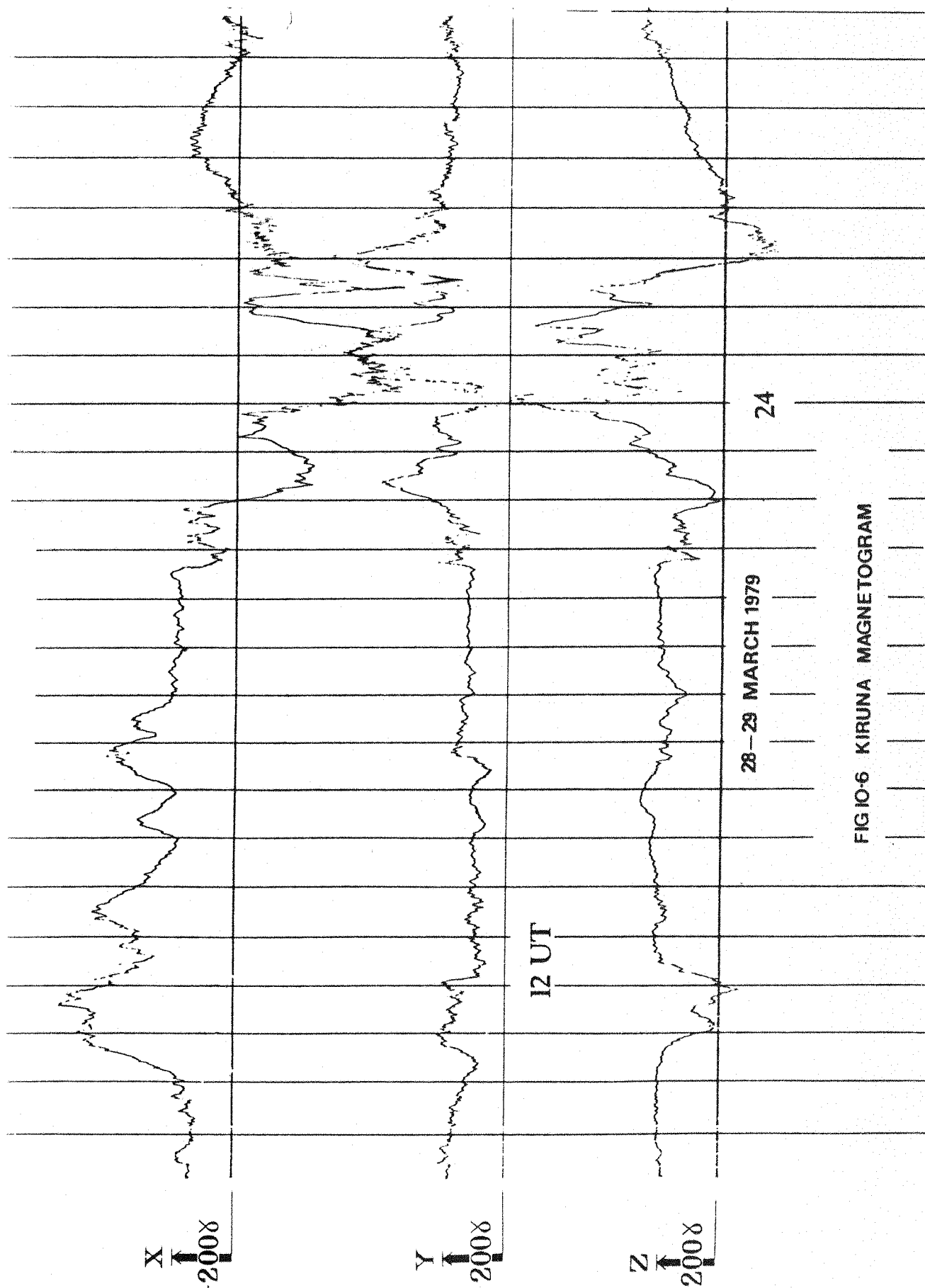
Table 10.2c H α Solar Flares Between 1200 UT and 1600 UT

Start UT	End UT	Start UT	End UT
1200	- (1)	1359	- (1)
1220	- (1)	1421	- (1)
1243	1315	1433	1437
1341	1345	1623	1658

- (1) End time unknown

Table 10.2d Three-hourly indices: K_p

Three Hour Interval	1	2	3	4	5	6	7	8
Index	4	4-	4	5+	6-	5-	3	5+



FIGIO-6 KIRUNA MAGNETOGRAM

in a better estimate of the frequency of the resonance peak.

Figure 10.7 shows the resonant frequency variations of the first five modes during the specified period. The odd order modes were generally stronger than the even order modes which often failed to show statistically significant peaks.

10.4.4 Interpretation

The diurnal variations presented in figure 10.7 are more noisy than those normally presented by other research workers. This is, however, not surprising since the latter are generally based upon either, an average of many diurnal variations or, frequency estimates derived from longer integration periods than those used in this study.

The enhanced variability exhibited by the higher order modes is due both, to the degraded signal to noise power ratio and, also, to the fact that these modes are influenced in a complicated fashion by the degree of E and F region ionization (Madden and Thompson, 1965).

Of particular interest are the short term variations of resonant frequencies which are correlated between one mode and another. Three such incidents have been identified and the variations are summarised in table 10.3.

Incidents one and two occurred during the SID events starting at ~ 1247 UT and ~ 2040 UT. On both occasions, mode 1 showed a decrease of the resonant frequency during the disturbance. During event one mode 3 also exhibited a frequency decrease but a slight increase during event two. Mode 5 showed a frequency increase during event one; no statistically significant variation occurred during event two. At these times other modes either showed statistically insignificant variations, or alternatively, no resonant frequency estimate was possible because of their low field strength. The computer models of Madden and Thompson (1965) predict a frequency decrease (mode 1: 0.1 Hz to 0.4 Hz) for all modes during an SID.

The third event (not an SID) occurred between 1415 and 1500 UT during which time the resonant frequency for mode 1 (and possibly for mode 2) increased and that of mode 3 (and possibly mode 5) decreased. Such opposite variations of modes 1 and 3 fit the predictions of Madden and Thompson (1965) for periods of enhanced E region rather than D region ionization. Table 10.2 shows no SID near this time even

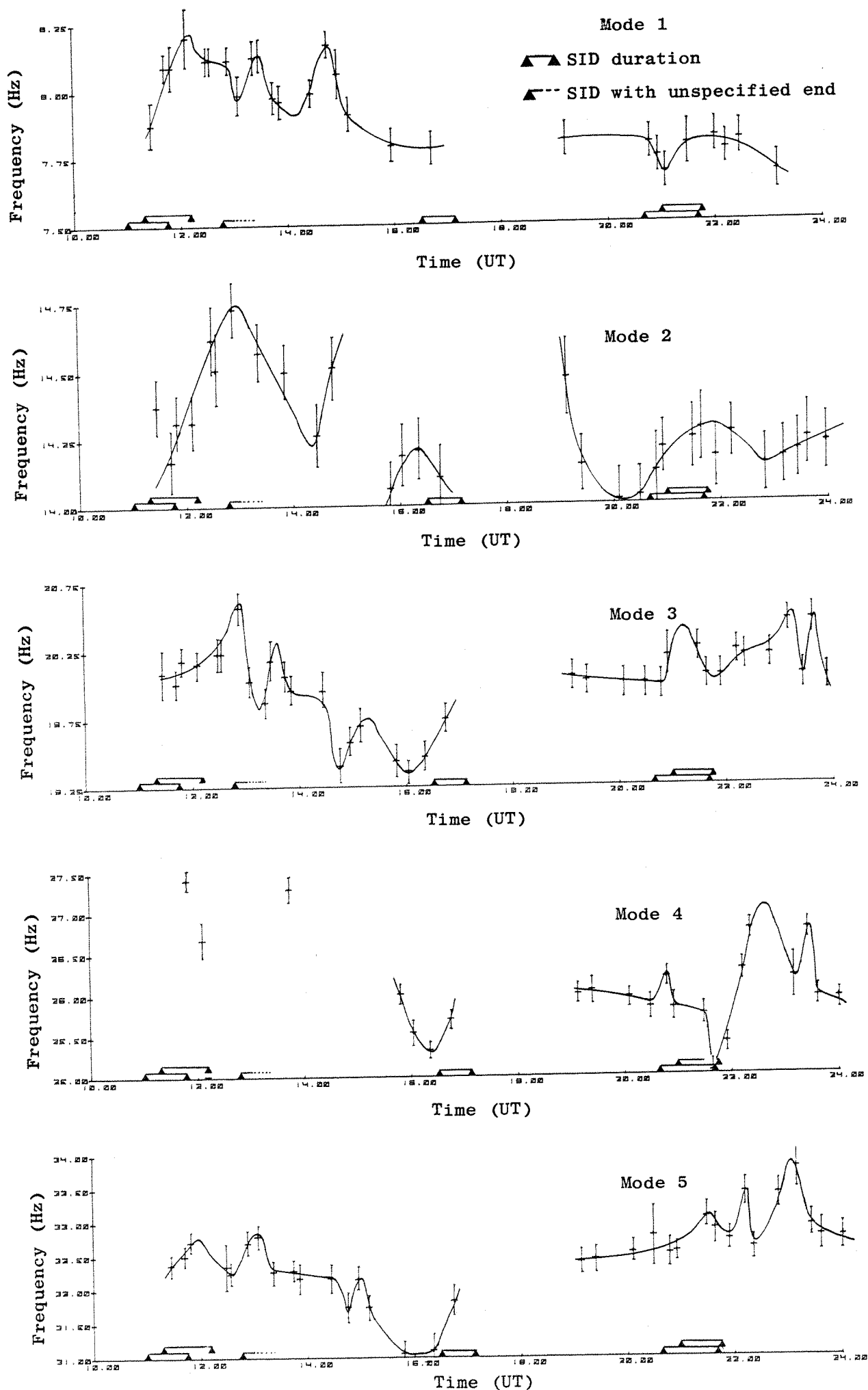


Fig. 10:7 Schumann Resonance Mode Variations Measured In Auroral Scandinavia On 28 March 1979.

Event Number	UT	Frequency Change				
		Mode 1	Mode 2	Mode 3	Mode 4	Mode 5
1	~1300	Down	No change	Down	No data	Up
2	~2100	Down	No change	Up	(1)	(1)
3	~14.30	Up	No data	Down	No data	No change ⁽²⁾

(1) General variability before, after, and during this time; no significantly enhanced variation at the time of the SID.

(2) Some indication of a downward frequency change.

Table 10.3 Summary Of Schumann Resonance Frequency Variations

though two H α flares occurred. It is concluded that the flare associated X-ray flux was low, causing no D region effect. E region modification may, however, have taken place due to (flare associated) enhanced EUV, rather than X-ray, radiation in the band 10 Å to 100 Å (Hargreaves, 1979). This study thus provides possible confirmation of the predictions of Madden and Thompson (1965) for mode variations caused by enhanced E region ionization.

10.4.5 Conclusions

Statistically significant short term variations in Schumann resonance mode frequencies have been identified during two SID events and at one other time.

The SID variations of the first order mode are in general agreement with theoretical predictions; however, the higher order modes are at variance with expectations. Chapman and Llanwyn Jones (1964) report an increase in the mode one frequency during a polar cap absorption event which could be considered, in terms of the area affected, as a small scale SID. Their variation is opposite to that described in this study and predicted theoretically.

On one other occasion the mode variations have been explained in terms of a modification to the E region ionization.

This short study has demonstrated one potential application of the ELF receiving system described in earlier chapters. Further analysis of Schumann resonance frequency variations at the times of SID's and other similar events should be undertaken with the view to confirming these results.

CHAPTER ELEVEN

Some Further Suggestions For ELF Research

11.1 The Future For Broad Band Goniometer Experiments In The Scandinavian Auroral Zone

The effectiveness of the present goniometer system for use in Scandinavia is demonstrated by Cannon et al. (1980), Madden (1981) and also by this thesis. There remains a store of interesting data yet to be analysed, see for example section 5.7.

Experience gained during the course of these experiments indicates, however, that the equipment, which was originally designed for use at Halley Bay, Antarctica ($L \sim 4$), could be modified to enhance its performance in Scandinavia.

One improvement would be to overcome the present limitation on system sensitivity caused by strong interfering signals. Unless these are sufficiently attenuated the minimum recordable signal (limited by the ~ 60 dB tape recorder dynamic range) is greater than the minimum detectable signal. The present design provides filtering of just three VLF transmitters, using notch filters, while mains interference is only limited by the response of the input transformer below resonance, see figure 3.3. Both are inadequate for Scandinavian operation where such interfering signals are both stronger and more numerous than they are at Halley Bay.

The primary improvement, however, would be one overcoming the amplitude resonance at ~ 1 kHz. Although the resonance counteracts the attenuation of signals near the waveguide cut off (1.7 kHz) it also reduces confidence in goniometer bearings of signals near this frequency. The resonance is of little consequence at $L \sim 4$, where the emission frequencies are generally > 3 kHz but falls centrally in the auroral zone ($L \sim 6$) emission band.

Adjustment of the resonance to a higher or lower frequency than 1 kHz would alleviate this problem but at the expense of an enhanced response to either mains or VLF transmitter interference.

It is suggested that a dedicated Scandinavian goniometer system be designed with the following characteristics:-

- (i) In the new goniometer system a low input impedance preamplifier should be used to provide a flatter frequency response. In the present design the high Q 1kHz resonance is provided by the high Q preamplifier input transformer which is itself maintained by the high input impedance of the preamplifier input stage. It is this high Q resonance which makes the channel amplitude and phase matching difficult and reduces confidence in the bearings.
- (ii) The system 3 dB bandwidth should be reduced to lie between 0.5kHz and 3 or 4kHz with sufficiently high gain and sensitivity over this range to compensate for attenuation, near and below cut off in the earth-ionosphere waveguide. This is provided, at present, by the amplitude resonance. Filtering should be severe enough above, and below, the passband to prevent any substantial reduction in sensitivity by mains or VLF transmitter interference.
- (iii) For additional mains rejection consideration should be given to the use of a mains commutating filter, similar to that described in chapter 8. Woolliscroft (private communication, 1979) reports that the mains interference is very strong near the Andøya rocket range. The high rejective qualities of the commutating filter would be particularly useful in this instance.
- (iv) At present the pulse phase reference is recorded on a separate channel to the signal since its high harmonic content would cause signal interference if recorded on the same channel. Smith, (private communication, 1979) has suggested the use of a sine wave, rather than a pulse (chapter 3) for azimuthal calibration. A pulse phase reference was originally adopted because bearing analysis involved the use of a travelling microscope to measure the distance (proportional to the phase) between a calibration pulse and a minimum in the signal modulation envelope; both displayed on a sonogram (Jarvis, 1976). Since the semi-automatic whistler analyser (section 3.6) uses correlation techniques a sine wave, with, for instance, zero crossings indicating north-south, would be equally adequate. Use of a sine wave might allow the calibration wave (55 Hz), the signal (0.5kHz to 3kHz) and the clock time coding (2.5kHz, 5kHz, 10kHz) to be mixed onto the same channel. This would release a track for subsequent recordings or, alternatively, for non-goniometered ELF/VLF recordings. The effect of modulating the incoming signal is to spread it into two sidebands, 55 Hz apart, making identification and spectral measurement difficult under high resolution. A parallel channel representing the R.M.S. addition of

non-goniometered signals from the two channels would supplement the azimuthal information with good spectral information.

11.2 Some Further 'Pip' Experiments

Chapters 6 and 7 have shown that the ELF pips were produced by an ionospheric effect and various generation mechanisms have been proposed. Much work remains, however, and this should be pursued with vigour. It is proposed that this should occur in three stages.

The first should be a search for pips in previously recorded background data in order to extend the data base of the present study. Goniometer recordings made by the Southampton Group during February 1976 and February/March 1977 will be of particular use since on these occasions stations were operated at both Tromsø and Sodankylä. During other Scandinavian campaigns the stations were located in Norway only and consequently triangulation will be extremely inaccurate if the source region is always located above Finland.

The second stage should be an experiment specifically designed to study ELF pips. Goniometer stations should be located in Sweden and Finland so that they can accurately monitor any movements of the generation region. The generation region is believed to be due to a two station interference effect (mechanism 3) or a > 2 station interference effect (mechanism 4). If such an experiment shows an infinite number of generation regions, along the bisector between any two transmitters then this would be indicative of a type three mechanism. If only specific generation locations could be identified then this would be indicative of a type four mechanism. Such an experiment should be conducted on a twenty-four hour schedule in order to ascertain the complete diurnal variation. Parallel monitoring of other geophysical parameters such as magnetic activity and ionospheric absorption should also be conducted. In particular a careful analysis of data from the Finnish magnetometer chain, and EISCAT could be used to **correlate accurately** the electrojet position with the goniometer derived pip sources. In addition the candidate transmission frequencies should be monitored at their carrier frequencies. The pip transmission schedules at each frequency should be carefully monitored since this could help to define the causative transmitters. The depth of modulation is also unknown at present.

The third stage is somewhat speculative and proceeds with the premise that the pip source does occur within the electrojet. It is

proposed that this demodulation mechanism might provide an extremely cheap, quasi-real time, hourly measure of the electrojet latitude over Finland. Consider three or four unmanned goniometer stations each with a bandwidth of only $\sim 1\text{kHz} \pm 20\text{ Hz}$. Each would switch on automatically shortly before the start of the pips storing the goniometered pip signal and calibration data either on magnetic tape or in other store. On interrogation by a central station, possibly Sodankyla, this information would be transmitted over an RF or telephone link. A desk top computer controlled correlator, or dedicated software, would perform a cross correlation between signal and calibration pulse (wave), and, using its stored azimuthal calibration data translate this into a bearing. By interrogating each goniometer station in turn the pip source, i.e. electrojet position, could be quickly determined.

REFERENCES

- Adjepong, S.K., Analyses Of Time Series Representing The Intensity Of VLF Chorus And Other Related Geophysical Phenomena, Ph.D. thesis, University of Southampton, U.K., 1972.
- Akasofu, S.I., Polar And Magnetospheric Substorms, D. Reidel Publ. Co., Holland, 1968.
- Akasofu, S.I., Discrete, Continuous and Diffuse Auroras, Planet Space Sci. 22, 1723 - 1726, 1974.
- Akasofu, S.I., Physics Of Magnetospheric Substorms, Astrophysics And Space Science Library, D. Reidel, Holland, 1977.
- Analog Devices, Data Sheet For The Model 606 Instrumentation Amplifier, 1974.
- Angerami, J.J., A Whistler Study Of The Distribution Of Thermal Electrons in the Magnetosphere, Tech. Rept. No. 3412 - 7, Stanford University, 1966.
- Axford, W.I., Magnetospheric Convection, Reviews of Geophysics, 7, 421 to 459, 1969.
- Axford, W.I., and C.O. Hines, A Unifying Theory Of High Latitude Geophysical Phenomena and Geomagnetic Storms, Can. J. Phys., 39, 1433 - 1464, 1961.
- Bailey, V.A. and D.F. Martyn, The Influence Of Electric Waves On The Ionosphere, Phil. Mag., 18, 369, 1934.
- Balser, M. and C.A. Wagner, Diurnal power variations of the earth-ionosphere cavity modes and their relationship to worldwide thunderstorm activity, J. Geophys. Res., 67, 2, 619 - 625, 1962a.
- Balser, M. and C. Wagner, On Frequency Variations Of The Earth-Ionosphere Cavity Modes, J. Geophys. Res., 67, 4081 - 4083, 1962b.
- Balser, M. and C. Wagner, Effect of a high-altitude nuclear detonation on the earth-ionosphere cavity, J. Geophys. Res., 68, 4115 - 4118, 1963.
- Balsley, B.B., W.L. Ecklund and R.A. Greenwald, V.H.F. Doppler spectra of radar echoes associated with a visual auroral form. J. Geophys. Res., 78, 1681, 1973.
- Banks, P.M. and J.R. Doupnik, A review of auroral zone electrodynamics deduced from incoherent scatter radar observations, J. Atmos. Terr. Phys., 37, 951, 1975.
- Barrington, R.E., T.R. Hartz and R.W. Harvey, Diurnal distribution of ELF, VLF and LF noise at high latitudes as observed by Alouette 2, J. Geophys. Res., 76, 5278, 1971.

- Bartels, J., N.H. Heck, and H.F. Johnston, The Three-Hour Range Index Measuring Geomagnetic Activity, J. Geophys. Res., 44, 411, 1939.
- Belrose, J.S., Low and Very Low Frequency Radio Wave Propagation, AGARDograph XXIX, Radio Wave Propagation P IV, 1968.
- Belrose, J.S., W.L. Hatton, C.A. McKerrow, R.S. Thain, The Engineering Of Communications Systems For Low Radio Frequencies, Proc I.R.E. 47, P661 - 680, 1959.
- Belrose, J.S. and I.A. Bourne, The Electron Distribution And Collision Frequency Height Profile For The Lower Part Of The Ionosphere (The D and Lower E Regions), Conf. on Radio Wave Propagation, Ottawa, VOL 1 P.79, 1966.
- Bendat, J.S. and A.G. Piersol, Random data: Analysis and measurement procedures, J. Wiley and Son, N.Y. U.S.A., 1971.
- Benoit, C., J. Etcheto, and R. Gendrin, Mesure automatique des variations de fréquence des résonances de la cavité terre-ionosphère, Annales de Géophysique, 1967.
- Blake, L.V., Antennas, Wiley, New York, U.S.A., 1966.
- Blakeman, R.B., and J.W. Tukey, The Measurement of Power Spectra, Dover Publications Inc., New York, 1958.
- Blixhavn, B. and L.T. Lyngdal, Omega Synchronised Clock For Data Aquisition System, NICP Report No. 7601, Norwegian Institute Of Cosmic Physics, P.O. Box 1038, Blindern, Oslo 3, Norway, 1976.
- Brekke, A. and C.L. Rino, High Resolution Altitude Profiles Of The Auroral Zone Energy Dissipation Due To Ionospheric Currents, J. Geophys. Res., 83, P.2517 - 2524, 1978.
- Brice, N., An Explanation of Triggered Very Low Frequency Emissions, J. Geophys. Res., 68, 15, 4626 - 4628, 1963.
- Brice, N., Fundamentals of Very Low Frequency Emission Generation Mechanisms, J. of Geophys. Res., 69, 21, 4515 to 4521, 1964.
- Broeker, B., Commutating Filter Techniques, Application Note AN-534, Motorola Semi-conductor Products Inc., 1970.
- Bullough, K., A.R.W. Hughes, T. Hudson, D. Dickinson, P. Broomhead, P. Tomlinson, The Sheffield University VLF Experiment On The Satellite Ariel 3, Journal of Scientific Instruments (Journal of Physics E) Series 2, Vol 1, 77, 85, 1968.
- Bullough, K., and J.L. Sagredo, VLF goniometer observations at Halley Bay Antarctica - I. The Equipment and measurement of signal bearing, Planet Space, Sci., 21, 899 - 912, 1973.
- Bullough K., A.J. Smith, G. Garside and A.M. Dealey, The Semi-Automated Whistler Analyser, URSI Conf. Proc., Lima, Peru, August 1975.
- Buneman, O., Excitation of field aligned sound waves by electron streams, Phys. Rev. Lett., 10, 71, 285 to 287, 1963.

- Burgess, B. and T.B. Jones, The Propagation of LF and VLF Radio Waves With Reference To Some Systems Applications, The Radio and Electronic Engineer, Vol. 45, 1, P 47, 1975.
- Burr Brown, The UAF41 Universal Active Filter, Burr Brown, Watford, U.K., 1976.
- Burton, E.T., Atmospherics detected on submarine cables, Nature, 126, 55, 1930.
- Burton, R.K. and R.E. Holzer, The origin and propagation of chorus in the outer magnetosphere, J. Geophys. Res., 79, 1014, 1974.
- Cahill, L., R.A. Greenwald, and E. Nielsen, Auroral radar and rocket double-probe observations of the electric field across the Harang discontinuity, Geophys. Res. Lett., 5, 687, 1978.
- Cannon, P.S., A Radio Receiver For The Frequency Range 1Hz to 1kHz, M.Sc. Thesis, Dept. of Electronics, University of Southampton, U.K., 1976.
- Cannon, P.S., R. Brittain, M. Madden and M.J. Rycroft, The Southampton University VLF Goniometer Operations Manual, Dept. of Physics, University of Southampton, U.K., 1979.
- Cannon, P.S., Gibbons W., Madahar R., Woolliscroft L. ELF/VLF Wave Field Measurements At The Time Of The Launch of Skylark SL1424. Conf. Proc. 5th E.S.A. Symposium On European Rocket And Balloon Programmes And Related Research, Bournemouth, 1980.
- Cantarano and Pallotino, A Low Noise FET Amplifier For A Spaceborne Magnetometer, Electronic Eng., Sept. 1970.
- Cashion, R.E., Hunt G.A., Lavanceau J.D., Precise Time Recovery From Transit Satellites, Radio Science, 14, 4, 715 - 719, 1979.
- Chapman, F.W., Llanwyn Jones D., Earth Ionosphere Cavity Resonances And The Propagation Of Extremely Low Frequency Radio Waves, Nature, 202, 654 - 657, 1964.
- Clayton, R., Operational Amplifiers, Butterworths, London, 1971.
- Cross, A.F., Time Code Receiver Clock, Wireless World, Vol. 82, Feb. 1976.
- Davies, K., Ionospheric Radio Waves, Blaisdell Publishing Company, U.S.A., 1969.
- Duffin, W.J., Electricity and Magnetism(Ch. 9) McGraw Hill, London, 1965.
- Dungey, J.W., Interplanetary magnetic field and the auroral zones, Phys. Rev. Letters, 6, 47 - 48, 1961.
- Dungey, J.W., The Magnetosphere, Sci., Prog., Oxf. 63, 315 - 333, 1976.

- Eckersley, T.L., Musical Atmospherics, Nature, 135, 104 - 5, 16, 1935.
- Ecklund, W.L., B.B. Balsely, and D.A. Carter, A preliminary comparison of F-region plasma drifts and E region irregularity drifts in the auroral zone, J. Geophys. Res., 82(1) 195 - 197, 1977.
- European Broadcasting Union, Extracts from the 1975 Geneva Plan, E.B.U. Brussels, Belgium, 1979a.
- European Broadcast Union, Annual list of LF/MF stations in the European Area, E.B.U. Brussels, Belgium, 1979b.
- Everhard-Bakker, A.E., M.J. Rycroft, N.A. Heard and A.J. Smith, ELF and VLF Radio Emissions Following A Barium Shaped Charge Release At $L \approx 6.5$, Cospar Space Research XVI, 1976.
- Farley, D.T., A plasma instability resulting in field aligned irregularities in the ionosphere. J. Geophys. Res. 68, 22, 6085 - 6097, 1963.
- Feldstein, Y.I., Planetary Space Sci. 14, 121, 1966.
- Finnish Broadcasting Co. Ltd., Observed Ionospheric Cross-Modulation On Long And Medium Waves, The Finnish Broadcasting Co. Ltd., Measuring Station, Helsinki, Finland, 1977.
- Finnish Broadcasting Co. Ltd., LF/MF Stations In U.S.S.R., As Notified To The I.F.R.B., The Finnish Broadcasting Co. Ltd., Measuring Station, Helsinki, Finland, 1979.
- Fuchs, J., A Report To The National Academy Of Sciences, National Research Council, Wash., D.C., Pub. 581, 105, P.11, 1938.
- Galejs, J., Terrestrial Propagation Of Long Electromagnetic Waves, Peragamon Press, 1972.
- Getmantsev, G.G., N.A. Zuikov, L.F. Mironenko, et al., Combination frequencies in the interaction between high power short wave radiation and ionospheric plasma, Pisma Zh. Eksp. Teor, Fiz. 20, 229, 1974 (JETP Lett. 20, 101, 1974).
- Giles, P.G., P.J. Hart, I. Thomas, Radio Clock For The Reception And Display Of M.S.F. Time Code Transmissions, Mullard Tech. Comm., No. 140, Oct. 1978.
- Girling, B., A Time Code Generator, B.Sc. Report, Dept. of Electronics, University of Southampton, U.K. 1977.
- Graeme, J., Electronic Design, 2, Jan 21, 1971.
- Greenwald, R.A., W. Weiss, E. Nielsen, N.R. Thomson, STARE: A new radar auroral backscatter experiment in northern Scandinavia, J. Geophys. Res., 13 (6), 1021 - 1039, 1978.
- Gurevich, A.V., Non-linear Phenomena In The Ionosphere, Springer-Verlag, New York, 1978.

- Haerendel, G., Project Porcupine, Summary of Scientific Objectives and Instrumentation, Max-Planck-Institut für Physik Und Astrophysik, 8046 Garching, 1976.
- Hargreaves, J.K., The Upper Atmosphere and Solar-Terrestrial Relations, Van Nostrand Reinhold, England, 1979.
- Hartz, T.R. and N.M. Brice, The general pattern of auroral particle precipitation, Planet Space Sci., 15, 301, 1967.
- Heikkila, W.J., The morphology of auroral particle precipitation, Space Res. XII, 1972.
- Heikkila, W.J., Electric field topology near the dayside magnetopause, J. Geophys. Res., 83, 1071, 1978.
- Helliwell, R.A., Whistler-triggered periodic very-low frequency emissions, J. Geophys. Res., 68, 5387 - 5395, 1963.
- Helliwell, R.A., Whistlers and Related Ionospheric Phenomena, Stanford University Press, U.S.A., 1965.
- Helliwell, R.A., A Theory Of Discrete VLF Emissions from the Magnetosphere, J. Geophys. Res., 72, 19, 4773-4787, 1967.
- Hibberd, F.H., Ionospheric self-interaction of radio waves, J. Atmos. Terr. Phys. 6, 268 - 279, 1955.
- Ho, D. and L.C. Bernard, A fast method to determine the nose frequency and minimum group delay of a whistler when the causative spheric is unknown, J. Atmos. Terr. Phys., 35, 881 - 887, 1973.
- Holmgren, G., R. Bostrom, M.C. Kelley, P.M. Kintner, R. Lundin, U.V. Fahlen, E.A. Bering, W.R. Sheldon, Artificial Stimulation Of Auroral Electron Acceleration By Intense Field Aligned Currents, Geophys. Res., Lett., 6, 10, 1979a.
- Holmgren, G., R. Bostrom, M.C. Kelley, P.M. Kintner, R. Lundin, U.V. Fahlen, E.A. Bering, W.R. Sheldon, Trigger an active release experiment that stimulated auroral particle precipitation and wave emissions, Submitted to J. Geophys. Res., 1979b.
- Honeywell Co., Manual for the Saicor SAI51B time compression analyser, Hauppauge, New York, U.S.A., 1970.
- Huage, R., and F. Soraas, Precipitation Of $> 115\text{KeV}$ Protons In The Evening And Forenoon Sectors In Relation To The Magnetic Activity, Planet. Space Sci., 23, 1141, 1975.
- Jarvis, M.J., An Investigation Of The Morphology Of Whistler Ducts By Triangulation Using VLF Goniometer Receivers, Ph.D. Thesis, University of Southampton, U.K., 1976.
- Jespersen, M., A. Haug, and B. Landmark, Electron Density And Collision Frequency Observations In The Arctic D-Region, Electron Density Profiles In Ionosphere and Exosphere, Proc. Nato Advanced Study Institute, Finse Norway, 1966.
- Jordan, E.C., K.G. Balmain, Electromagnetic Waves And Radiating Systems, Prentice Hall, P. 640 - 641, 1968.

- Kamide, Y. and S.I. Akasofu, The auroral electrojet and global auroral features, *J. Geophys. Res.*, 80, 3585, 1975.
- Kamide, Y. and A. Brekke, Auroral electrojet current density deduced from the Chatanika radar and from the Alaska meridian chain of magnetic observatories, *J. Geophys. Res.*, 80, 587, 1975.
- Kamide, Y.R. and A. Brekke, Altitude of the eastward and westward auroral electrojets, *J. Geophys. Res.*, 82, 2851, 1977.
- Kapustin, I.N., R.A. Pertsovskii, A.N. Vasil'ev et al., Generation of radiation at combination frequencies in the region of the auroral electric jet. *Pis'ma Zh. Eksp. Teor. Fiz.* 25, 248, 1977 (*J.E.T.P. Lett.*, 24, 228, 1977).
- Keefe, T.J., H. Etzold, and C. Polk, Detection And Processing Of ELF (3 - 30 Hz) Natural Electromagnetic Noise Final Rept. Pt. 1 U.S.A.F. Contract No. F19628 - 70 - e - 0090, University of Rhode Island, U.S.A., 1973.
- Kisabeth, J.L. and G. Rostoker, Development of the Polar Electrojet during Polar Magnetic Substorms, *J. Geophys. Res.* 76, 6815, 1971.
- Koons, Dazey, Garnier, Girolani, VLF transmissions from Katford (Norway) to Scatha, *Cospar Conf. Proc.*, 1980.
- Knott, K.F. and L. Unsworth, Mains Rejection Tracking Filter, *Wireless World*, October, 1974.
- Landmark, B., The Ionosphere, *AGARD Lect. Ser. No. 29.*, Ch. 2, 1968.
- Little, C.G., and H. Leinbach, Some measurements of high latitude ionospheric absorption using extraterrestrial radio waves, *Proc. I.R.E.*, 46, 334 - 348, 1958.
- Madden, T., W. Thompson, Low-Frequency Electromagnetic Oscillations Of The Earth-Ionosphere Cavity, *Reviews of Geophysics*, 3, 2, 211 - 253, 1965.
- Madden, M.A., M.J. Rycroft, and N.E. Smith, Ground-based ELF/VLF observations at high latitudes during the passes of Geos - I and ISEE - 1 and 2, *Space Sc. Rev.* 22, 465 - 479, 1978.
- Madden, M., Some Studies Of Whistlers Recorded Using Goniometers At High Latitudes, M. Phil. Thesis, Dept. of Physics, University of Southampton, U.K., 1981.
- Maezawa, K., Magnetospheric Convection Induced by the Positive and Negative Z Components Of The Interplanetary Magnetic Field: Quantitative Analysis Using Polar Cap Magnetic Records, *J. Geophys. Res.*, 81 (13), 2289 - 2303, 1976.
- Matsumoto, H., and I. Kimura, Linear and non-linear cyclotron instability and VLF emissions in the magnetosphere, *Planet. Space Sci.*, 19, 567 - 608, 1971.
- McPherron, R.L., Magnetospheric Substorms, *Reviews of Geophysics and Space Physics*, 17, 4, 657 - 681, 1979.

- Meacham, R., British Broadcasting Corporation Monitoring Service, Caversham, U.K., 1979.
- Metzger, J., Bipolar and FET Op-Amps, Electronics Products Magazine, June, 1977.
- Montbriand, L.E., A Simple Method For Calculating The Local Time Of Corrected Geomagnetic Midnight, J. Geophys. Res., 75, 28, 5634, 1970.
- Morgan, D., Detection And Analysis Of VLF Triggered Emissions, Ph.D. Thesis, Dept. of Physics, University of Sheffield, U.K., 1976.
- Motchenbacher, C.D., and F.C. Fitchen, Low-Noise Electronics Design Wiley-Interscience Publication, 1973.
- Nambra, S., Polarisation phenomena of low-frequency waves, Proc. IRE, 19, (11), 1988, 1931.
- Ness, N.F., C.S. Scarce, and S. Cantarano, Probable Observations Of The Geomagnetic Tail at 10^3 Earth Radii by Pioneer 7, J. Geophys. Res. 72, 3769, 1967.
- Ness, N.F., Magnetometers for space research, Space Sci. Rev., 11, 459, 1970.
- Nielsen, E., and R.A. Greenwald, Variations In Ionospheric Currents and Electric Fields In Association With Absorption Spikes During The Substorm Expansion Phase, J. Geophys. Res., 83 (A12), 5645 - 5654, 1977.
- N.O.A.A., Solar Geophysical Data, U.S. Department of Commerce, Boulder, Colorado, U.S.A., 417, Pt I, May, 1979a.
- N.O.A.A., Solar Geophysical Data, U.S. Department of Commerce, Boulder, Colorado, U.S.A., 423, Pt II, Nov. 1979b.
- Orr, D., Magnetic pulsations within the magnetosphere: a review, J. Atmos. Terr. Phys., 35, 1, 1973.
- Orr, T., Designing And Using Active Filters, Part 2, Electronics Today International, August 1977.
- Ott, W.E., Minimize Noise Problems With Instrumentation Amplifiers, Electron Products Magazine, June 17, 175 - 177, 1974.
- Pope, J.H., A high-latitude investigation of the natural very low frequency electromagnetic radiation known as chorus, J. Geophys. Res., 68, 83, 1963.
- Potemra, T.A., Current Systems In The Earths Magnetosphere, Reviews of Geophysics and Space Physics, 17, 4, 640 - 656, 1979.
- Ratcliffe, J.A., The Magneto-Ionic Theory and its Applications to the Ionosphere, Cambridge Univ. Press, 1959.
- Ratcliffe, J.A., The Magnetosphere, Comtemp. Phys., VOL 18, 2, 165 to 182, 1972.
- Runyon, R.P., and A.H. Haber, Fundamentals of Behavioral Statistics, Addison-Wesley Publishing Company, 1971.

- R.C.A., COS/MOS Integrated Circuits, R.C.A. Corporation, Sunbury-on-Thames, Middx, England, 1977.
- Reiger, E., H. Foeppl, G. Haerendel, A. Valenzuela, I.A. Zhulin, V.I. Gaidansky, V.S. Dokoulin, Yu. Ya. Ruzhin, and T.J. Hallinan, The Barium Ion Jet Experiment Of Porcupine 2, Space Research, Vol. XIX, 1979.
- Rishbeth, H. and O.K. Garriott, Introduction To Ionospheric Physics, Academic Press, New York and London, 1969.
- Rosenbauer, H., H. Grunwaldt, M.D. Montgomery, G. Paschmann and N. Sckopke, Heos 2 Plasma Observations In The Distant Polar Magnetosphere: The Plasma Mantle, J. Geophys. Res., 80, 2723, 1975.
- Rogister, A., and D'Angelo, Type 2 irregularities in the equatorial electrojet, J. Geophys. Res. 75, 19, 3879 - 3887, 1970.
- Rostoker, G., Geomagnetic Indices, Reviews of Geophysics and Space Physics, 10, 4, 935 - 950, 1972.
- Rostoker, G., J.C. Armstrong, A.J. Zmuda, Field-Aligned Current Flow Associated With Intrusion Of The Substorm-Intensified Westward Electrojet Into The Evening Sector, J. Geophys. Res., 80 (25), 3571 - 3579, 1975.
- Russell, C.T., and R.C. Elphic, Initial ISEE Magnetometer Results, Magnetopause Observations, Sub. to Space Science Reviews, 1978.
- Rycroft, M.J., Resonances of the Earth-Ionosphere Cavity Observed At Cambridge England, Radio Science, J. Res. NBS, Vol. 69D, 1965.
- Rycroft, M.J., VLF Emissions In The Magnetosphere, Radio Sci., 7, 8 and 9, P. 811 - 830, 1972.
- Rycroft, M.J., Whistlers And Discrete ELF/VLF Emissions, Proceedings of the NATO Advanced Study Institute, Spatinad, Norway, April, 1974.
- Rycroft, M.J., Active Experiments In Space Plasmas, Nature, 287, 7, 4 Sept. 1980.
- Rycroft, M.J. and A. Mathur, The determination of the minimum group delay of a nose whistler, J. Atmos. Terr. Phys., 35, 2177 - 2182, 1973.
- Salt, J., Pictorial Atlas Of The World, Hamlyn, 1976.
- Schumann, W.O., Über die Strahlung slosen Eigenschwingungen einer leitenden Kugel, die von einer Luftschicht und Einer Ionenspharenhülle umgeben ist, Z. Naturforsch., 7a(2), 149 - 154, 1952.
- Shawhan, S.D., Magnetospheric Plasma Wave Research 1975 - 1978, Rev. of Geophys. And Space Phys., 17, 4, P. 705, June 1979.
- Showen, R.L., Artificial Heating Of The Lower Ionosphere, J. Geophys. Res., 77, 10, 1923 - 1933, 1972.

- Signetics, Signetics Applications, Signetics International Corp., Penge, London, England, 1974.
- Siren, J.C., STARE radar observations as applied to launch conditions for Andøya rocket "18.211 UE/IE", Working document circulated to participating members of rocket 18.211 UE/IE; I.P.S.T., University of Maryland, U.S.A., 1977.
- Siren, J.C., J.R. Doupnik, and W.L. Ecklund, Comparison of auroral currents measured by the Chatanika Radar with 50MHz backscatter observed from Anchorage, J. Geophys. Res., 82, 25, 3577 - 3583, 1977.
- Smith, A.J., Experiments On The Goniometer VLF Antenna, Internal Rept., Dept. of Physics, University of Sheffield, U.K., 1970.
- Smith, A.J. and K. Bullough, The Sheffield University VLF Manual, Sheffield University Physics Dept., U.K., 1976.
- Smith, A.J., I.D. Smith, A.M. Deeley and K. Bullough, A semi-automated whistler analyser, U.R.S.I. Conf., Helsinki, Finland, August, 1978.
- Smith, R.L., Propagation Characteristics Of Whistlers Trapped In Field-Aligned Columns Of Enhanced Ionization, J. Geophys. Res., 66, 11, 3699 - 3707, 1961.
- Smith, R.L., Helliwell, R.A., Yabroff I.W., A Theory Of Trapping Of Whistlers In Field-Aligned Columns Of Enhanced Ionization, J. Geophys. Res., 65, 3, 815, 1960.
- Spectral Dynamics, The SD350-6 Digital Signal Analyser With Internal Translator, Spectral Dynamics, San Diego, U.S.A., 1978.
- Spectral Dynamics, Model 13262-1 Hard copy recorder, Spectral Dynamics, San Diego, U.S.A., 1979.
- Stassinopoulos, E.G., World Maps Of Constant B,L and Flux Contours, NASA Rept., SP-3054, 1970.
- Stiles, G.S., R.A. Helliwell, Frequency-time behaviour of artificially stimulated VLF emissions, J. Geophys. Res. 80, 608, 1975.
- Stoner, Demagnetizing Factors For Ellipsoids, Phil. Mag., 7, 36, 803 - 821, 1945.
- Storey, L.R.O., An Investigation Of Whistling Atmospherics, Phil. Trans. Roy. Soc. (London), A, 246, 113 - 41, 1953.
- Strangeways, H.J., An Investigation Of The Propagation Of Whistlers In Magnetospheric Ducts By Means Of Ray Tracing, Curve-Fitting, And Direction Finding Techniques, Ph.D. Thesis, University of Southampton, 1977.
- Stubbe, P. and H. Kopka, Modulation of the Polar Electrojet by Powerful HF Waves, 82, 16, 2319 - 2325, 1977.
- Stubbe, P. and H. Kopka, Ionospheric Modification Experiments In Northern Scandinavia - "A Description Of The Heating Project, Max-Planck-Institute Fur Aeronomie, W. Germany, MPAE - W - 02 - 79 - 04, 1979.

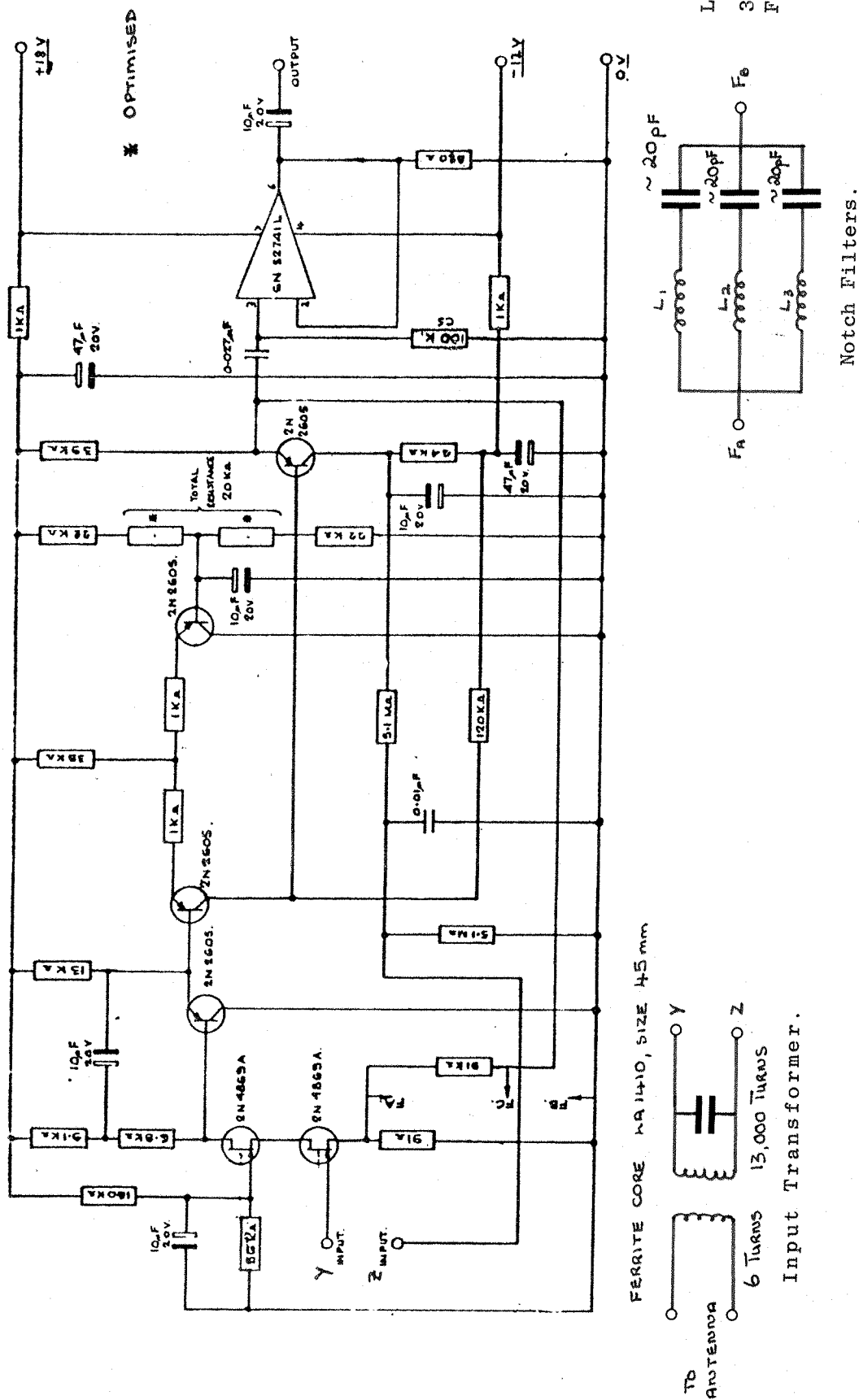
- Sugiura, M., Identifications of the polar cap boundary and the auroral belt in the high altitude magnetosphere: A model for field aligned currents, J. Geophys. Res., 80, 2057, 1975.
- Tarcsai, G., Routine whistler analysis by means of accurate curve fitting J. Atmos. Terr. Phys., 37, 1447 to 1457, 1975.
- Taylor, W.W. and D.A. Gurnett, Morphology of VLF emissions observed with the Injun 3 satellite, J. Geophys. Res., 73, 5615, 1968.
- Telcon Metal Ltd., Mu Metal Alloys, Telcon Metals Ltd., Manor Royal, Crawley, Sussex, 1975.
- Tellegen, B.D.H., Interaction between radio waves, Nature, 131, 840, 1933.
- Terman, F.E., Radio Engineers Handbook, McGraw Hill, 1943.
- Texas Instruments, Bifet Op-Amp Family, Bulletin CB-248/U.K., 1977.
- Thomas, G.R. and D.A. Bryant, Proposed U.K. High Latitude Rocket Campaign In Late 1976/Early 1977, ESRO SP107, 1975.
- Thomas, L., The lower ionosphere, Journal Atmos. Terr. Phys., 33, 157 - 195, 1971.
- Thorne, R.M., E.J. Smith, K.J. Fiske, and S.R. Church, Intensity Variations Of ELF Hiss And Chorus During Isolated Substorms, Geophys. Res. Lett., 1, 193, 1974.
- Thorne, R.M., S.R. Church, W.J. Malloy and B.T. Tsurutani, The local time variation of ELF emissions during periods of substorm activity, J. Geophys. Res., 82, 1585, 1977.
- Tobey, G. and J. Graeme, Operational Amplifiers, Design And Applications, Burr Brown Series, McGraw Hill, U.S.A., 1978.
- Tsurutani, B.T. and E.J. Smith, Postmidnight chorus, a Substorm Phenomenon, J. Geophys. Res. 79, 118, 1974.
- Turco, R.P., and C.F. Sechrist, An investigation of the ionospheric D region at sunrise, 1, Time variations of ozone, metastable molecular oxygen, and atomic oxygen, Radio Sci., 7, 703 - 716, 1972.
- Turunen, T., P.S. Cannon and M.J. Rycroft, Generation of ELF Radio Signals In The Auroral Ionosphere By Non-Linear Demodulation Of LF And/Or MF Transmissions, Nature 286, 375 - 377, 24 July, 1980.
- Ungstrup, E. and I.M. Juckerott, Observations of chorus below 1500 cps at Godhavn Greenland from July 1957 to December, 1961, J. Geophys. Res., 68, 2141, 1963.
- U.S. Naval Observatory, Washington D.C. 20390, Time Series Publications Series 1, Worldwide Primary VLF and HF Transmissions, Feb. 1979.

- Utlaut, W.F., Ionospheric Modification Induced by High-Power HF Transmitters - A Potential for Extended Range VHF-UHF Communications and Plasma Physics Research, Proc. IEEE, 63, 7, 1022 - 1043, 1975.
- Wagner, R.A., A.L. Snyder, and S.I. Akasofu, The Structure of the Polar Ionosphere during Exceptionally Quiet Periods, Planet, Space Sci., 21, 1911, 1973.
- Wait, J.R. and A.M. Conda, Pattern of an Antenna on a Curved Lossy Surface, I.R.E. Trans On Antennas and Propagation - 6, 348 - 359, 1958.
- Walker, J.C.G., Active Experimentation With The Ionospheric Plasma, Rev. Geophys. and Space Phys., 17, 4, 1979.
- Wallis, D.D., C.D. Anger, and G. Rostoker, The Spatial relationship of auroral electrojets and visible aurora in the evening sector, J. Geophys. Res., 81 (16), 2857 to 2869, 1976.
- Wiens, R.G., and G. Rostoker, Characteristics of the Development of the Westward Electrojet During the Expansive Phase of the Magnetosphere Substorm, J. Geophys. Res., 80, 16, 2109 - 2128, 1975.
- Willis, J.W. and J.R. Davis, Radio Frequency Heating Effects on Electron Density in the Lower E region, J. Geophys. Res., 78, 25, 5710 - 5717, 1973.
- World Radio and T.V. Handbook, Billboard Publications, Canarby Street, London, U.K., 1979.
- Watt, A.D., E.L. Maxwell and E.H. Whelan, Low-Frequency Propagation Paths In Arctic Areas, Journal of Res. Nat. Bur. Standards - D Radio Propagation, Vol. 63D, No. 1, July - August, 99 to 112, 1959.
- Yabroff, I., Computation Of Whistler Ray Paths, J. Res. NBS, 65D, 485, 1961.

APPENDIX ONE

Goniometer System Preamplifier

The goniometer system preamplifier is based upon a design by Cantarano and Pallotino (1970), the circuit diagram, for which, is shown in figure A1.1.



APPENDIX TWO

A2.1 Circuit Description Of The Digital Time Encoded Clock

The following is a brief description of the clock circuit described in Chapter 4 and based on the work of Blixhavn and Lyngdal (1976) and Girling (1976).

A2.2 Preamplifier and Omega Receiver Figures A2.1 and A2.2

A preamplifier with a JFET input stage, tuned to 10.2kHz amplifies the signal from a long wire antenna. The signal is fed by coaxial cable to the "Omega Receiver", where it is suitably amplified and filtered at 10.2kHz, before being fed to the Omega Detector.

A2.3 Omega Detector Figures A2.3 and A2.4

The Omega Receiver output is fed to a commutating 10.2kHz bandpass filter (4051) which is driven by the divided output of a crystal oscillator. The filter output passes to a 4071 level detector, the output of which triggers a 4017 monostable. After being successfully triggered this locks out the detector against noise for eight or nine seconds, (as indicated by a LED). The monostable also triggers two other monostables. One gates the signal to a 4040 counter for 0.4 seconds. Providing this succeeds in counting to 3072 the signal is accepted as an Omega pulse, not noise, and the 4013 flip flop suitably loaded. This in turn enables the 4048 8 input AND gate when the seconds counter LSB is 4 or 5. The output from this gate enables the time adjustment gate, 4016. The second monostable provides a pulse to reset a 4510 reference counter which starts counting. The counter is programmed by setting a thumb wheel switch, see Fig. A2.5. When dealing with signals from Omega, Norway, this represents the time difference between zero seconds and the time of the 10.2kHz pulse, see Chapter 4. The reference counter is compared to the seconds counter LSB and the comparator outputs used to control the 4016 time adjustment gates. These admit 100Hz, or 200Hz (providing 10ms or 5ms control) or neither to a 4518 divider chain. Note that this only occurs when the LSB is 4 or 5 in order that correction does not take place into the wrong 10 second interval. The comparator state is indicated by panel mounted LED's, see figure A2.5.

A2.4 Display, Seconds, Minutes and Hours Counters Figures A2.5, A2.6, A2.7, A2.8.

The display is a 9 digit liquid crystal display suitably driven by 4543's. This is a departure from the design of Blixhavn and Lyngdal (1976) who used an LED display. All time information is multiplexed on four common buses, Q_1 , Q_2 , Q_3 and Q_4 at 1.6kHz. The time format and nomenclature are shown in figure A2.15. Note these are shown as two 16 bit words.

The operation of all counters is similar. The dual B.C.D. counter 4518 provides the two digits of each group with each digit gated through the 4016 switch when its associated strobe line is high. The counter outputs are fed asynchronously to the 4021 shift register when the P/S line is high, being read out as one of two 16 bit lines when the P/S line is low. Only days and hours, or minutes and seconds information can be encoded.

A2.5 Day Counter Figure A2.9

The day counter is similar. A flip flop is used, however, to count the hundred days and provision is included to reset after 365 or 366 days. The 4068 and 4022 combine to reset the day count to logic one rather than zero after a complete cycle.

A2.6 Display Multiplexers, Set Time Debounce, Time Marker Figure A2.10

The figure shows three separate circuits, only the time marker will be discussed here.

The time marker switch selects the appropriate signals and feeds them to a 4528 monostable which produces 0.25 second pulses, except for the second pulses which are 0.07 seconds long. These pulses, together with the long interval pulses, see figure A2.16, are gated through an exclusive OR gate to drive a pair of opto-couplers.

A2.7 Time Encoder Figure A2.11

A 1.3MHz clock is divided by a 12-stage counter (4040) to give the FSK modulation and carrier frequencies of 2.5kHz, 5kHz and 10 kHz. The external clock (417Hz) is used to read the time from the 4021 registers

(figures A2,6,7,8,9) when the P/S line is low. (The P/S line is a differentiated 1Hz signal). This is then suitably gated through to a 4013 flip flop and thence to 4011 nand gates which form the modulator. The flip flop is set to one by the 4022 output on the second pulse of every six pulse cycle. It is then reset to zero on the sixth count for a logic one on the day or minute input, or on the fourth and sixth counts for logic zero. The Q and \bar{Q} outputs of the 4013 are then used to gate the FSK carrier signals. Pulse width modulation of the carriers is thus accomplished.

A2.8 Time Encoder Mixer And Decoder Filtering. Figure A2.12.

The encoder consists of a mixer which adds the time encoded FSK signal to a low pass filtered goniometer calibration pulse. The output is recorded on one channel of the tape recorder.

On replay the decoder separates these mixed signals by high pass filtering the FSK coded signal and low pass filtering the calibration signal. Both signals are fed to comparators to reconstitute the pulses. For the calibration pulse this is set to give a sharp pulse $\sim 0.8\text{ms}$ long.

A2.9 Time Decoder. Figure A2.13.

The monostable 4528 and flip flop 4013 form an FSK discriminator. The 4528 time constant is set midway between 5kHz and 10kHz. Any input frequency higher than this produces a steady 1 output, whilst lower frequencies produce a train at that frequency. A steady "1" on the monostable Q output causes a "1" at the flip flop output. A '0' (caused by the flip flop timing out) causes the flip flop to reset to '0' but since the input is delayed by the CR network, the D input is still at '0' when the next clock pulse occurs. Hence the output remains at '0'. Consequently the 10kHz signals are decoded as logic 1 and the 5kHz signals as logic '0'.

The following monostable (4528), with a time constant of 1.2ms, forms a pulse width decoder. Its purpose is to generate a sampling pulse which occurs after a pulse corresponding to a '0' signal has finished but before a pulse corresponding to a '1' signal has finished. This signal is used to clock the 4015 shift registers which are fed from the FSK demodulator output. The parallel shift register outputs feed 4016 analog gates which are enabled in turn by a one of nine output from the 4017 multiplexer. See figure A2.10.

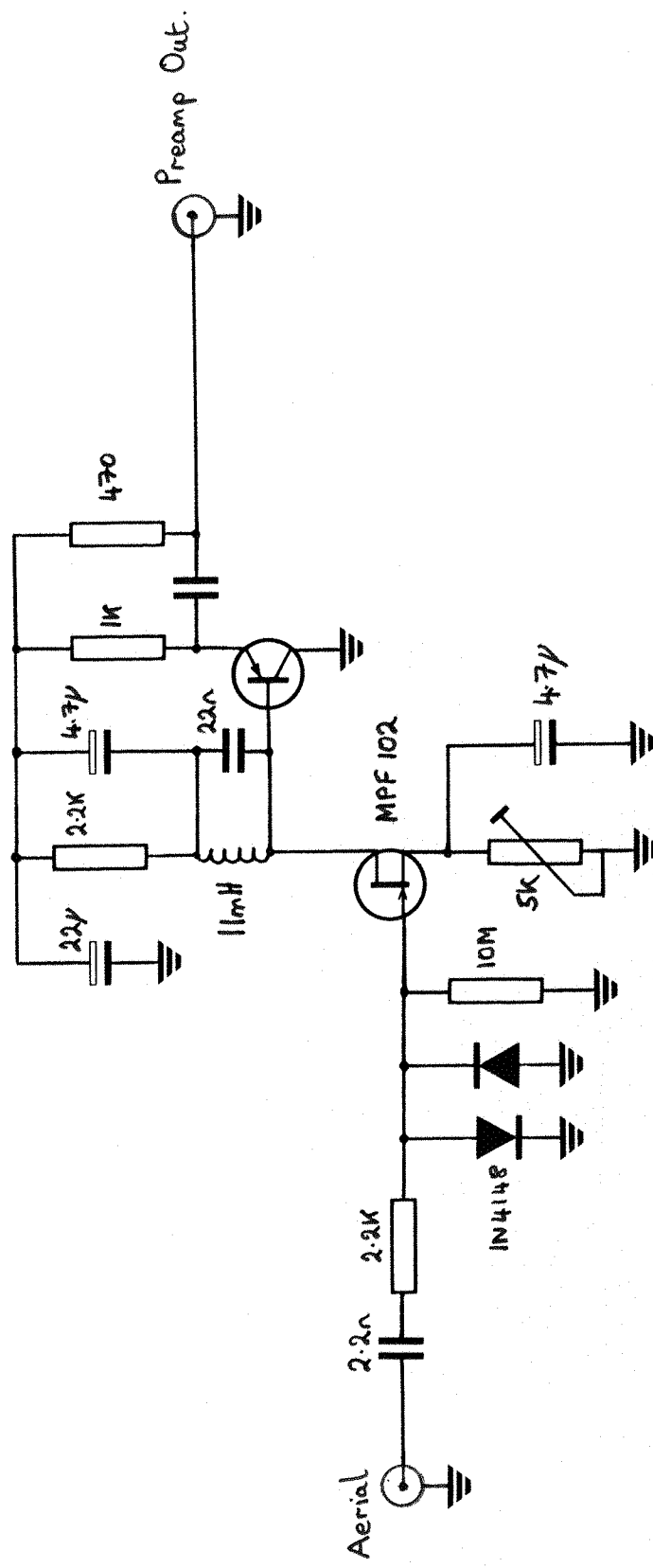


Fig. A 2:1 Omega Clock Preamplifier.

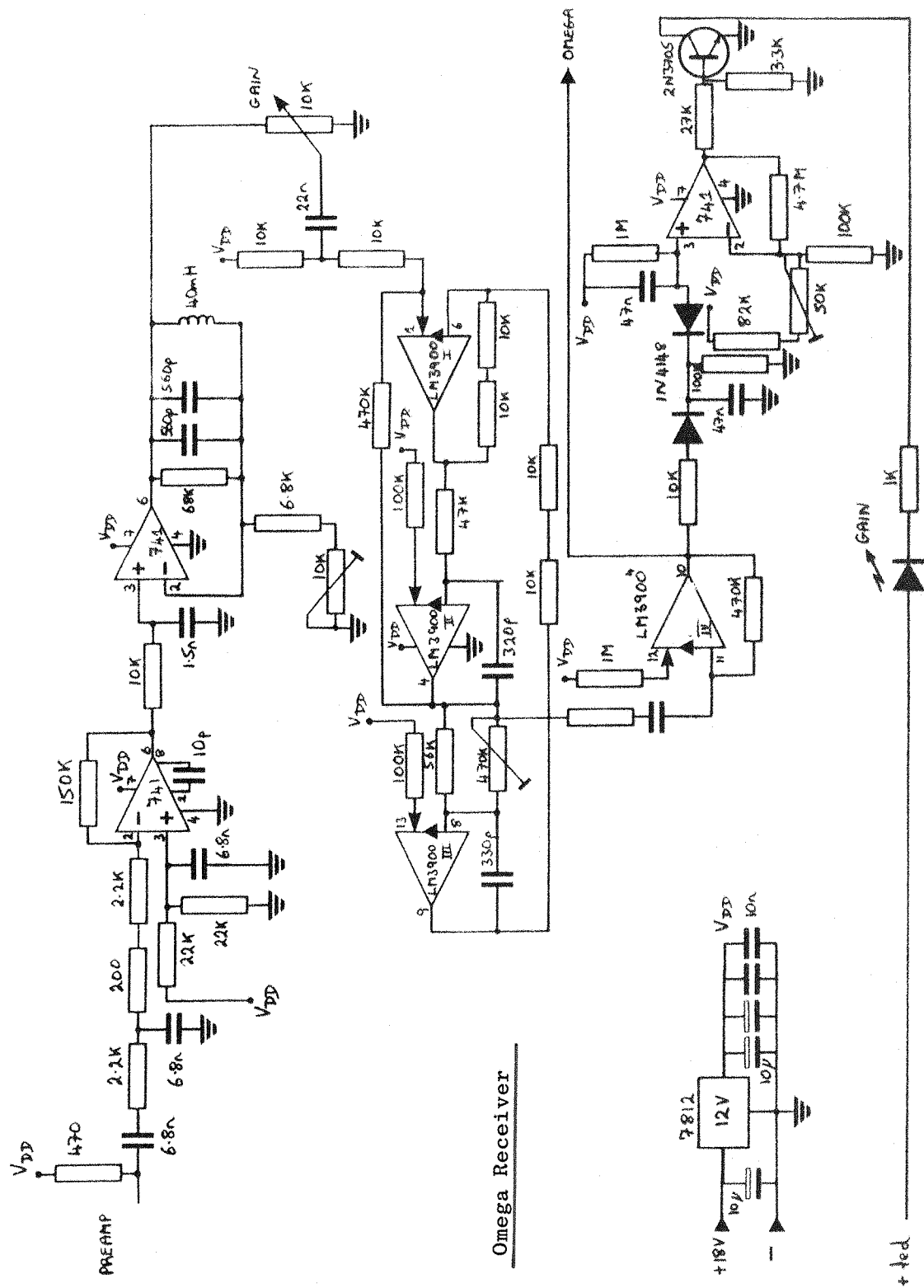
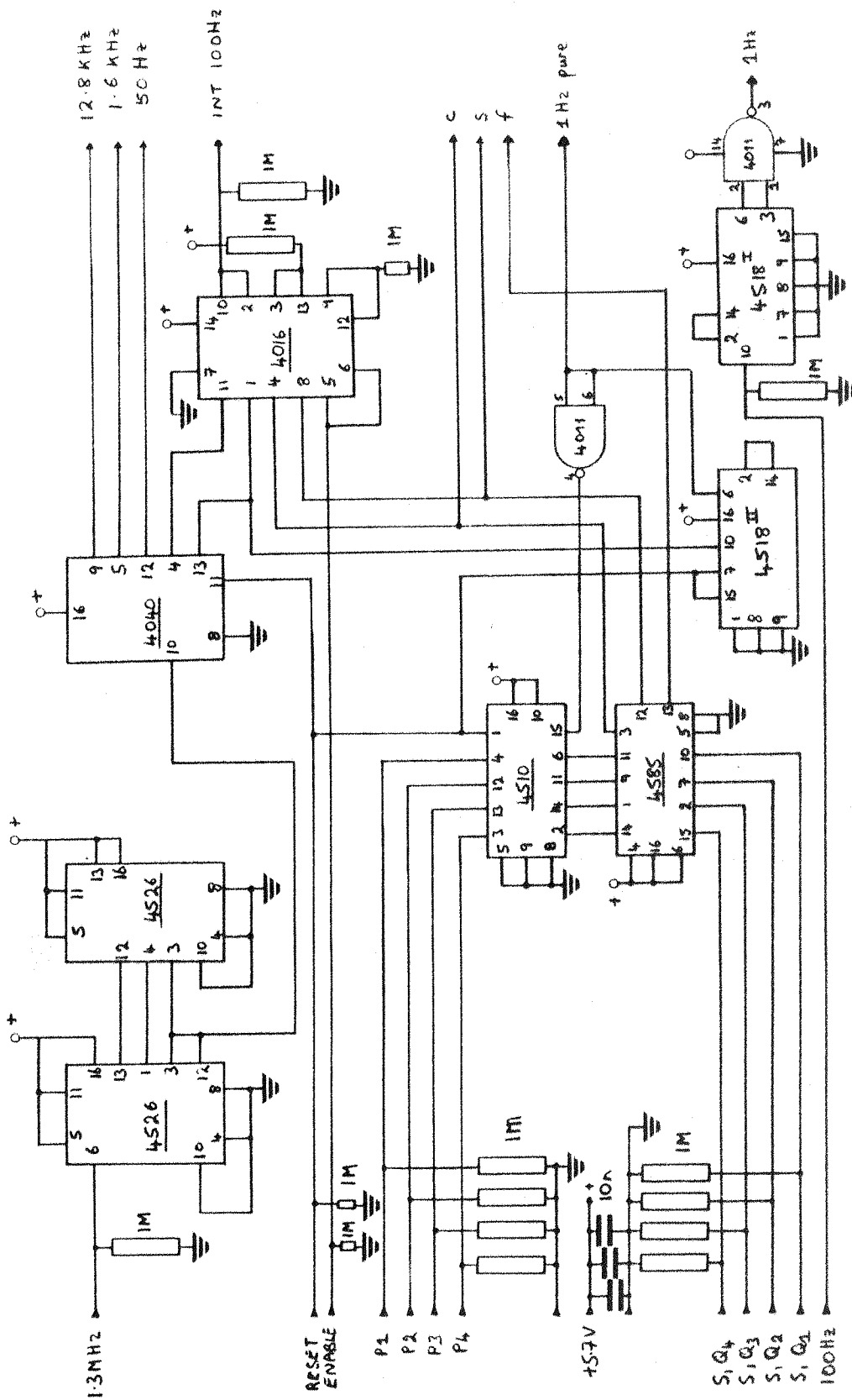
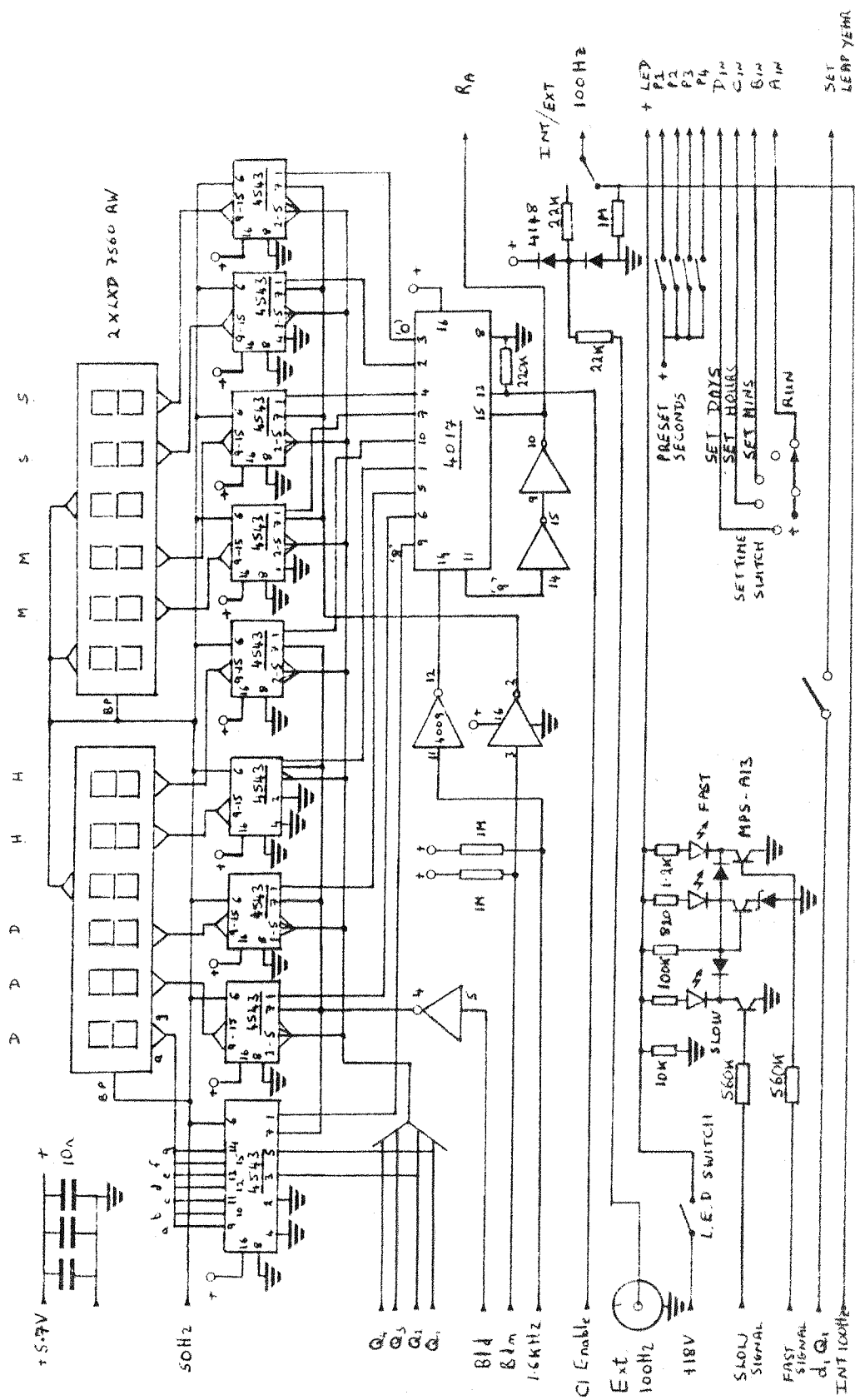


Fig. A2:2 Omega Receiver





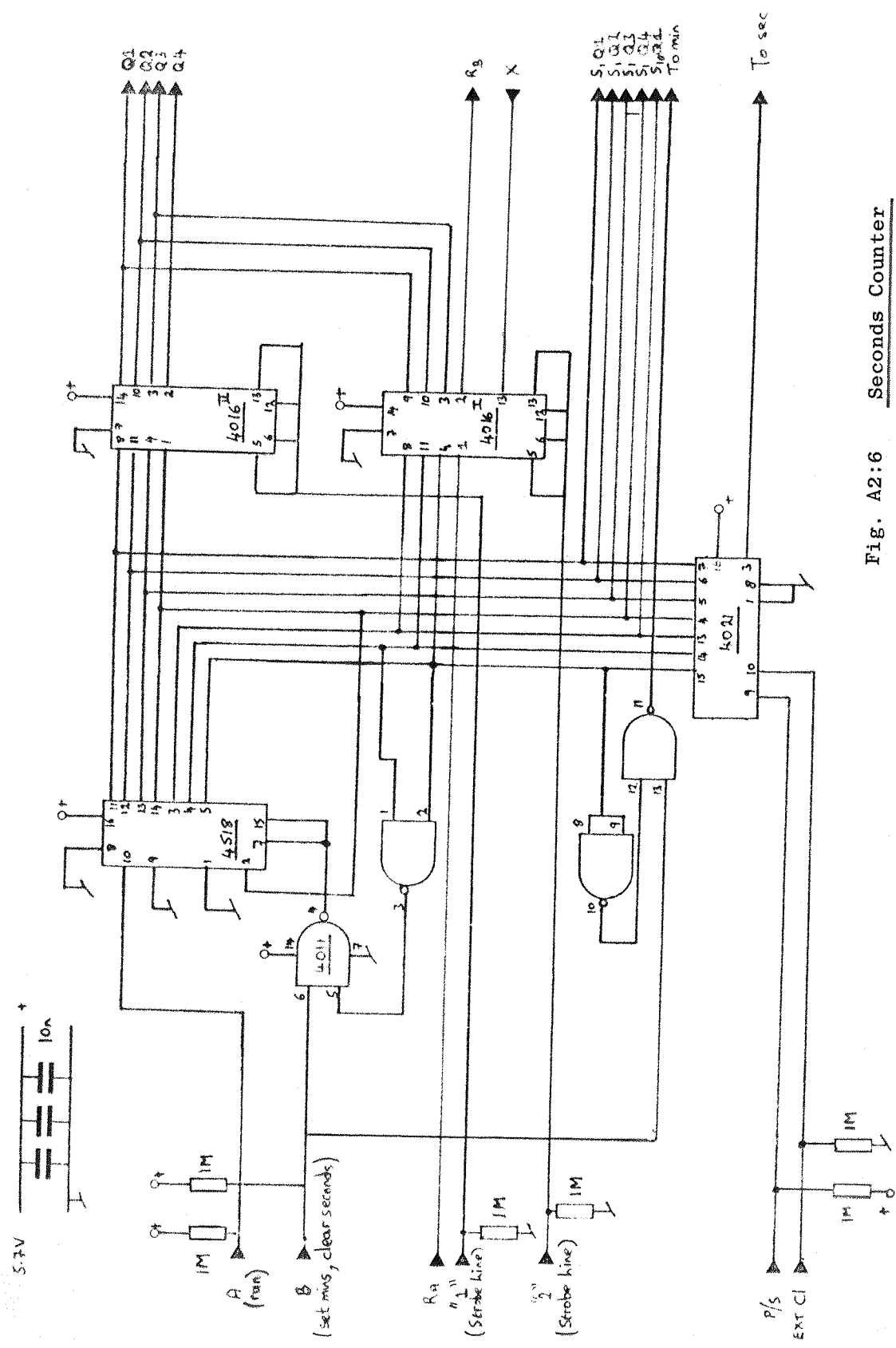


Fig. A2:6 Seconds Counter

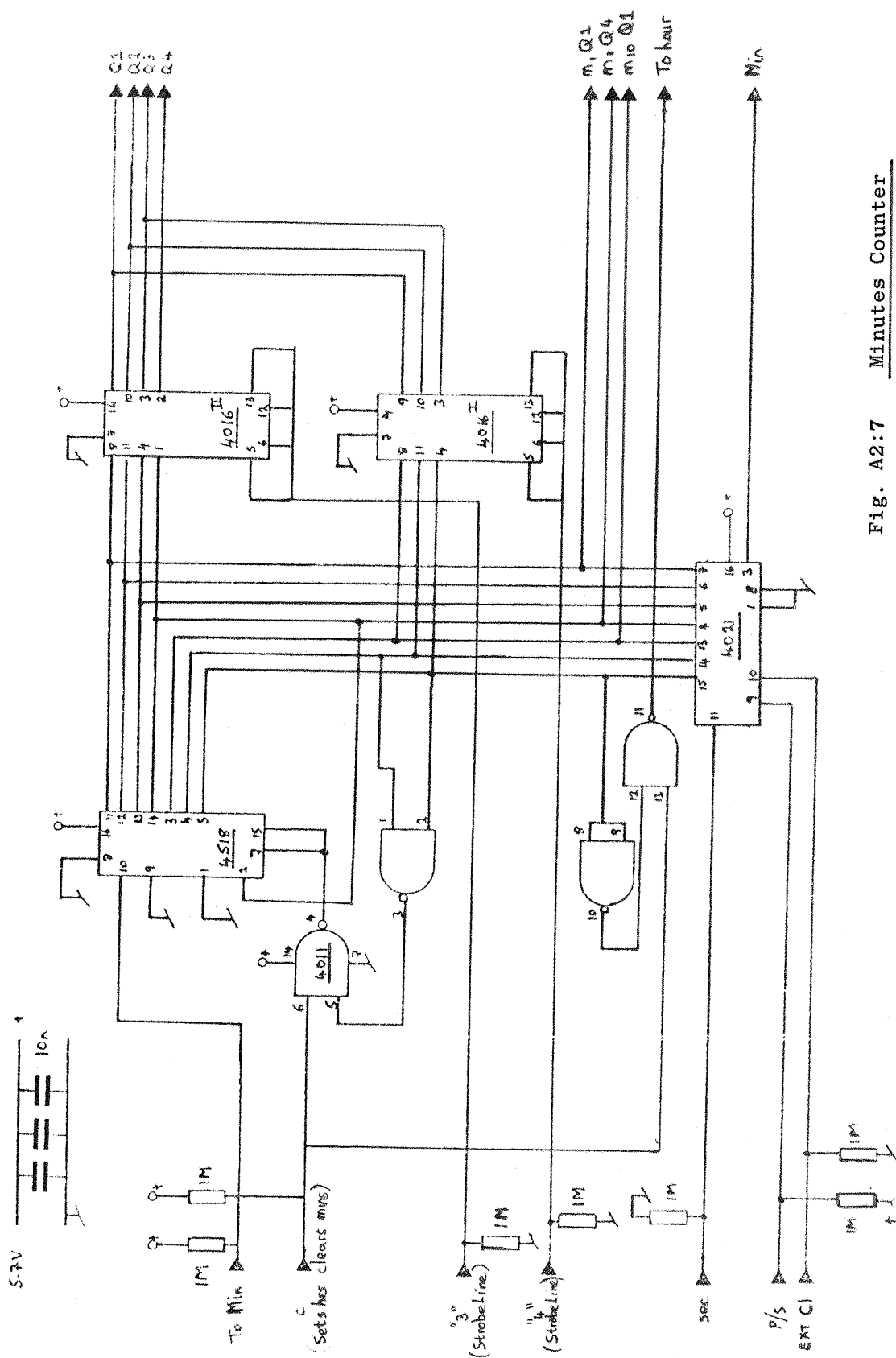
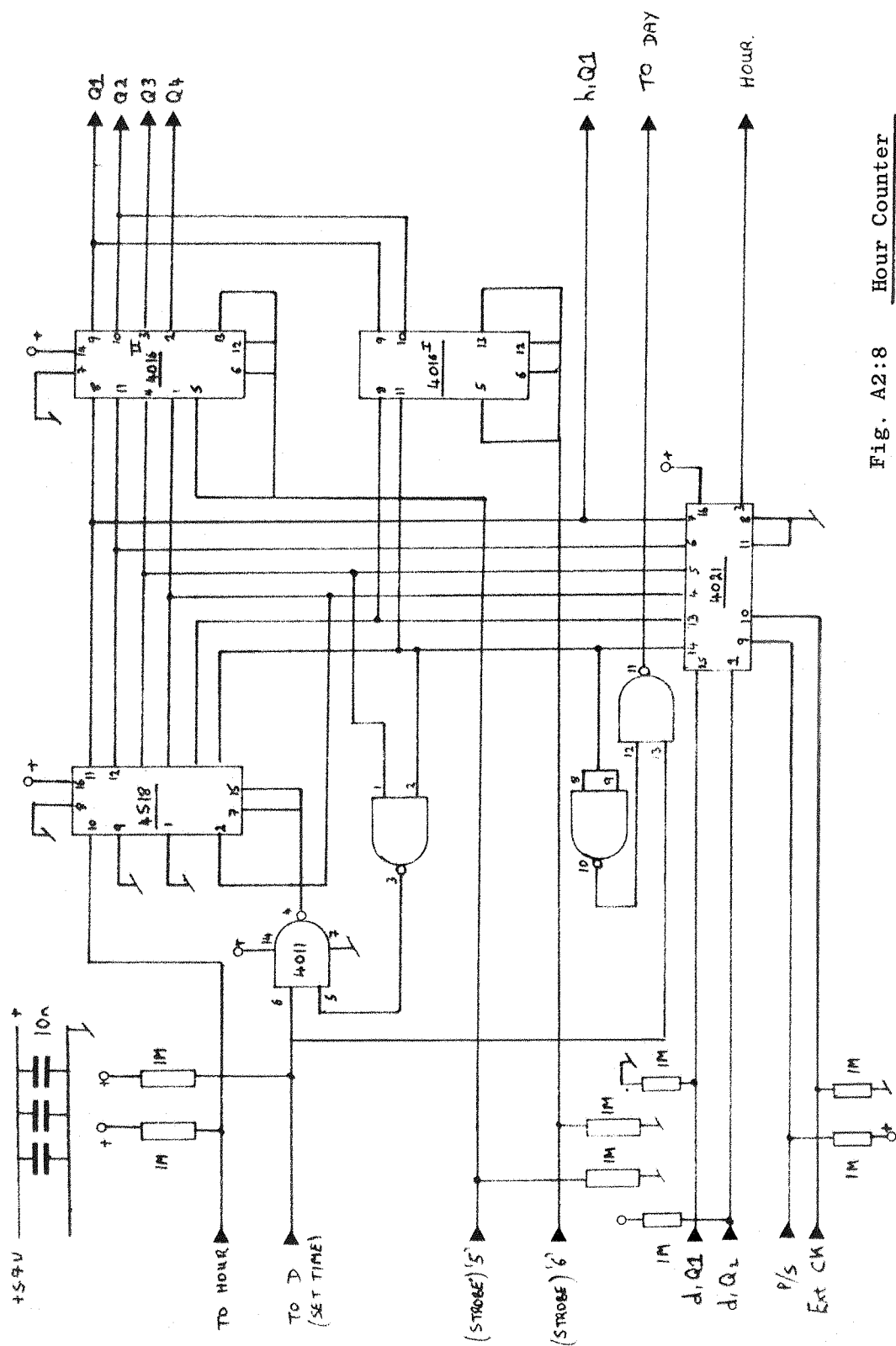


Fig. A2:7 Minutes Counter



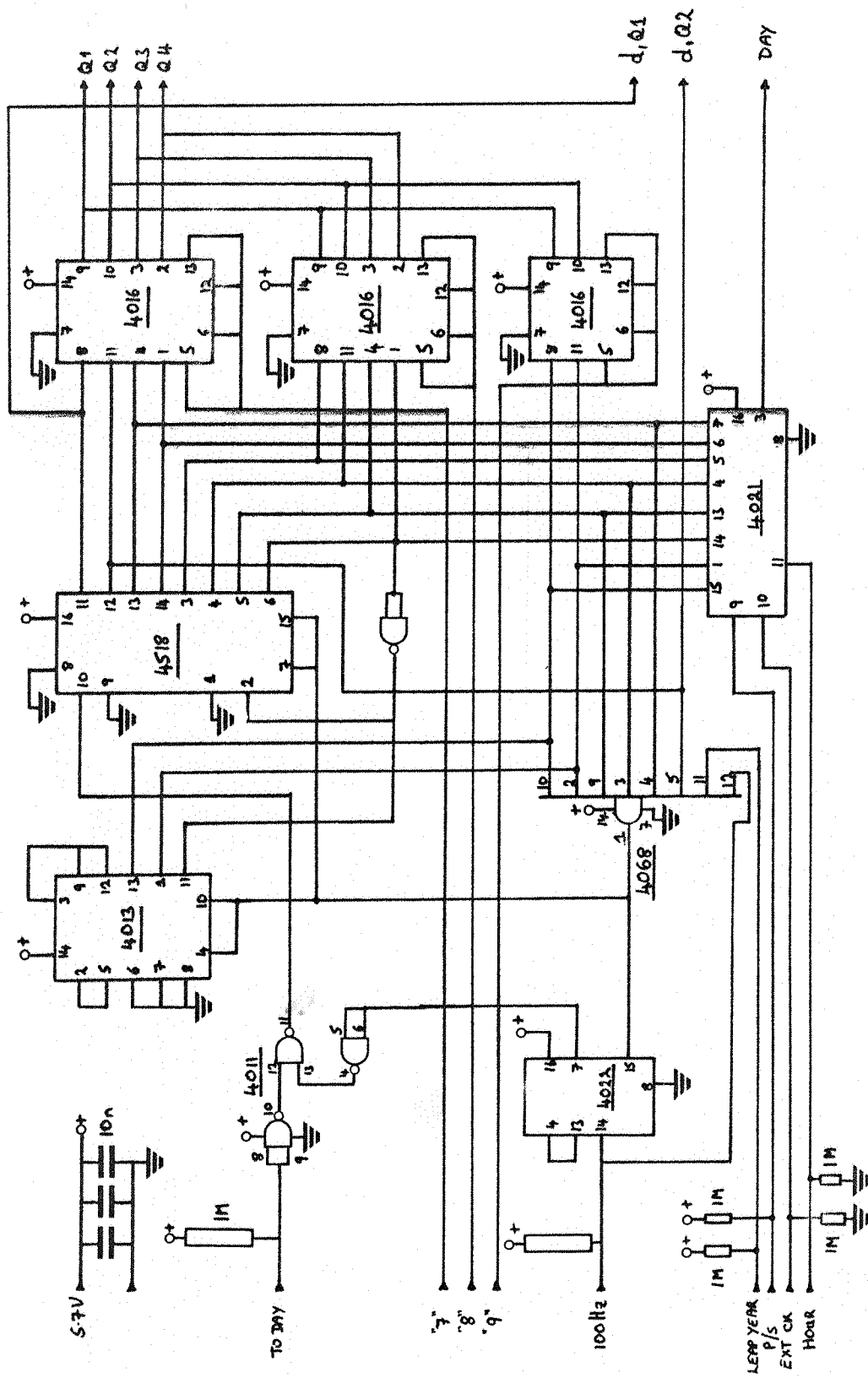


Fig. A 2:9 Day Counter.

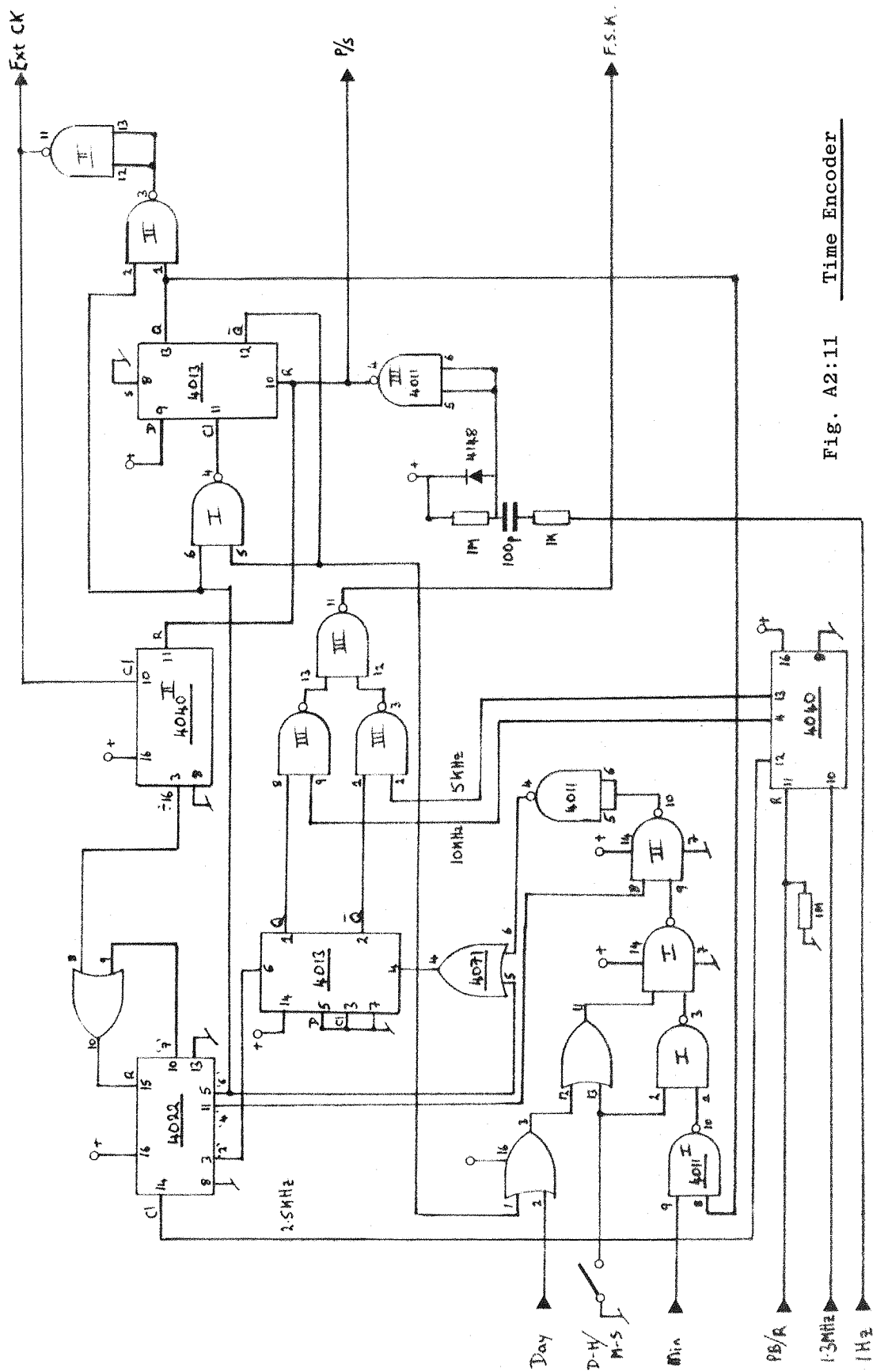


Fig. A2:11 Time Encoder

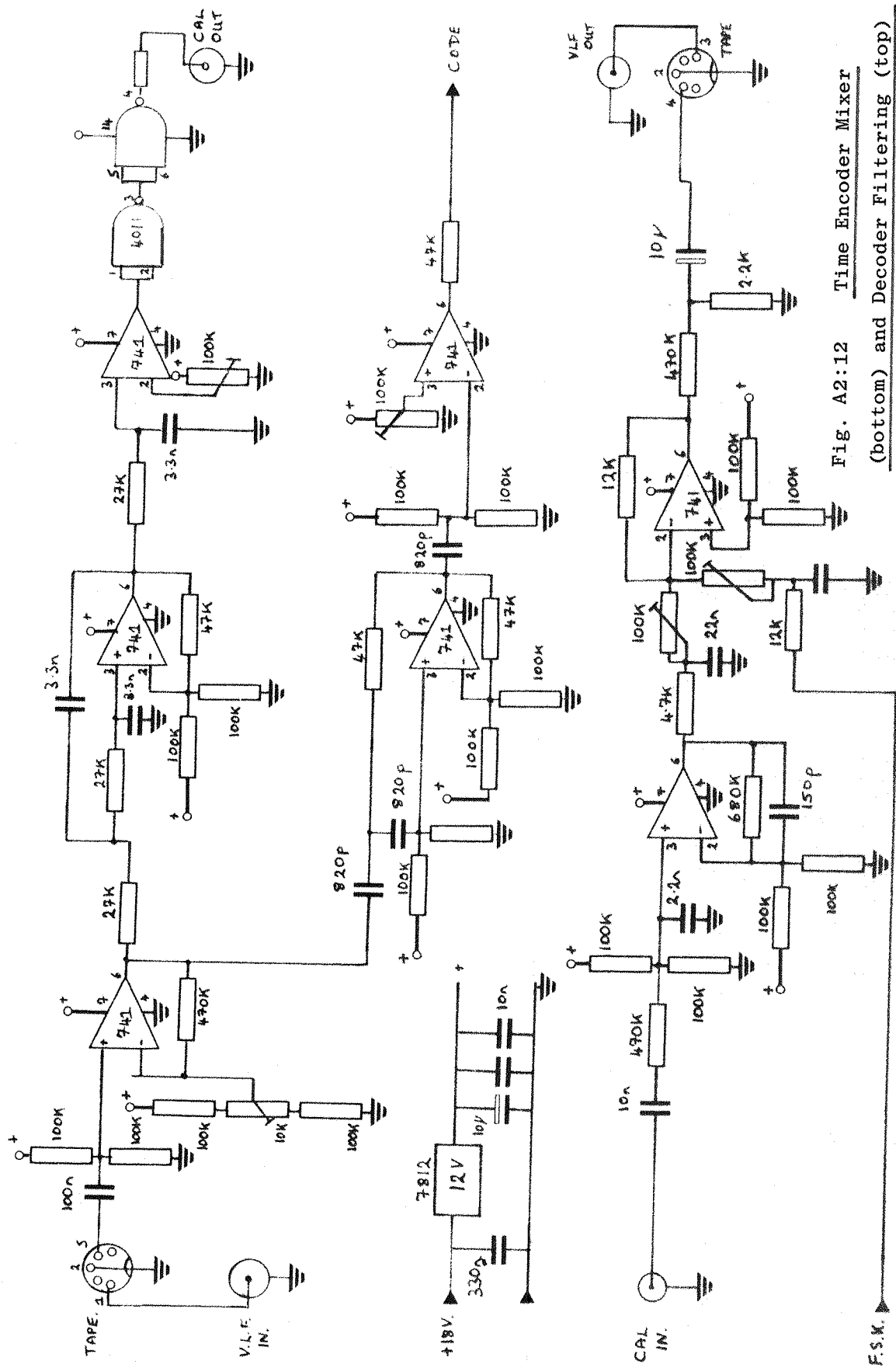


Fig. A2:12 Time Encoder Mixer

(bottom) and Decoder Filtering (top)

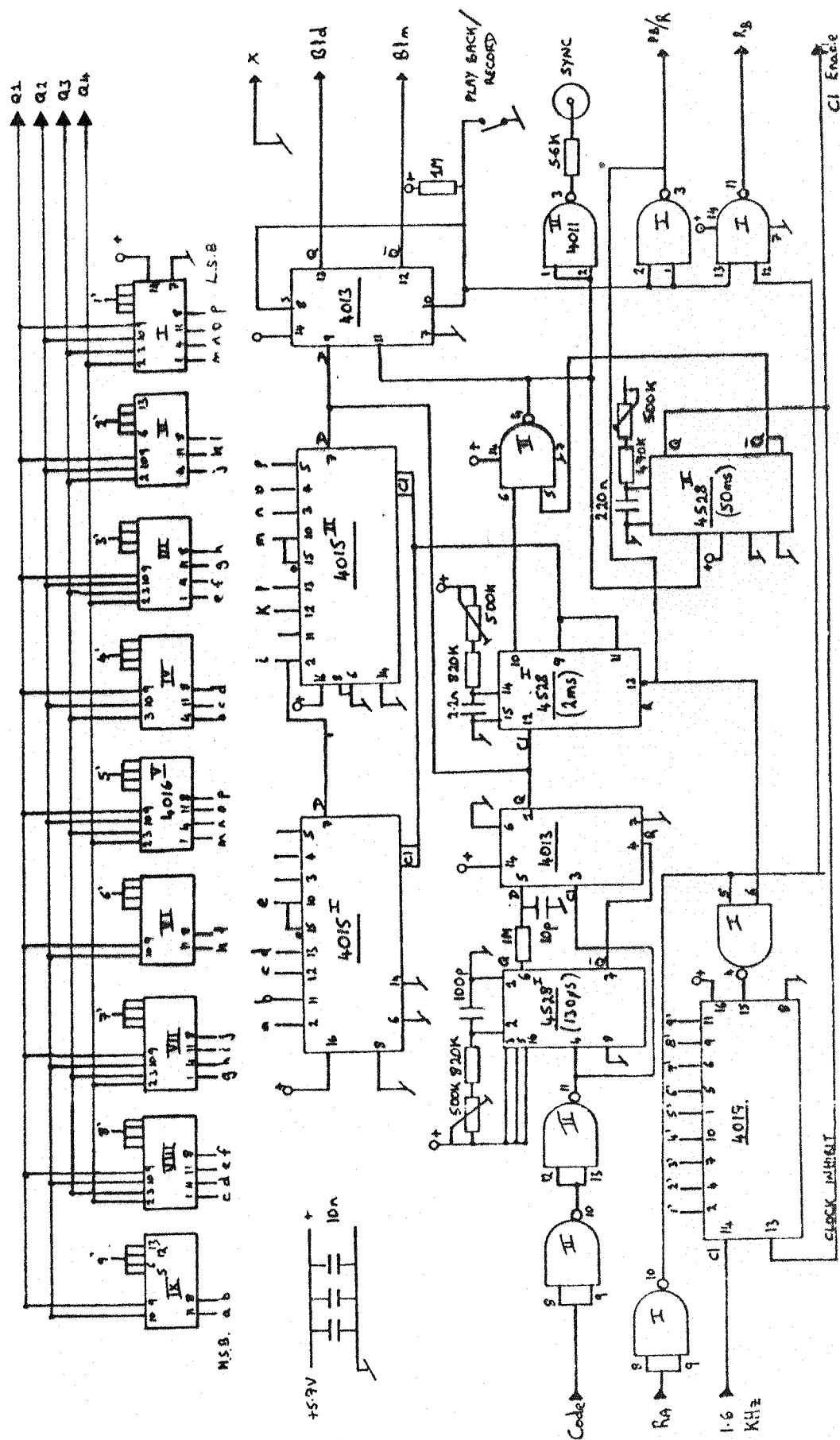


Fig. A 2:13 Time Encoder.

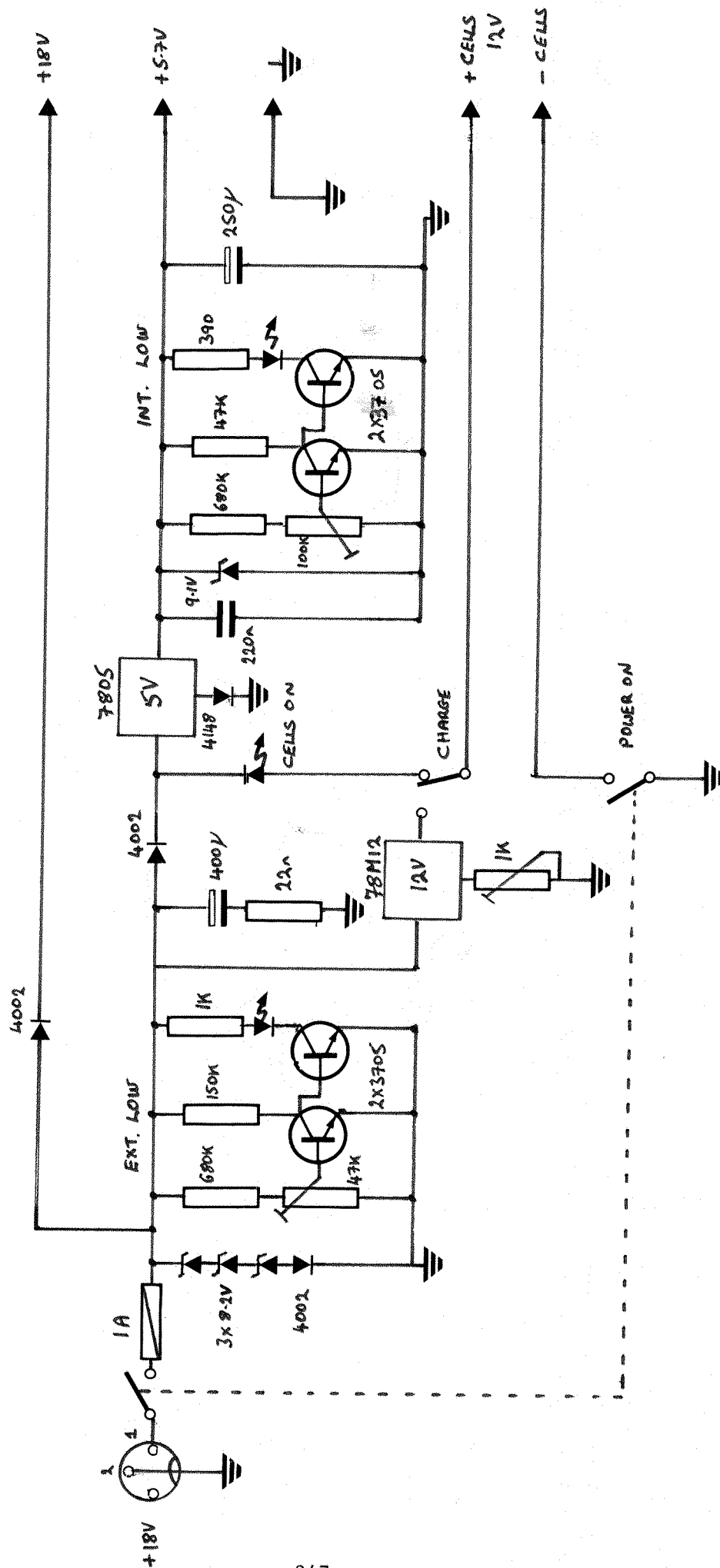


Fig. A 2:14 Regulated Power Supply and Charger.

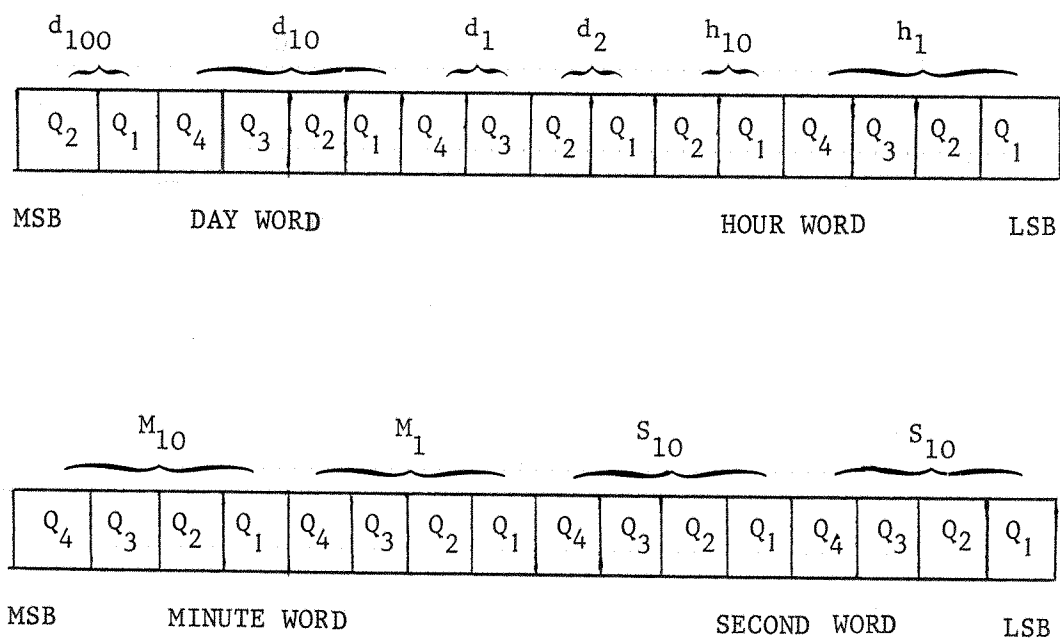


Fig. A2.15 Time Code Format

<u>SETTING</u>	<u>LONG INTERVAL</u>	<u>SHORT INTERVAL</u>
OFF	NO MARKS	NO MARKS
DAY	1/DAY	1/HOUR
HOUR	1/HOUR	1/10 MIN.
10 MIN.	1/10 MIN.	1/MIN.
MIN.	1/MIN.	1/10 SEC.
10 SEC.	1/10 SEC.	1/SEC.

Fig. A2.16 Time Marker Output

APPENDIX THREE

Field Site Operation Of The ELF Receiver System

A3.1 Introduction

Figure A3.1 shows a schematic of the wiring between the various units. All equipment is powered by 5 ampere-hour lead acid gell batteries charged from a constant current charger. The preamplifier and receiver have separate power supplies. It is assumed that the comb filter is placed subsequent to IC13a, see section 8.7.

A3.2 Setting Up

Below are listed those steps which must be followed to correctly set up the ELF system.

- 1) With power and lock up antenna connected, connect a signal generator to the receiver input, switch the receiver comb filter to the antenna lock up mode and sweep the generator to ascertain whether it is possible to obtain a stable notch at 50 Hz, indicating that a suitable comb filter lock up signal is available. If yes proceed to step 3.

- 2) If no, use the internal crystal oscillator to lock up the filter.

- 3) Set up the system as shown in figure A3.1, switch the range to 0.3Hz to 700Hz and the notch filters out.

- 4) Measure the signal level at test point 2 and adjust the gain of IC7a, figure 8.9, to obtain a value ~ 1.5 volts peak to peak. This is the maximum signal which can be applied to the variable notch filters without causing signal clipping.

- 5) Measure the signal level at test point 3 and adjust the gain of IC13a, figure 8.10 to obtain a level of ~ 5 volts peak to peak. This value is limited by the comb filter FET inverter, see figure 8.13.

- 6) Monitor the receiver output and if required utilise the variable notch filters provided. Increase the gain of IC13a to bring the maximum peak to peak level back to 5V.

- 7) Switch the range selector firstly to 0.3Hz to 40Hz and then 200 Hz to 700 Hz and adjust the gain of IC9c and 10b (figure 8.9) to obtain a similar voltage at test point 3 to that obtained on the 0.3Hz to 700Hz range. This enables the ranges to be changed without affecting tape recorder settings.

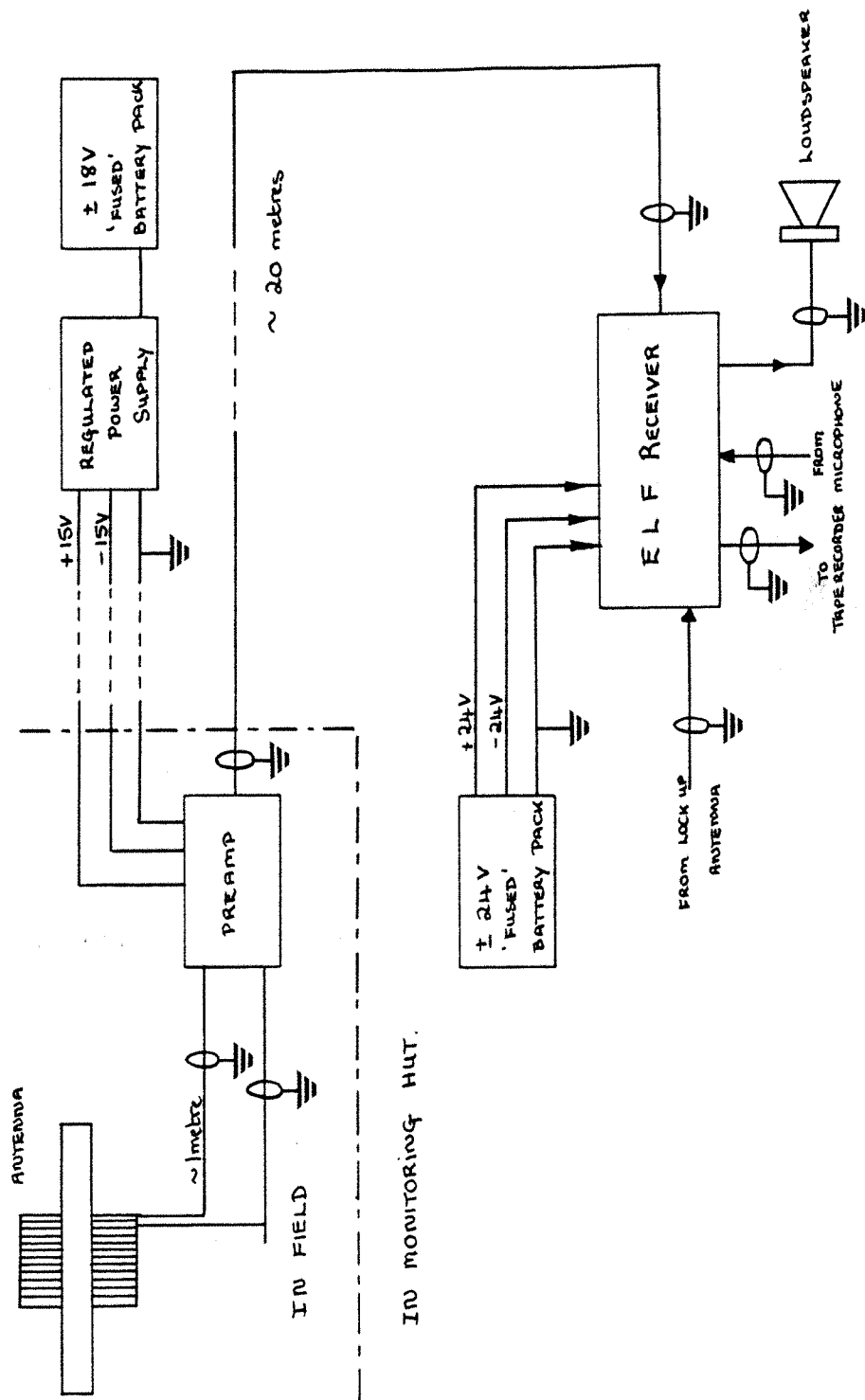


Fig. A3:1 ELF Recording System (one channel only shown)

APPENDIX FOUR

A Helmholtz Coil Calibration System

In order to test and calibrate the ELF antenna described in chapter 9, a uniform and calculable laboratory magnetic field was required. To provide this a Helmholtz coil system was developed. Since the antenna was designed to operate across the mains fundamental and harmonic frequencies a high field strength was provided in order to reduce corruption of the injected signal by laboratory noise.

Bullough et al. (1968) give the time varying magnetic field at the centre of a single turn square Helmholtz coil as:-

$$B = \frac{1.7 i}{\ell} \times 10^3 \text{ pT}$$

where ℓ = length of the coil side (metres), i = current in the coil (mA, RMS), and the distance between coils is $\ell/2$. For N turns on each coil:

$$B = \frac{1.7 N i}{\ell} \times 10^3 \text{ pT} \quad \text{equation A4.1}$$

Each square coil was constructed from three turns of copper wire, one coil being wound near the laboratory ceiling and one coil being wound near the laboratory floor giving a value of $\ell = 5.95 \text{ m}$.

The coils were driven in parallel from a current amplifier which was itself fed from a signal generator. The current amplifier is shown in figure A4.1 and can deliver a maximum of 300 mA RMS into the coil and current limiting resistor. (The Helmholtz coil is assumed purely resistive since its reactance at 1kHz is only $\sim 1\Omega$).

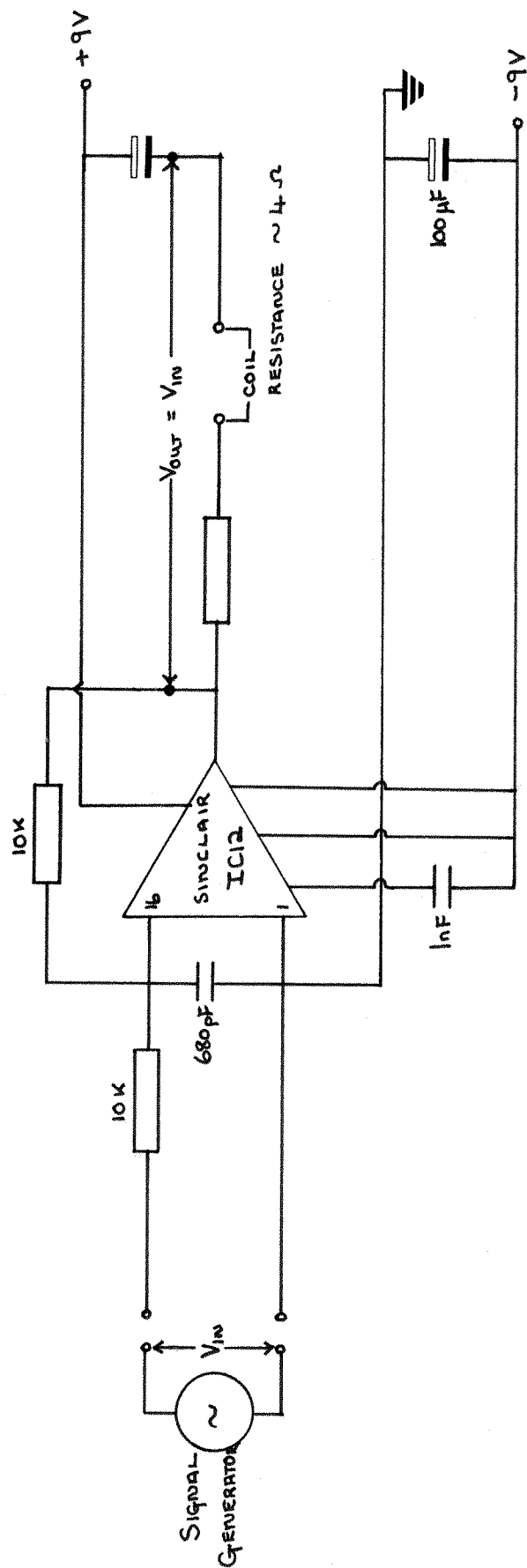


Fig. A4:1 Helmholtz Coil Current Booster.